ELECTROKINETIC BARRIER AND REMEDIATION WITH SOLAR ENERGY

By

Ahmed M.A. Yassin Mahmoud

This thesis is submitted in partial fulfillment of the requirements for the degree of

Master of Science in Engineering in Environmental Engineering (MSc Eng)

Faculty of Graduate Studies

LAKEHEAD UNIVERSITY

Thunder Bay, Ontario, Canada

March 2012

ABSTRACT

Electrokinetics is a promising technique to prevent/ minimize the migration of pollutants to the soil and/or groundwater and to remediate contaminated slurries. Electrokinetics requires a low-level direct current (dc) between an anode and a cathode. This results in electro-osmosis, electro-migration and electrophoresis along with electrolysis reactions. An electrokinetic barrier utilizes electro-osmosis, electro-migration and a soil zone with high pH created near the cathode to prevent the migration of contaminants. Electrophoresis accelerates the sedimentation of contaminated slurry whereas electro-osmosis and electro-migration remove water and pollutants from the slurry. Solar energy is an environmentally friendly renewable source capable of providing sufficient electric field for electrokinetics, particularly in remote areas.

This study consisted of two parts. Part one investigated electrokinetic barrier to minimize heavy metal contamination in clayey sand. Part two explored electrokinetic remediation of two clay slurries contaminated with a heavy metal. Copper, a common heavy metal pollutant, was used to prepare the influent for part one of the study and to artificially contaminate the slurry in part two. Solar energy provided the electric field with one and two-dimensional configurations.

The results showed that electrokinetic barrier was effective in significantly minimizing the migration of copper in the soil. Electro-migration was found to be the dominant mechanism in hindering the movement of copper. The copper adsorption capacity of the soil near the cathode was profoundly increased after the test. Electrokinetics accelerated the sedimentation and was successful in the dewatering and

decontamination of the slurry. In this study, solar energy provided sufficient electric field for electrokinetics.

DEDICATION

This dissertation is dedicated to of my grandparents Abdallah, Hasiba, Ihasan and Abdaljaleel may their souls rest in peace.

ACKNOWLEDGEMENTS

First of all, I would like to express my gratitude to Allah (God) for providing me the blessings to complete this thesis.

I would like to express my sincere gratitude to my helpful supervisor, Dr. Eltayeb Mohamedelhassan for his great supporting, helpful discussions, and corrections throughout the program.

Special gratitude to my uncle Dr. Ali Mahmoud for his endless care, support and continuous encouragement.

My grateful thanks goes to my parents, my mother Ekram and my father Mohammed for their loving, understanding, prayers, and for energizing me by their blithe spirit.

I am sincerely appreciating my colleagues Ikrema, Obai, Majed and Shazali for their help and support.

Finally, I would like to thank all other people that deserved acknowledgements for their help and assistance in the last two years.

TABLE OF CONTENTS

LIST OF TABLES

LIST OF FIGURES

CHAPTER ONE

INTRODUCTION

1.1 GENERAL

Heavy metals contamination of subsurface soils and groundwater from landfills leachate, mine tailings, industrial wastes and other sources is posing a significant hazard to human health and the environment. Acid mine drainage represents a major source of contamination by heavy metals to the soil and groundwater. Although many soil remediation technologies are available, electrokinetics has various advantages; including ease of operation, in-situ remediation and abilities to remediate fine grained soils with very low permeability (Reddy and Cameselle, 2009). Electrokinetics is a promising and innovative technique to prevent or minimize the spread of pollutants to the groundwater and soil.

In geo-environmental engineering field, most of the work on electrokinetics has been performed to remove the contaminants out of the soil (Lageman et al., 1989; Acar et al., 1992; Probstein and Hicks, 1993; Acar and Alshawabkeh, 1996; Alshawabkeh and Acar, 1996). Electrokinetics is the application of a low-level direct current (dc) between positively charged electrode (anode) and negatively charged electrode (cathode) inserted into the ground. This results in electro-osmosis, electro-migration and electrophoresis transports along with electrolysis reactions.

Only few studies have investigated the practicability of using electrokinetics to create subsurface barriers in order to prevent contaminants migration (Narasimhan and Ranjan, 2000; Lynch et al., 2007). An electrokinetics barrier utilizes inverse electro-osmosis and electro-migration along with the created zone of high pH to prevent or limit the spread of contaminants. In remote areas, the accessibility of the large equipment to the contaminated site is a major limitation to conventional barriers. Solar powered electrokinetics barrier is an innovative option for the remote areas (Mohamedelhassan, 2011).

In addition to their environmental hazards, contaminated sediments such as mining, industrial, and dredging wastes contain significant clay and colloidal fractions. This results in a very long settling period by gravity. Electrokinetics technique can be used to remediate the sediments. The remediation includes accelerating the sedimentation process, dewatering of sediment, and removing the heavy metals.

Very few researchers attempted to investigate the use of solar cell as a power supply in electrokinetic applications. The power produced by solar cell is environmentally friendly and can be used in sites located in remote areas without active power lines. Moreover, solar cells produces dc electric field that is usable in electrokinetic applications without alteration (i.e. without dc transformer) which can cut the electricity transmission expenses and eliminate power losses in the transmission lines. Yuan et al. (2009) showed that the cost of the electric power was reduced when solar cells were used to generate the power for an electrokinetic remediation study.

1.2 OBJECTIVE OF THE STUDY

This study consists of two parts. The first part investigated integrated solar powered electrokinetic barrier to prevent/minimize heavy metal contamination. The second part explored the remediation of slurries contaminated with a heavy metal.

The objectives of part-1 are:

- To examine the effectiveness of electrokinetic barrier powered by solar energy in preventing the spread of heavy metals contamination.
- To monitor the change in the properties of the soil after the test.
- To propose an electrode arrangement and spacing for field applications.

The objectives of part-2 are:

- To investigate the electrokinetic remediation of contaminated slurries using solar energy as source of power.
- To test and develop an applicable electrode configuration for field applications.

Several laboratory experiments were conducted with one and two-dimensional electrode configurations. Copper (Cu^{+2}) was selected as it is a common heavy metal pollutant.

1.3 ORGANIZATION OF THE THESIS

This thesis consists of seven chapters. Chapter One introduces the scope of the study and briefly describes the thesis. Chapter Two discusses the theoretical aspects of the electrokinetic phenomena, the idea of the electrokinetic barrier and electrokinetic remediation of contaminated slurries.

Chapter Three presents the tests carried out to characterize the soils used in this research including geotechnical properties tests, adsorption/desorption tests and zeta potential tests. Chapter Four describes the experimental program followed in this study. This chapter demonstrates the soil preparation procedure, experiment equipment, testing procedure and the data collection methods.

In Chapter Five, the results obtained from the electrokinetic barrier tests with one and two-dimensional configurations were presented and discussed. This chapter discusses current and voltage distributions, effluent collection and copper migration of the tests conducted. Furthermore, mathematical model was used to evaluate the effectiveness of the one-dimensional configuration. Optimization of the two-dimensional electrodes arrangement was also presented.

Chapter Six presents and discusses the results of the electrokinetic sedimentation and dewatering/decontamination test. In this chapter, novel two-dimensional configurations were introduced and investigated for electrokinetic sedimentation. Chapter Seven includes conclusion and recommendations for future work.

CHAPTER TWO

LITERATURE REVIEW

2.1 INTRODUCTION

The term electrokinetics refers to processes that result from applying direct current (dc) electric field through a heterogeneous substance. A soil mass is considered a heterogeneous substance which consists of solids, water, and/or gas. In geotechnical and environmental engineering, electrokinetics can be defined as the application of low dc electric field across mass of soil to mobilize or promote the movement of water, suspended particles, and/or various chemical species towards their preferred electrodes (Mitchell and Soga, 2005).

The electrokinetic phenomena have a history dating back two centuries. In 1808, Reuss applied a dc electric field to a clay-water mixture. The electrical gradient between the electrodes induced movement of water from the positively charged electrode (anode) towards the negatively charged electrode (cathode) through the capillary and when the electric field was removed the flow of water stopped (Acar and Alshawabkeh, 1993). Over the years theoretical understanding of electrokinetic phenomena has been introduced and improved by many researchers.

As the knowledge of electrokinetic processes increased during the past decades, electrokinetic soil remediation has been generously studied. However, the application of

electrokinetics as an effective barrier to minimize or block the migration of pollutants in soil has limited studies (e.g. Narasimhan et al., 2000; Lynch et al., 2007).

Electrokinetics has been used successfully to reduce volume of slurry-type tailing wastes (Acar et al., 1989). Contaminated slurries typically contain clay, colloidal fraction and contaminants. As a result of the high water content of the contaminated slurries, potential environmental hazards existed. Electrokinetic processes can be used to accelerate the settling of slurry-type waste and remove the contaminants (Chung et al., 2006).

In this chapter, the fundamentals of electrokinetics are reviewed, including the three main transport mechanisms: electro-osmosis, electro-migration and electrophoresis. In addition, the chemical reactions associated with electrokinetics and their effects are discussed. The basic principles of electrokinetic barriers and recent studies are presented. The remediation of contaminated slurry through electrokinetic sedimentation and dewatering is discussed.

2.2 ELECTRO-CHEMISTRY OF SOIL

The reaction of water with fine grained soil cannot be fully appreciated without an understanding of the architecture of both the clay particles and the water on an atomic scale. The clay minerals have electrical properties which affect their movement towards one another as well as their reaction to water. A brief review of clay mineralogy and clay water interaction is presented in the following section.

2.2.1 Clay Mineralogy

Clay minerals are small complex aluminum silicates composed of two basics units (i) silica tetrahedron (Figure 2.1 (A)) and (ii) aluminum octahedron (Figure 2.1 (B)). The different clay minerals group are characterized by the stacking arrangements of the basic units e.g. 1:1 (1 silica tetrahedron: 1 aluminum octahedron) and 2:1 (2 silica tetrahedron: 1 aluminum octahedron) (Mitchell and Soga, 2005). Table 1.1 lists properties of three common clay minerals (i.e. kaolinite, montmorillonite and illite). Knowledge of the nature of clay became better understood in the 1930s with the advancements in X-ray diffraction technology to analyze the molecular nature of clay particles.

Isomorphous substitution, or the substitution of different similar-sized cations for those present in the crystal structure without changing in the structure, is common in clay minerals and is an important factor in their behaviour. Common cations replacement in clay minerals includes aluminum (Al^{+3}) for silicon (Si^{+4}), magnesium (Mg^{+2}) for aluminum (Al^{+3}), and ferrous iron (Fe^{+2}) for magnesium (Mg^{+2}) in the ideal tetrahedral or octahedral sheets. Isomorphous substitution and broken bonds in the structure of clay minerals result in a charge deficiency in the crystal structure and a net negative charge on the mineral's surface (Mitchell and Soga, 2005).

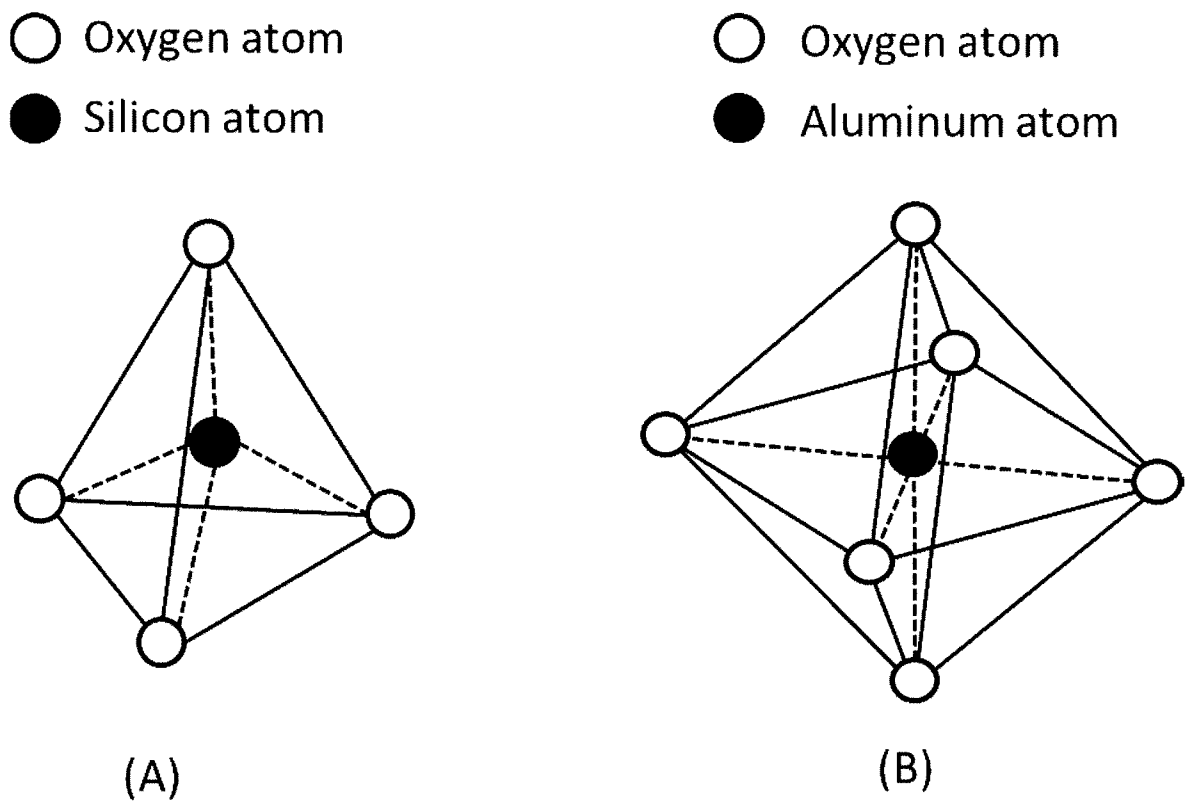

Figure 2.1 A: Silica tetrahedron, B: Aluminum octahedron.

Table 2.1 Properties of the three common clay minerals (Mitchell and Soga, 2005)

Parameter	Kaolinite (1:1)	Smectite (Montmorillonite) (2:1)	Illite (2:1)
Bonding	Hydrogen bond and Van der waals bond	Van der waals bond and exchangeable cations	K ions
Particle size	~ 0.2 – 2 μm	~ 0.1 μm	~ 0.1 – 0.2 μm
Cation exchange capacity	3 – 15 meq/100g	80 – 150 meq/100g	10 – 40; if no K: up to 150 meq/100g
Specific surface area	10 – 20 m^2/g	up to 700-840 m^2/g	65 - 100 m^2/g
Atterberg limits:			
LL	30 – 110	100 – 900	60 – 120
PL	25 – 40	50 – 100	30 – 60
Isomorphous substitution	One Si in each 400 by Al	In every 6 Al by one Mg; In 15% of Si by Al	1/4 Si replaced by Al

2.2.2 The Cation Exchange Capacity

The quantity of the exchangeable cations required to neutralize the surface charge density of clay is termed the cation exchange capacity (CEC). CEC is expressed in

milliequivalent per gram of dry soil (meq/g) and can be estimated in the laboratory (Hillel, 1982). The rate of cation exchange varies with clay type, solution concentration, temperature and pH. However, in general exchange reactions in the kaolinite minerals are almost instantaneous. In illite, a few hours may be needed for completion because a small part of the exchange sites may be between unit layers. A longer time is required in smectite because the major part of the exchange capacity is located in the inter-layer regions. The CEC of the clay decreases in low pH environment which creates suitable condition for the metal ions to remain in the pore solution (desorption) and thereby can be extracted more easily. The high pH environment increases the likelihood of precipitation of ionic species (Ricart et al., 2001).

2.2.3 Clay-water Electrolyte System

In a wet phase, clay particles attract cations (positively charged ions) in the fluid composition to stay electrically neutral. Cations develop high concentration zone near the particle surface, with tendency for them to diffuse away in order to have equal concentrations in the fluid. An electrical attraction induced by the negatively charged clay particle surfaces hinders the diffusion of cations (Yeung, 1994).

The negatively charged surface influences the nearby distribution of ions in solution, attracting ions of opposite charge (cations) towards the surface and repelling ions of equal charge (anions) away from the surface. At the same time, the cations tend to diffuse away from soil particle surface to equilibrate the ion concentration in solution.

The charged surface and the distributed charge are together termed the diffuse double layer (Mitchell and Soga, 2005).

The Stern-Gouy-Chapman theory has been successfully applied to explain the behavior of clay particles in clay-water-electrolyte interaction. Mitchell and Soga (2005) described this theory in detail considering the effects of electrolyte concentration, pH, temperature and the permittivity of pore fluid. The diffuse double layer consists of an inner layer (Stern layer) and an outer diffuse layer (Gouy layer). In the Stern layer, cations are strongly held by clay surfaces whereas in the Gouy layer the balancing cations are held by electrostatic attraction to maintain the electrical stability.

2.2.3.1 Zeta potential

The term zeta potential, ζ, is defined as the electrical potential at the solid-liquid interface (sparks, 1998). ζ is located between the Stern layer and the Gouy layer as shown in Figure 2.3.

The magnitude of the ζ represents the strength of the repulsion between colloid particles. Values of ζ are in the range of +50 mV to -50 mV and for most clayey soils ζ is in the range of 0 to -50 mV. ζ is highly influenced by the solution pH and ionic strength (Young, 1994).

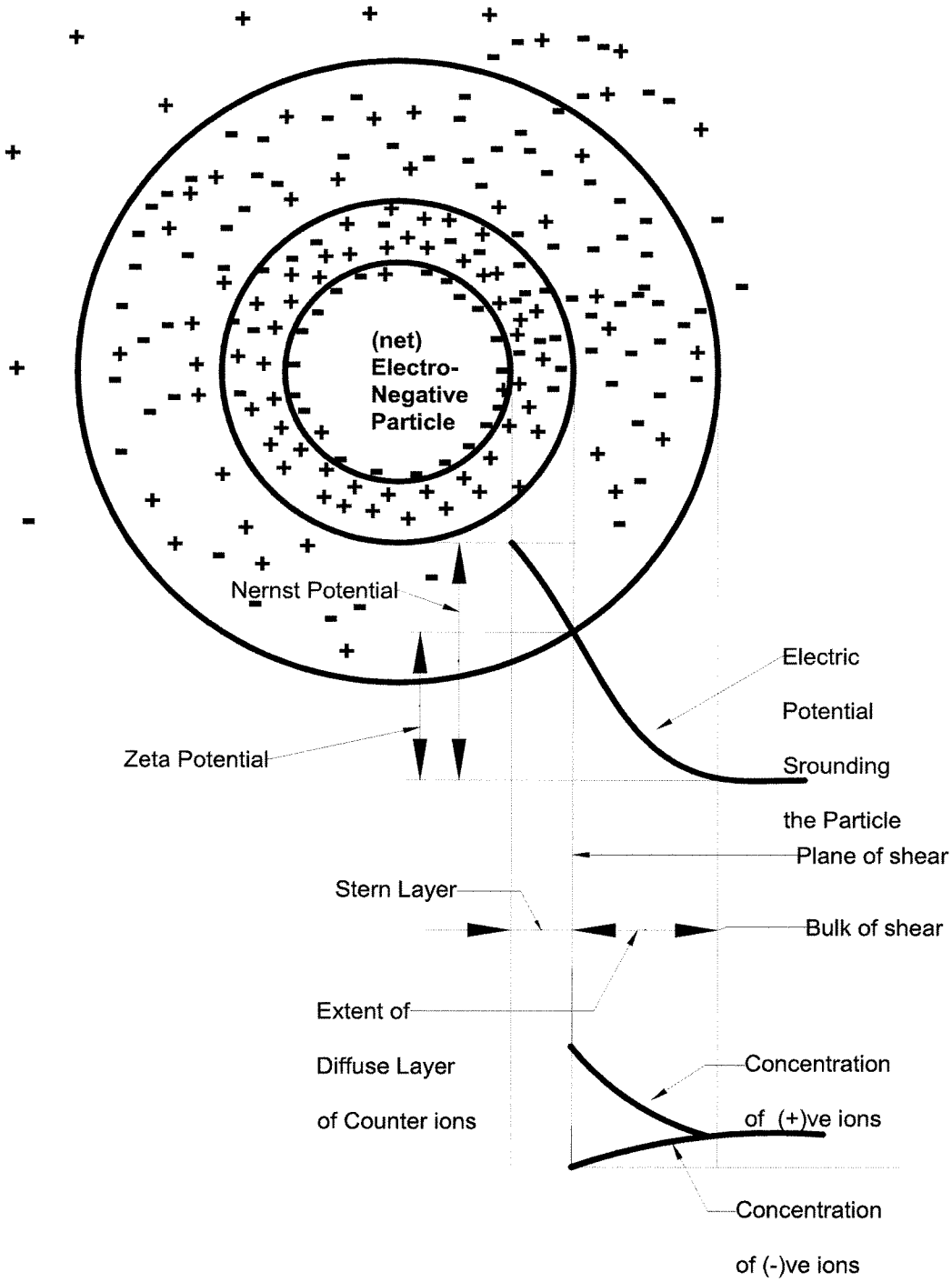

Figure 2.2 The diffuse double layer components (Water Quality and Treatment, 1999).

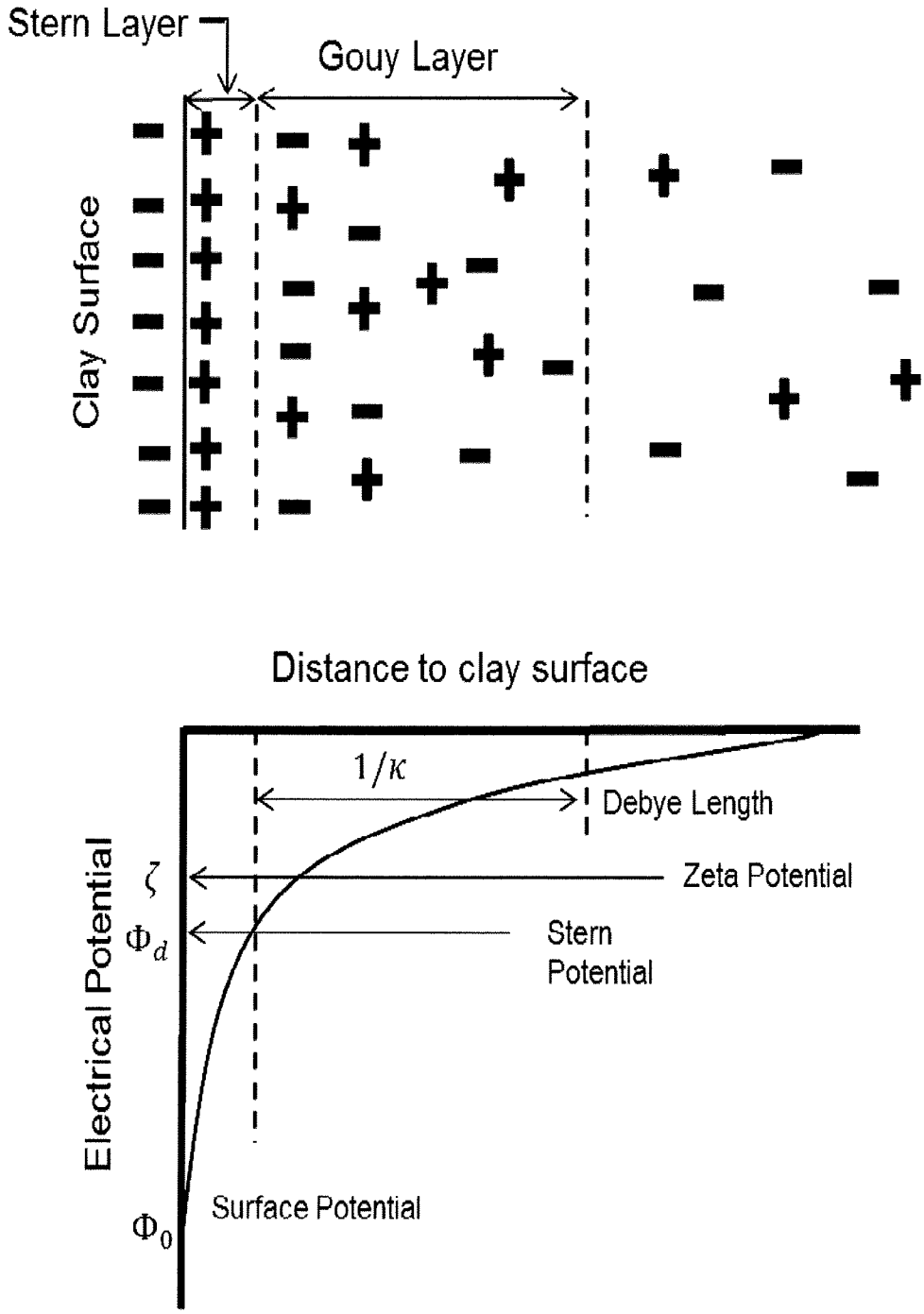

Figure 2.3 The Stern-Gouy-Chapman model (Shang et al., 1994).

2.2.4 Soil Electrical Conductivity

Electrical conductivity (EC) is the ability of a material to transmit an electrical current and is commonly expressed in units of S/m (Siemens per meter) (Virkutyte et al., 2002). The conductivity of soil primarily depends on the concentration and the mobility of the ions present in the pore fluid (e.g. contaminants) and the moisture content of soil. As the moisture content decreases, the soil conductivity may become too low for an effective electrokinetic application process.

2.3 ELECTROKINETIC PHENOMENA

Electrokinetic is the application of a dc electric field across a moist soil mass. The dc induces three distinct transport mechanisms, namely; electro-osmosis, electro-migration and electrophoresis along with electrolysis reactions. Figure 2.4 illustrates the phenomena.

2.3.1 Electro-osmosis

Electro-osmosis is the movement of pore fluid through mass of soil under an applied dc electrical field. The water migrates from the anode towards the cathode. Electro-osmosis was mathematically explained by many scientists. Helmholtz-Smoluchowski model is the most accepted theory and it's commonly used to determine the rate of the electro-osmotic flow. Other theories proposed to explain the phenomenon included Schmid model and Gray-Mitchell approach, which are discussed in the following sections.

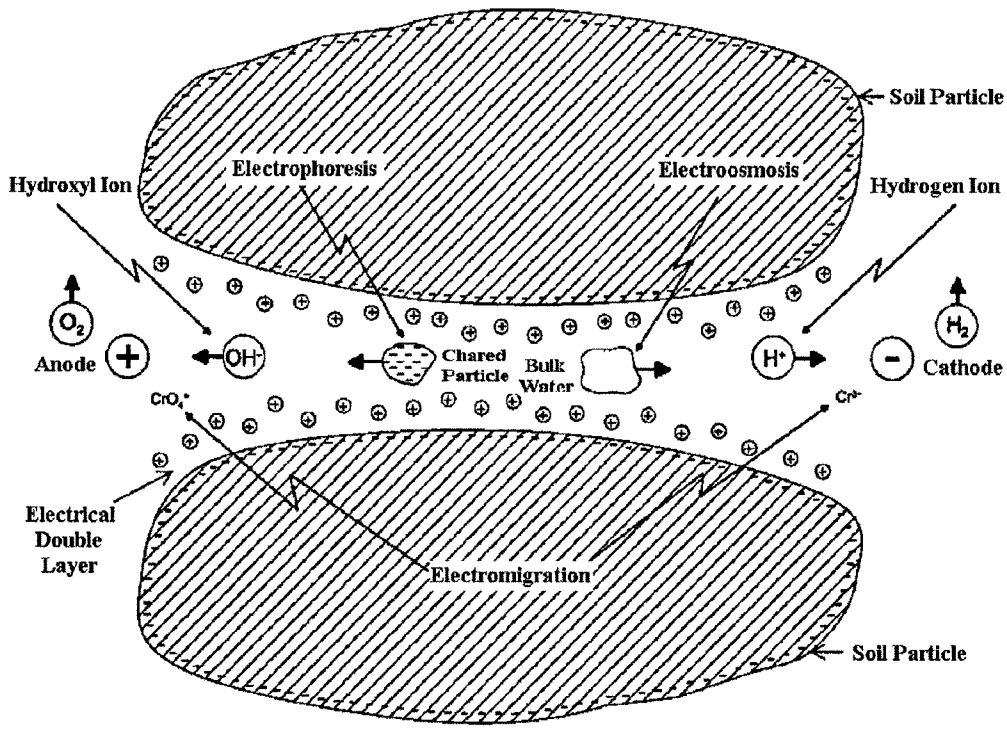

Figure 2.4 Electrokinetic phenomena (USEPA report, 1998)

2.3.1.1 Helmholtz-Smoluchowski model

In 1879, Helmholtz sat up his theory regarding electro-osmosis which was modified by Smoluchowski in 1914 (Yeung, 1994). The Helmholtz-Smoluchowski model treats the capillary as an electrical condenser with ions of one sign on the wall surface and mobile ions of opposite sign in a layer in the liquid near the wall surface as shown in Figure 2.5. The mobile shell of counter-ions is assumed to drag water through capillary by plug flow (Mitchell and Soga, 2005).

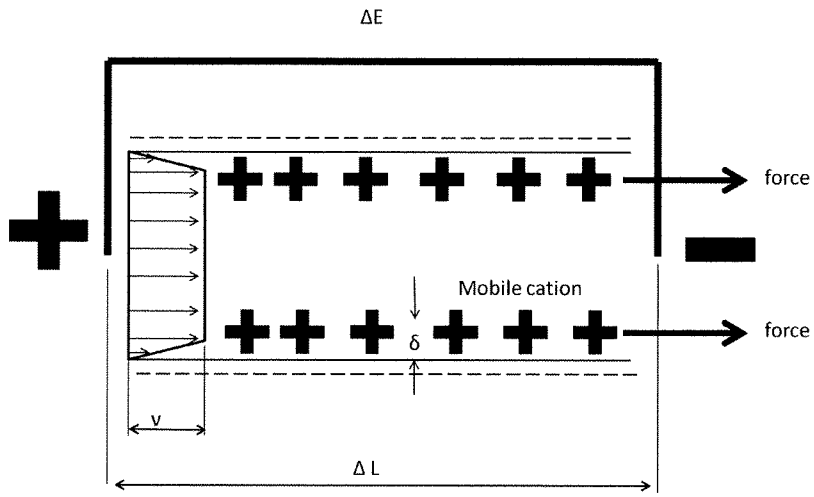

Figure 2.5 Schematic of Helmholtz-Smoluchowski model.

The flow rate of water is controlled by the balance between the applied electric field inducing the water movement and the frictional force between the liquid and the wall. The velocity gradient (1/s) between the wall and the centre of the positive charge is v/δ where v (m/s) is the velocity of flow, and δ (m) is the distance between the wall and

the centre of the plane of mobile charge. Therefore, the drag force per unit area (N/m^2) is $\eta v/\delta$ where η ($N{\cdot}s/m^2$) is the viscosity. The electrical force per unit area is σE, where σ is the surface charge density (C/m^2) and E is the electric field intensity (V/m). At equilibrium, the drag force equals the electric field force:

$$\eta \frac{v}{\delta} = \sigma E \qquad [2.1]$$

or

$$\sigma \delta = \eta \frac{v}{E} \qquad [2.2]$$

The sign of ζ is opposite to the sign of the mobile ions, and zeta potential, ζ (V), is given by:

$$\zeta = -\frac{\sigma\delta}{\varepsilon} \qquad [2.3]$$

where ε (F/m) is the permittivity of the pore fluid.

Substituting Eq. [2.3] into Eq. [2.2] and rearranging gives:

$$v = -\frac{\zeta \varepsilon}{\eta} E \qquad [2.4]$$

For a single capillary of cross-sectional area, a (m^2), the velocity of flow, , is:

$$v = -\frac{\zeta \varepsilon}{\eta} E\, a \qquad [2.5]$$

For a bundle of N capillaries within the entire cross-sectional area normal to the direction of flow, A (m^2), the total electro-osmotic flow rate, q_A (m^3/s), is:

$$q_A = N\, q_a = -\frac{\zeta\, \varepsilon}{\eta}\, E\, N\, a \qquad [2.6]$$

For a porous medium with porosity, n, the cross-sectional area of the voids is n A which is equal to a :

$$q_A = -\frac{\zeta\, \varepsilon}{\eta}\, E\, n\, A \qquad [2.7]$$

Casagrande (1949) derived an empirical equation to describe electro-osmosis flow rate, analogous to Darcy's low for the hydraulic flow rate:

$$q_A = k_e\, E\, n\, A \qquad [2.8]$$

where k_e ($m^2/s{\cdot}V$) is the coefficient of electro-osmotic permeability

Comparing Eq. [2.8] to Eq. [2.7], the coefficient of electro-osmotic permeability, k_e, given by the Helmholtz-Smoluchowski model is:

$$k_e = -\frac{\zeta\, \varepsilon\, n}{\eta} \qquad [2.9]$$

k_e is not constant along the distance between the anode and the cathode as it is dependent on the zeta potential which is sensitive to the change of the pH and the ionic strength. The values of k_e can be determined experimentally (Mitchell and Soga, 2005).

2.3.1.2 Schmid model

The Helmholtz-Smoluchowski model assumes a negligible extension of the counter-ions layer into the pores and it doesn't consider the excess of ions over those needed to balance the surface charge. Schmid (1951) proposed a theory that accounts for the counter-ions in the pores by assuming uniformly distributed counter-ions throughout the pores. In the Schmid model, the electro-osmosis flow rate, q_A (m^3/s), is given by:

$$q_A = \frac{A_0 F_0 r^2 n}{8\eta} EA \qquad [2.10]$$

where A_o (equivalents/m^3) is the concentration of surface charges in the pore fluid, F_o (96485 C/equivalent), is the Faraday's constant and r (m) is the radius of capillary.

The coefficient of electro-osmotic permeability, k_e (m^2/s V), given by the Schmid theory is:

$$k_e = \frac{A_0 F_0 r^2 n}{8\eta} \qquad [2.11]$$

Schmid theory suggests that k_e is dependent on the pore size and porosity and independent of the zeta potential and permittivity.

2.3.1.3 Gray-Mitchell approach

Gray and Mitchell (1967) developed a rational approach on the basis of Donnan's theory of membrane equilibria. The basis of the Donnan theory is that at equilibrium the chemical potentials of the internal and external phases are equal and electroneutrality is maintained in both phases (Yeung, 1994).

Gray and Mitchell (1967) introduced a distribution coefficient, R, defined as the ratio of cations to anions in the internal phase for a symmetrical electrolyte. R is given by:

$$R = \frac{C^+}{C^-} = \frac{1+\sqrt{1+y^2}}{-1+\sqrt{1+y^2}} \quad [2.12]$$

In which

$$y = \frac{2\,C_0\gamma\pm}{A_0\overline{\gamma}} \quad [2.13]$$

where C_o (equivalent/m^3) is the concentration in external solution, $\gamma \pm$ is the mean molar activity coefficient in external solution, $\overline{\gamma}$ is the mean molar activity coefficient in the double layer, and A_0 (equivalent/m^3) is the surface charge density per unit volume of pore fluid. A_0 is proportional to the cation exchange capacity of the soil by the expression (Gray and Mitchell, 1967):

$$A_0 = \frac{(CEC)\rho_w}{w} \quad [2.14]$$

where CEC (equivalent/kg of soil) is the cation exchange capacity of the soil, w (%) is the water content of the soil and ρ_w (kg/m^3) is the density of water.

Higher R values indicate higher exclusion of co-ions and greater electro-osmotic water transport (Mitchell and Soga, 2005; Young 1994). In this case, electro-osmotic flow is less affected by an increase in the pore water salinity.

2.3.2 Electro-migration

Electro-migration is the movement of ions in the pore fluid under the influence of an electrical field. Positive ions (cations) migrate towards the cathode while negative ions (anions) are transported to the anode. As a result, ions tend to concentrate near the oppositely charged electrode (Reddy et al., 2006). The ionic migration is relative to the ions concentration in the pore water and the electric field intensity (Kim et al., 2005). The mobility for specific ions is significantly affected by the soil electrical conductivity, pH, porosity, tortuosity and initial concentration of the ions (Acar and Alshawabkeh, 1993).

Electro-migration of ions is quantified by the effective ionic mobility. Effective ionic mobility is the velocity of the ion in the soil under the influence of electric field intensity. The ionic mobility in a soil mass and the diffusion coefficient of an ion in dilute solution are related by the Nernst–Einstein equation (Koryta, 1982):

$$u_j^* = \frac{D_j z_j F}{R T} \tau n \qquad [2.15]$$

where u_j^* (m^2/s V) is the effective ionic mobility, D_j (m^2/s) is the diffusion coefficient of species j in dilute solution, z_j is the charge of chemical species j, F (96487 C/mol) is the Faraday's constant, R (8.314 J/ mol K) is the universal gas constant and T (K) is absolute temperature. According to Acar and Alshawabkeh (1993), the mass transport rate of ions due to electro-migration can be as high as 10 times the transport rate due to electro-osmosis.

2.3.2.1 Ionic mobility of copper

Copper (Cu) is a common species that has +1 and +2 valence states when electrolysed. It can form anionic or cationic complexes. The solubility of copper is governed by the pH and a low pH value is needed to keep copper dissolved in the soil (Virkutyte et al., 2002). In the presence of an electric field, almost all copper is transported towards the cathode (Virkutyte et al., 2002). Reddy and Parupudi (1997) suggested that some copper that may be found near the anode is due to copper's capability of forming different ligands present in the soil. Ottosen et al. (2004) suggested that copper is mobile at high pH. The ion mobility of copper in a free solution is 5.56×10^{-4} cm^2/s V (Mitchell and Soga, 2005).

2.3.4 Electrophoresis

Electrophoresis is the movement of charged particles and colloids under the influence of an electrical field. Similar to the electro-migration, charged particles and colloids that are suspended in fluid move under the electrostatic attraction/repulsion of the charged electrodes. Electrophoresis is negligible in compacted soil compared to electro-osmosis and electro-migration, yet electrophoresis is exceptionally important in treatment of soil suspension systems, i.e. slurry ponds (Mitchell and Soga, 2005).

Von Helmholtz was the first to derive electrophoretic mobility which represents the electrophoresis phenomenon. The equation was later corrected by Smoluchowski to include the permittivity and nowadays written as (Mitchell and Soga, 2005):

$$u_{ek} = \frac{\zeta \varepsilon}{\eta} \quad [2.16]$$

where u_{ek} (m^2/s V) is the electrophoretic mobility.

2.4 CHEMICAL PROCESSES ASSOCIATED WITH ELECTROKINETICS

Several processes arise in the soil due to the application of dc electric field, which lead to changes in the soil properties. The major processes are hydrolysis reactions at the electrodes, induced changes in pH value, adsorption and desorption of ions and changes in zeta potential (Acar and Alshawabkeh, 1993). Combinations of these processes affect the electrokinetic phenomena and are discussed in the following sections.

2.4.1 Electrolysis Reactions

The main electron transfer reactions that occur at electrodes during the application of dc electric field are the electrolysis of water (Acar and Alshawabkeh, 1993). Electrolysis of water releases hydrogen ion (H^+) at the anode and hydroxide ions (OH^-) at the cathode building up sharp acid-base fronts. The electrolysis of water is given by:

Anode Reaction: $2H_2O - 4e^- \rightarrow O_2 (g) + 4H^+$ [2.17]

Cathode Reaction: $2H_2O + 2e^- \rightarrow H_2 (g) + 2 OH^-$ [2.18]

The hydrogen ions (H^+) decrease the pH and form an acid front near the anode. The acid front is carried towards the cathode by electro-migration, electro-osmosis

(i.e. advection) and chemical diffusion. At the same time, an increase in the concentration of hydroxide ions (OH^-) elevates the pH near the cathode. The OH^- ions have a tendency to migrate towards the anode by electro-migration and chemical diffusion. The extent of migration depends on the buffering capacity of the soil.

The buffer capacity is an indicator of a system capacity to resist the pH changes resulting from adding strong base/acid. In a soil with low buffering capacity, a distinct pH gradient ranging from 2 (near the anode) to 12 (near the cathode) is generally developed. The solubility of metal-hydroxides is directly influenced by the pH of the solution. Most metals are soluble at low pH values, whereas high pH values encourage precipitation of the metals. High pH values may also result in the formation of heavy metals negative complexation, which migrate towards the zone of acid-base junction and eventually precipitating in this zone as insoluble hydroxides (Acar and Alshawabkeh, 1993; Probstein and Hicks, 1993). At high pH, charged metal ions tend to precipitate reacting with hydroxyls ions during the application of the dc electric field as follows:

$$M^{+n} + n\,(OH)^- \rightarrow M\,(OH)_n \downarrow \qquad [2.19]$$

where M is the metal and n is the metal charge.

At low pH, the hydrogen ions react with heavy metals precipitated in soil to release charged cations in the pore fluid as:

$$nM\,(OH)_n^- + 2\,n\,H^+ \rightarrow n\,M^{+n} + 4\,H_2O \qquad [2.20]$$

2.4.2 Generation of pH Gradient

Acid and base fronts rise due to the electrolysis of water. The acid front travels towards the cathode while the base front moves in the opposite direction towards the anode. Since the ionic mobility of hydrogen ions is 1.75 times that of the hydroxide ions, the H^+ ions dominate the system chemistry (Acar and Alshawabkeh, 1993). Consequently, the migration of the acid and base fronts takes place at different rates. The migration of the two fronts considerably impacts the electrochemical properties of the soil and the removal of contaminants (Alshawabkeh and Acar, 1996). Due to its faster rate of propagation, the acid front affects the surface charge characteristics and the cation exchange capacity of the clay (Eykholt and Daniel, 1994).

The high pH at the cathode encourages precipitation of heavy metals into the soil near the cathode. Acidic front in turn causes the dissolution and desorption of metals from the soil solids into the pore fluid. The acidification of the soils enhances desorption of the metals by exchange of the metal ion for hydrogen ion (Acar and Alshawabkeh, 1993).

In some instances, adsorption of some metals in soils with high pH is desirable, particularly if the metals are migrating towards the neighbourhood environment. Zeta potential and the degree adsorption/desorption of ions are to a great extent pH dependent. Therefore, the change in pH during an electrokinetic application has to be considered as it may significantly affect the outcome.

2.4.3 Changes of Zeta Potential

As discussed, changes in pH are experienced at both the cathode and anode due to electrolysis reactions. There is a relationship that exists between pH and the zeta potential. West and Stewart (1995) studied this relationship for kaolinite clay using dilute kaolinite suspension at various pH levels. The results showed that kaolinite suspensions experienced an increased in zeta potential values (i.e. became less negative) with a decrease in pH. For example, at pH of 12.3 the zeta potential was -32 mV compared to zero at pH of 3. The presence of H^+ ions at low pH values cause a build-up of positive charges near the clay surface and thereby neutralizes the clay surface and subsequently decreases the zeta potential. At high pH values, the zeta potential decreases (i.e. becomes more negative). The value of zeta potential can be determined experimentally by the electrophoretic mobility (Sposito, 1989). The direction of electro-osmotic flow in soil is dictated by the sign of the zeta potential on particle surfaces as it is shown by Eq. [2.10].

2.4.4 Adsorption and Desorption into/from Soil Particles

Adsorption and desorption refer to the transformation of ions between pore fluid and the soil particle surface via cation exchange. Adsorption is defined as the attraction of an aqueous species (e.g. contaminants) to the surface of a solid, while desorption is the reverse process and it is responsible for the release of contaminants from the soil surface (Mitchell and Soga, 2005).

Adsorption and desorption are affected by changes in soil pH caused by the electrolysis reactions. At high pH values, adsorption normally takes place whereas desorption occurs at low pH (Acar and Alshawabkeh, 1993). The pH dependent adsorption/desorption behaviour is determined by performing batch tests using the soil and contaminant of interest at constant concentration and varying pH (Alley, 1993).

Along with the pH, adsorption and desorption depend on the type and ionic strength of the contaminant, the soil type and the pore fluid characteristics. It has been well established that ionic strength has significant effects on the adsorption/desorption behaviour of heavy metals by soils (Chen, 1996; Undabeytia et al., 2002; Phillips et al., 2004; Xu and Zhao, 2005). As a result of the adsorption process, contaminants get immobilized which is preferable in terms of minimizing their migration and spread. Desorption is critical for removing a contaminant from soil by a remediation process. This means that despite the opposite nature of adsorption and desorption, they can both be utilized in the control and removal of heavy metals pollution. The adsorption and desorption of copper in soils have mostly been discussed by employing empirical models, such as Langmuir and Freundlich equations (Arias et al., 2002, 2005; Phillips et al., 2004).

2.4.5 Electrode Materials and Configuration

Many electrode materials are commonly used in electrokinetic applications. Two main factors should be taken into consideration when selecting the material. First, the electrode material should be selected to avoid or minimize the adverse reactions by-

products of the material with the hydrogen and hydroxyl ions generated at the electrodes. For example, metallic electrodes may dissolve as a result of electrolysis reaction at the anode and introduce corrosive products into the soil as:

$$M_A \rightarrow M_A^{+n} + n\,e \qquad [2.21]$$

where the M_A refers to the electrode material, n is the metal charge.

Second, the material should be selected to minimize the voltage loss at the soil electrode interfaces. Often, it is very difficult to achieve both. For example, the use of non-metallic electrodes will not produce unwanted by-products compared with metallic electrodes. However, the voltage loss at the soil-electrode interfaces is higher with non-metallic electrodes as reported by previous researchers (e.g. Lockhart, 1983; Mohamedelhassan and Shang, 2001).

2.4.6 Intermittent Current

Intermittent current is the use of on and off cycles for the applied electric field during an electrokinetic process. It can improve the electrokinetic process by altering the polarization process of the ions of opposite signs in the double layer. In the diffuse double layer, the stationary clay particles (negatively charged) are surrounded by the mobile cations (positively charged). The applied dc electric field results in redistribution of charges (polarization) in the double layer, which is against the applied electric field. As a result, the polarization decreases the efficiency of electrokinetics by reducing the electro-osmosis flow. The intermittence allows the double layer to restore its original

charge distribution and thereby increase the efficiency of the electro-osmosis process (Mohamedelhassan and Shang, 2001). Many researchers had reported a significant increase in electro-osmosis flow rate by intermittent current (e.g. Sprute and Kelsh, 1976; Mohamedelhassan and Shang, 2001), while few studies showed that intermittent current has no influence on the flow rate (e.g. Lockhart and Hart, 1988).

2.4.7 The Applied Electric Field

The applied electric field in an electrokinetic process affects the electro-osmosis flow and electro-migration. The stronger the electric field, the higher the electro-osmosis flow and electro-migration as per Eqs. [2.8] and [2.15]. However, the rate of increase is not linear and the efficiency of electric field reaches a plateau at higher electric field as noted by previous researchers (Lockhart, 1983; Shang, 1997). Furthermore, at high electric field, significant energy is lost in heating which is not beneficial to the process. Shang et al. (1996) performed series of tests to determine the coefficient of electro-osmosis permeability, k_e, an indicator for the rate of consolidation for a range of electric field intensity. It was reported that k_e decreased as the electric field increased.

Mohamedelhassan and Shang (2001) studied the effect of applied voltage on the magnitude of the voltage drop at the soil-electrode interfaces. The test was conducted for a range of applied voltages where the voltage loss at the soil-electrode interfaces was measured. To quantify the voltage drop, an efficiency factor, β, was introduced as:

$$\beta(\%) = \frac{V_e}{V_0} \times 100 = \frac{V_0 - (\Delta V_A + \Delta V_C)}{V_0} \times 100 \qquad [2.21]$$

where V_e (V) is effective voltage, V_0 (V) is the applied voltage, ΔV_A (V) is the voltage loss at soil-anode interface and ΔV_c (V) is the voltage loss at soil-cathode interface. They suggested that due to voltage loss at the soil-electrode interfaces, the electric field that contributes to electro-osmosis and electro-migration is the effective electric field intensity, E_c (V/m), defined as:

$$E_c = \frac{\beta E_0}{100} \qquad [2.22]$$

where E_0 (V/m) is the electric field intensity.

In one-dimensional electric field configuration, the electrodes cover the entire area perpendicular to the direction of flow and the electric field a cross the soil is uniform. In two-dimensional configuration, the electric field depends on the distance between the electrodes. The number of electrodes required for two-dimensional configuration depends on spacing between electrodes of the same polarity. Decreasing spacing between electrodes minimizes the area of inactive electric field, but increases the cost of the process.

2.5 ELECTROKINETIC APPLICATIONS

Soil, subsurface and groundwater contamination are pollution issues that concern the public and environmental professionals. Electrokinetic remediation is a promising and an innovative technique to remediate contaminated soil, sediments and prevent/minimize the migration of pollutants to the groundwater and/or soil. There are

several potential applications of electrokinetic for environmental engineering such as: (i) electrokinetic sedimentation and dewatering, (ii) electrokinetic extraction (removal) of contaminants, and (iii) electrokinetic barrier and fencing. In recent years, a major portion of geo-environmental engineering researches has been devoted to electrokinetic remediation for removal of organic and inorganic contaminants from soils (e.g. Acar and Alshawabkeh, 1993, 1996; Acar et al., 1994, 1996; Reddy and Cameselle, 2009). Limited studies have been conducted regarding the application of electrokinetic barrier (Narasimhan and Ranjan, 2000). Electrokinetic barrier and treatment of contaminated slurries by electrokinetic sedimentation and dewatering are discussed in the following sections. Solar power is presented as an innovative and cost effective source of energy for electrokinetic applications.

2.5.1 Electrokinetic Barrier to Prevent/Minimize Migration of Contaminants

One solution to the spread of heavy metals pollution is by confining the contaminant. Conventional containment technologies like slurry walls, grout curtains and sheet pile cut-off walls are expensive to construct and require the use of specialized large equipment. Furthermore, the availability of suitable access by the large equipment to the contaminated site is a major limitation of the conventional techniques, particularly in remote areas. Under these conditions, electrokinetic barrier is a better alternative as installing the electrodes surrounding the contaminated zone can be achieved with portable equipment (Reddy and Cameselle, 2009).

Using the electrical fields to prevent the contaminant migration was conceived by Lageman et al. (1989) who introduced the phrase “electrokinetic fence”.

They successfully used the technique to prevent the migration of heavy metal contaminants including lead, copper, zinc and cadmium during electrokinetic remediation of an abandoned factory site.

Mitchell and Young (1990) mentioned that stand alone electrokinetic barrier counters flow may be effective to stop the movement of contaminants. Electro-osmosis and electro-migration can effectively prevent the cationic contaminants from migration through compacted clay liner. In clayey soil, the movement of water due to electro-osmosis is highly significant when compared to the flow of water under a hydraulic gradient. The values of hydraulic conductivity can differ by orders of magnitude but the coefficient of electro-osmotic conductivity is generally in the range of 1×10^{-8} to 1×10^{-10} ($m^2/s\cdot V$) (Mitchell and Soga, 2005).

The total contaminant flux under an electric potential can be calculated as (Acar and Alshawabkeh, 1993; Reed et al., 1996):

$$J_i = D_i^* \nabla(-c_i) + \left[\frac{|z_i|}{z_i}\right] c_i u_i^* \nabla(-\mathrm{E}) + c_i q_e \qquad [2.23]$$

where D_i^* (m^2/s) is the effective diffusion coefficient, c_i (mg/L) is the concentration of contaminant i, z_i is the valence of contaminant i, u_i^* (m^2/s V) is the effective ionic mobility of contaminant i, U (V) is the electric field and q_e (m/s) is the electro-osmosis flux.

The first term on the right hand side of Eq. [2.23] quantifies the transport of the contaminant due to the concentration gradient (i.e. diffusion). The second and the third terms represent the contaminant transport by electro-migration and electro-osmosis, respectively. The mass flux by electro-migration in most cases is at least one order of magnitude greater than that by diffusion (Acar and Alshawabkeh, 1993). The effective ion mobility, u_i^*, which quantifies electro-migration, is a function of the contaminant's molecular diffusion coefficient, valence, soil porosity, and tortuosity. As shown by Eq. [2.15].

Electro-osmosis flux, q_e, is given by:

$$q_e = k_e E \qquad [2.24]$$

and

$$q_A = q_e A \qquad [2.25]$$

or

$$q_A = k_e E A \qquad [2.26]$$

where k_e ($m^2/s \cdot V$) is the electro-osmosis permeability, E (V/m) is the electric field intensity, q_A (m^3/s) is the electro-osmosis flow rate and A (m^2) is the cross-sectional area perpendicular to the direction of flow.

In an electrokinetic barrier, the hydraulic flow goes in a direction opposite to the electro-osmotic flow and the electro-migration. The hydraulic flow is given by Darcy's law equation:

$$q_h = k_h\, i \qquad [2.27]$$

where k_h (m/s) is the hydraulic conductivity of the soil and i (m/m) is the hydraulic gradient.

The transport of the contaminant by the hydraulic flow can be expressed by:

$$J_h = q_h\, c_i \qquad [2.28]$$

By adding the hydraulic transport, Eq. [2.28], to Eq. [2.23] and rearranging terms, the total contaminant flux for the contaminant under an electric field can be calculated as:

$$J_i = D_i^* \nabla(-c_i) + c_i q_h - c_i q_e - \left[\frac{|z_i|}{z_i}\right] c_i\, u_i^* \nabla(-\mathrm{E}) \qquad [2.29]$$

Figures 2.5 and 2.6 show two possible scenarios for the migration of contaminants and the concepts of electrokinetic barrier. The first scenario simulates the migration of acid mine drainage from reactive tailings. The contaminants travel with the hydraulic flow towards the uncontaminated ground. The second scenario is the migration of the infiltrated contaminant into the ground water flow. The cathode electrodes are installed facing the contaminants where electro-osmotic and electro-migration fluxes are in opposite direction to the contaminant migration by the hydraulic flow. Near the cathode,

the base front increases the pH and subsequently the adsorption capacity of the soil. Thus, create an environment suitable to immobilize and precipitate the contaminants by chemical reactions and adsorptions.

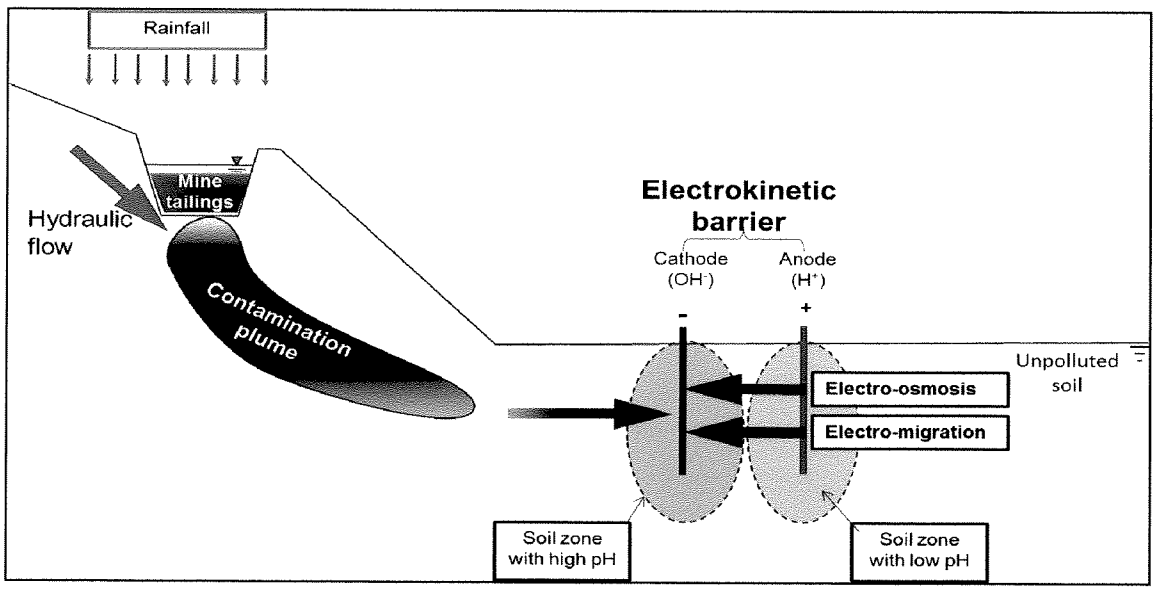

Figure 2.5 First contaminant migration scenario and the electrokinetic barrier.

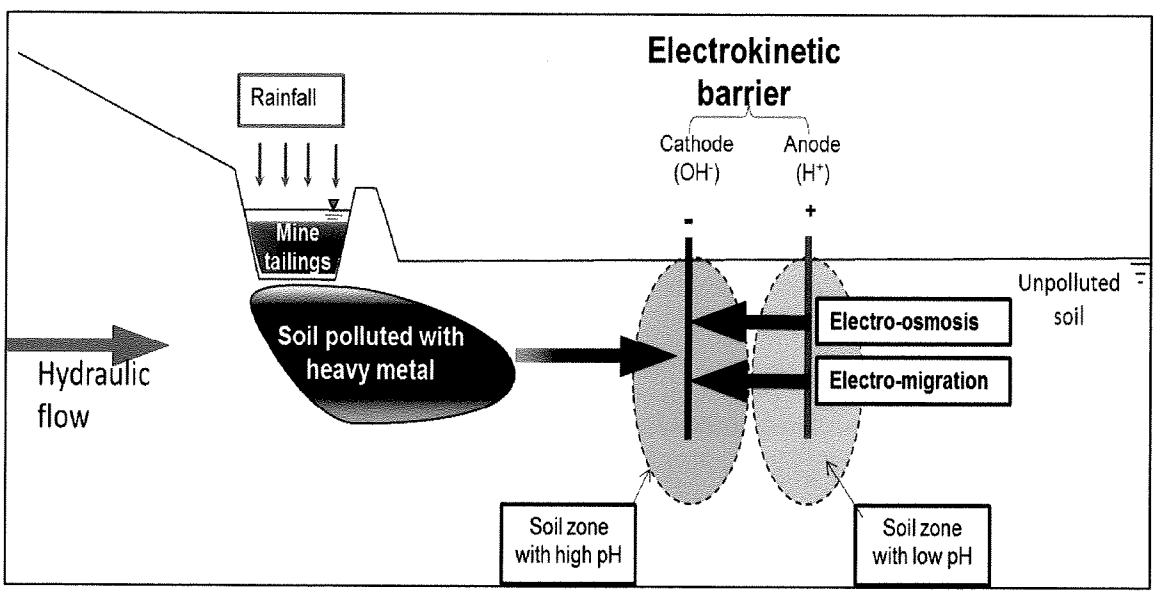

Figure 2.6 Second contaminant migration scenario and the electrokinetic barrier.

Lynch et al. (2005) conducted one and two-dimensional tests to evaluate the effectiveness of electrokinetic barriers with different voltages to stop the spread of cadmium. The results indicated that electrokinetic barrier with electric field intensity of 50 V/m can prevent or significantly reduce the spread of cadmium contamination by hydraulic gradients of 7 for the one-dimensional test and 1.3 for the two-dimensional test. Reeve and Lynch (2007) carried out one-dimensional test with pulsed voltage to investigate the possibility of using solar power supply in an electrokinetic barrier. At night the power was shut down to simulate solar energy. The results suggested that the contaminant advancement may be stopped or significantly reduced by using solar energy.

2.5.2 Electrokinetic Remediation of Contaminated Slurries

Sediments such as mining wastes, industrial wastes and dredging wastes are increasing extensively due to the growth in industrialization and population in all over the world. Sediments of impoundment and landfill are usually placed hydraulically as slurry by open dumping (Chung et al., 2005). Design problems associated with these impoundment and landfill include storage capacity, densification of filling materials, embankment stability, migration of contaminated pore fluid, and final land use. These sediments contain significant clay and colloidal fractions which results in a very long settling period by gravitational forces. The environmental hazards of this type of sediments are real challenges in waste management. Therefore, it is often necessary to accelerate settlement of the sediment in order to reduce the volume prior to performing remediation and pollutant extraction techniques (Buckland et al., 2000). Electrokinetic

remediation techniques have been used in volume reduction for slurry/sediment and/or contaminants removal (Acar, 1989). Many applications of electrokinetic remediation of sediments have been documented (Reddy and Cameselle, 2009).

2.5.2.1 Electrokinetic sedimentation

The remediation of contaminated slurry consists of two main phases: sedimentation and dewatering/decontamination. Both of these processes are accelerated by the use of electrokinetics. There are many parameters that affect the particles settling velocity. The most influential parameters are the particle size and shape, fluid viscosity, solid concentration, specific gravity and interaction between adjacent particles (Shang, 1997). The application of Stokes' law to determine the sedimentation velocity of a suspension is only valid for a suspension of low solid concentration ratio. Kynch (1952) found that for suspensions with higher solid concentrations Stokes' law was inadequate to predict sedimentation velocity. He developed the theory of the hindered settling. The sedimentation velocity during the free and the hindered settling can be expressed as (Mohamedelhassan and Shang, 2001):

$$U = \beta u n^r \qquad [2.30]$$

where U (m/s) is the sedimentation velocity, β is the coefficient of free settling, u (m/s) is the particle velocity, n is the porosity of the sediment and r is the coefficient of sedimentation for a slurry.

The sedimentation parameters in Eq. [2.30], i.e. β and r, are affected by electrokinetics on the slurry sediment. β represents the statistical average of the settling velocities of particles that defines the clear water-suspended solid interface (mudline). The mudline drop represents the settling of particles with finer grain sizes in the suspension as the suspension contains various ranges of the grain size. β and r are functions of the physical, chemical and mineralogical properties of the suspension and can be determined via experiments. r controls the settling velocity in the hindered settling stage where the porosity, n, in Eq. [2.30] is less than 1. With n approaching 1 (an infinitely dilute suspension), the sedimentation velocity would be constant. Hence the sedimentation velocity can be expressed as (Shang, 1997):

$$U = \beta u \qquad [2.31]$$

2.5.2.1.1 Free settling

Free settling is simply the settlement of soil particles due to gravity and it is dependent on the density and diameter of the particles as well as the density and viscosity of the fluid (water in this case). The following equation characterizes free settling:

$$u_g = \frac{g(\rho_s - \rho_w)d^2}{18\eta} \qquad [2.32]$$

where u_g (m/s) is the particle settlement due to gravity, g (9.81 m/s^2) is the acceleration due to gravity, ρ_s (kg/m^3) is the density of the particle, ρ_w (1000 kg/m^3) is the density of

water, d (m) is the diameter of the particle and η (kN s/m^2) is the dynamic viscosity of water.

Since soil consists of varying grain sizes, the particle settling velocity of a soil suspension is not uniform. An average particle settling velocity introduced by Eq. [2.33]:

$$\overline{u_g} = \sum_{i=1}^{N}(f_i - f_{i+1})\left(\frac{u_{g(i)}+u_{g(i+1)}}{2}\right) \quad [2.33]$$

where f_i is the fraction of suspension finer than the grain size d_i and $u_{g(i)}$ is the gravitational settling velocity of an individual particle with grain size d_i (m/s).

When a dc electric field is applied to a clay suspension with electrodes configuration of the cathode at the top and the anode at the bottom, clay particles will move towards the anode by electrophoresis which can be used to accelerate sedimentation of clay suspensions. The velocity of individual particles induced by electrophoresis is (Mohamedelhassan and Shang, 2001):

$$u_{ek} = \frac{\varepsilon_w \zeta}{\eta} E \quad [2.34]$$

where u_{ek} (m/s) is the particle velocity induced by electrokinetics (electrophoresis), ε_w (F/m) is the permittivity of water, ζ (mV) represents the zeta potential, η (N s/m^2) is dynamic viscosity of water and E (V/m) is the electric field intensity.

Equation [2.34] is derived assuming clay slurry with extremely small particles. The calculated u_{ek} is independent of the particle grain size. It is irrelevant to consider this

induced settlement by electrokinetics when particle sizes are large (i.e. sand) since the negative charges which are found in clay would not exist and the zeta potential would be extremely small.

The average particle settling velocity induced by gravity and electrokinetics $\bar{u}$, is given by:

$$\bar{u} = \overline{u_g} + u_{ek} = \sum_{i=1}^{N}(f_i - f_{i+1})\left(\frac{u_{g(i)}+u_{g(i+1)}}{2}\right) + u_{ek} \quad [2.35]$$

Consider a suspension containing grain sizes ranging primarily from silt (5μm < d <75μm) to clay (d < 5μm). The free settling process is represented by the linear drop of the mudline with time when the porosity of the suspension, n, is approximately equal to 1. Therefore, in the experimental analysis the free settling velocity, U_f, can be directly measured as the rate of drop of the mudline (Mohamedelhassan and Shang, 2001):

$$U_f = \beta\bar{u} \quad [2.36]$$

With varying solid concentrations, the change in β will give a good indication of the impact of the applied electric field on the free settlement. U_f represents the settling of the finer particles with the lower settling velocity, particularly, clay particles with the grain size d < 5 μm.

2.5.2.1.2 Hindered settling

Hindered settling is a process which begins to occur as particles begin to collide as they settle down and as a result the settling velocity decreases. Over time, the hindered settling zone increases and the solids concentration increases. As a result, the porosity, n, can no longer be assumed to equal 1, but instead it becomes a significant factor with a value <1. The coefficient of sedimentation, r, must also be considered as it becomes a controlling factor. The following equation defines the hindered settling velocity, U_h :

$$U_h = \beta \bar{u} n^r = U_f n^r \qquad [2.37]$$

$$\log(\frac{U_h}{U_f}) = r \log(n) \qquad [2.38]$$

The change in the coefficient of sedimentation represents the effects of the applied electric field as:

$$r = r_g - \Delta r \qquad [2.39]$$

where r_g the coefficient of sedimentation due to gravity and Δr is is the change in the coefficient of sedimentation by the electric field.

The decrease in the coefficient of sedimentation by electrokinetics (Δr) leads to an increase in the hindered settling velocity at a specific porosity.

Mohamedelhassan and Shang (2001) illustrated 3 zones of the particle settling velocity as shown in Figure 2.7. Zone 1, in which the grain size is less than 1 μm and the velocity is primarily induced by electrokinetics (u_{ek}). Zone 2, in which the grain sizes range between 1 and 5 μm. The overall settling velocity of the particles is the summation of the gravitational and electrokinetic settling velocities ($u_g + u_{ek}$). Zone 3, in which the grain size is larger than 5 μm and the gravitational forces predominantly control the overall particle settling velocity.

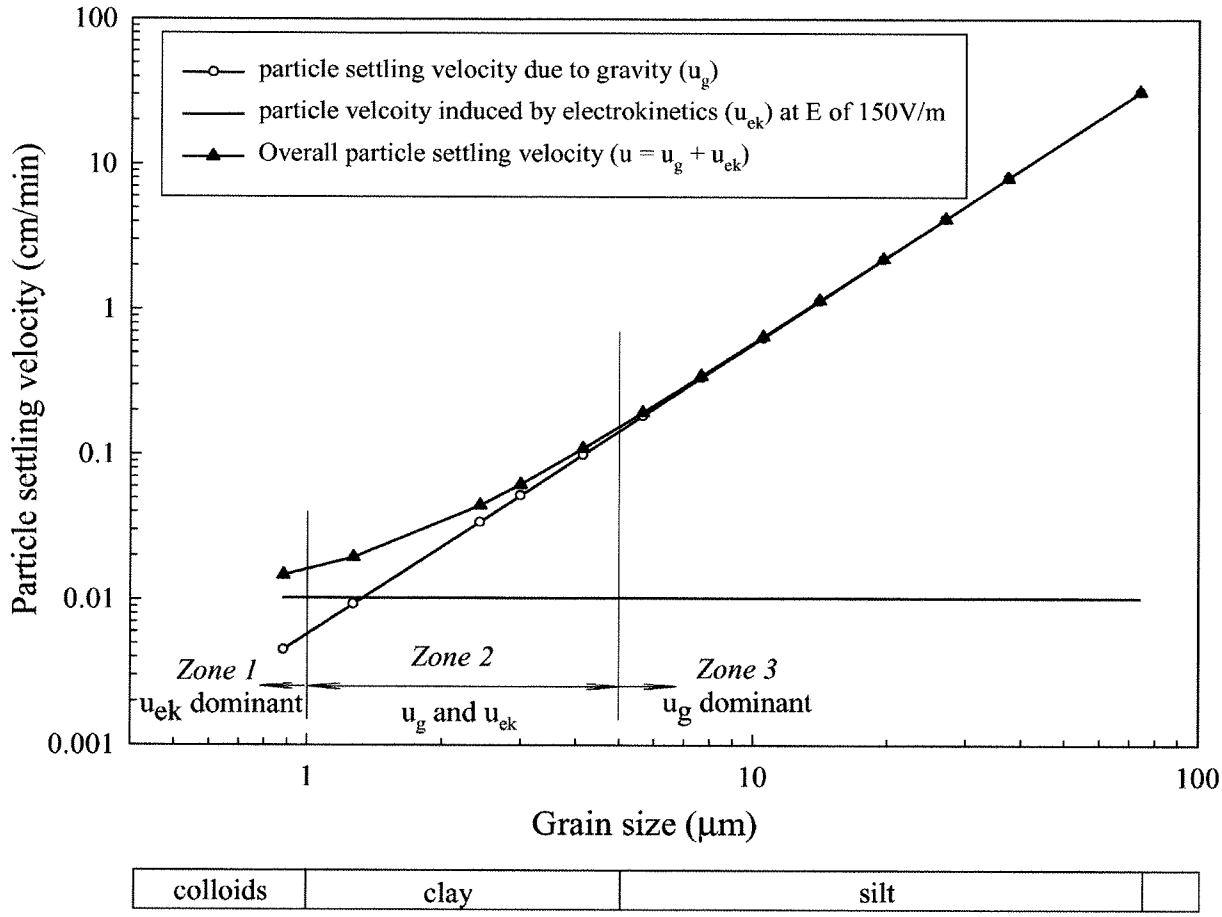

Figure 2.7 Particle settling velocity vs. the grain size (Mohamedelhassan and Shang, 2001)

2.5.2.2 Electrokinetic consolidation-dewatering

It is extremely difficult to use conventional dewatering methods for clayey soil, as the pore sizes are very small. Electro-osmotic flow is an attractive method of dewatering clayey soils and suspensions as it is relatively insensitive to pore size and pore size distribution. Due to electro-osmosis, the water flows towards the cathode, where it is drained away. If no water is allowed to enter at the anode, then consolidation of soil would occur.

As a following process to the electrokinetic sedimentation, electrokinetic dewatering can be applied to the settled contaminated solids (thickener). Electrokinetic dewatering mainly use electro-osmosis to decant the water from the thickener. The research on electrokinetic dewatering started in the 1960s. The United States Bureau of Mines pioneered the research and development of electrokinetic dewatering of tailings from mineral and coal processing. Sprute and Kelsh (1975, 1980) reported several successful field applications. The Australian Commonwealth Scientific and Research Organization began the research on electrokinetic dewatering of tailings in the late 1970s (Lockhart, 1986). More than 60 tailings from coal preparation plants, sand washing plants, mineral processing and water purification plants were tested.

Chung et al. (2005) conducted laboratory experiments on artificially contaminated sediments, applying electrokinetic sedimentation and dewatering. Polarity reversal was employed after the settlement process was finished. The researchers achieved rapid volume reduction and contaminants removal.

2.6 SOLAR ENERGY AS SOURCE OF POWER

Over the last decade solar energy has gained the attention of scientists and the general public, leading to a multitude of beneficial applications. Although, a solar cell can be an excellent candidate for power supply in electrokinetic applications, very few researchers attempted to investigate its use. The use of solar cells as a source of power can cut the electricity transmission expenses and eliminate power losses in the transmission lines. Furthermore, the power produced by solar cell is environmentally friendly and can be used in sites located in remote areas without active power lines. Also, solar panel produces dc electric field that is usable in electrokinetic applications without alteration (i.e. without dc transformer). The expected reduction in solar cell prices as the technology continues to improve can significantly reduce the initial cost of a solar power system.

The power generated by solar cell panel depends on the duration of the day and the weather conditions. This can cause oscillation in the power supply during the day, besides intervals of zero voltage at night. As discussed before, intermittent current can be beneficial to the outcome of an electrokinetic process. Thus, electrokinetic remediation with solar cells can improve the process by the intermittent resulting from periods of zero voltage at night.

Yuan et al. (2009) investigated the use of solar cell in electrokinetic remediation of kaolinite clay contaminated with cadmium. Three set of laboratory experiments were carried out. The first one on a cloudy rainy day, the second one in a sunny day, and the

third set was a control test conducted with a continuous dc power supply. The voltages generated were found to be different, where the highest voltage was during the sunny day and the lowest was during the cloudy day. The efficiency of cadmium removals in the three tests was however comparable. Yuan et al. (2009) reported that in China the cost of electrokinetic remediation with solar cell panel was 40% of that carried by electric power from the grid.

2.7 CONCLUSIONS

Electrokinetics appears to be a viable alternative for soil and groundwater contamination remediation and/or prevention. Numerous studies have been performed with varying degrees of success. In general, electrokinetics is found to be effective in moving contaminants and/or water in the soil, and therefore it can be used to remediate contaminated soils or prevent the spread of pollution. The application of the electric field has several effects on the soil, water, and contaminants. These effects include electro-migration, electro-osmosis, changes in pH, and electrophoresis. The present study is consisting of two parts: the first part investigated the effectiveness of electrokinetic barrier in preventing contaminant migration; the second part explored the electrokinetic remediation of contaminated slurries. The use of the solar energy as source of power was introduced in the both applications.

Researches in recent years have demonstrated several applications of electrokinetic phenomena in the fields of geotechnical and environmental engineering. Only few studies have investigated the feasibility of using electrokinetics in creating subsurface

barriers to prevent the contaminant migration (Narasimhan and Ranjan, 2000; Lynch et al., 2007). The idea of an electrokinetic barrier is simple. A counter-gradient opposite in direction to that of the groundwater hydraulic gradient is created by the continuous or periodic application of an electrical field between rows of electrodes. This will stop the movement of water within that region and prevent the migration of contaminants. In this study, the effectiveness of electrokinetic barriers is investigated. Solar energy as source of power is an innovative option for electrokinetics applications. Mohamedelhassan (2011) conducted one-dimensional laboratory study to investigate the use of electrokinetic barrier powered by solar panel to prevent contamination of clayey soil by hydraulic flow. Solar power supply was used to generate electric field for electrokinetic barrier. The effectiveness of the solar powered barrier is compared with effectiveness of a barrier that used dc power supply for electricity. Electrokinetic remediation of slurries has been used in volume reduction for slurries and contaminants removal. The dewatering/decontamination remediation consists of the two phases; electrokinetic sedimentation and electrokinetic consolidation. Solar energy is potential source of energy to provide sufficient current for the remediation processes.

The main objectives of this study are: (i) to assess the effectiveness of electrokinetic barrier in preventing or minimizing heavy metal contamination using one- and two-dimensional electric field configurations, (ii) to investigate the effectiveness of electrokinetics in increasing the settling velocity, decreasing the volume and removing heavy metal from contaminated slurries and (iii) to explore feasibility of using stand-alone solar power as source of energy for the tests.

Chapter Three

Material properties and Characterization

3.1 INTRODUCTION

Three types of soil were used in this study; kaolinite clay, sand and bentonite. Kaolinite rich clay was obtained from Plainsman clay in Medicine Hat, Alberta. The sand was obtained from an open pit in Thunder Bay, Ontario. A commercial Bentonite was brought from Tru-Bore. Geotechnical, chemical, and/or mineralogical tests were performed on the Plainsman clay, sand and bentonite.

3.2 GEOTECHNICAL CHARACTERIZATION

3.2.1 Plainsman Clay

Atterberg limits, specific gravity, soil classification, particle size distribution, cation exchange capacity and X-ray diffraction tests were carried out on the clay soil to identify its geotechnical, physical and chemical properties. Table 3.1 summarizes the results of the tests.

Table 3.1 The clay soils properties

Test	Property	Plainsman's clay	85%Plainsman's clay -15% bentonite
Specific gravity	G_s	2.65	2.62
Atterberg limits	Liquid Limit, LL	41	62
	Plastic Limit, PL	19	20
	Plastic Index, PI	22	42
Grain size distribution	Sand (%)	0	0
	Silt (%)	58	49
	Clay (%)	42	51
Classification	USCS symbol	CL	CH
Cation Exchange capacity	CEC (meq/100g)	8.9	28
Mineralogy	Dominant clay mineral(s)	Kaolinite	Kaolinite, Montmorillonite

3.2.1.1 Atterberg limits

The liquid and plastic limits were determined following the American Society of Testing and Materials (ASTM) procedure D4318 (ASTM, 2005).

3.2.1.2 Specific gravity

The density of the soil was calculated following ASTM D854 (ASTM, 2006).

3.2.1.3 Soil classification

The Unified Soil Classification System (USCS) group symbol of the Plainsman clay is CL and the group name is lean clay.

3.2.1.4 Grain size distribution

Hydrometer tests were conducted to estimate the distribution of the particle sizes in accordance with ASTM D422 (ASTM, 2007). Figures 3.1.A and 3.1.B show the grain size distribution for the Plainsman clay and the Plainsman clay-bentonite mixture (85% Plainsman clay and 15% bentonite), respectively.

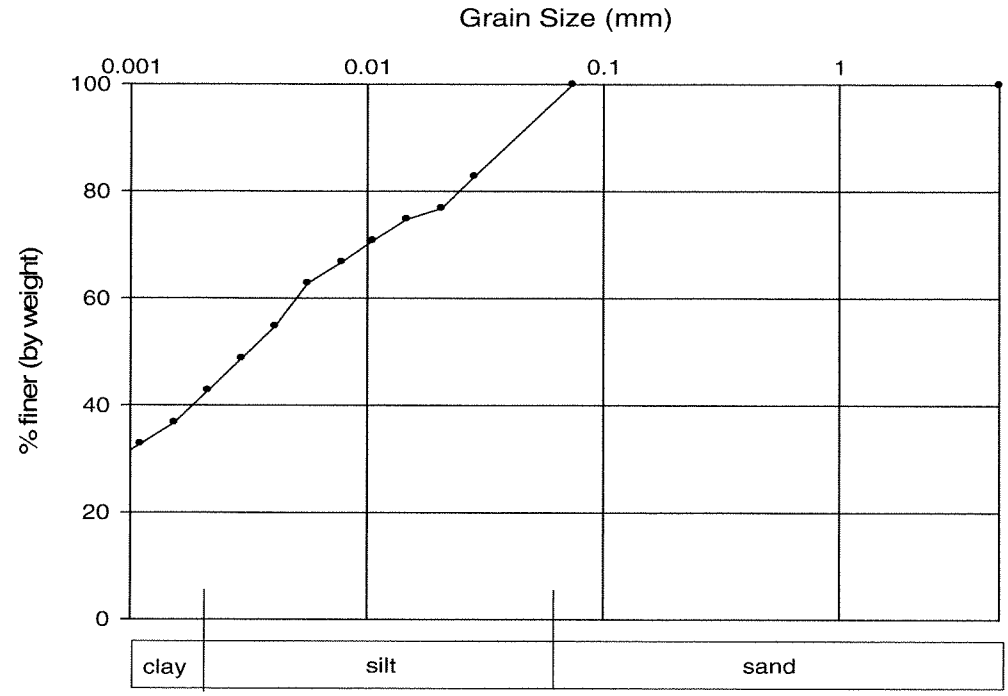

Figure 3.1.A Grain size distribution for Plainsman clay.

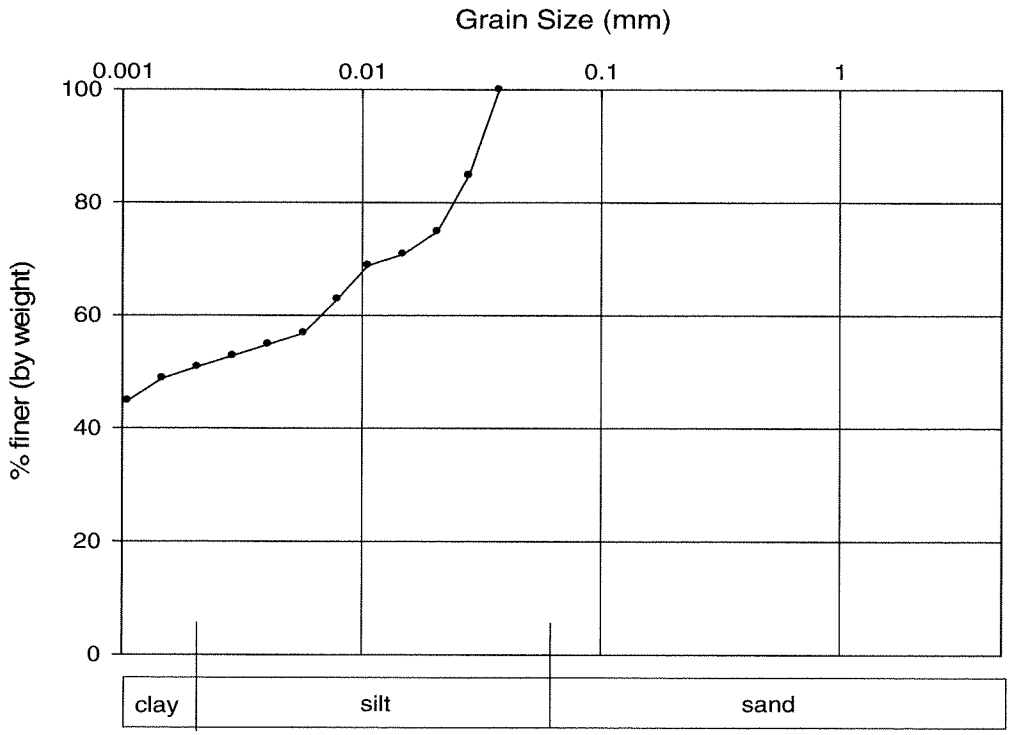

Figure 3.1.B Grain size distribution for Plainsman clay-bentonite mixture.

3.2.1.5 Cation exchange capacity (CEC)

The cation exchange capacity (CEC) tests were conducted in Lakehead University Centre for Analytical Services (LUCAS). The CEC was 8.9 meq/100 g for the Plainsman clay. CEC for the Plainsman clay-bentonite mixture was found to be 28 meq /100 g.

3.2.1.6 X-ray diffraction

The X-ray diffraction seen in Figure 3.2 showed that kaolinite is the dominant clay mineral in the Plainsman clay soil. The test was conducted without crushing the soil which may explain the low percentage of kaolinite shown by the test.

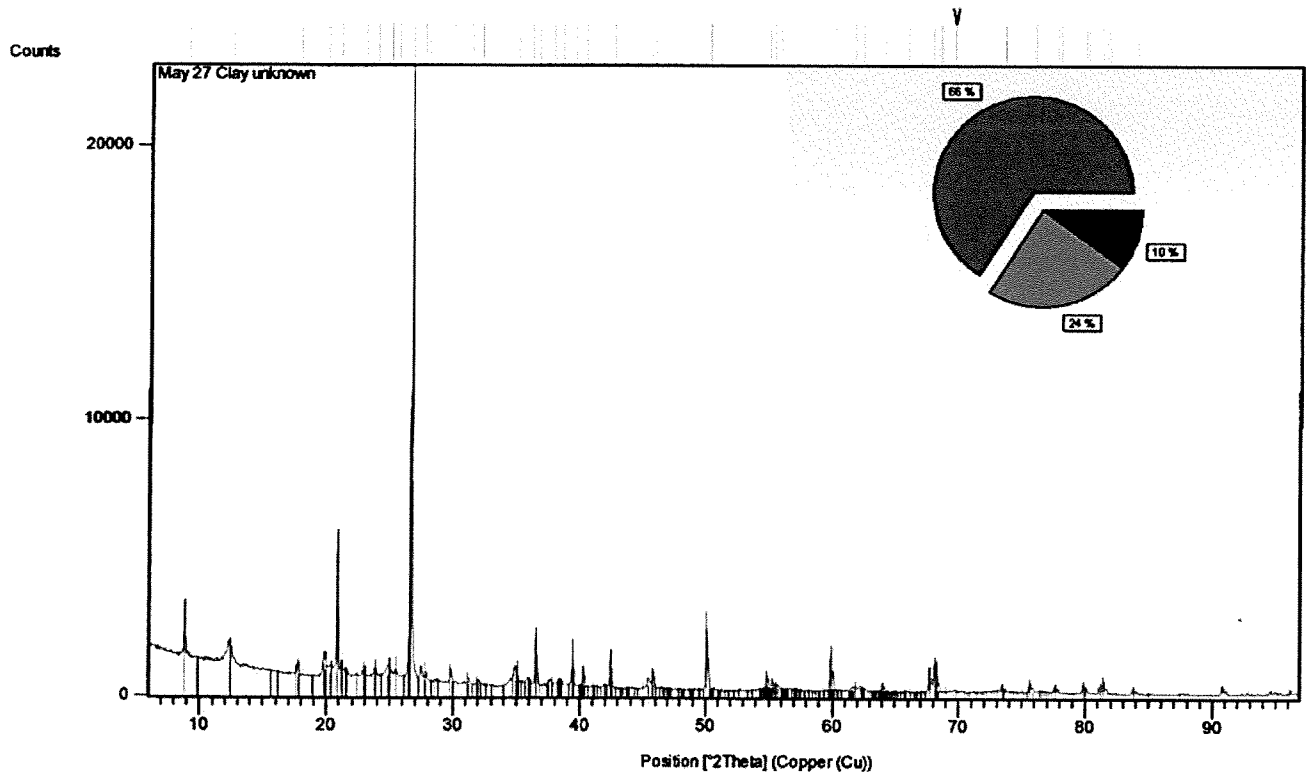

Figure 3.2 X-ray diffraction pattern for the Plainsman clay soil.

3.2.2 Bentonite Clay

Tru-Bore commercial bentonite was used to prepare a Plainsman clay-bentonite mixture. Bentonite was mixed by ratio 15% of the total mass. The mixture was used in the sedimentation tests. The mixture properties are presented in Table 3.1.

3.2.3 Sand

The sand used in this study was sieved through sieve No. 10 (2.0 mm) and retained on sieve No. 40 (0.425 mm). The sand was washed and dried prior to the test. Figure 3.3 shows the grain size distribution for the retained sand used. The USCS group symbol of the sand is SP (poorly graded sand). The specific gravity of the sand was 2.7.

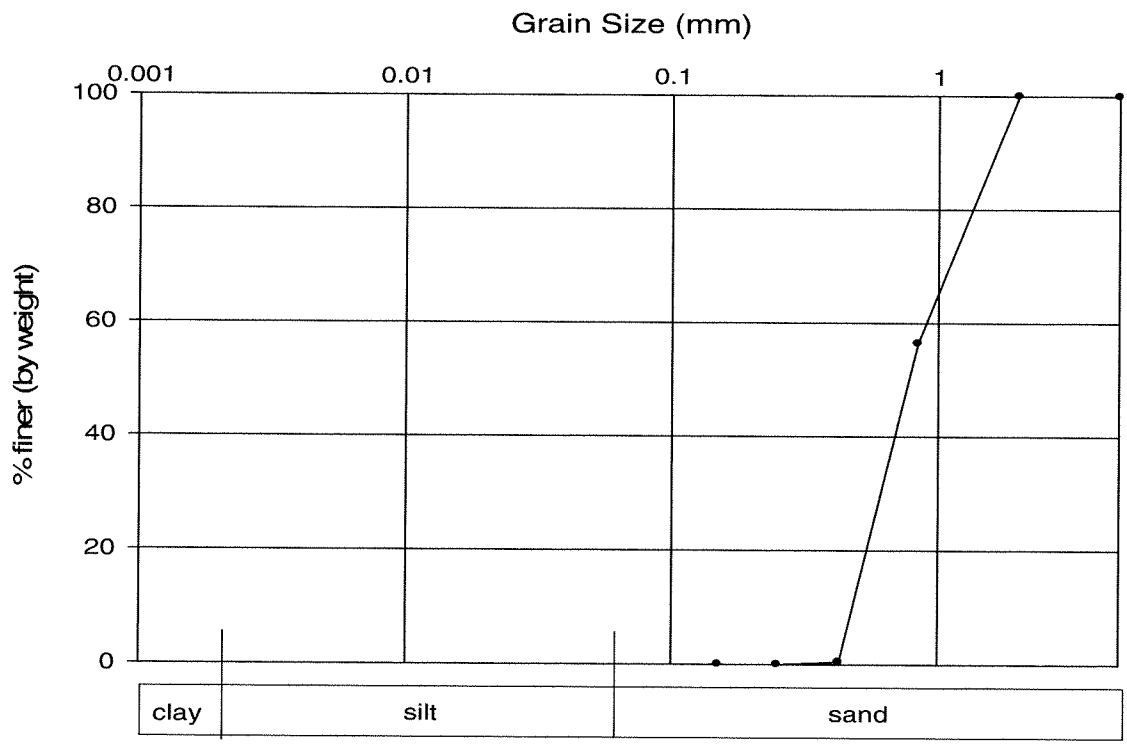

Figure 3.3 Grain size distribution for sand.

3.3 ADSORPTION AND DESORPTION TESTS

The adsorption and desorption of heavy metals by clay mineral surfaces and soils in general have mostly been discussed by employing empirical models, such as Langmuir and Freundlich equations (Atanassova and Okazaki, 1996). Electrokinetic processes change the soil pH and consequently alter the soil adsorption/desorption capabilities. In this study, series of tests were conducted to investigate the adsorption and desorption behaviour of copper into/from soil at various pH values and ionic strengths. The tests methodology described in the following section was adapted from Yuan et al. (2007). Each of the adsorption and desorption test was carried out in triplicate.

3.3.1 Copper Adsorption Test

The adsorption capacity of the soil is important in order to estimate the heavy metal adsorbed by soil solids and that free in the soil pore fluid. Batch equilibrium tests were conducted to evaluate the copper adsorption characteristics of the Plainsman clay, the primary soil used in this study.

One liter of 0.01 M $NaNO_3$ solution was prepared as background electrolyte, where a mass of 0.85 g of NaNO3 was mixed with 1000 mL deionized water. A mass of 0.268 g of $CuCl_2$ $2H_2O$ was added to 100 mL of the background solution to obtain 1000 mg/L copper concentration. Six extra solutions with copper concentration of 500, 250, 100, 50, 20 and 5 mg/L were obtained by consecutive dilution of the 1000 mg/L solution using the electrolyte solution.

1 g of the dry soil was placed into a 50 mL Erlenmeyer flask and then 14 mL of the copper solution was added to each flask. The pH of the mixture was adjusted to 5.75±0.25 using nitric acid (HNO_3) and/or sodium hydroxide (NaOH). The flask was placed in a table shaker that was shaking at 120 rpm. The soil-copper mixture was left to equilibrate in the table shaker at the room temperature for 24 h. The pH of the soil-copper solution was measured during the equilibration time using the pH-electrode Sentix 41-3 (WTW-multi 340i) and readjusted when needed.

The soil-copper solution was transferred to a 20 mL centrifuge tube. The tube was placed in a laboratory centrifuge (82012-800 VWR) and centrifuged for 10 minutes at 4000 rpm to separate the liquid from the suspension solids. Afterward, 1 mL of the supernatant from the centrifuge tube was drawn into 20 mL plastic tube and then diluted with 9 mL of deionized water. The diluted sample was sent to the Inductivity Coupled Plasma-Optical Emission Spectroscopy (ICP-OES) to determine the copper concentration.

The batch test results were used to construct the adsorption isotherms. From the results, Langmuir model was found to best represent the isotherm, and to determine the maximum adsorption capacity of the soil. Langmuir equation as given by (Atanassova and Okazaki, 1996):

$$\frac{C_e}{S} = \frac{1}{K_L M_L} + \frac{C_e}{M_L} \qquad [3.1]$$

where C_e (mg/L) is the equilibrium concentration of the supernatant, S (mg/g) is the amount of copper adsorbed per g soil, K_L (L/mg) is the Langmuir constant and M_L (mg/g) is the Langmuir maximum adsorption capacity.

The results of the initial copper concentration (C_i) and the equilibrium concentrations (C_{e1}, C_{e2} and C_{e3}) were obtained by ICP-OES. Table 3.2 presents the results and the factors of the Langmuir equation. Figure 3.4 shows that the absorbed amount of copper increased with the increase of the copper-solution concentration (ionic strength). From the results of the model, the Langmuir equation was found to be:

$$C_e/S = 0.25\ C_e + 19.22 \qquad [3.2]$$

Coefficient $R^2 = 0.988$

$K_L = 1.3\times10^{-2}$ (L/mg)

$M_L = 3.98$ (mg/g)

Table 3.2 Summary of copper adsorption test results - Langmuir isotherm model

C_i (initial copper concentration in the solution) (mg/L)	equilibrium concentrations (mg/L)			C_e (average equilibrium concentration) (mg/L)	S (amount absorbed by the soil) (mg/g)	C_e/S (g/L)
	1	2	3			
5.33	0.76	0.73	0.89	0.80	0.063	12.58
21.70	7.49	0.52	1.54	3.19	0.259	12.29
48.43	20.12	9.80	2.95	10.96	0.525	20.89
96.21	24.53	25.40	30.37	26.77	0.972	27.53
274.50	126.80	127.70	126.00	126.83	2.079	61.35
511.20	286.80	316.70	308.80	304.10	2.899	104.88
1001.1	690.80	735.60	780.70	735.70	3.714	198.08

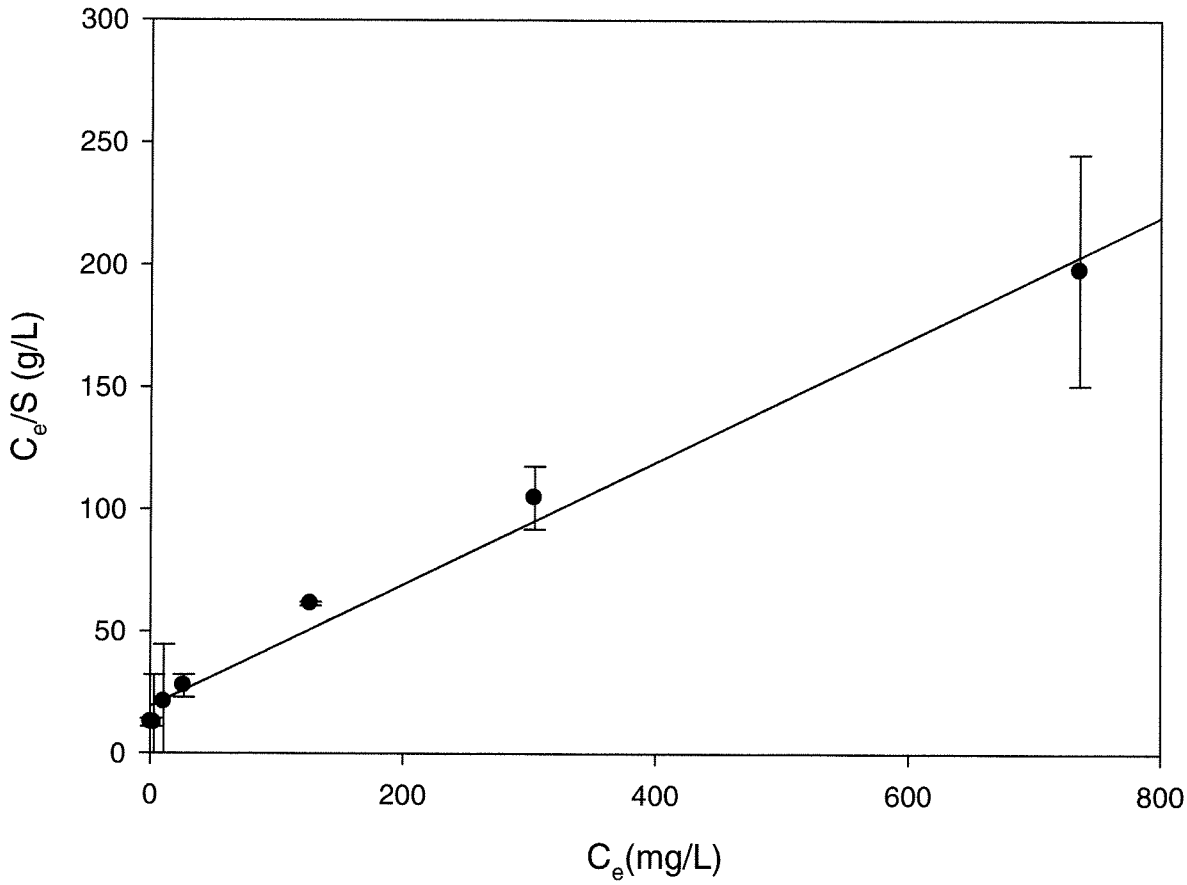

Figure 3.4 Copper adsorption isotherm.

3.3.2 Copper Desorption Test

Yuan et al. (2007) concluded that desorption of copper is influenced by ionic strength and the pore fluid pH. Electrokinetic processes result in developing a pH gradient along the soil and thereby affect the adsorption/desorption characteristics of the soil.

Two tests series were conducted to evaluate desorption of copper from the soil. In the first test series, the effect of the copper concentration on desorption was evaluated with a fixed pH. The second test series investigated the effect of the pH on desorption of copper from soil samples with similar copper concentration.

3.3.2.1 Effect of copper concentration

The tests were conducted using the soil samples from the adsorption test series in Section 3.2.1. The soil samples contained different amounts of adsorbed copper (60 to 3720 mg Cu/ kg soil). The amount of copper desorbed in each test was obtained and compared with the initial amount of copper adsorbed into the soil sample.

After drying and grinding the soil samples used in the adsorption test, 14 mL of 0.01 M $NaNO_3$ solution was added to 1 g of soil and the mixture was left for 24 h in the table shaker at 120 rpm. During the equilibration time the pH of the solutions was kept at 5.75±0.25 using strong nitric acid (HNO_3) and/or sodium hydroxide (NaOH). The soil-solution tubes were centrifuged for 10 min at 4000 rpm. 1 mL of the supernatant from each tube was drawn into a 20 mL plastic tube, and then diluted with 9 mL of deionized water. The diluted sample was sent to ICP-OES to determine the copper concentration.

Table 3.3 shows the results obtained from the tests. The copper adsorbed by the soil ranged from 63 to 3714 mg copper/ kg soil. The average of copper desorbed in the solution was used to calculate the equilibrium amount desorbed of copper per gram soil, the following equation shows the calculation procedure:

$$D_e = \frac{(D_{ave} - C_0)\left(\frac{mg}{L}\right)}{1\ g\ of\ soil} \times 0.014\ L \times \frac{1000\ g}{Kg} \qquad [3.3]$$

D_{ave} is the average desorption equilibrium copper concentrations D_{c1}, D_{c2} and D_{c3} (mg/L). D_e is the desorbed amount of copper (mg/kg), C_0 (mg/kg) is the initial concentration of copper in the sodium nitrite solution (zero).

Figure 3.5 shows that the desorbed copper increased with the increase of the initial adsorbed copper. The desorbed copper represents the amount that can easily be removed from the soil. The highest desorbed copper of 371 mg/kg was obtained from the highest initial adsorbed copper of 3714 mg/kg. This represents about 16.5% of the adsorbed copper amount.

Table 3.3 Summary of the copper desorption test results for different copper concentrations

S amount adsorbed (mg/Kg)	Desorption equilibrium concentrations (mg/L)			D_{ave} Average equilibrium concentrations (mg/L)	D_e Amount desorbed (mg/kg)	D_e/S (%)
	1	2	3			
63	0.092	0.2952	0.1498	0.18	2.51	3.98
259	1.224	0.2537	0.3102	0.60	8.34	3.22
525	3.338	3.053	1.858	2.75	38.50	7.33
972	4.279	4.209	5.031	4.51	63.09	6.49
2079	15.03	15.75	14.67	15.15	212.10	10.20
2899	29.44	30.12	32	30.52	427.28	14.74
3714	41.85	41.55	47.93	43.78	612.87	16.50

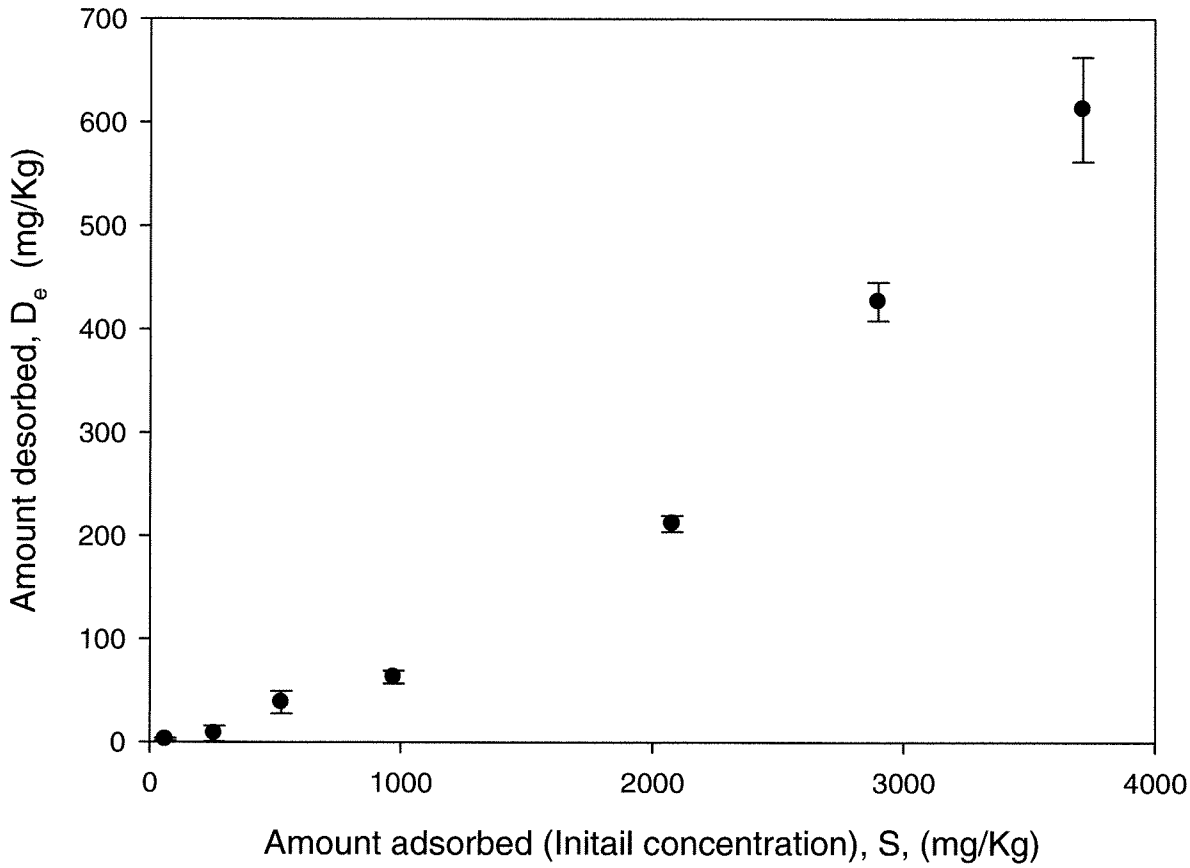

Figure 3.5 Amount desorbed, D_e, vs. initial adsorbed copper, S, at pH of 5.75±0.25

3.3.2.1 Effects of pH

This test series was conducted using soil samples with the same copper concentration and different pH values. The soil sample was air dried after it has been artificially contaminated to adsorb 355 mg copper per kg of soil.

1 g of the dried contaminated soil was weighted into each of 5 Erlenmeyer flask (50 mL). 14 mL of 0.01 M $NaNO_3$ solution was added to each Erlenmeyer flask. The pH of the solution was adjusted to 2, 4, 6, 8 and 10 using nitric acid (HNO_3) and/or sodium hydroxide (NaOH). Then the soil-solution mixtures were placed on the table shaker with 120 rpm for 24 h. During the equilibration time the pH was measured and readjusted when needed. After 24 h, the mixtures were transferred to 20 mL centrifuge tubes. Then the tubes were centrifuged for 10 min at 4000 rpm.1 mL of the supernatant from each tube was drawn into 20 mL plastic tube, then diluted with 9 mL of deionized water. The diluted samples were sent to ICP-OES to determine the copper concentration.

Table 3.4 shows the results obtained from the test and the calculation of the amount desorbed at each pH value. Figure 3.6 illustrates that the amount of copper desorbed increased with the decrease of pH. At pH of 2 (acidic environment) the amount desorbed was about 271 mg/kg represents 80% of the total adsorbed copper. At pH of 8 and 10 (alkaline environment), the desorbed percentage of copper was less than 0.5%.

The electrolyte reactions that result from the electrokinetic processes increase the pH near the cathode. This high pH zone near cathode increases the adsorption of the copper by the soil. Therefore, the employment of an electrokinetic barrier can improve

the adsorption characteristics of part of the soil barrier and thereby generate a trap zone for the heavy metal(s).

Table 3.4 Summary of copper desorption test results for different pH values.

pH	S_i Initial Copper Concentration (mg/kg)	Desorption Equilibrium concentration mg/L			D_e Average concentration (mg/L)	D_d Amount desorbed (mg/kg)	D_d/S_i percentage desorbed (%)
		1	2	3			
2	355	20.55	18.27	19.42	19.41	271.79	76.55
4	355	14.81	13.99	10.42	13.07	183.03	51.55
6	355	1.56	3.09	2.24	2.30	32.15	9.05
8	355	0.13	0.14	0.09	0.12	1.68	0.47
10	355	0.09	0.05	0.05	0.06	0.89	0.25

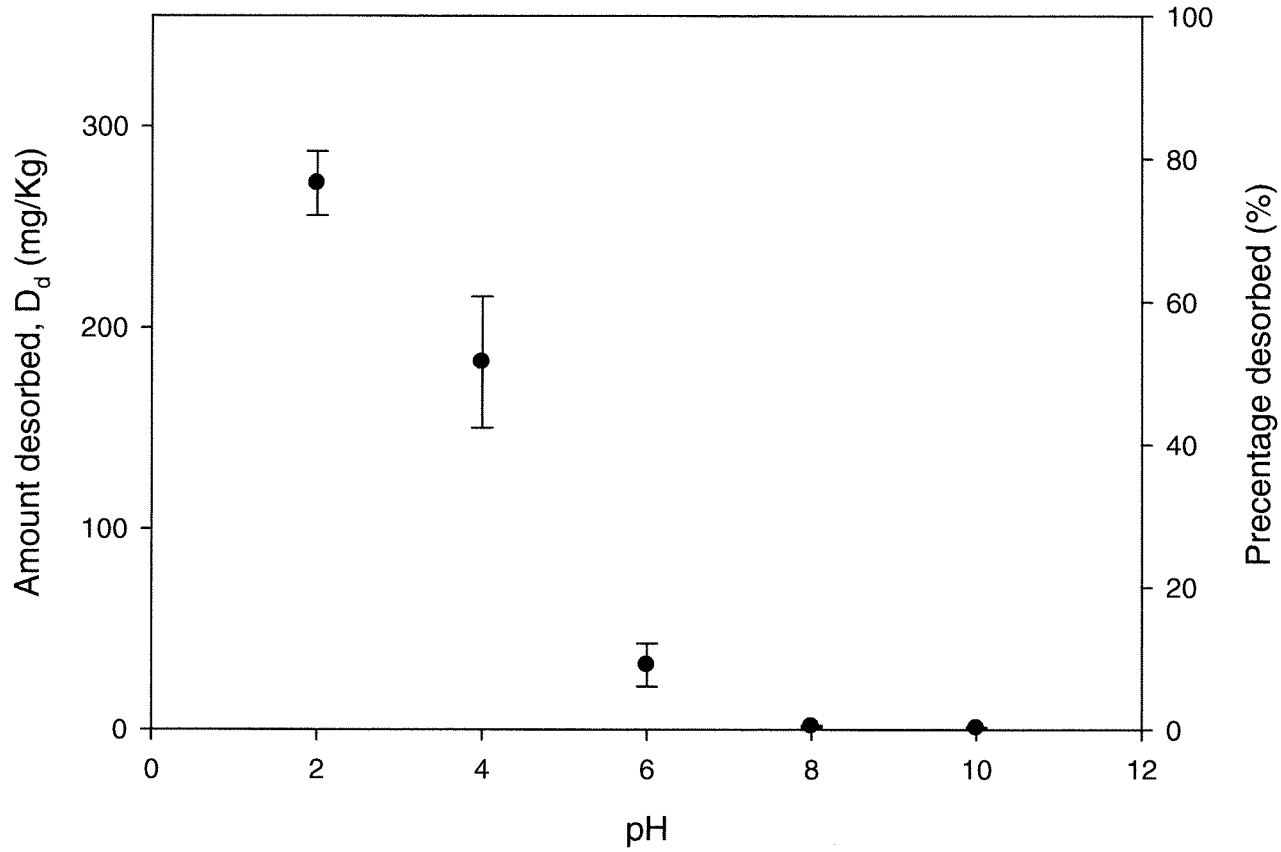

Figure 3.6 Amount of copper desorbed, D_d, vs. pH for soil with initial copper concentration of 355 mg/ kg of dry soil.

.

3.4 ZETA POTENTIAL TESTS

Electro-osmosis and electrophoresis are greatly affected by the magnitude of the zeta potential, ζ. Thus, it is an important factor in the electrokinetic remediation (Mitchell and Soga, 2005).The most important factors that affect ζ are pH and the ionic strength. ζ value on its own without quoting its environment, i.e. pH and the ionic concentration, is a virtually meaningless number. Therefore, zeta potential tests are typically designed to detect the value of ζ for specific pH and electrical conductivity (ionic strength) for a clay sample.

In this study, the zeta potential tests were conducted using varies pH and electrical conductivity for four clay samples. Buffer solutions pH of 2, 4, 6, 8, and 11 were made for the tests using potassium phosphate salt (K_3PO_4) with the hydrochloric acid (HCl), citrate with HCl, citrate with sodium hydroxide (NaOH), TRIS (organic compound) with HCl, boric acid (H_3BO_3) with NaOH, respectively. The ionic strength of the buffers was calculated to remain with molarity of 0.05 M. Each buffer solution was diluted with deionized water to acquire electrical conductivity of 500, 1000, 2000, 5000 and 10000 µS/cm. The electrical conductivity was adjusted using the multi 340i conductivity probe.

Four clay samples kaolinite, kaolinite spiked with 400 mg copper/ kg of dry soil, bentonite, and 85% kaolinite-15%bentointe mixture spiked with 2000 mg copper/kg of dry soil. Each clay sample tasted with pH range 2 – 11, and altered electrical conductivity.

The two samples spiked with copper were taken from the same slurries which tasted for the sedimentation (discussed in Chapter Four). The 20% solid concentration of each slurry mixture was air dried and grounded before it was sieved through sieve # 200 (75 μm).

ζ values were measured using Zeta-Meter 3.0 (Figure 3.7). Zeta-meter device is a microprocessor based instrument that uses electrophonic cell to track the particles during the applied voltage. Following the instrument manual, 0.2 g of each clay sample was diluted into 500 ml buffer solutions with known pH and electrical conductivity.

Figures 3.8 and 3.9 show ζ vs. the pH and electrical conductivity for the four soils tests. As shown by the Figures 3.8-A to 3.8-C, ζ decreased (become more negative) with the increase of the pH. For example, for kaolinite (Figures 3.8-A and 3.9-A) with electrical conductivity of 10000 μS/cm, ζ was 2 at pH of 2 and -38 mV for pH of 10. In low pH environments clay particles tend to release cations into the electrolyte solution, whereas the hydrogen ions replace the cations. This results in a decreased diffuse double layer and consequently an increase in ζ (Shang et al., 1994). As seen in Figures 3.8-A and 3.9-A, for pH values < 5, at similar pH, ζ decreased (become less negative) with the increase of the electrical conductivity, e.g. at pH of 4, ζ at electrical conductivity of 500 μS/cm > ζ at 1000 μS/cm > ζ at 2000 μS/cm, etc. For pH > 5, the trend was reversed. For example, at pH of 8, ζ at 500 μS/cm < ζ at 10000 μS/cm. The trend of ζ with pH and electrical conductivity observed in the bentonite clay (see Figures 3.8-C and 3.9-C) was identical to the trend of ζ for the kaolinite clay. As shown in Figures 3.8-A and 3.8-C,

ζ values for the bentonite samples were slightly higher than the values of the kaolinite samples.

Figures 3.8-B and 3.9-B show ζ values for the kaolinite clay spiked with 400 mg copper/kg soil. As seen in the figures, in general, ζ increased with the increased of the pH and the decrease of the electrical conductivity. The highest ζ value was reported in the sample with the highest pH (11) and lowest electrical conductivity (500 μS/cm). The lowest ζ was reported in the test with 10000 μS/cm (highest value) and pH of 2 (lowest).

Figure 3.8-D and 3.9-D show ζ values for the 15% bentonite-85% kaolinite mixture. As seen in the figures, the trends of ζ are in general similar to the trends of the kaolinite samples and the bentonite samples. Thus, for pH values < 5, at similar pH, ζ decreased with the increase of the electrical conductivity and for pH > 5, the trend was reversed.

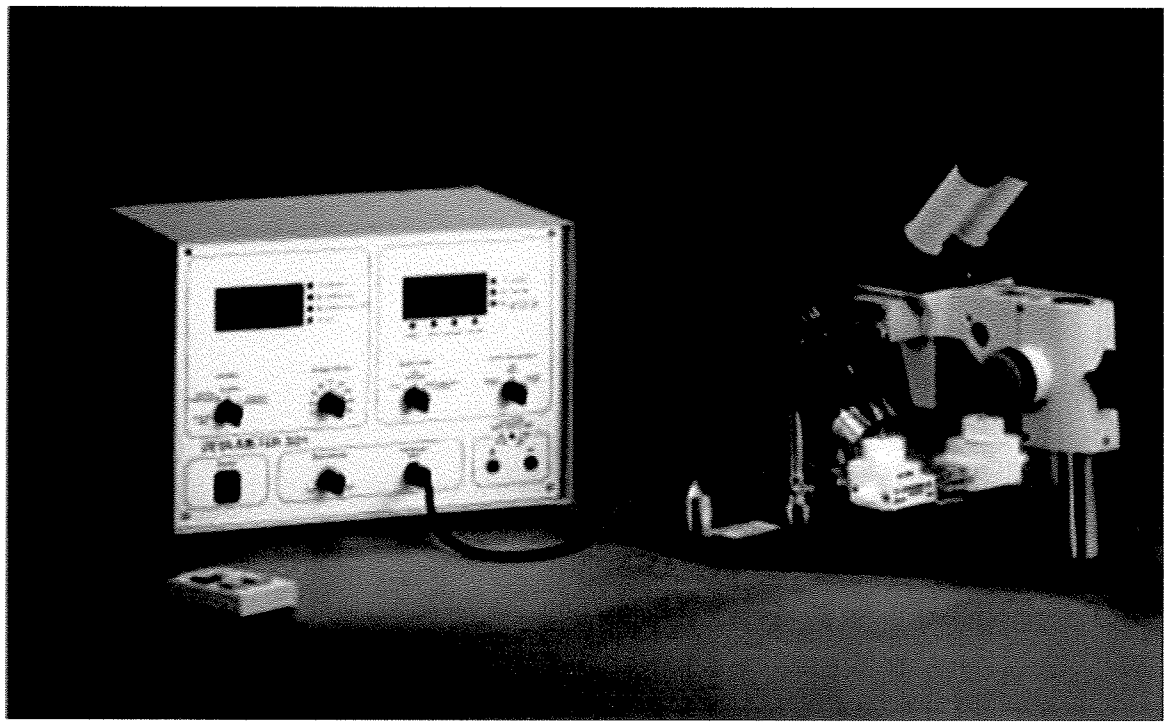

Figure 3.7 Zeta meter device.

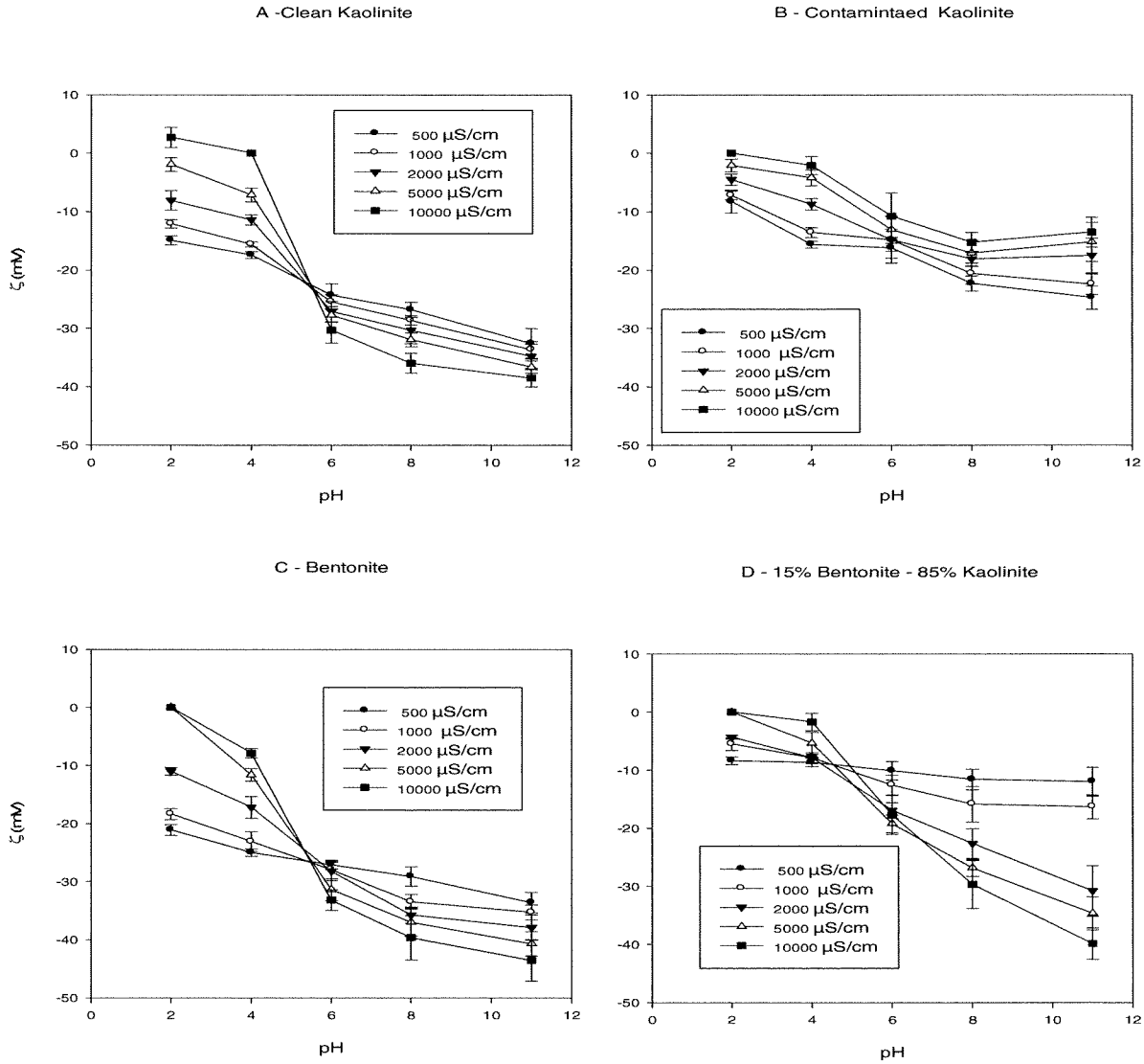

Figure 3.8 Zeta potential, ζ, vs. pH.

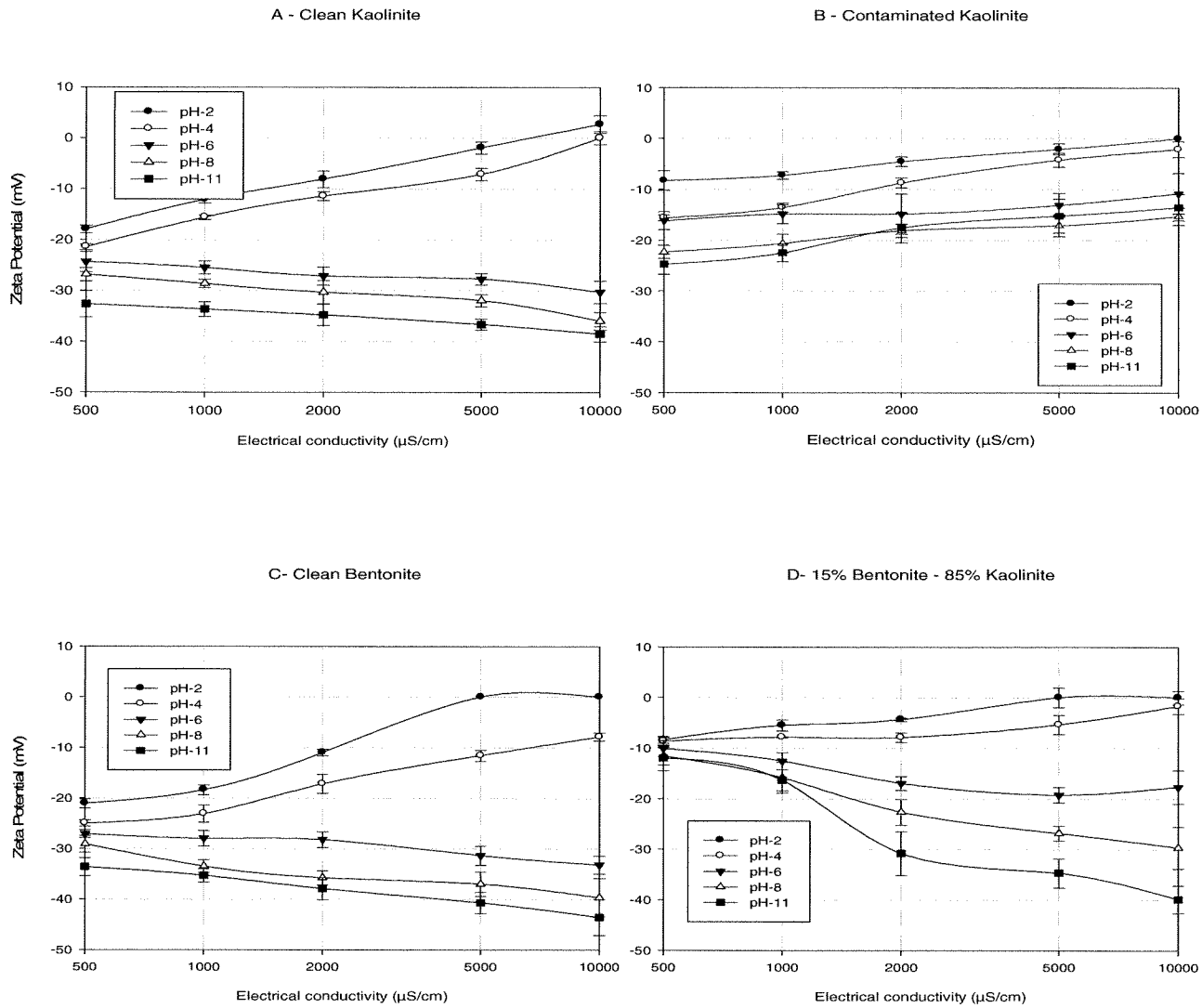

Figure 3.9 Zeta potential, ζ, vs. electrical conductivity.

CHAPTER FOUR

EXPERIMENTAL PROGRAM

4.1 INTRODUCTION

In this study, the experimental program consisted of two parts. Part one investigated the effectiveness of solar powered electrokinetic barrier. In part two, the feasibility of solar electrokinetic remediation of contaminated sediments was explored.

4.2 PART 1: SOLAR POWERED ELECTROKINETIC BARRIER

In this part of the research, laboratory experiments were carried out to investigate the use of solar energy to create an electrokinetic barrier. The effectiveness of stand-alone solar system to block/minimize the migration of contaminants through the soil was explored. The experiments were conducted using one and two-dimensional electric field configurations. Each configuration was tested using two types of source of power; solar cells and dc power supply. A control test without electric field was carried out for comparison.

4.2.1 Material Properties

The soil tested was prepared by mixing natural sand with clay. The soil mixture was 80% (by mass) sand and 20% clay. The sand particles passed through sieve No. 10 (2 mm) and retained on sieve No. 40 (0.425 mm). The clay, inorganic grey clay, was obtained from Plainsman in Medicine Hat, Alberta. Kaolinite is the predominant clay mineral of the Plainsman clay. According to the Unified Soil Classification System

(USCS), the group symbol for the soil mixture is SC and the group name is clayey sand. The specific gravity of the mixture is 2.68. Table 3.1 presents the soil properties of the clay.

4.2.2 Experiment Apparatus

4.2.2.1 Electrokinetic cell

Four electrokinetic cells were designed and constructed using Plexiglas plates 155 mm in thickness. The dimensions of the cell tank are 285 × 125 × 250 mm (Length × width × height). Two movable perforated Plexiglas plates (250 × 125 mm) were installed in groves on the cell wall to adjust the soil length to 200 mm. Two drainage valves were placed in the anode and cathode reservoirs. Figure 4.1 shows schematic of the electrokinetic cell.

4.2.2.2 Laboratory devices

Laboratory equipment were used for handling, testing and analysis of the soil samples. A mechanical mixer was used to blend the soil with copper and/or water. Multi 340i-WTW set was used for measuring the pH and electrical conductivity of the soil and water samples. Digital table shaker with speed range of 0 – 500 rpm was used to ensure the solid-solution interaction. A bench scale centrifuge with maximum speed of 4000 rpm was used to separate the fluid from the soil. A dc power supply and solar cells panel were used to generate the electric field. The copper concentration of the supernatant was sent to Lakehead University Centre for Analytical Services (LUCAS) where the Inductivity Coupled Plasma-Optical Emissions Spectrometer (ICP-OES) was used to determine the copper concentration.

4.2.3 Testing Procedure

4.2.3.1 Soil preparation

The soil was mixed in batches of equal size. The batch was prepared by pouring 8 kg of dry sand, 2 kg of dry Plainsman clay and 2 litres of tap water into the bucket of the mechanical mixture. The mixing was allowed for enough time to homogenous soil mixture with water content of 20%. The mixture was stored in an air tight pail. The mixing process was repeated to prepare enough soil mixture for the tests at hand.

4.2.4.1 Copper solution

Copper (II) chloride dihydrate ($CuCl_2.2H_2O$) was selected to prepare the copper solution. 26.89 g of $CuCl_2 \cdot 2H_2O$ was added to 10 liter of water for copper concentration of 1000 mg/L. The pH of the solution was measured and reduced to 2 using hydrochloric acid (HCL) in order to simulate acid mine drainage. The contaminated solution kept in a covered container.

4.2.4.2 One-dimensional configuration

Two identical perforated graphite electrodes, one serving as anode and the other as cathode, were placed vertically in direct contact with the soil at 194 mm from each other (see Figure 4.2-A). The dimensions of electrode were 200 × 125 × 3 mm (Height × width × thickness) and the electrodes cover the entire soil area perpendicular to the direction of flow. A geotextile filters were inserted between the electrodes and the

perforated Plexiglas plates. The soil packed into the cell was weighted in order to calculate the bulk density and the porosity of the soil.

The cathode reservoir was filled with the copper solution. The anode reservoir was empty with the drainage valve opened and connected to scaled flask. In some tests, the solar power was simulated using a dc power supply based on the output of a solar cells panel. The dc power supply was turned on during the day for 12 h and turned off during the night for 12 h. The continuous powered test was conducted using a continuous dc electrical field. The control test was carried without an electric field.

The pore volume of the soil sample was about 1750 mL and accordingly, an accumulated effluent of 2000 mL (1.14 pore volume) was selected to terminate the control test. The electrokinetic barrier tests (solar powered and the dc continuous powered) were terminated at a duration equivalent to the time required by the control test for 2000 mL effluent.

4.2.4.3 Two-dimensional configuration

In the two-dimensional configuration, two graphite electrodes each with dimensions 200 × 10 × 10 mm (Height × Length × Width) served as the anode and the cathode. The electrodes were installed at the edge of the soil specimen 180 mm from each other. The electrodes covered 8% of the soil area perpendicular to the flow. A procedure similar to that in the one-dimensional configuration was followed. Figure 4.3.A shows schematic diagram for the two-dimensional configuration.

4.2.4 Data Collection, Soil Sampling and Testing

Four water samples were collected from the effluent of the control test. The water samples were tested for pH and the electrical conductivity using the multi 340i-WTW-meter. The copper content in the water samples was determined using ICP-OES. After terminating the control test, two representative soil samples were used to determine the copper concentration in the soil and in the pore fluid. In the electrokinetic test with one-dimensional configuration, the soil specimen was divided into 4 sections (see Figure 4.2.B). The soil was divided into 12 sections in the electrokinetic test with two-dimensional configuration as seen in Figure 4.3.B. The water content was determined for each soil section. A soil sample from each section was air-dried for 72 h and then ground and tested for pH, and the copper content. For pH determination, 5 g of the air-dried soil was mixed with 10 mL of deionized water and the pH of the mixture was determined by a pH-electrode. The pore fluid copper concentration was tested by agitating 2 g of air-dried soil sample with 5 mL deionized water for 1 h in a table shaker at 120 rpm. The soil-water mix was then centrifuged at 4000 rpm for 10 min. The supernatant was test tested for copper content using ICP-OES. A 2.2 g of the dry soil was mixed with 11 mL of the concentrated nitric acid (HNO_3). The mixture was agitated for 12 h in the table shaker at 150 rpm. Afterward the mixture was centrifuged for 20 min at 4000 rpm. The supernatant was diluted and tested for copper content by ICP-OES.

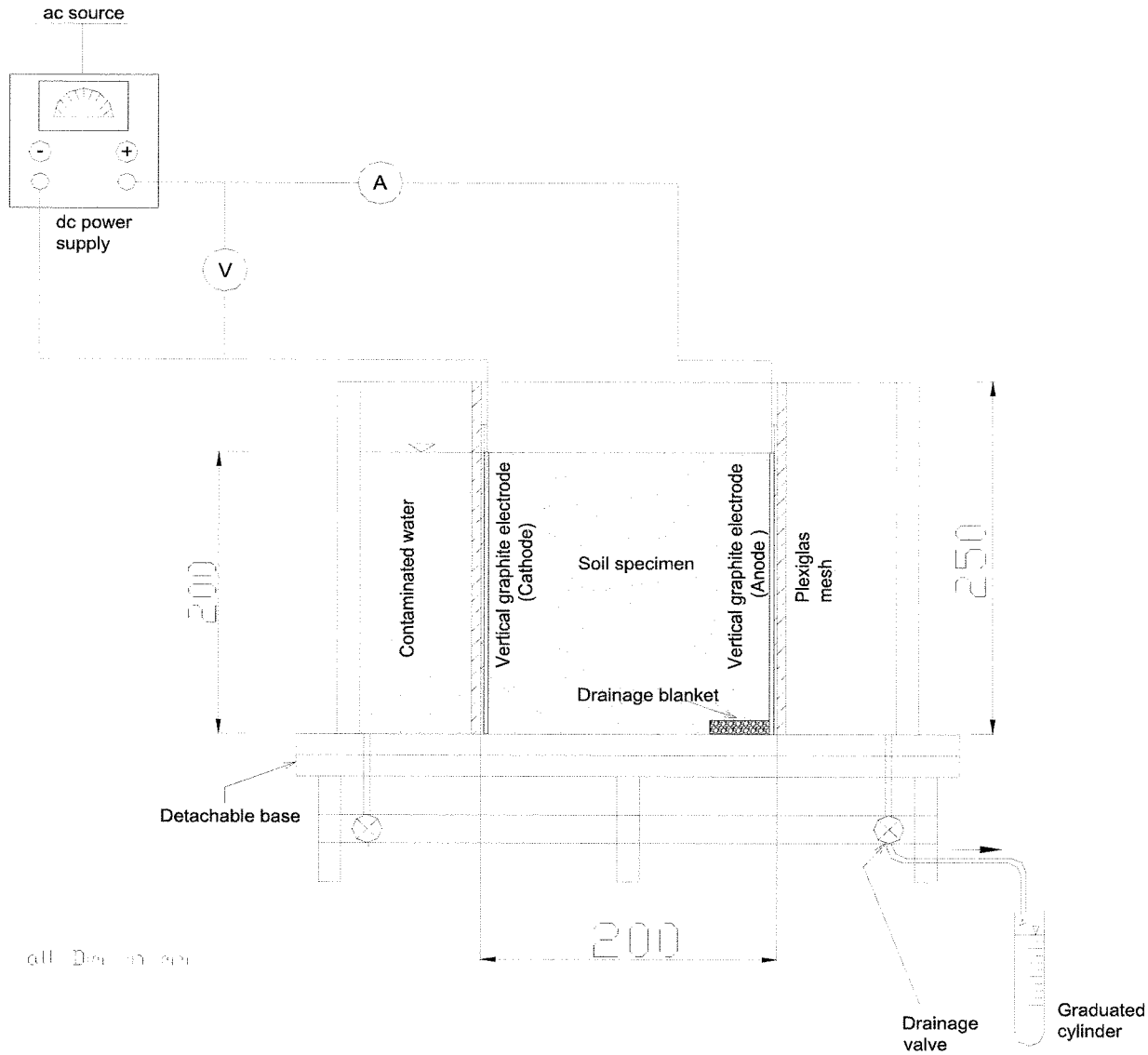

Figure 4.1 Schematic diagram of electrokinetic cell.

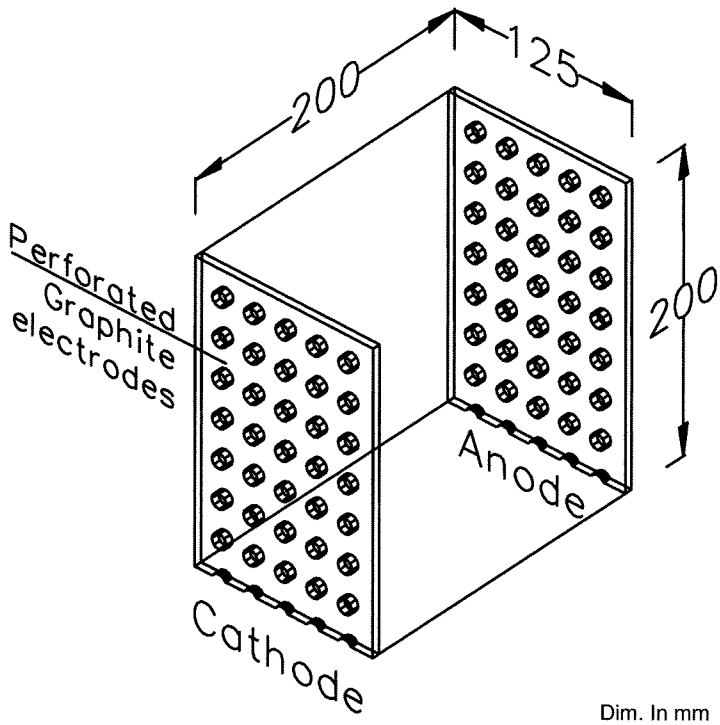

Figure 4.2.A One-dimensional configuration of the electrokinetic barrier.

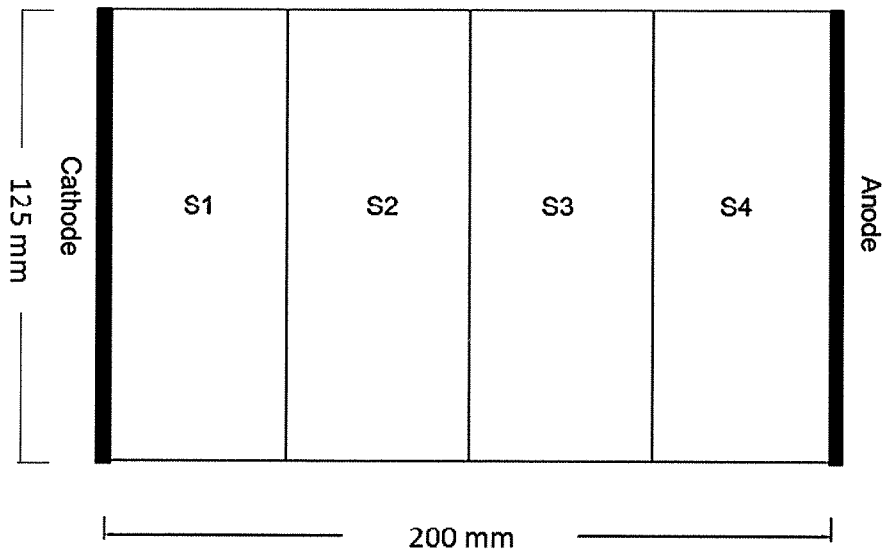

Figure 4.2.B One-dimensional configuration sampling sections (plan view).

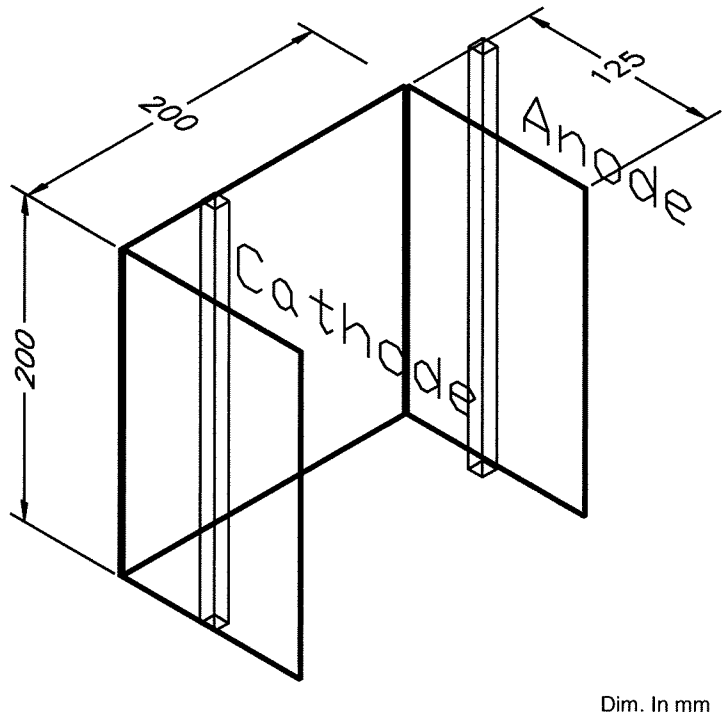

Figure 4.3.A Two-dimensional configuration of the electrokinetic barrier.

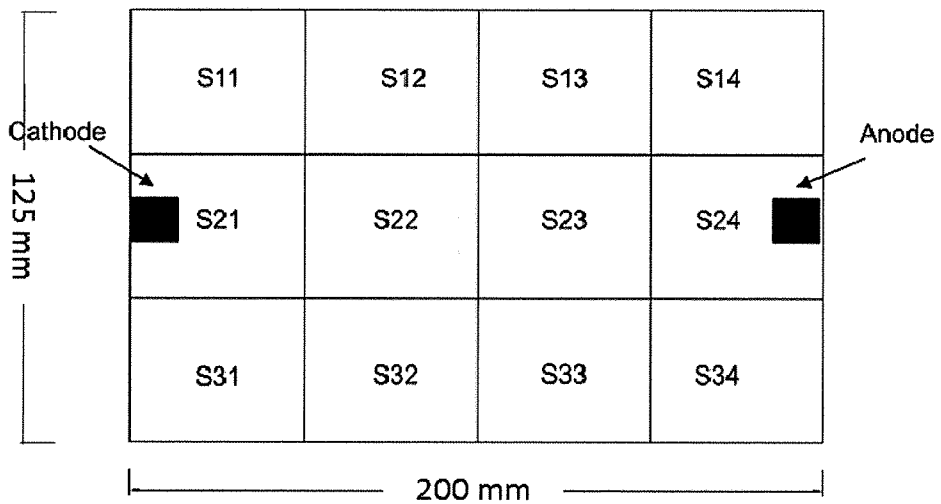

Figure 4.3.B Two-dimensional configuration sampling sections (plan view).

4.3 PART 2: SOLAR ELECTROKINETIC REMEDIATION OF CONTAMINATED SLURRIES

The tests were conducted using one-dimensional (1-D) and two dimensional (2-D) electric field configurations. Solar panels were used to provide the electric field. The clay slurries were prepared using two types of clay soils with a range of solid contents. The slurries were artificially contaminated with predetermined amount of copper. The 1-D configuration tests were carried out in two phases. Phase 1 examined electrokinetic sedimentation whereas in phase 2 electrokinetic dewatering/decontamination were investigated. Electrokinetic sedimentation was further investigated in the 2-D configuration tests.

4.3.1 Material Properties

Two clay soils were used to prepare the slurries. The first clay was obtained from Plainsman clay in Medicine Hat, Alberta. Kaolinite is the predominant clay mineral in the Plainsman clay (hereafter referred to as kaolinite). The second soil is a mixture of 85% (by weight) kaolinite and 15% Bentonite. According to the Unified Soil Classification System, the group symbols for kaolinite is CL (lean clay) and the kaolinite-bentonite mixture is CH (fat clay). The properties of the two soils are summarized in Table 3.1. Copper (II) chloride dihydrate ($CuCl_2 \cdot 2H_2O$) was selected to artificially contaminate the slurries.

4.3.2 Experiment Equipment

4.3.2.1 One-dimensional test column

Two identical cylindrical electrokinetic columns were designed and manufactured for this study. The column, 300 mm long and 125 mm in diameter, was made from a 6 mm thick transparent Plexiglas tube (see Figure 4.4). The base of the column consisted of 115 mm in diameter and 35 mm long chamber. A valve was fixed to the bottom of the base. The column and the chamber were tied to 3 steel legs 150 mm in length. Three ports that can accommodate voltage probes were mounted on the wall of the column. A scale was glued along the wall of the column to monitor the mudline movement. Two identical perforated graphite electrodes, 6 mm thick, were cut to the diameter of the cell. One electrode was fitted with a geotextile filter into the bottom chamber and the other were attached to a Styrofoam block and floated on the slurry during the test. Figure 4.5 shows the dewatering phase of the test.

4.3.2.2 Two-dimensional test column (configuration-A)

A novel electrodes configuration (configuration-A) was used in the electrokinetic cell described in Section 4.3.2.1. A graphite electrode was cut to the diameter of the cell (125 mm) as the cathode. A 3 mm diameter coated steel bar was fixed into the centre of the cathode. The coated bar connected to 10 mm thick graphite anode with dimensions of 20 × 20 mm. Figure 4.6 shows schematic diagram of the configuration.

4.3.2.3 Two-dimensional tank

A rectangular tank, 270 × 230 × 280 mm (Length × Width × Height) constructed from 6 mm thick Plexiglas was used for the tests with 2-D electrode configuration (see Figure 4.7). The tank was scaled vertically in order to monitor the settlement height during the test. Five graphite bars, were used as electrodes. Four bars, each 230 mm long × 20 mm wide × 5 mm thick, were placed at equal distance to cover the surface area of the tank (270 × 230 mm) and served as a cathodes. The four bars were assembled with a Styrofoam block to be floated during the settlement. The fifth bar, 270 mm in length × 20 mm in width × 5 mm in thickness, was placed at the bottom of the tank centred to the cathode bars and served as the anode.

4.3.2.4 Laboratory devices

The laboratory instruments described in Section 4.2.2.2 were used

4.3.2.5 Squeezer-cell

Soil pore fluid squeezer cell was manufactured to recover the pore fluid of the wet soil. The cell consists of a steel chamber with inner dimension of 50 mm diameter and 100 mm length, drainage base, and steel piston. Porous plate with filter paper is placed on a grove in the base.

4.3.2.6 Solar cell panels

A solar panel (NT-175U1) was used as the model for stand-alone solar system. The solar cells panel dimensions are 1590 mm× 820 mm, (Figure 4.8), and the peak outputs of the panel are 44 V, 4.27 A and 175 Wh. The longitude and latitude of Thunder Bay, Ontario, where the tests were conducted, are 89°14' W and 48°24' N. The cell panel was mounted on wooden frame at an angle 48° to the horizontal for optimum exposure and placed in a fenced yard open to the sky.

4.3.2.6.1 Solar cell power simulation

The output from the solar panel was recorded from sunrise to sunset for one day during winter time. The voltage output was read in 15 minute intervals during the first hour after sunrise and last hour before sunset due to the rapid change in the output. During the constant daylight hours the output was recorded every hour. The voltage was recorded for a total of 9.25 h. Figure 4.9 shows the voltage distribution. A logical sequence of voltages was comprised to reflect the average voltages found throughout the day starting with 20.2 volts then go to the maximum voltage 44.4 V before it goes down again to 15.6 V. Figure 4.9 shows the solar panel voltage output during a winter day time.

4.3.3 Testing Procedure

4.3.3.1 Slurry preparation

The slurry was prepared by thoroughly mixing predetermined amounts of dry soil, tap water and copper (II) chloride dihydrate using a mechanical mixer. The solids

concentrations (mass of dry soil/ mass of water) used in the study were 10, 15, 20 and 25%. The copper concentration in the kaolinite slurry was 400 mg of copper per kg of dry soil. In the kaolinite-bentonite slurry, the concentration was 800 mg of copper per kg of dry soil. The slurry was kept in covered container for 48 h prior to the test to allow adsorption of the copper by the clay. Table 4.1 shows the slurry mixtures content.

4.3.3.2 One-dimensional configuration

The 1-D tests were carried out in two phases. Phase-1 investigated electrokinetic sedimentation of contaminated slurry and phase-2 investigated the dewatering and decontamination of the contaminated sediment. The slurry was poured into the electrokinetic column with the valve in the base chamber closed. The electric field was immediately applied via the graphite electrodes with the bottom electrode serving as the anode and the top electrode as the cathode (phase-1). The height of clay/water interface (i.e. mudline) was monitored and recorded at time intervals of 0, 2, 4, 8, 15, 30, 60 min and then every 2 h along with the electric current. The sedimentation (i.e. phase-1) was considered completed when the height of the mudline remained the same for 4 h.

After the completion of the phase-1, the water above the mudline was removed. Some of the water was reserved for parametric testing. In phase-2 (dewatering) the polarity of electrodes was reversed with the top electrode serving as the anode and the bottom electrode as the cathode. The valve on the base chamber was kept open during phase 2. The voltage, electric current and volume of water collected were monitored and recorded. An identical control test was carried without electric field for both phases 1 and 2 to provided base line data for comparison. The voltage was adjusted during both

phases of the test to simulate the outputs solar panel (see Section 4.3.2.6.1). Table 4.2 shows the titles of the tests conducted.

4.3.3.3 Two-dimensional configuration-A

Electrokinetic sedimentation tests were carried using a novel 2-D configuration. The electrokinetic column was used to conduct the tests following the same procedure used in the 1-D tests. Table 4.2 shows the titles of the tests conducted.

4.3.3.4 Two-dimensional configuration-B

The kaolinite-bentonite slurries were tested using a bigger scale with a novel 2-D configuration. The electrokinetic cell in Section 4.3.2.3 (see Figure 4.7) was used to perform the tests. The slurry was poured into the tank. The electric field was directly applied via the four graphite electrodes bars with the bottom electrode serving as the anode and the top electrode as the cathode. A maximum voltage of 44 V similar to that of the 1-D test was applied. The mudline was monitored and recorded at time intervals of 0, 2, 4, 8, 15, 30, 60 min and then every 2 h along with the electric current. The sedimentation was considered completed when the height of the mudline remained the same for 4 h. Table 4.2 shows the titles of the tests conducted.

4.3.4 Data Collection and Testing

In the 1-D tests, after the sedimentation phase (phase 1), water samples were collected above the mudline. Using the multi 340i-WTW set, the water samples were tested for pH. The copper concentration was determined using ICP-OES. After completing the

second phase, the treated soil was divided into two equal sections. The soil in each section was tested for pH, water content and the copper content. Part of the soil was used to recover a pore fluid sample using the squeezing cell described in Section 4.3.2.5. The pore fluid was tested for pH and copper concentration. The rest of the soil was air-dried for 72 h, ground and then used to determine the total copper concentration. A 2.2 g of the dry soil was mixed with 11 mL of the concentrated Nitric acid (HNO_3). The mixture was agitated for 12 h using a digital table shaker at 150 rpm. Afterward, the mixture was centrifuged for 20 min at 4000 rpm. The supernatant was diluted then sent to be tested by ICP-OES.

Table 4.1 Slurry mixtures contents

Slurry Type	Solid Concentration	Water in 10 kg of Slurry (kg)	Solid Mass in 10 kg of slurry (kg)	Copper II Chloride in 10 kg of slurry (g)
Kaolinite (spiked with400 mg copper /kg dry soil)	10%	9	1	1.07
	15%	8.5	1.5	1.62
	20%	8	2	2.15
	25%	7.5	2.5	2.69
85% Kaolinite + 15% Bentonite (spiked with 800 mg/ kg dry copper)	10%	9	(0.850 kaolinite + 0.150 Bentonite)	2.15
	15%	8.5	(1.275 kaolinite + 0.225 Bentonite)	3.22
	20%	8	(1.700 kaolinite + 0.300 Bentonite)	4.30
	25%	7.5	(2.125 kaolinite + 0.375 Bentonite)	5.38

Table 4.2 Summary of tests carried out in part 2 of the study.

Slurry Type	Initial solid concentration	Test Title	Electrodes Configuration
Kaolinite	10%	C-10K	Control test (0 V)
		EK-10K	One dimensional
		EKA -10K	Configuration-A
	15%	C-15K	Control test (0 V)
		EK-15K	One dimensional
		EKA-15K	Configuration-A
	20%	C-20K	Control test (0 V)
		EK-20K	One dimensional
		EKA-20K	Configuration-A
	25%	C-25K	Control test (0 V)
		EK-25K	One dimensional
		EKA-25K	Configuration-A
85%Kaolinite-15%Bentonite	10%	C-10B	Control test (0 V)
		EK-10B	One dimensional
		EKA-10B	Configuration-A
		EKB-10B	Configuration-B
	15%	C-15B	Control test (0 V)
		EK-15B	One dimensional
		EKA-15B	Configuration-A
		EKB-15B	Configuration-B
	20%	C-20B	Control test (0 V)
		EK-20B	One dimensional
		EKA-20B	Configuration-A
		EKB-20B	Configuration-B
	25%	C-25B	Control test (0 V)
		EK-25B	One dimensional
		EKA-25B	Configuration-A
		EKB-25B	Configuration-B

EK: electrokinetic

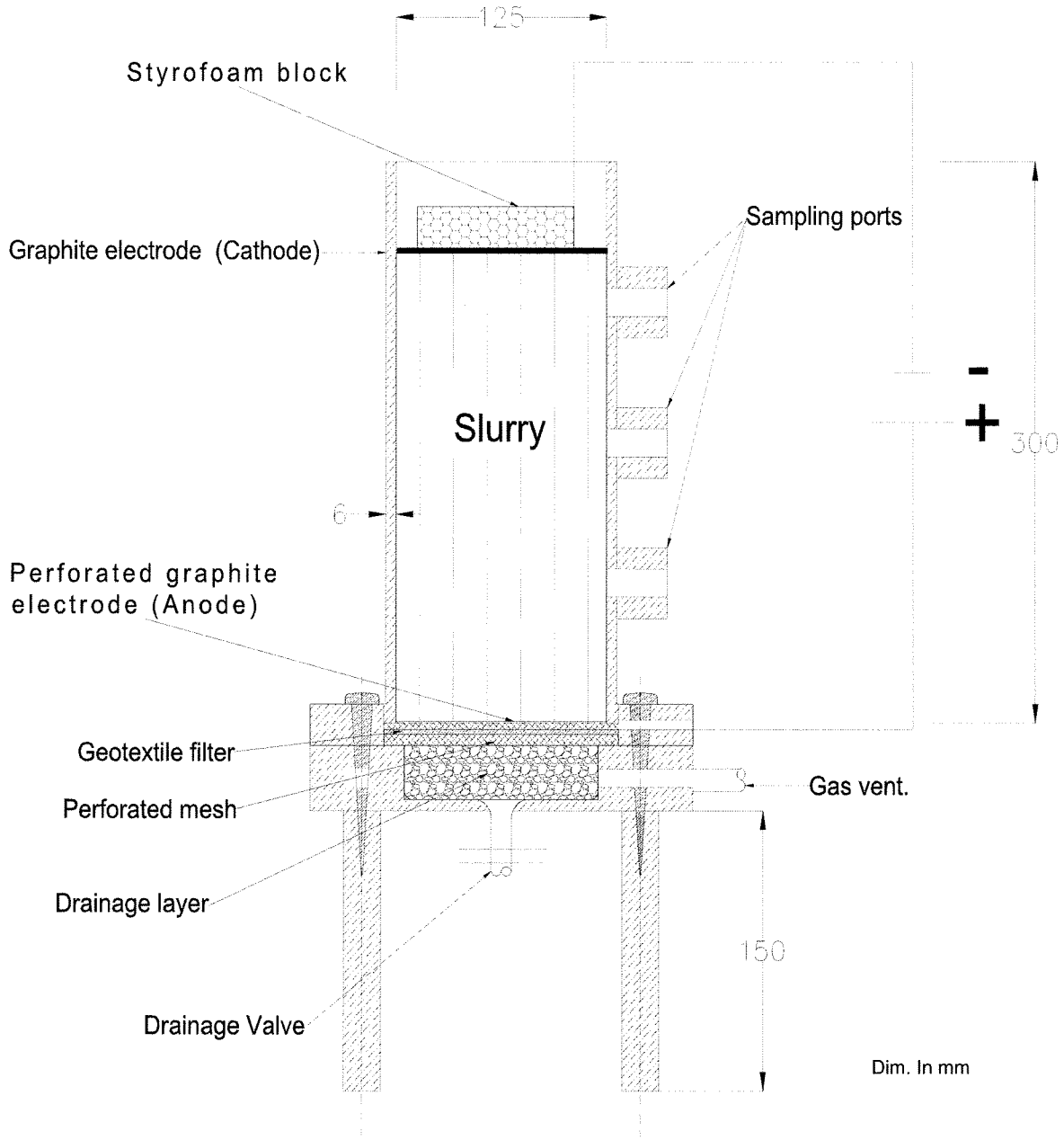

Figure 4.4 Schematic of electrokinetic column - sedimentation setup.

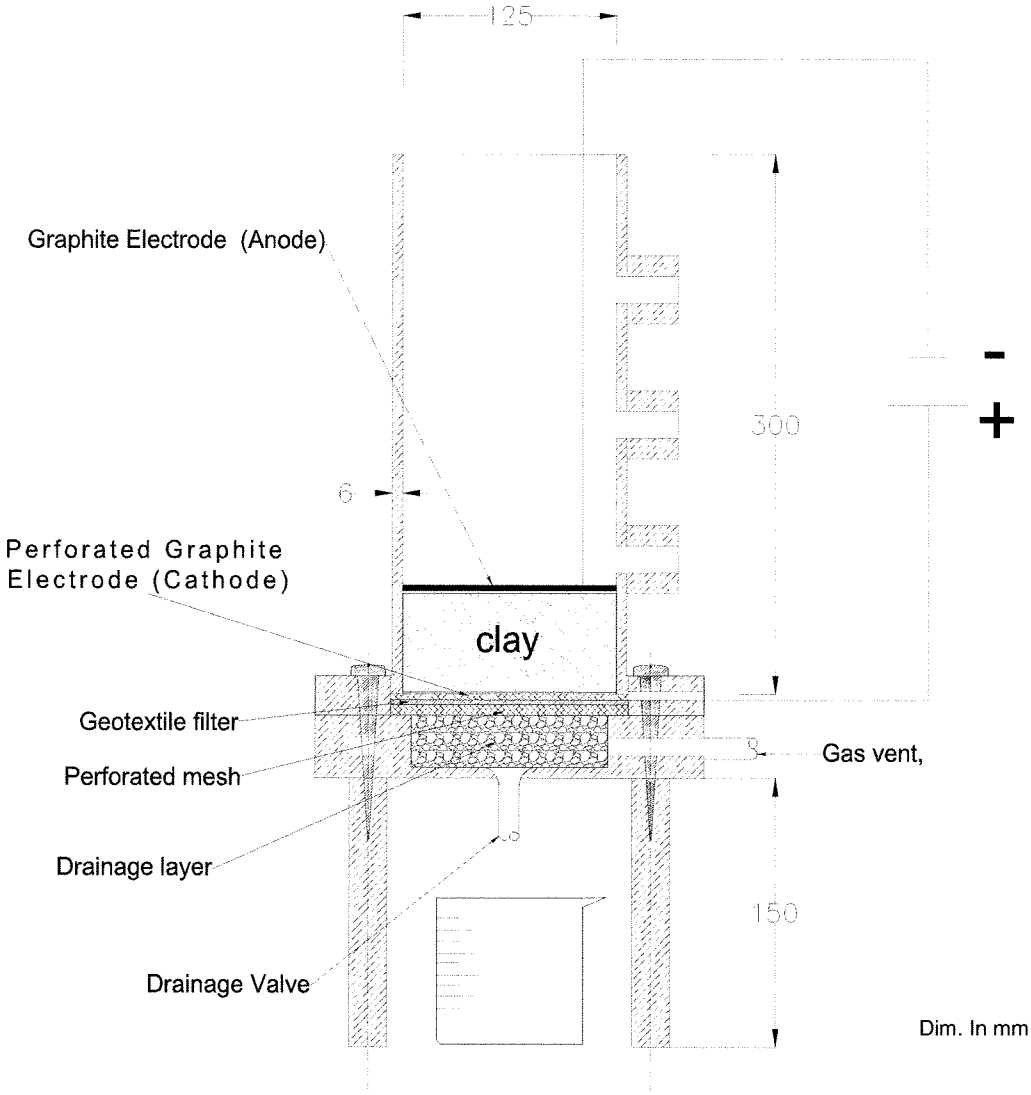

Figure 4.5 Schematic of electrokinetic column - dewatering setup.

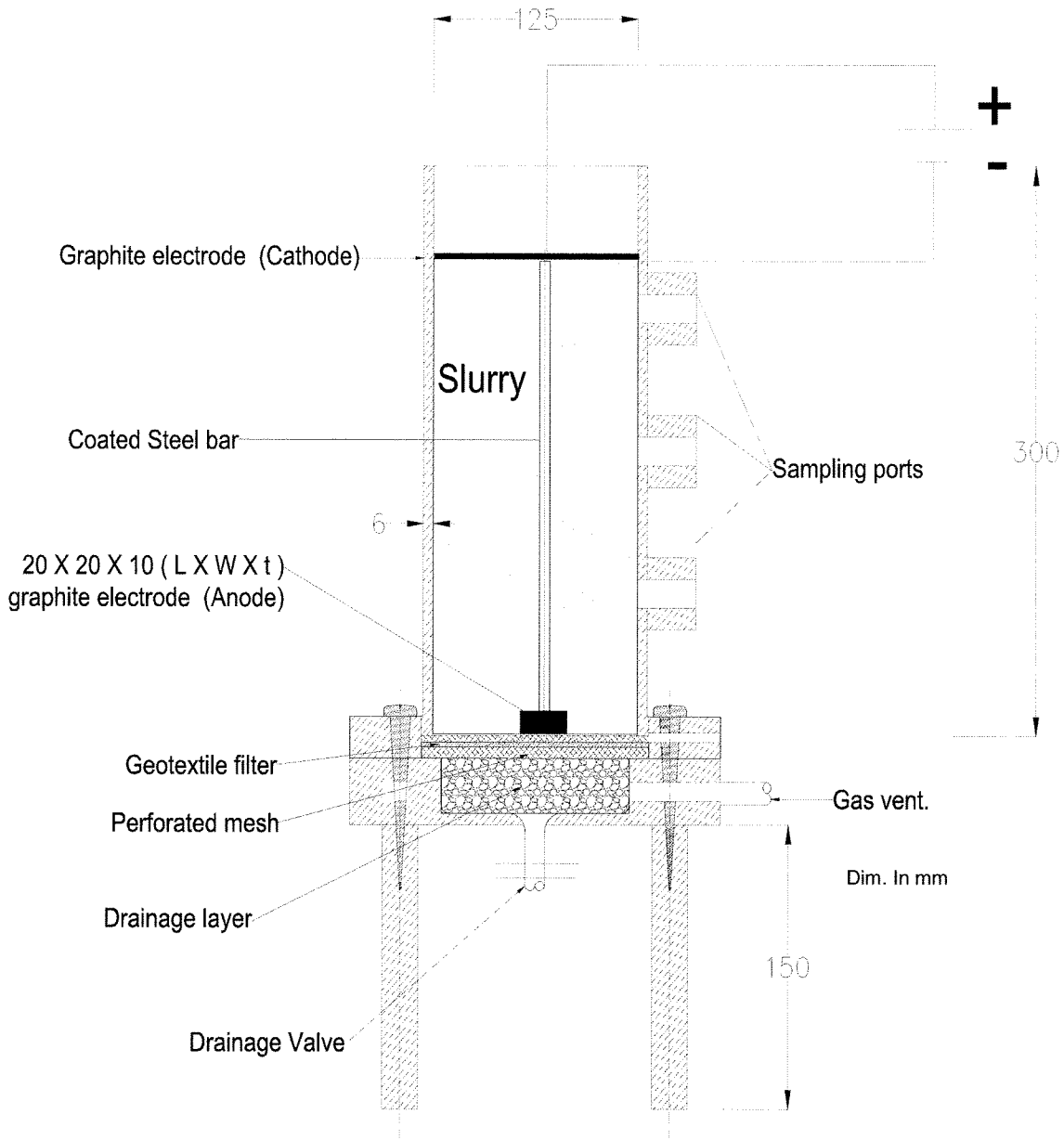

Figure 4.6 Schematic of two-dimensional sedimentation - configuration-A.

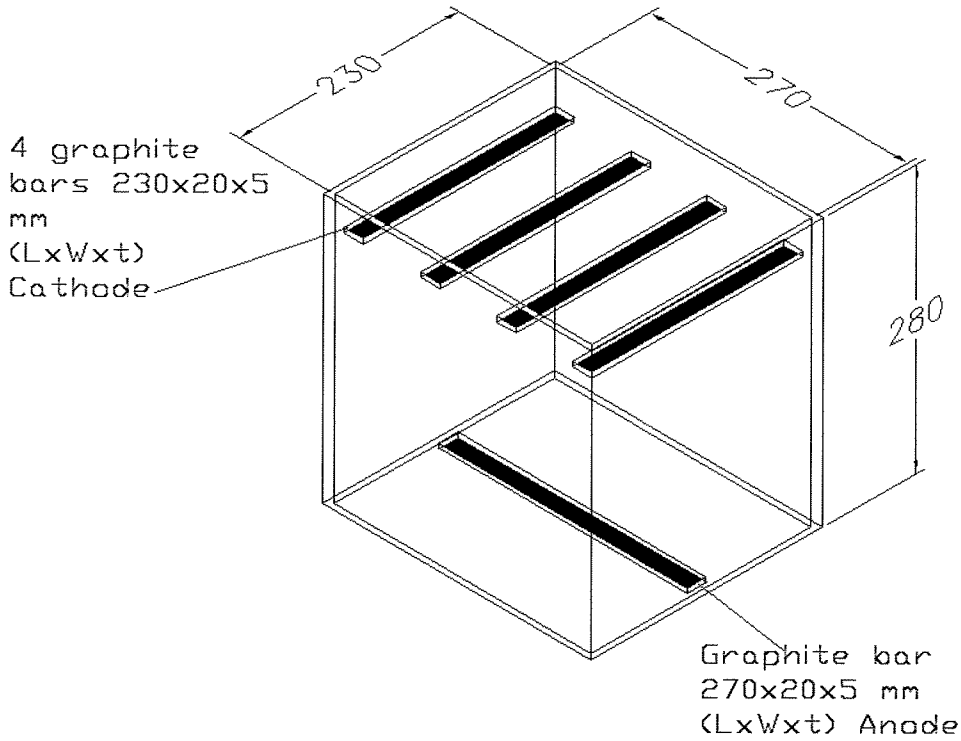

Figure 4.7 Schematic of two-dimensional sedimentation test - configuration-B.

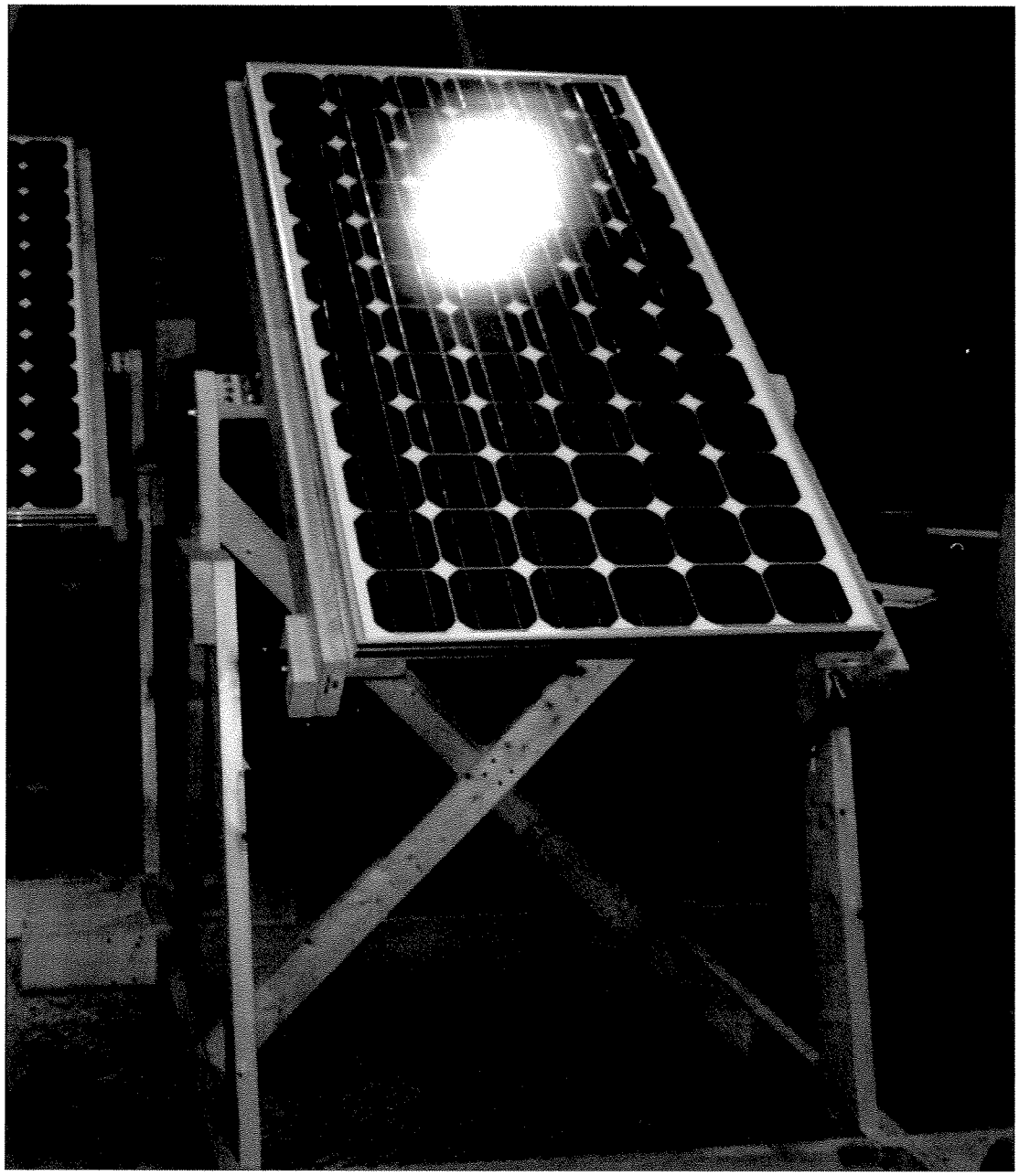

Figure 4.8 Solar cells panel.

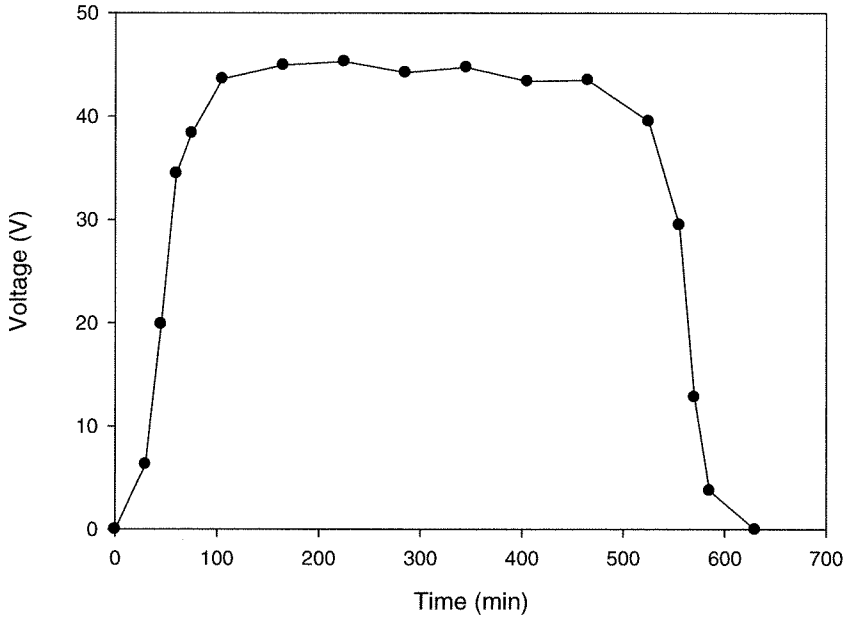

Figure 4.9 Voltage output of the solar cell during a winter day (14/01/2011).

CHAPTER FIVE

RESULTS: INTEGRATED SOLAR POWERED ELECTROKINETIC BARRIER

5.1 INTRODUCTION

Electrokinetics requires only low-level of direct electric current. An electrokinetic barrier can prevent the movement of contaminations into adjacent clean land by utilizing electro-osmosis, electro-migration and electrolysis reactions (Lynch et al., 2007). In remote areas with no active power lines, solar energy is an attractive option to provide sufficient electric field for electrokinetics. In this study, solar cells were proposed to generate the electric field required to prevent/minimize migration of heavy metals through the soil. Low pH water containing copper was used to simulate acid mine drainage. This chapter presents the results and discusses the efficiency of a stand-alone solar system as source of power for an electrokinetic barrier with one and two-dimensional configurations as discussed in Chapter Four. Computer modeling for the electric filed of the two-dimensional configuration was performed using a finite element software (QUICKFIELD^{TM}, Tera Analysis Ltd., 2011). Accordingly, optimization of the electrodes arrangement is discussed.

5.2 TEST PROCEDURE

Four identical electrokinetic cells were used to conduct the experiments. The procedure described in Section 4.2.3 was followed. A control test was carried out without an

electric field and the effluent water was monitored and recorded. Samples were taken from the effluent water every 500 mL. Based on the time required to collect just over 1 pore volume (1750 mL) in the control test (about 192 h), four tests were performed with an applied voltage of 10 V. Two of the tests were carried under one-dimensional (1-D) electric field configuration and the other two with two-dimensional (2-D) configuration (see Figures 4.2 and 4.3). For each configuration, the 10 V were applied continuously in one test (continuous-powered test) and only during the daytime in the other test (solar-powered test). During the electrokinetic test, the pH of the contaminated water (upstream) was monitored and adjusted to 2 when required. The effluent of each test was collected and tested for copper concentration and pH. At the end of the control test, soil samples were taken from two different locations for testing the residual copper concentration in the soil. In the 1-D configuration test, the soil specimen was extracted from the cell and divided into 4 equal sections. The soil from each section was thoroughly mixed and then air-dried and grounded before used for copper concentration testing. At the end of the 2-D test, the soil specimen was extruded and sectioned into 12 parts (see Chapter Four). Each part was air-dried, grounded, assorted and reserved for sampling and testing. Each of the 12 parts was tested for the total copper content in the soil, the copper content in the pore fluid, and the pH of the soil. The copper in the pore fluid was recovered by adding 5 mL of deionized water to 2 grams of air dried soil. For the total copper content in the soil the procedure described in Chapter Four was followed. The pH was measured by mixing 5 g of dry soil with 10 mL of deionized water.

5.3 RESULTS AND DISCUSSION

The control test was used to simulate the advancement of copper contamination through a soil in the absent of a barrier system. Solar-powered and the continuous-powered electrokinetic barrier tests were compared with the control test. Optimization of the electrodes arrangement is discussed in terms of electric field intensity simulated using QUICKFILED^{TM} (Tera Analysis Ltd., 2011).

5.3.1 One-Dimensional Configuration

5.3.1.1 Volume of effluent collected

Figure 5.1 shows the volume of water collected during the control test, 1-D electrokinetic solar-powered and 1-D electrokinetic continuous-powered tests. In the control test, 2000 mL were collected during 192 h. Through the same period, 660 mL (33% of the control effluent) were collected from the solar-powered test and only 40 mL (2%) from the continuous-powered test. In the solar-powered test, most of the effluent (90 %) was collected during the night time (i.e. period of zero applied voltage) and only very small portion of the effluent (10%) was collected during the day (applied voltage of 10 V) electric. The much lower volume of water collected in the electrokinetic tests clearly indicates that electro-osmotic flow was successful in countering the hydraulic flow.

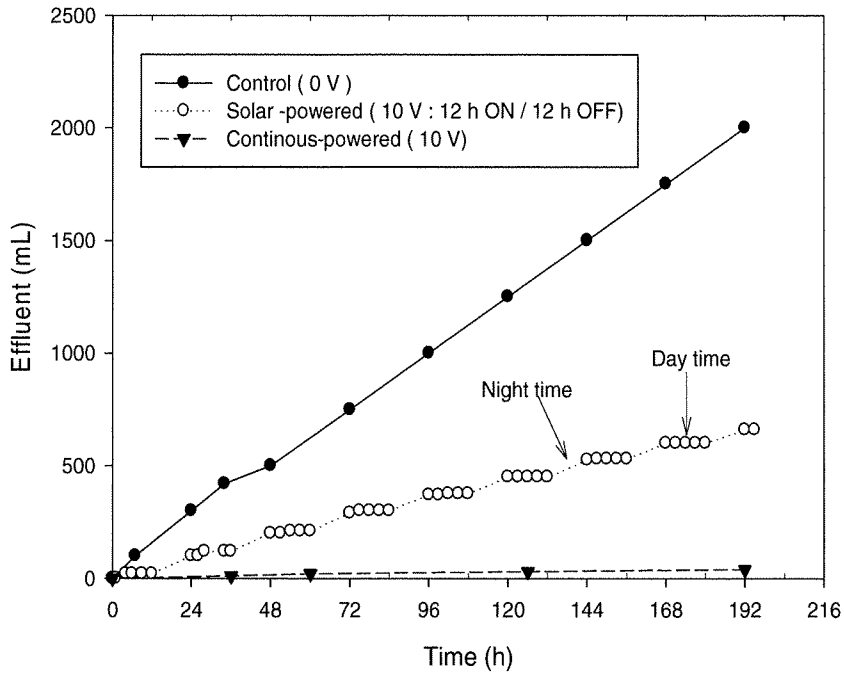

Figure 5.1 Cumulative volume of the effluents during the 1-D tests.

5.3.1.2 Electric current

Figure 5.2 shows the voltage and the electric current during the 1-D continuous-powered test. The electric current started around 10 mA and slightly decreased during the early hours of the test. The current then gradually increased and reached a peak of 38 mA about 80 h from the start of the test. After the peak, the current gradually decreased and reached 12 mA at the end of the test. The change in electric current with time, as shown in Figures 5.2, resulted from the change in electrical conductivity of the soil during the test. The bulk electrical conductivity of a soil mass is a byproduct of the conductivity of the pore fluid and the soil solids. In general, the pore fluid is more conductive than the solids and thereby dominates the conductivity of the soil. During the first half of the test, the conductivity of the pore fluid was increasing as the copper concentration in the pore fluid was increasing due to chemical diffusion and advection. However, the advancement of the copper was countered by electro-osmosis and

electro-migration and as the advancement was ceased, the electrical conductivity of the soil and subsequently the electric current started to decrease. The changes in electrical conductivity and electrical current during an electrokinetic processes were also observed by other researchers (e.g. Narasimhan and Ranjan, 2000; Mohamedelhassan and Shang, 2003).

Figure 5.3 shows the voltage and the electric current during the 1-D solar-powered test. The peak voltage during day time was 10 V (electric field intensity of 50 V/m) and 0 during the night. The corresponding current started with 11 mA and then increased after 24 h to 50 mA. Figure 5.3 shows that for each day during the test, the highest current was reported at the start of the day and the lowest at the end of the day. Since the test was solar-powered, most of the transport of copper in the soil by diffusion and advection would occur during the period without electric field (i.e. during the night time). Subsequently, the highest electrical conductivity of the soil was at the end of the night time. Therefore, as the electric power was turned-on, the soil had the highest electrical conductivity and thereby the highest electric current was observed. The total energy consumption was 37.8 Wh in the continuous-powered test compared to 34.8 Wh in the solar-powered test.

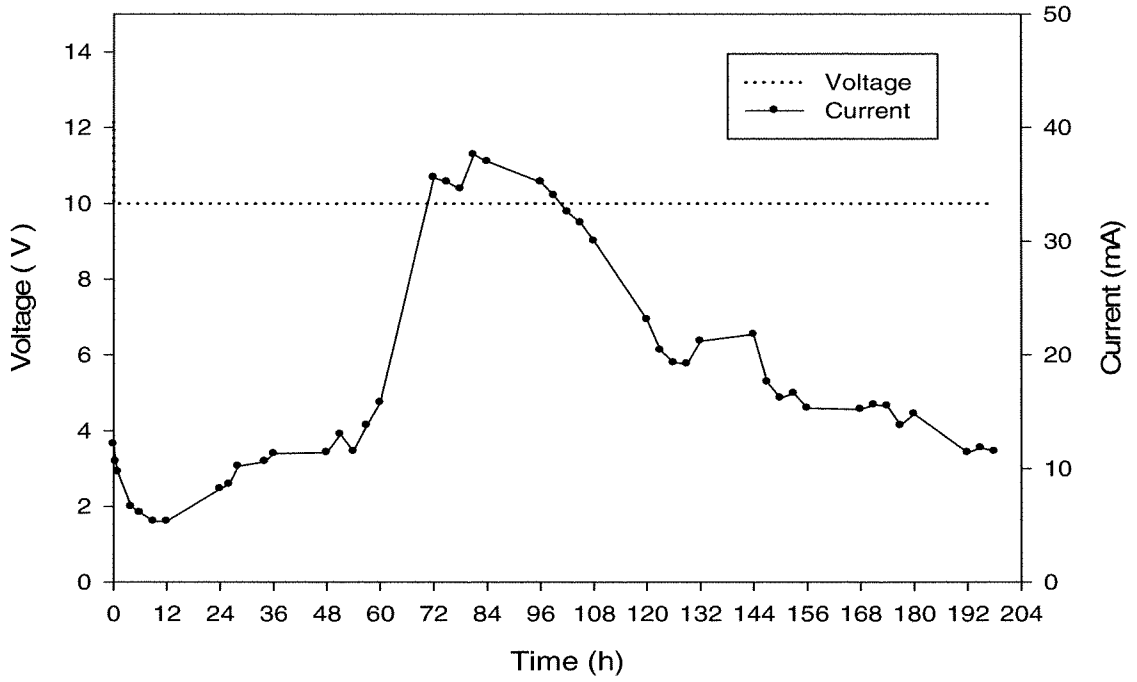

Figure 5.2 Applied voltage and electric current vs. time for continuous-powered test.

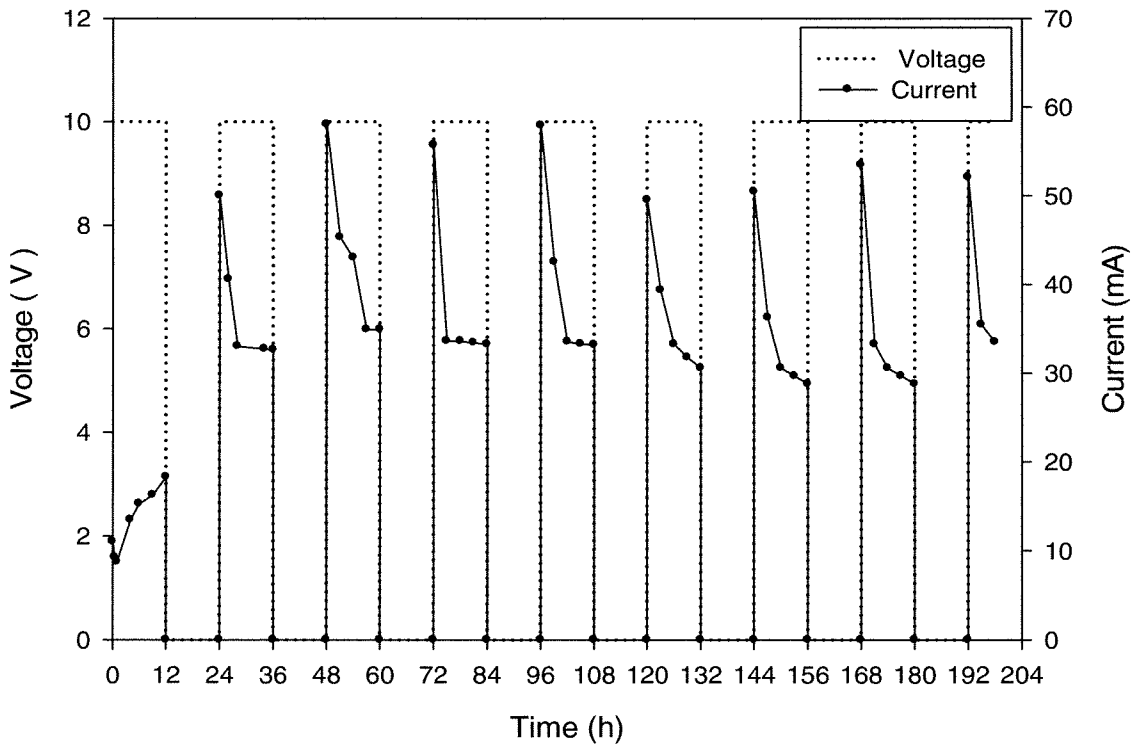

Figure 5.3 Applied voltage and electric current vs. time for solar-powered test.

5.3.1.3 pH profile in the soil at the end of the test

Figure 5.4 shows the pH profile of the control, continuous-powered and solar-powered tests. The initial pH of the soil was 7.5 and the pH of the influent copper solution was 2. The final pH of the soil in the control test decreased to 4.9 as the pore fluid of the soil was replaced by the copper solution. As shown in Figure 5.4, in the electrokinetic barrier tests, the pH was dependent on the distance from the electrode and the pH values of the continuous-powered test were in general slightly higher than the values of the solar-powered test. In agreement with electrolysis reactions at the electrodes, the highest pH values were found near the cathode and the lowest near the anode. Figure 5.4 shows that the lowest pH in the electrokinetic barrier tests (near the anode) was approximately similar to that of the control test. In general, as the pH increases, the capacity of the soil to retain heavy metals increases and subsequently the advancement of heavy metals through the soil is hindered and vice versa. The results showed that electrokinetic increased the capacity of the soil to retain heavy metals near the cathode as the pH increased from 4.9 in the control to 8.2 and 8.8 in the electrokinetic barrier tests. Even near the anode, the results showed the pH in electrokinetic barrier tests were similar to that in the control test despite the electrolysis reactions.

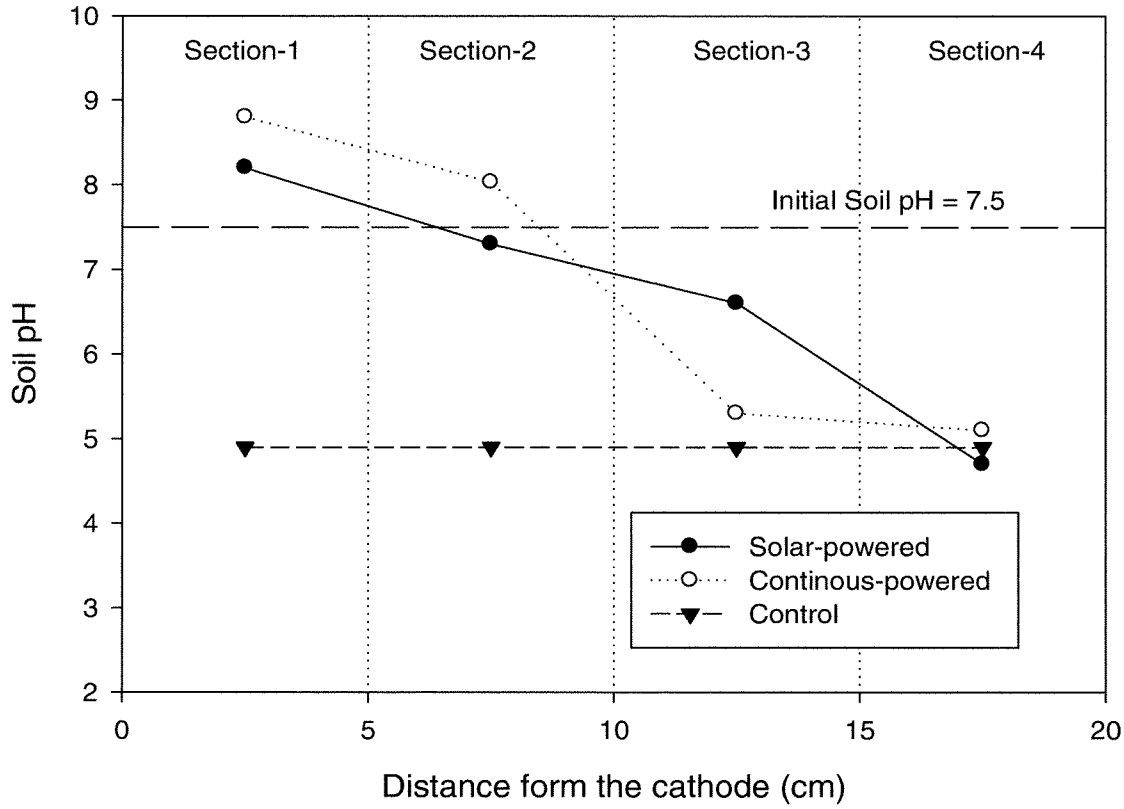

Figure 5.4 pH of the soil sections at the end of the 1-D tests.

5.3.1.4 Copper migration

In this section, the copper migration concentration at the end of tests are presented and discussed.

5.3.1.4.1 Control test

Figure 5.5 shows the copper concentration of the effluent concentration, the effluent to the influent ratio and pH during the control test. The test was terminated after a 1.14 pore volume (2000 mL) of effluent was collected. The figure shows that the concentration ratio of the effluent increased and the pH decreased with the pore volume. The figure also shows that 50% of the influent copper concentration was found at 0.8 pore volume (1400 mL) of the effluent. The observed copper prior to 1 pore

volume was primarily due to chemical diffusion and short flow paths. This presence of copper also indicates that the retardation factor of the soil was limited (i.e. adsorption by soil was low). This was to be expected as 80% of the soil was sand and the pH of the influent was kept at 2. Figure 5.6 shows the average of copper concentration of two representative locations in the soil specimen at the end of the control test. Approximately, 80% of the copper in the soil was found in the pore fluid and 20% was adsorbed by the soil solids. It must be noted that copper in the pore fluid is readily available to further advance into the soil downstream of the source. It is obvious that the soil barrier in the control test was unsuccessful in combating the advancement of the copper.

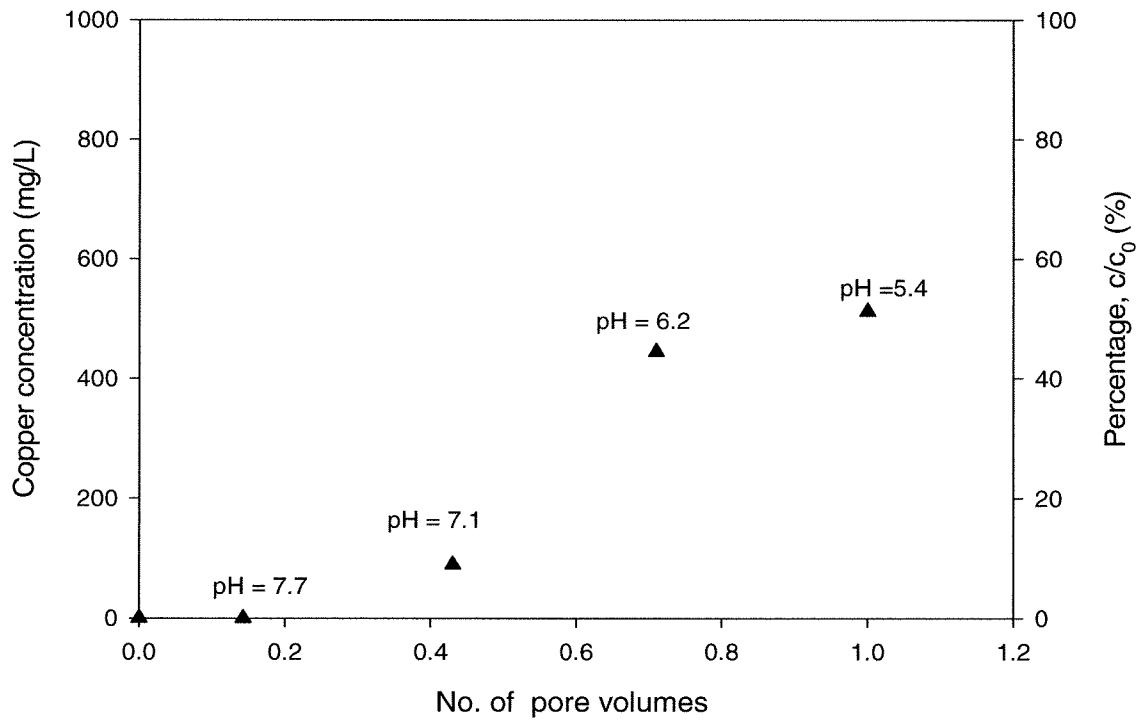

Figure 5.5 Copper concentrations and pH of the control test effluent (samples tested every 500 mL).

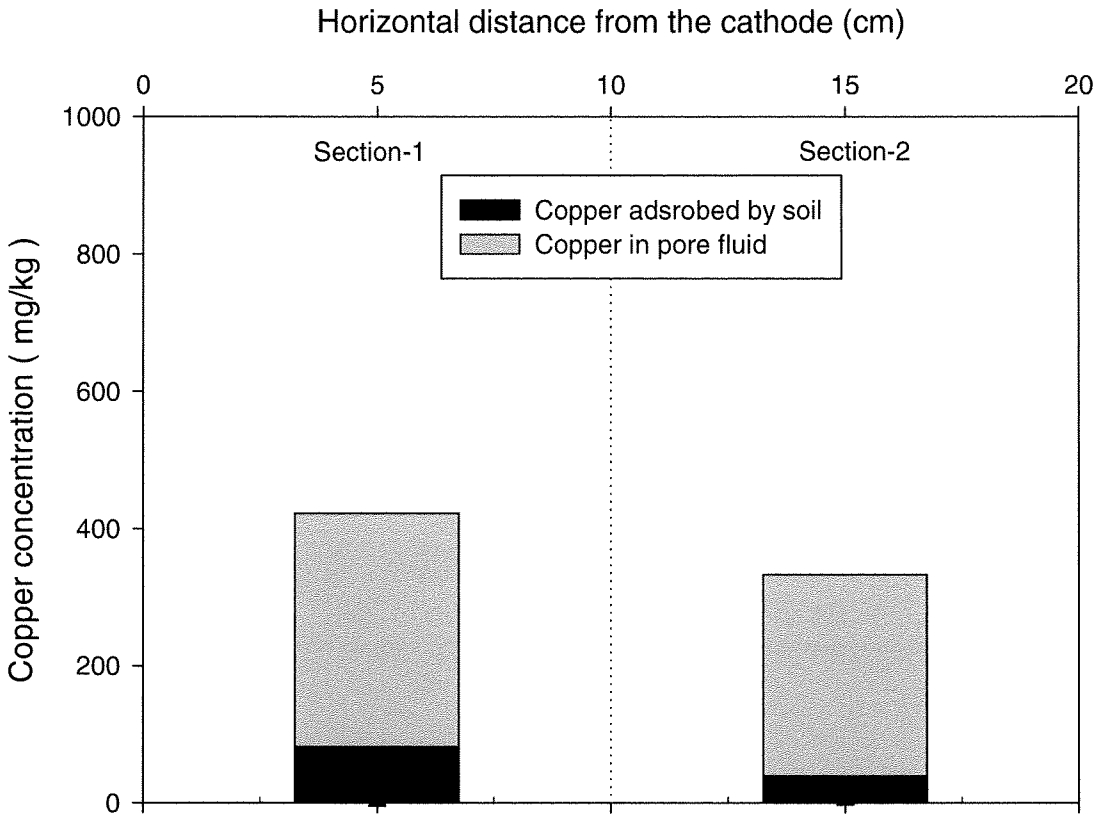

Figure 5.6 Copper concentration at the end of the control test.

5.3.1.4.2 Continuous-powered test

In the continuous-powered test, only 40 mL of effluent was collected at the end of the 192 h duration of the test. The pH of the effluent was 1.8 and the copper concentration was only 0.2 mg/L, representing a negligible 0.02% of the influent concentration compared to 54% in the control test. The low pH effluent resulted from the electrolysis reactions and production of hydrogen ions at the anode. Figure 5.7 shows the copper concentration in four sections of the soil specimen at the end of the test. The total copper in the soil is presented for the portion adsorbed by the soil solids and the portion free in the pore fluid. Figure 5.7 illustrates the ability of electrokinetic barrier to combat the copper movement and increase the capacity of the soil to adsorb the copper. As shown in the figure, negligible copper was found in section 3 and 4. That is

electrokinetic barrier prevent the movement of copper to the soil sections downstream of the influent (sections 3 and 4). Figure 5.7 shows high concentrations of copper in sections 1 and 2 and almost all the copper was adsorbed by the soil solids. The increase copper adsorbent capacity of the soil shown in sections 1 and 2 resulted from the higher pH values in the two sections as shown in Figure 5.4. In this test, the negligible amount of copper in the effluent and the soil sections downstream (sections 3 and 4) coupled with an increased adsorbent capacity of soil near the influent illustrated that electrokinetic barrier was effective in combating the movement of copper. Slimier electrokinetic barriers were reported by Lynch et al. (2005) and Mohamedelhassan, (2011).

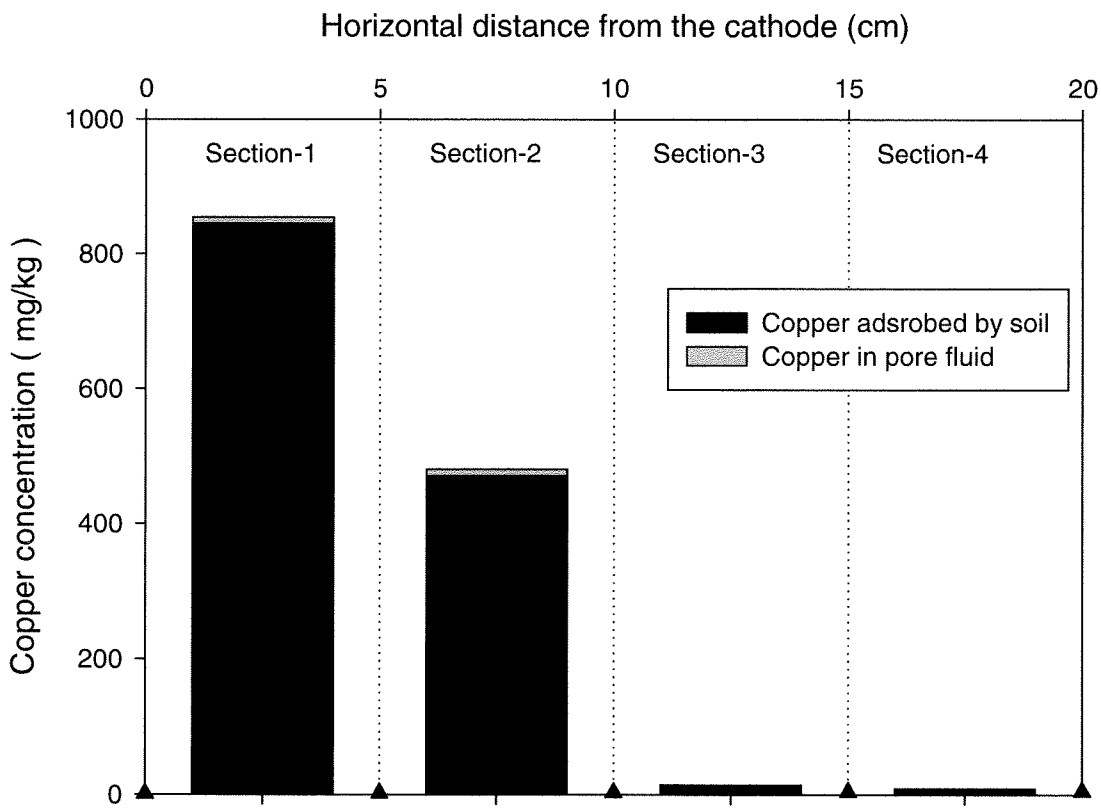

Figure 5.7 Copper Concentration at the end of the 1-D continuous-powered test.

5.3.1.4.3 Solar-powered test

As shown in Figure 5.1, 660 mL of effluent was collected by the end of the 192 h duration in the solar-powered test. The copper concentration in the effluent was 46 mg/L representing only 4.8% of the influent concentration and the pH was 2. The low pH of the effluent resulted from generated acidic front at the anode. Figure 5.8 shows the copper concentrations in the effluent of the three tests. As seen in the figure, while the copper concentration in the effluent was 54% of the influent at the end of the control test, only 4.8% of the influent concentration was found by the end of solar-powered test.

Figure 5.9 presents the total copper concentration in the four soil sections at the end of the solar-powered test. The copper adsorbed in soil solids were 531, 332, 108 and 36 mg/kg in sections 1, 2, 3 and 4, respectively. The corresponding copper concentrations in pore fluid were 63, 65, 25 and 40 mg/kg, respectively. Thus, in sections 1 and 2 and 3, most of the copper was adsorbed by the soil solids and therefore unavailable to be transported. In comparison with the control test, electrokinetics increased the adsorption capability of the soil near the influent by 550% and decreased the copper concentration in the pore fluid copper concentration. By increasing the capacity of the soil to adsorb copper and the deceasing the copper in the pore fluid, an electrokinetic barrier system can further combat the spread of copper pollution.

By comparing the effectiveness of the two electrokinetic barriers in terms of the copper concentration in the influent and the copper in the pore fluid, the continuous-powered barrier was superior to the solar-powered barrier. This was expected as the solar-

powered barrier received electric field during 50% of the testing time. However, the solar-powered barrier had significantly reduced the copper concentration in the effluent and in the soil pore fluid as compared with the control barrier. The results found in this study are analogous to results in former studies (e.g. Nowicki, 2005; Reeve, 2007 and Laden, 2008).

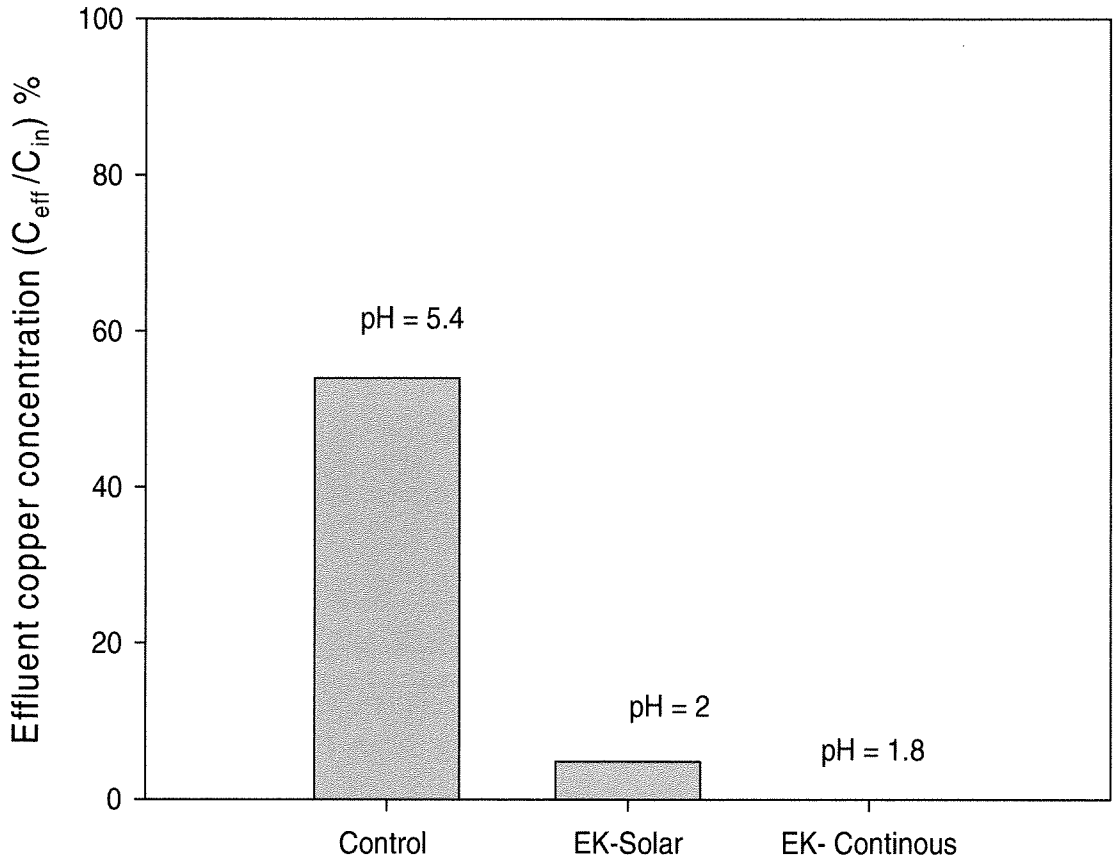

Figure 5.8 Effluents copper concentration at the end of the control, solar-powered and continuous-powered tests.

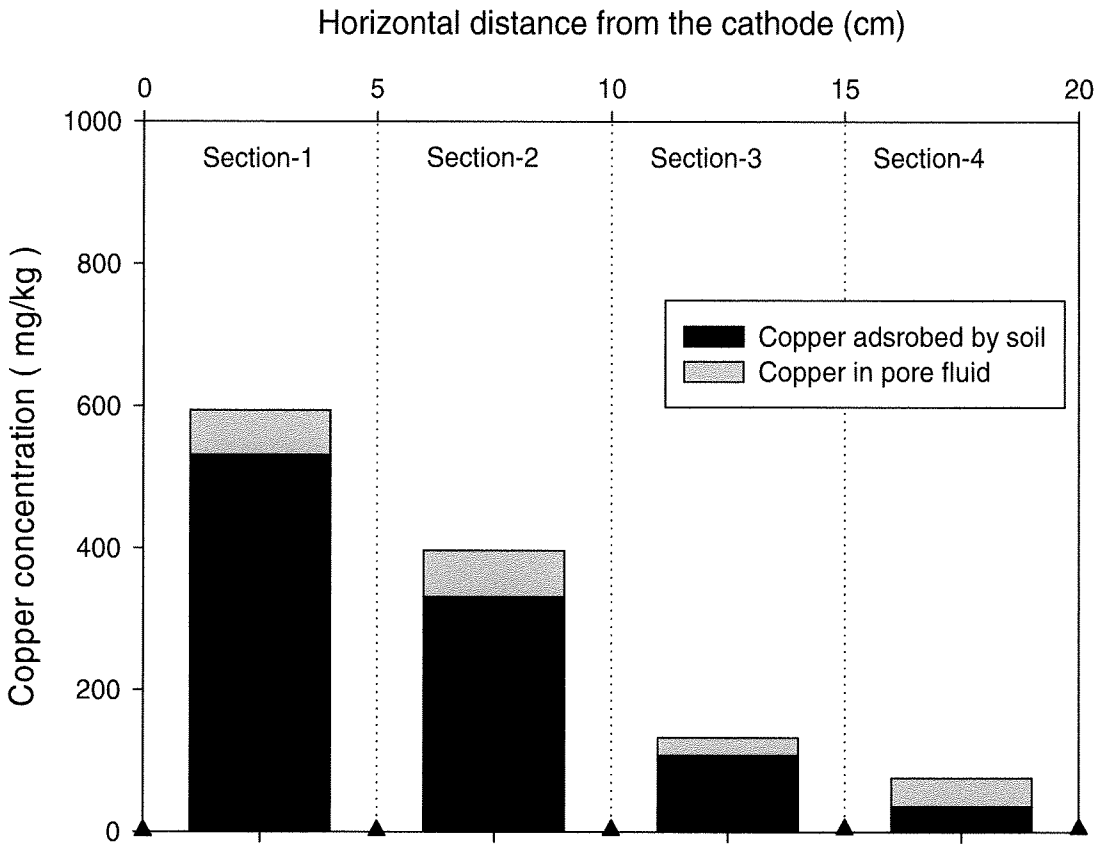

Figure 5.9 Copper concentration at the end of the 1-D solar-powered test.

5.3.2 Two-Dimensional Configuration

5.3.2.1 Volume of effluent collected

Figure 5.10 shows the cumulative volume of effluents for the control and the two-dimensional (2-D) solar-powered and continuous-powered electrokinetic tests during 192 h of testing. For the 2-D continuous-powered test, the effluent collected was 980 mL, 49% of the control and 0.56 the pore volume. Effluent of 1160 mL was collected from the solar-powered test (0.66 pore volume). Despite the increase in effluent collected compared with the 1-D tests, electro-osmosis with 2-D configuration was

successful in reducing the effluent flow as compared with the control. It is worth mentioning that the reduced effluent, 49% and 58% of the control, in the 2-D tests was induced by electrodes that covered only 8% of the area perpendicular to the direction of flow.

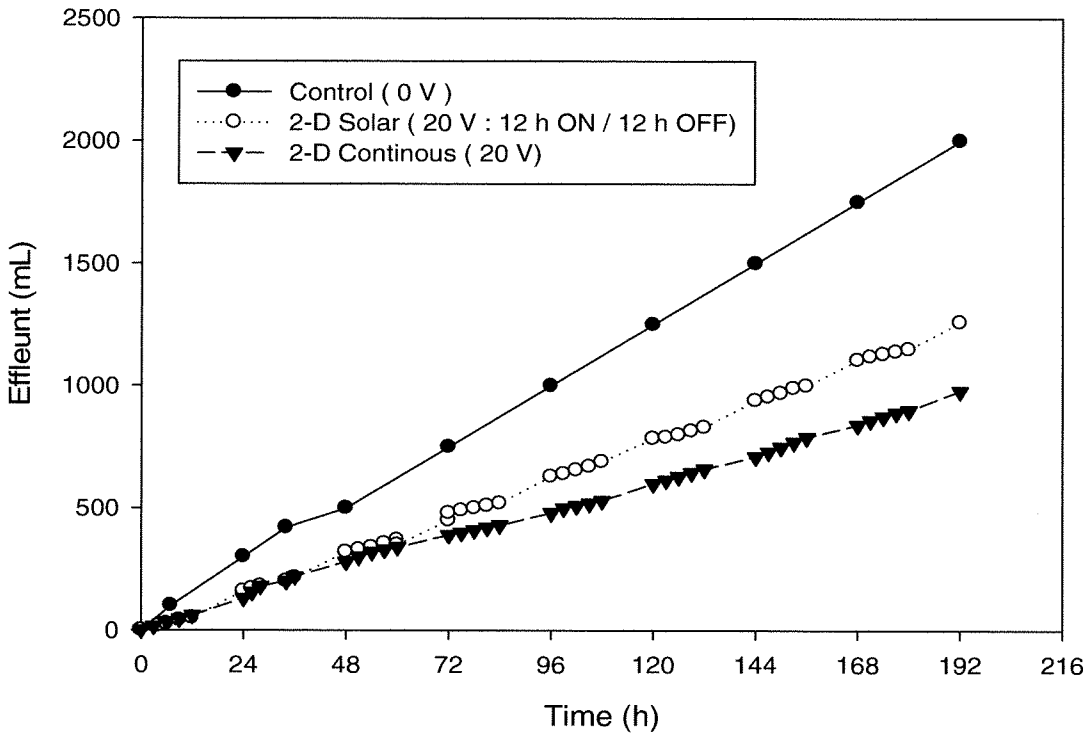

Figure 5.10 Cumulative volume of the effluents during the 2-D tests

5.3.2.2 Voltage and current

Figure 5.11 shows the voltage and the electric current during the test carried with 2-D continuous-powered. A 10 V where applied continuously during the test. The electric current was zero at the beginning and then increased with time and reached a peak of 24 mA about 72 h after the start of the test. The increase in the electric current with time resulted from the increase in electrical conductivity of the soil as the much more

conductive copper solution replaced the water in the soil pores. Progressively, the current sustained values of 23 to 20 mA until the end of the test, which indicated the existence of copper solution in the soil pores.

Figure 5.12 shows the voltage and the electric current during the 2-D solar-powered test. The electric current trend increased with time and reached a peak value of 27 mA and was 23 mA at the end of the test. The relatively higher current in the solar-powered test was caused by the higher electrical conductivity of the soil. The higher effluent was collected in the test means more pore fluid water was replaced by the much conductive copper solution and thereby a soil with higher electrical conductivity. The total energy consumption was 37.3 Wh for the continuous-powered test, while a 20 Wh was consumed at the solar-powered test.

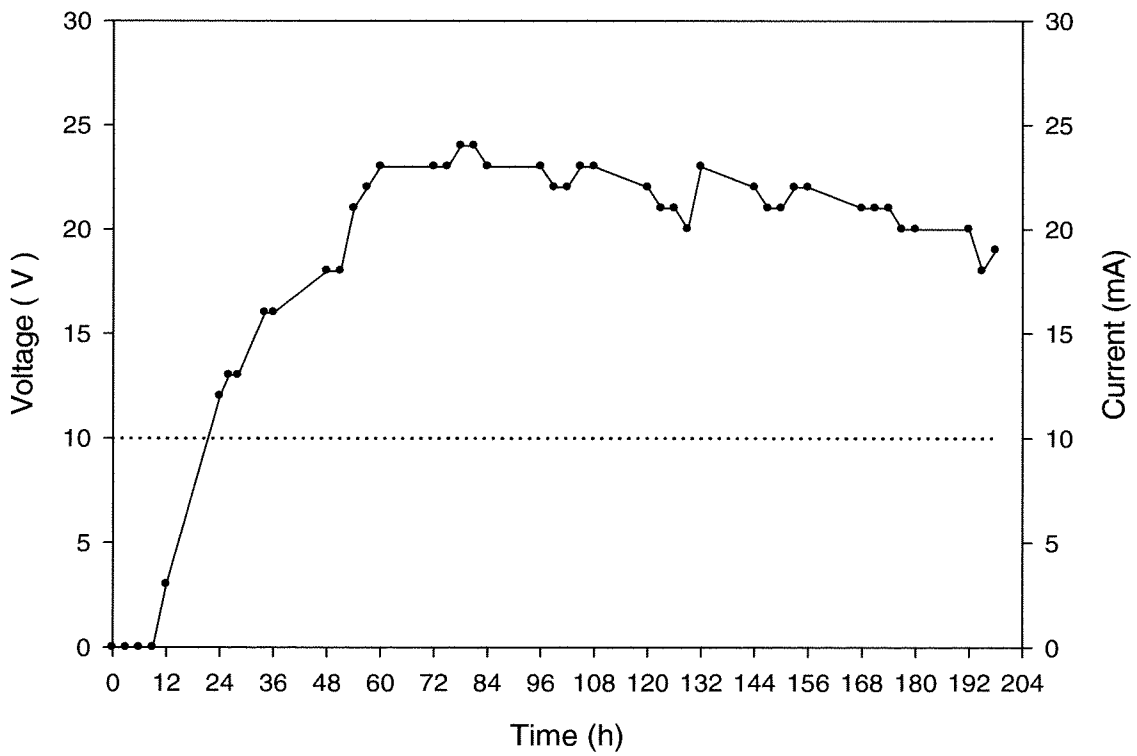

Figure 5.11 Applied voltage and electric current for the 2-D continuous-powered test.

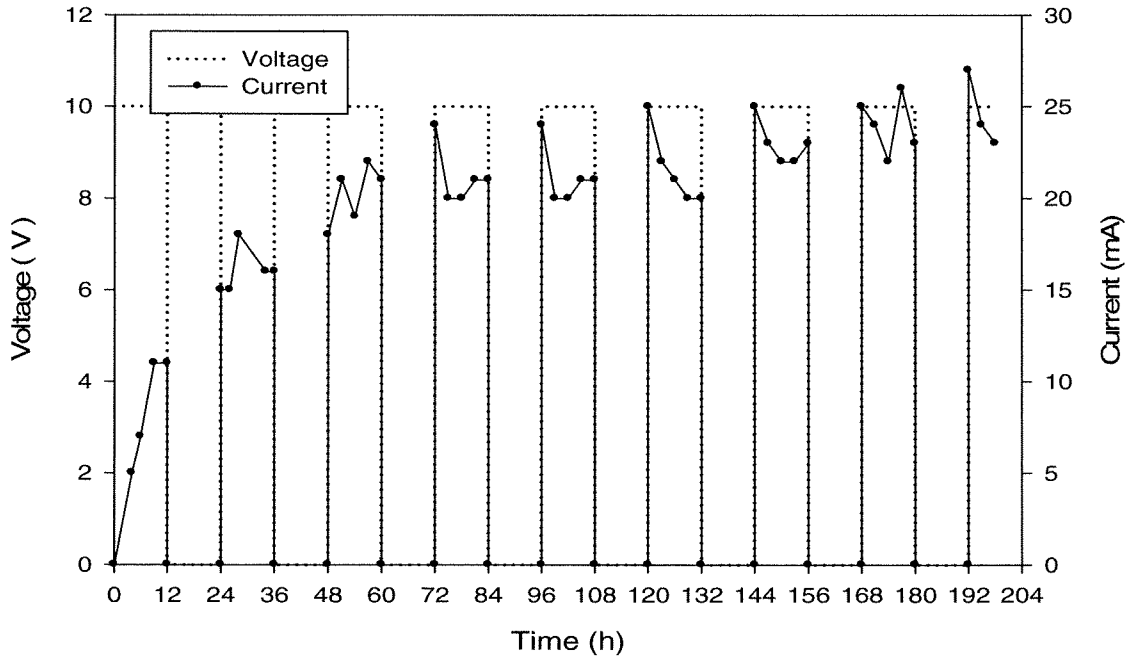

Figure 5.12 Applied voltage and electric current for 2-D solar-powered test.

5.3.2.2.1 Voltage and electric field intensity distribution for the two-dimensional configuration

Based on soil resistivity of 3 mS/cm (back calculated from the 1-D continuous-powered test), applied voltage of 10 V and two dimensional electrode configuration, the distributions of the voltage, U (V), and electric filed intensity, E, (V) were modeled using 2-D solver software QuickField™ (Tera Analysis Ltd, 2011). Figures 5.13.A and 5.13.B show U and E for the 2-D configuration. The voltage contour shows a maximum of 10 V at the anode and 0 at the cathode. As seen in Figure 5.13.A, the voltage contour lines were semi-elliptical near the electrodes and the voltage distribution was linear for most of the cell. Figure 5.13.B shows the minimum E values in the corners of the cell ranged between 0 to 10 V/m, while the maximum E (50 V/m) appears to act locally with semi-circular or semi-elliptical contours surrounding the electrodes. For the most of the cell,

E ranged between 30 and 40 V/m. Figure 5.13.C shows the voltage distribution at section A-A near the anode. As seen in the figure, 77% of the applied voltage was found near the cell walls. Figure 5.13.D shows the electric field intensity along at the centre of the electrokinetic cell. The average E is around 76% of the electric field intensity in the 1-D test (50 V/m).

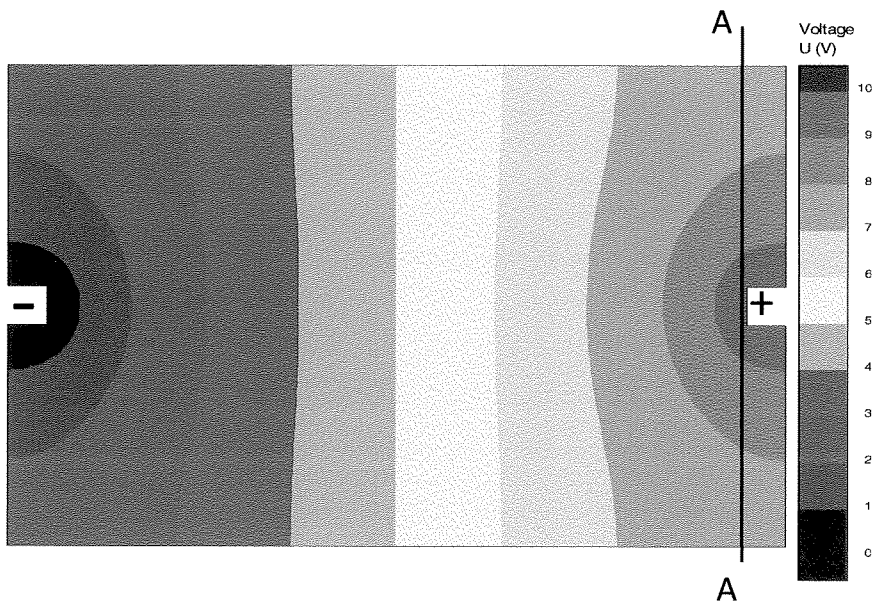

Figure 5.13.A Voltage distribution for the two-dimensional configuration (plan view).

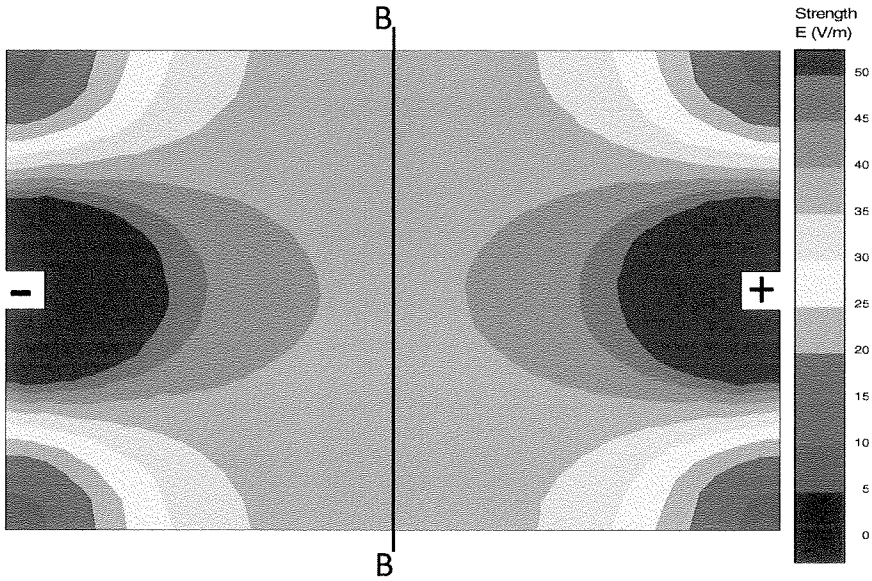

Figure 5.13.B Electric field intensity distribution for the two-dimensional configuration (plan view)

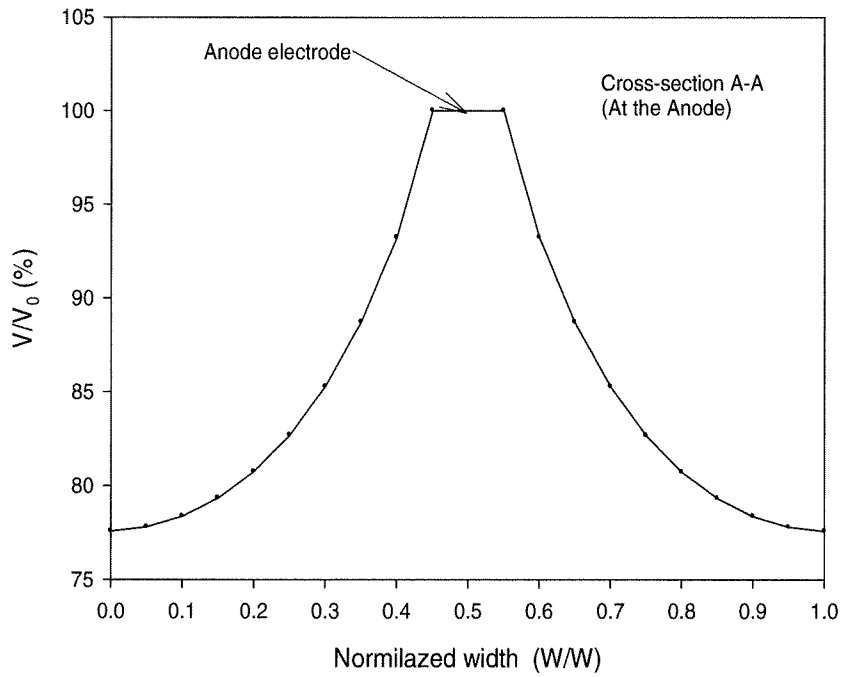

Figure 5.13.C Voltage distribution along cross section A-A near the anode.

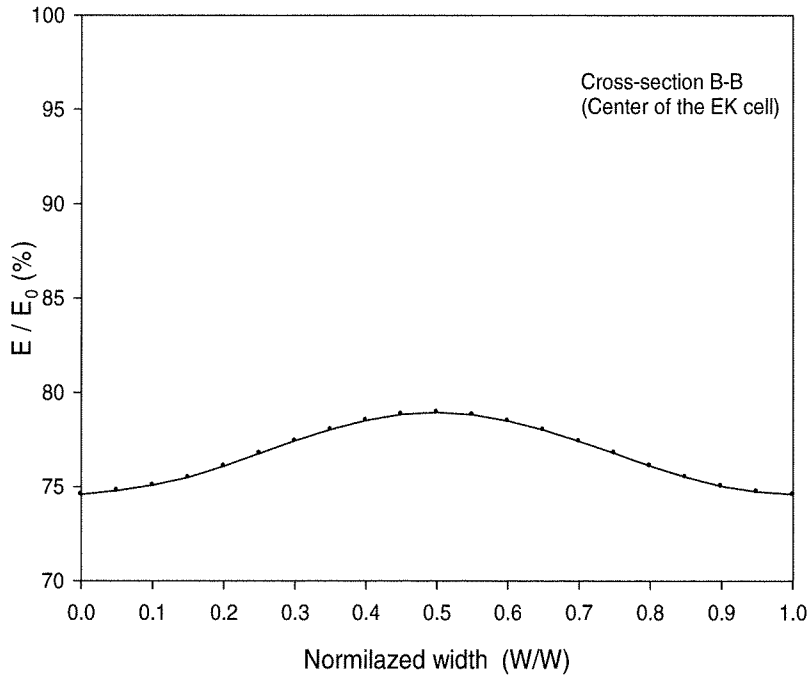

Figure 5.13.D Distribution of electric field intensity along cross section B-B at the centre of the electrokinetic cell.

5.3.1.3 pH distribution in the soil after the test

Figures 5.14.A and 5.14.B show the soil pH distribution in the 2-D continuous-powered and the 2-D solar-powered tests. The contours were produced using statistical software (SigmaPlot®). As expected, the highest pH values (> 7) were found around the cathode and the lowest (< 5) were near the anode. The high and low pH zones display semi-ellipsoidal shape of the contours with the basic front extending slightly further than the acidic front. This was due to the hydraulic flow. In the absent of a hydraulic gradient, the acidic front advances more than the basic front due to the smaller size of the hydrogen ions as compared to the hydroxide ions and the direction of electro-osmosis flow.

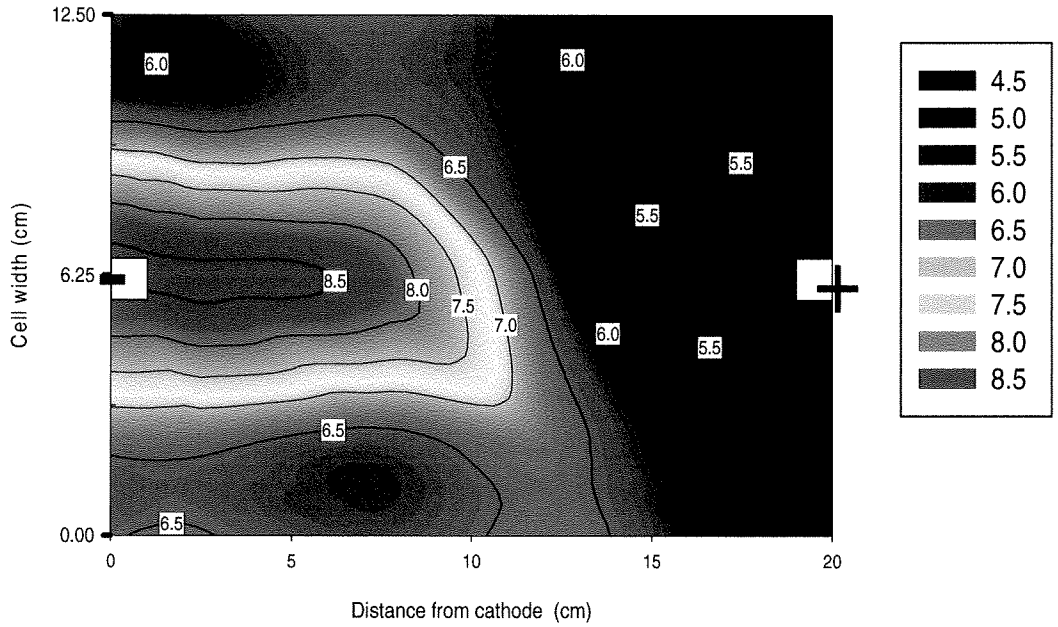

Figure 5.14.A pH distribution at the end of the 2-D continuous-powered test.

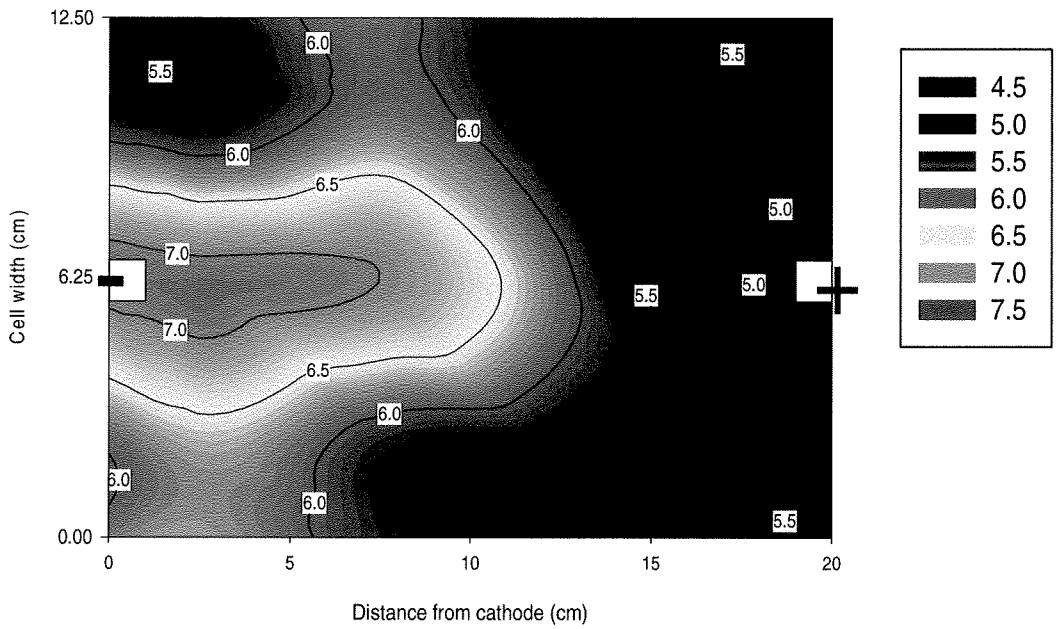

Figure 5.14.B pH distribution at the end of the 2-D solar-powered test.

5.3.1.4 Copper migration

5.3.1.4.2 Two-dimensional continuous-powered test

Figure 5.15 shows the copper concentrations in the effluent of the 2-D tests. The pH and the copper concentration in the continuous-powered test were 3.4 and 99 mg/L, respectively. This respected 10% of the influent concentration while the volume of the effluent was 0.56 pore volumes. From Figure 5.5, 25% of the influent copper concentration was found in the control effluent at the same 0.56 pore volumes. This reduction in copper concentration for the same effluent was due to electro-migration. Figures 5.16 and 5.17 show counters distribution of the total copper concentrations and the copper in pore fluid at the end of the 2-D continuous-powered test, respectively. The results were plotted using data obtained from 12 sampling points as described earlier in Chapter Four. The copper absorbed by the soil solids has been back-calculated and presented in Figure 5.18. The high pH around the cathode increased the amount of copper adsorbed by the soil (~ 600 mg/kg), accompanied by a lower copper concentration in pore fluid (~ 100 mg/ kg). Copper concentration in pore fluid was increased and the copper in the soil solids was decreased in the width side of the cathode zone. This can be explained by the low electric field intensity at the cell corners as seen in Figure 5.13.b. The Anode half was dominated by average of 200 mg/kg pore fluid copper concentration (nearly 60% of total copper concentration). Although that indicated copper advances, nevertheless, significant amount of copper was adsorbed by the soil.

5.3.1.4.3 Two-dimensional solar-powered test

Figure 5.15 shows the copper concentrations of the 2-D solar test effluent compared to the control test. The pH and the copper concentration were 3.9 and 198 mg/L, respectively. For effluent of 1260 mL (0.72 pore volumes), the influent copper concentration was 19% of the influent concentration compared to 45% was found in the control for the same pore volume (see Figure 5.5). This noticeably indicates the influence of the electro-migration and the success of the solar cell as source of power for electrokinetics. Figures 5.19 to 5.21 show contour distribution of the total copper concentrations, the copper in pore fluid and the copper absorbed by soil solid at the end of the 2-D solar-powered test, respectively. The result plotted using the data from 12 sampling points as described in Chapter Four (see Figure 4.3-b). The amount of copper adsorbed by the soil around the cathode to ~ 600 mg/kg, and near the anode was ~ 150 mg/kg as shown in Figure 5.21. The increase of the amount absorbed compared to the 2-D continuous test due to the introduction of the low pH influent during the nights. The pH distribution of the 2-D solar-powered test (Figure 5.14.B) was in good agreement with the amount of copper absorbed along with the copper concentration in pore fluid. Though that considerable amount of copper was found in the effluent, yet, solar-powered electrokinetics significantly increased the amount of copper adsorbed by the soil.

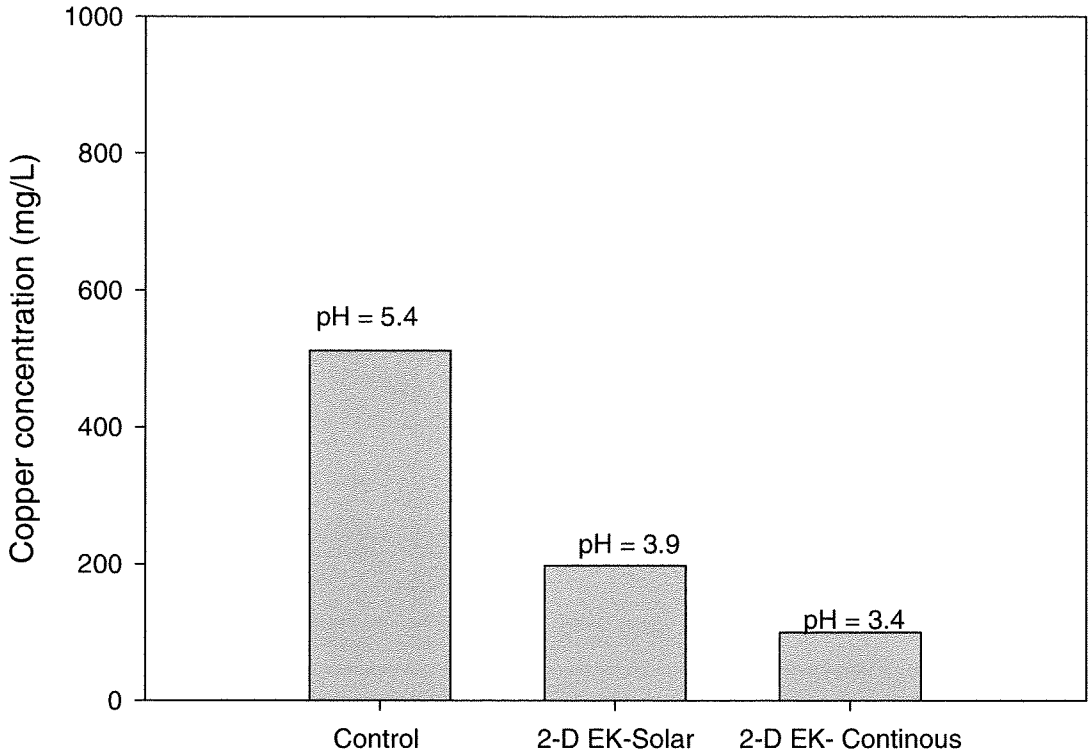

Figure 5.15 Effluent copper concentrations in the 2-D continuous-powered and solar powered tests and the control.

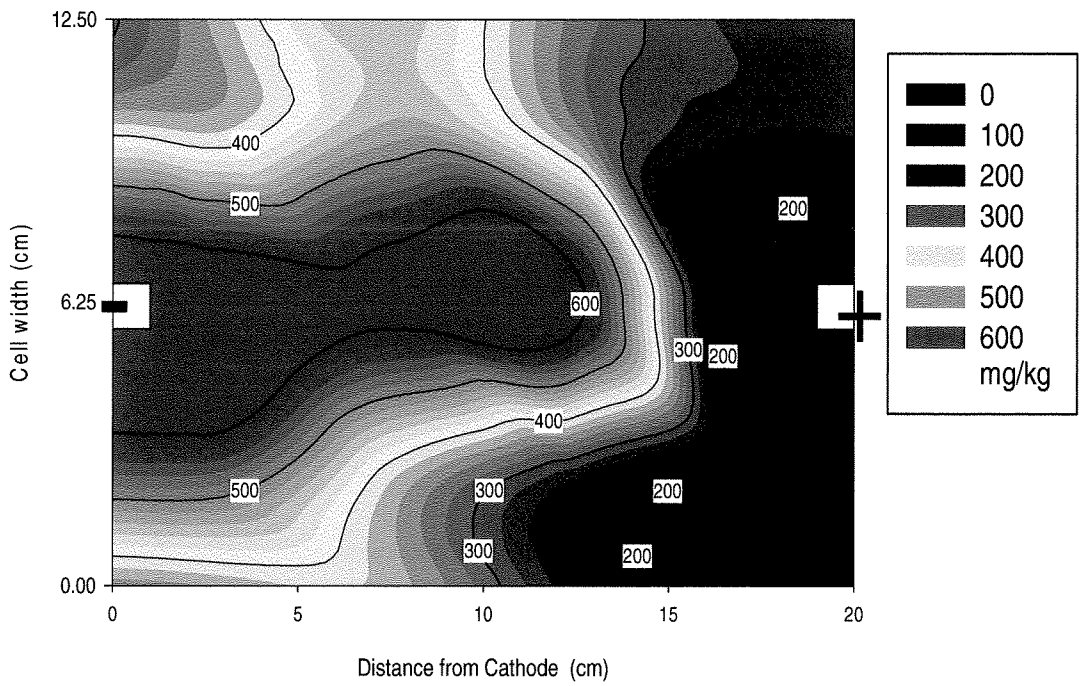

Figure 5.16 Distribution of total copper concentration at the end of the 2-D continuous-powered test.

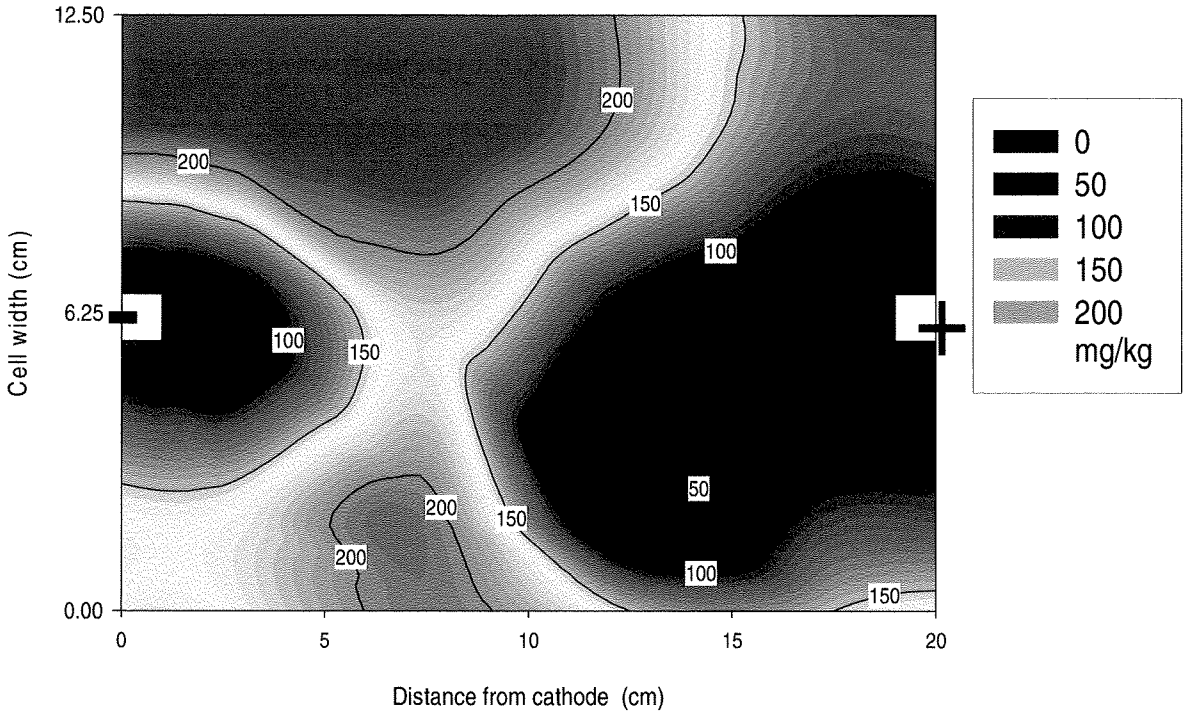

Figure 5.17 Distribution of copper concentration in pore fluid at the end of the 2-D continuous-powered test.

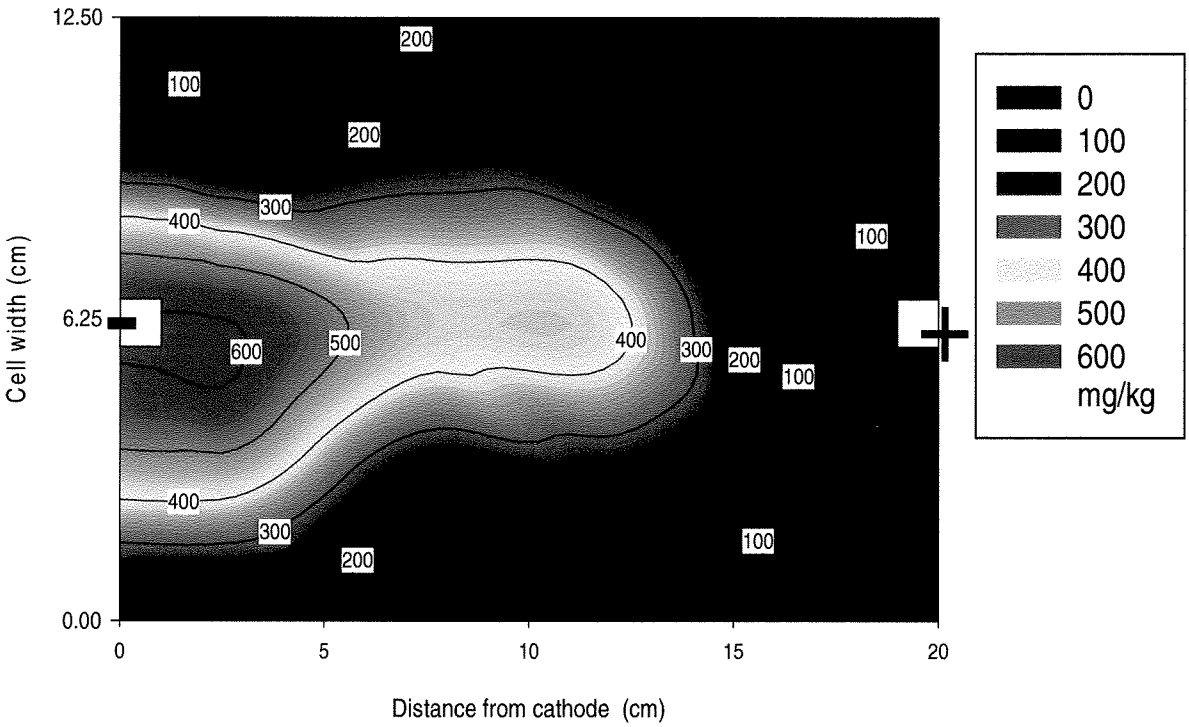

Figure 5.18 Distribution copper adsorbed by soil solids at the end of the 2-D continuous-powered test.

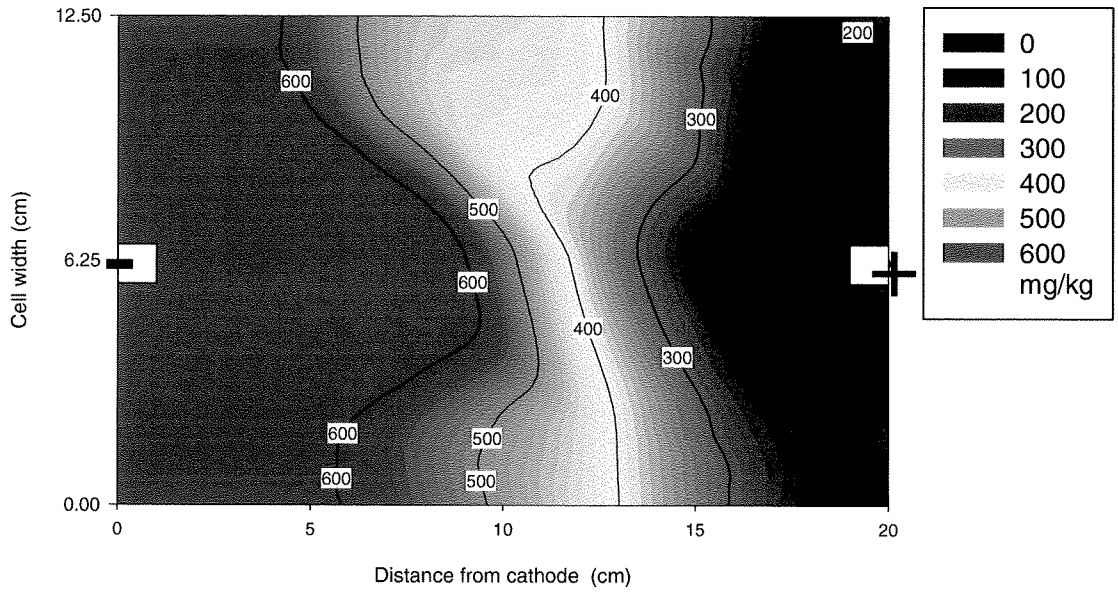

Figure 5.19 Distribution of total copper concentration at the end of the 2-D solar-powered test.

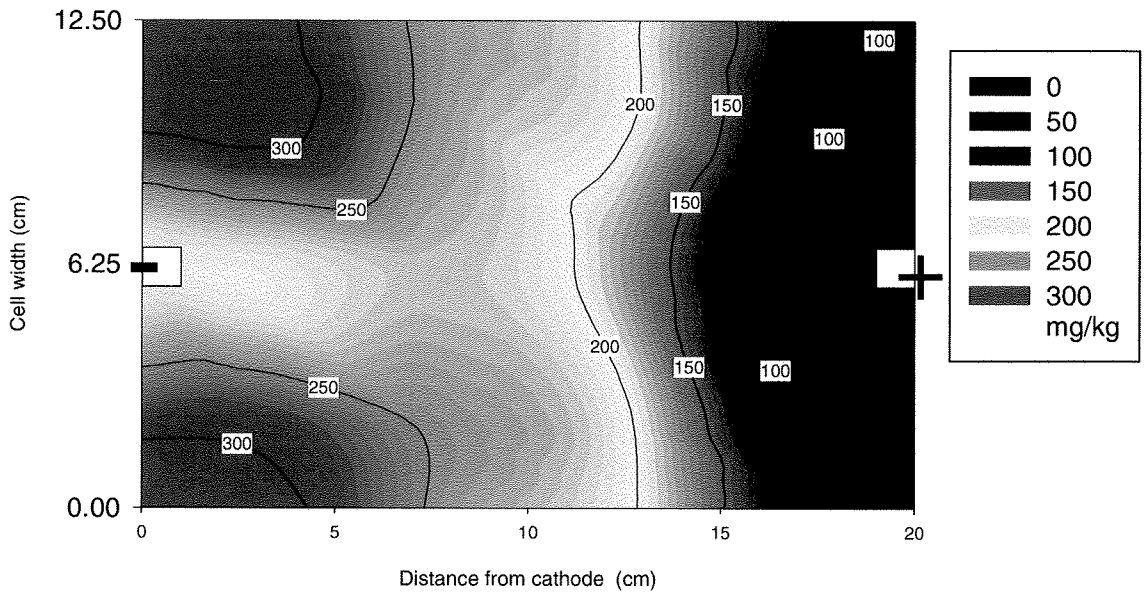

Figure 5.20 Distribution of copper concentration in pore fluid at the end of the 2-D solar-powered test.

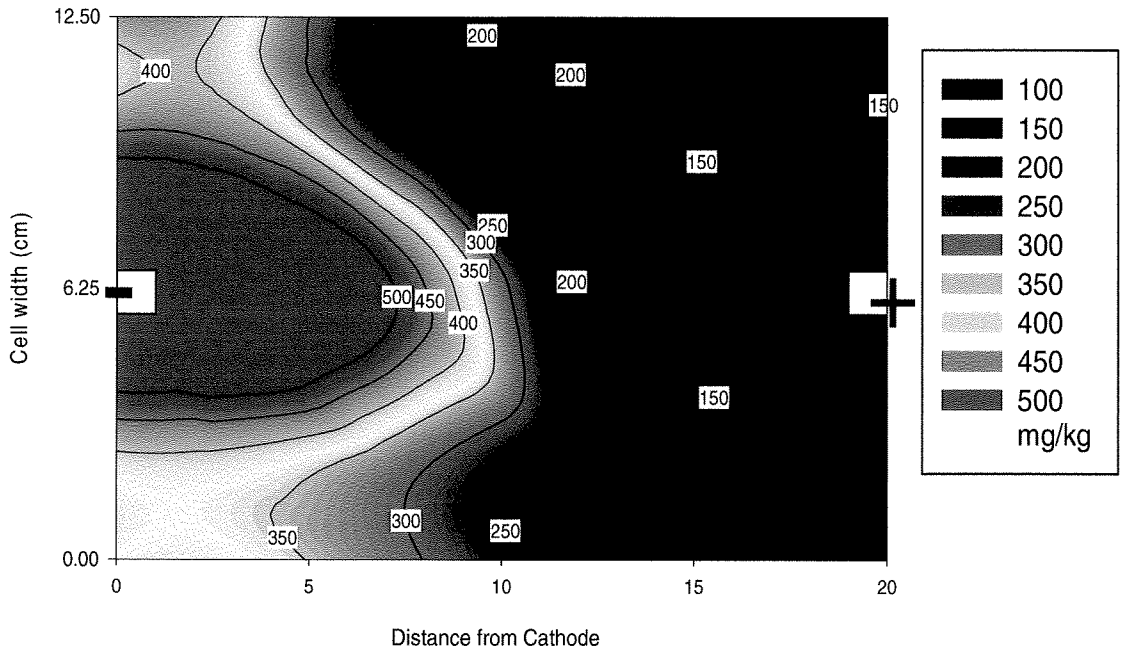

Figure 5.21 Distribution of copper adsorbed by soil solids at the end of the 2-D solar-powered test.

5.4 ELECTROKINETIC BARRIER EFFECT ON COPPER MIGRATION

Table 5.1 shows simple numerical assessment for the total mass flux of the one-dimensional tests conducted; control, continuous and the solar-powered. The total mass flux was determined using Eq. [2.29] in Chapter Two. The following sections review the assumption and the data used in the calculations.

5.4.1 Soil Hydraulic Conductivity

As shown in Figure 4.1, a drainage blanket, 40 mm × 10 mm (L × H), was maintained at the downstream side of the cell. The blanket was installed to accelerate the seepage velocity and accumulate about 1 pore volume of effluent within 7 to 9 days in the control test. Figure 5.1 shows that 1.14 pore volume of effluent was collected in the control test in 8 days (192 h). The corresponding average flow rate was 2.38 $\times 10^{-8}$ $m^3/s/m$. Figure 5.22 shows the flow net in the control test simulated using SEEP/W (GEO STUDIO, 2007). From the flow net, the saturated hydraulic conductivity, k_h, was determined to be 2×10^{-7} m/s.

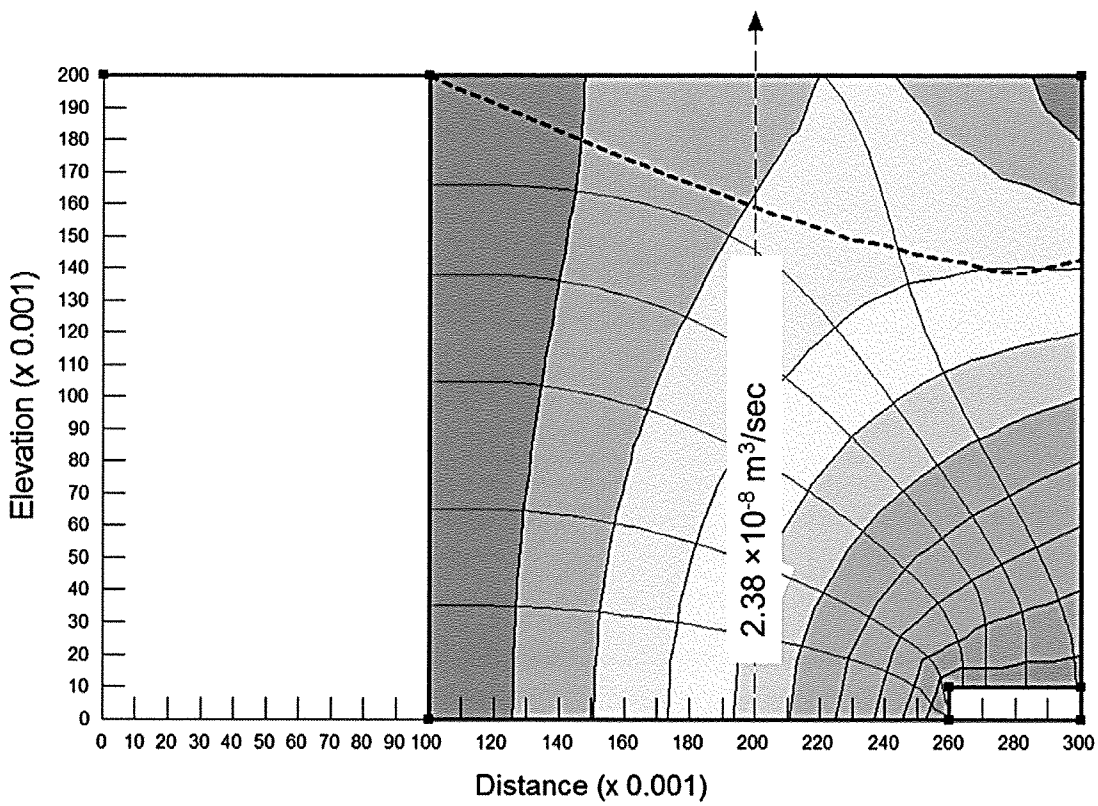

Figure 5.22 The flow net of the control test.

5.4.2 Diffusive Mass Flux

Diffusion is the process by which both ionic and molecular species dissolved in water move from areas of higher concentration to areas of lower concentration. The self-diffusion coefficient of copper, D_o, is 7.13×10^{-10} m^2/s (Mitchell and Soga, 2005). Effective soil porosity, n_e, of 0.25 and tortuosity, τ, of 0.35 were assumed as a baseline for the analysis. The effective diffusion coefficient, D^*, was determined to be 6.24×10^{-11} m^2/s. The mass flux due to diffusion is determined using Eq. [2.29]. The diffusive mass flux was considered to be a constant value for the tests conducted i.e. control, continuous and solar test.

5.4.3 Hydraulic Mass Flux

The advective mass flux due to the hydraulic gradient was determined directly from the flow rate of the control test. The flow was assumed to be one-dimensional flow with hydraulic gradient of 1 (m/m). The hydraulic conductivity k_h of 2×10^{-7} m/s as determined in section 6.4.1 was used. The hydraulic mass flux was determined using Eq. [2.29].

5.4.4 Electro-osmotic Mass Flux

The average electro-osmotic permeability, k_e, was determined from the balance of the effluent flow rate of the continuous and the solar test. For the continuous test, the

electro-osmotic flow rate was the difference between the control and the continuous tests effluents with electric field intensity, E, of 50 V/m. k_e of the soil in the continuous test was 2.27 × 10^{-9} m^2/s V. k_e of soil in the solar test was 3.1 × 10^{-9} m^2/s V determined using an average E of 25 V/m (50 V/m during the day time and zero during the night). The electro-osmotic mass flux was determined using Eq. [2.29].

5.4.5 Electro-migrative Mass Flux

The transport rate by electro-migration was determined using the effective the effective diffusion coefficient of the copper, D^*, as determined in Section 6.4.2. The effective ionic mobility, u_i^* was determined to be 4.86 10^{-9} m^2/s V The electro-migrative mass flux was calculated using Eq. [2.29].

5.4.5 Total Mass Flux

The total mass flux for the copper ions (Cu^{+2}) through the soil specimen was numerically determined. The copper concentration of the influent was ~1000 mg/L, the travel distance was 20 cm and the duration of the tests was 192 h. The total mass flux were determined for 0, 25, 50 V/m as the applied electric filed intensity of the control, solar-powered and continuous-powered test, respectively. For the control test, the total transport rate of copper from the influent to the soil specimen and effluent was 0.2 mg/m^2/s. The majority of copper was transported by the hydraulic flux and the contribution from diffusion was minor. For the continuous-powered test, the total mass

flux was zero. In this test, electro-migration and electro-osmosis countered the flux of copper by the hydraulic gradient and diffusion and thereby reduced the net flux as compared with the control. As shown in Table 5.1, the electro-migration flux was dominant as compared to the electro-osmotic flux. For the solar-powered test the total mass flux was 0.001 $mg/m^2/s$. Although the copper transport rate was in the direction of the anode, electrokinetics significantly minimized the total mass flux as compared to the control test. The electro-migration was governing the electrokinetic barrier mechanism. In fact, transport rate of Cu^{+2} due to electro-migration was approximately one order of magnitude higher than electro-osmosis as can be seen in Table 5.1. The numerical analysis are in good agreement with the test effluent results, where 512, 46 and 0 mg/L final copper concentrations were collected after 192 h from the control, solar, and continuous test, respectively.

Table 5.1 Numerical analysis of the copper mass fluxes for the one-dimensional tests.

Test #	Control test (0 V/m)	Continuous test (50 V/m)	Solar test (25 V/m)
Diffusive mass flux ($mg/m^2.s$)	3×10^{-4}	3×10^{-4}	3×10^{-4}
Hydraulic mass flux ($mg/m^2.s$)	0.2000	0.2000	0.2000
Electro-osmotic mass flux ($mg/m^2.s$)	-	-0.1134	-0.0775
Electro-migrative mass flux ($mg/m^2.s$)	-	-0.2432	-0.1216
Total mass flux J_{Cu} ($mg/m^2.s$)	0.2003	0	0.0012

5.5 FIELD APPLICATION SCENARIO

This section describes a theoretical modeling of a 2-D electrokinetic barrier and discusses the effects of its electrodes arrangement and spacing. Numerical simulations of contaminant transport under 2-D electric-field distributions can be used for predicting species transport (Alshawabkeh and Acar, 1992; Alshawabkeh and Acar, 1996; Narasimhan, 2000). Several factors affect electrode configuration and spacing. These factors include the soil properties, applied voltage, contaminant type, hydraulic flow and the cost of electrodes. Large electrode spacing reduces the installation costs, but may decrease the electric field and thereby the effectiveness of electrokinetics. It is essential to assess these variables prior to selecting the configuration and spacing (Alshawabkeh, 2001). Figure 5.23.A shows 3-D schematic illustration of a proposed solar powered electrokinetic barrier. Two rows of electrodes inserted into the ground, where the cathode electrodes facing the contaminated flow. This configuration is similar to the configuration of the 2-D laboratory tests conducted. Figure 5.23.B shows a plan view of the electrokinetic barrier, where L is the distance between cathode and anode and W is the spacing between the same-polarity electrodes (e.g. anode-anode or cathode-cathode).

Increasing the applied voltage will increase energy expenditure and cost of the process. Therefore, an optimum voltage should be appropriately selected along with the electrode arrangement and spacing. Assuming uniform field condition, with soil properties similar to the geotechnical, chemical and hydrological properties of the tested soil, a two-dimensional modeling for the electric field distribution of several electrodes

spacing was performed. The model was used to evaluate the effect of the same-polarity electrodes spacing, W, in the voltage and the electric field intensity distributions.

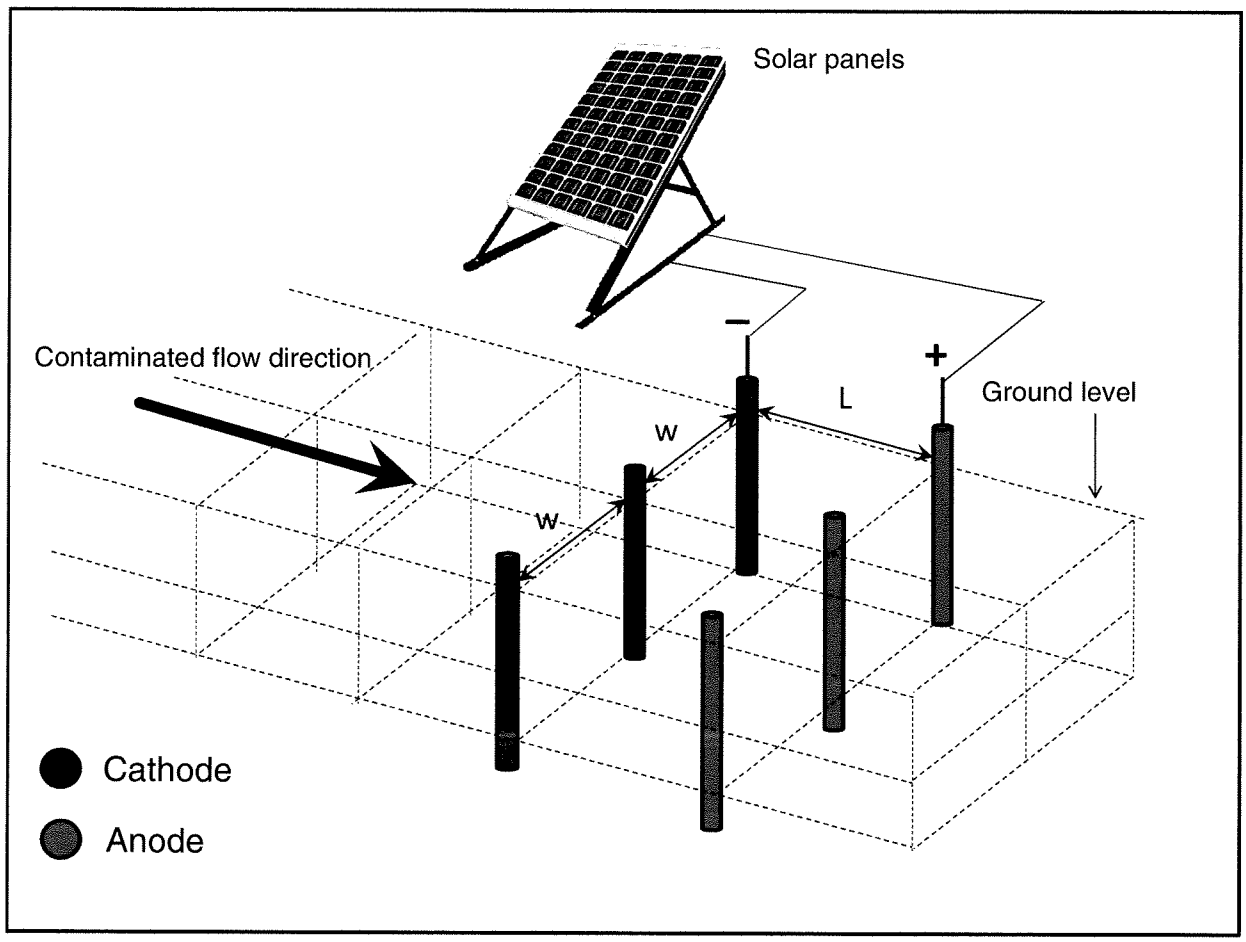

Figure 5.23.A 3-D schematic of the proposed solar powered electrokinetic barrier.

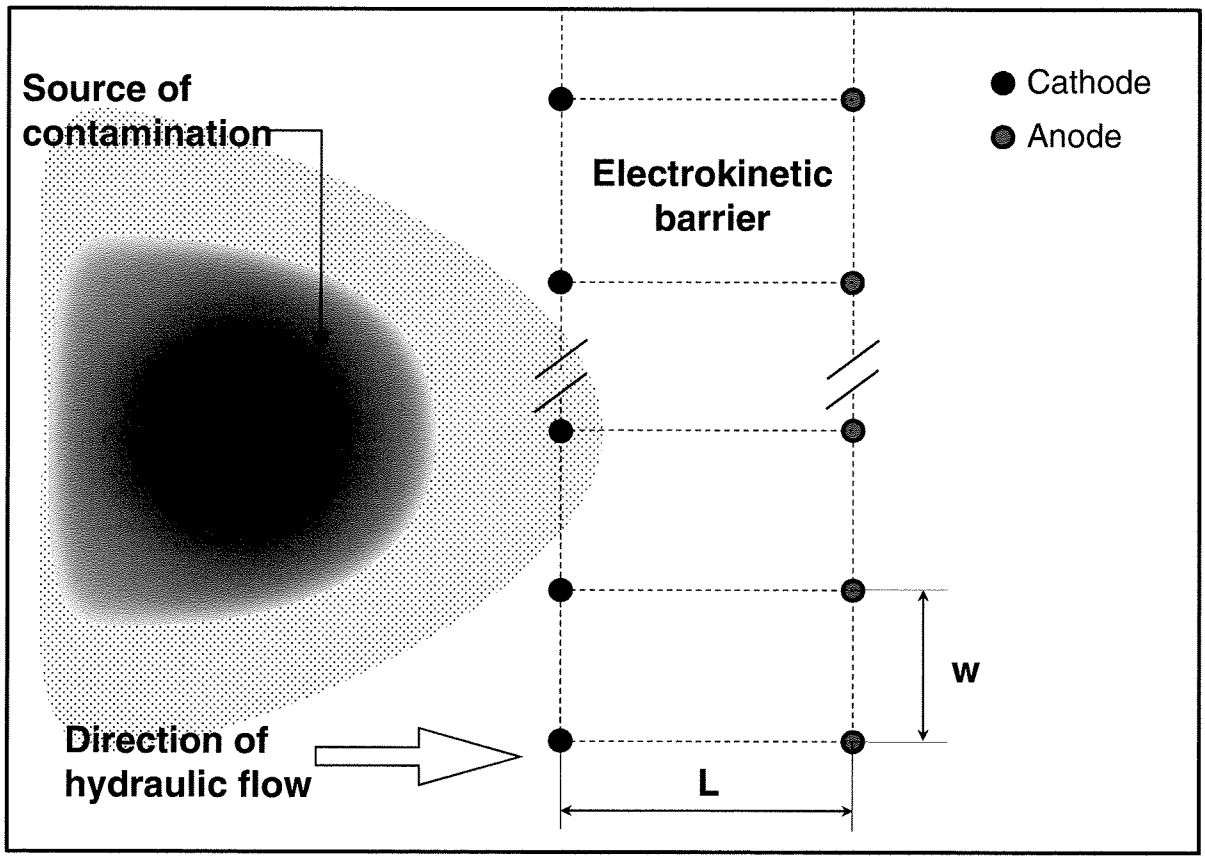

Figure 5.23.B Plan view of proposed solar-powered electrokinetic barrier.

5.5.1 Assumptions

- The field condition has a soil properties similar to the geotechnical, chemical and hydrological properties of the tested soil (e.g. the saturated hydraulic conductivity, k_h, is 2×10^{-7} m/s).
- The total width of contaminant exposure area is 6 m, and the electrokinetic barrier length (distance between cathode and anode) is 1 m.

- According to the results of the two-dimensional solar-powered test, an electric field intensity of 50 V/m considerably hindered the migration of the contaminants and increased the adsorption capacity around the cathode electrode. Therefore an electric field of 50 V was applied to achieve similar results to the laboratory test.

5.5.2 Electric Field Distribution

Figures 5.24.A to 5.27.B show the results of the 2-D electric field modeling for proposed spacing between electrodes with similar polarity. Each configuration was investigated for the voltage distribution and the electric field intensity. Similar to the voltage and electric field intensity distribution of the two-dimensional configuration tests (see Section 5.3.2.2.1), the voltage distribution at the anode along the width of the electrokinetic barrier (cross-section X-X) and the average electric field at the centre of the barrier (cross-section E-E) was plotted vs. the normalized width as shown in figures Figure 5.28.A and B.

According to the laboratory test results, 77% of the applied voltage and 75% of the maximum electric field intensity are required to hinder the copper migration. For the configuration W = 3 L, only 14% of the normalized spacing between the the same-polarity electrodes, W, has a voltage higher 77% of the applied voltage and the average electric field intensity was below 75%. For the configuration W = 2 L, only 21% of W is higher than the 77% of the applied voltage. Ninety percent of the normalized width has the voltage higher than the 77% for the configuration W= L. The electric field intensity is in good agreement with the laboratory test results. For the configuration (W=0.5L), the

voltage distribution was in range of 90 – 100% of the applied voltage distribution, almost similar to the 1-D configuration.

The configuration (W = L) was found to be the optimum spacing in term of the required values and cost. Although the spacing (W=0.5L) has the best results, but it increases the cost of the electrokinetic barrier.

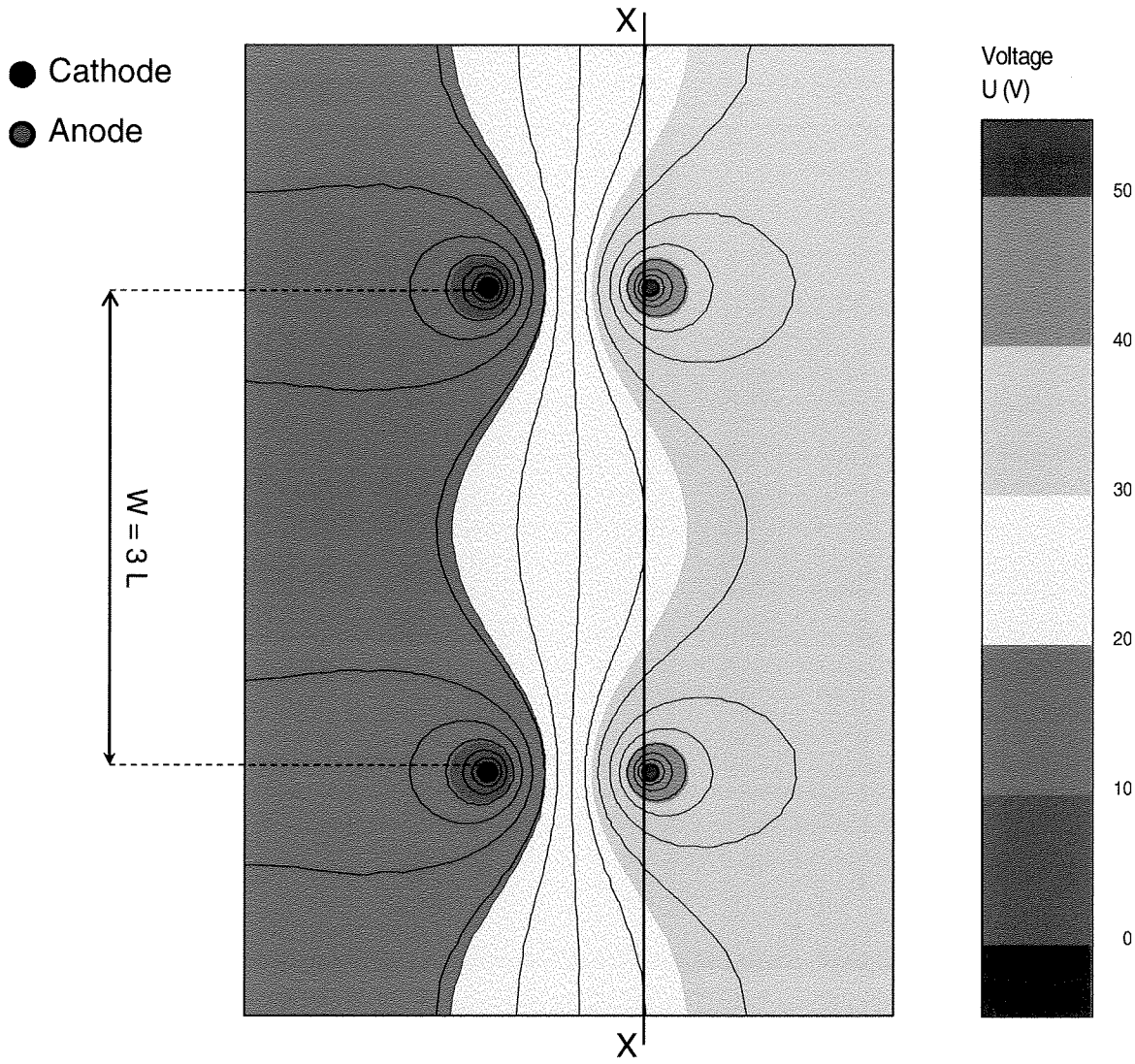

Figure 5.24.A Voltage distribution of the electrokinetic barrier with configuration of W = 3 L.

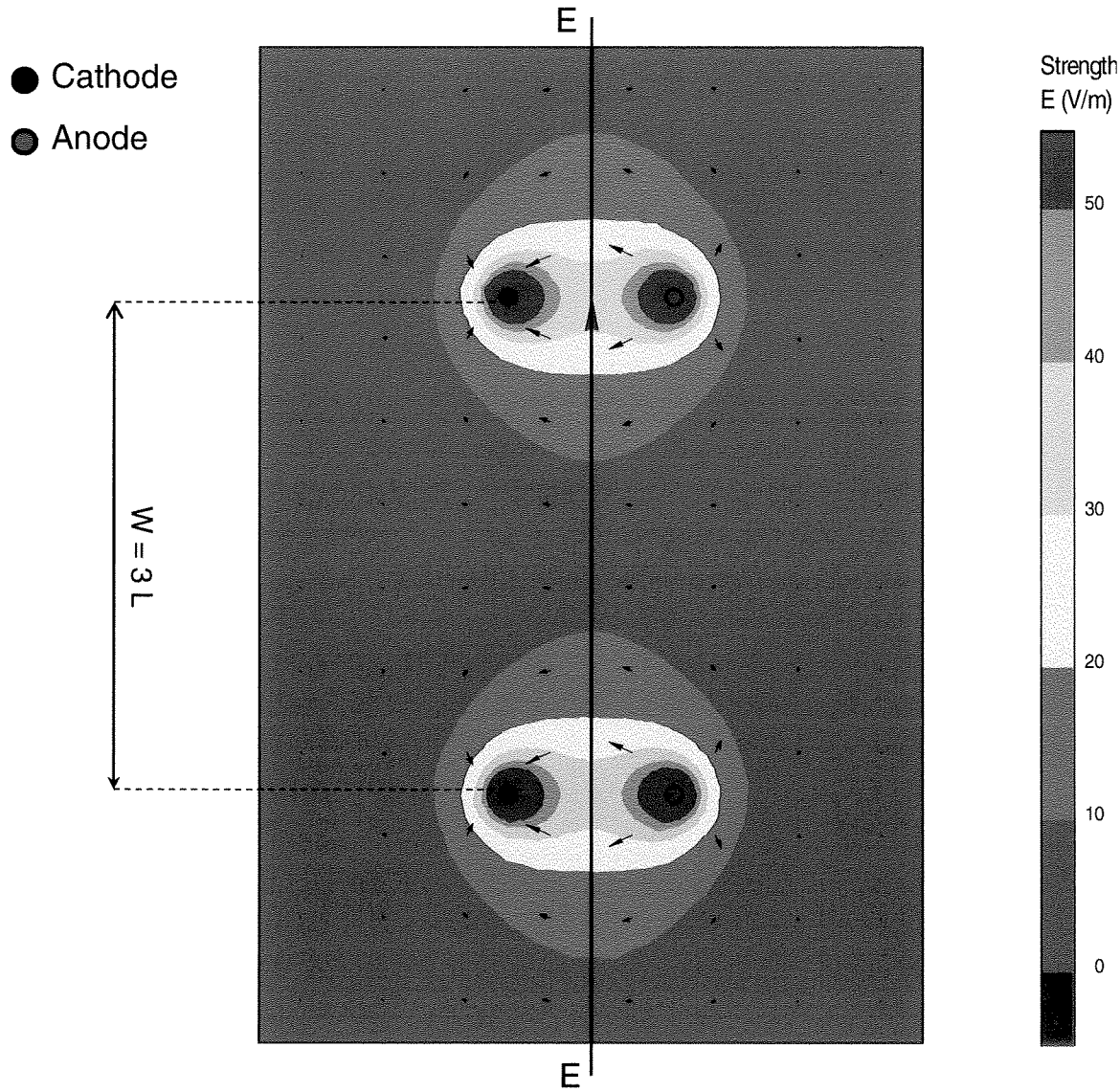

Figure 5.24.B Electric field intensity distribution of the electrokinetic barrier with configuration of W = 3 L.

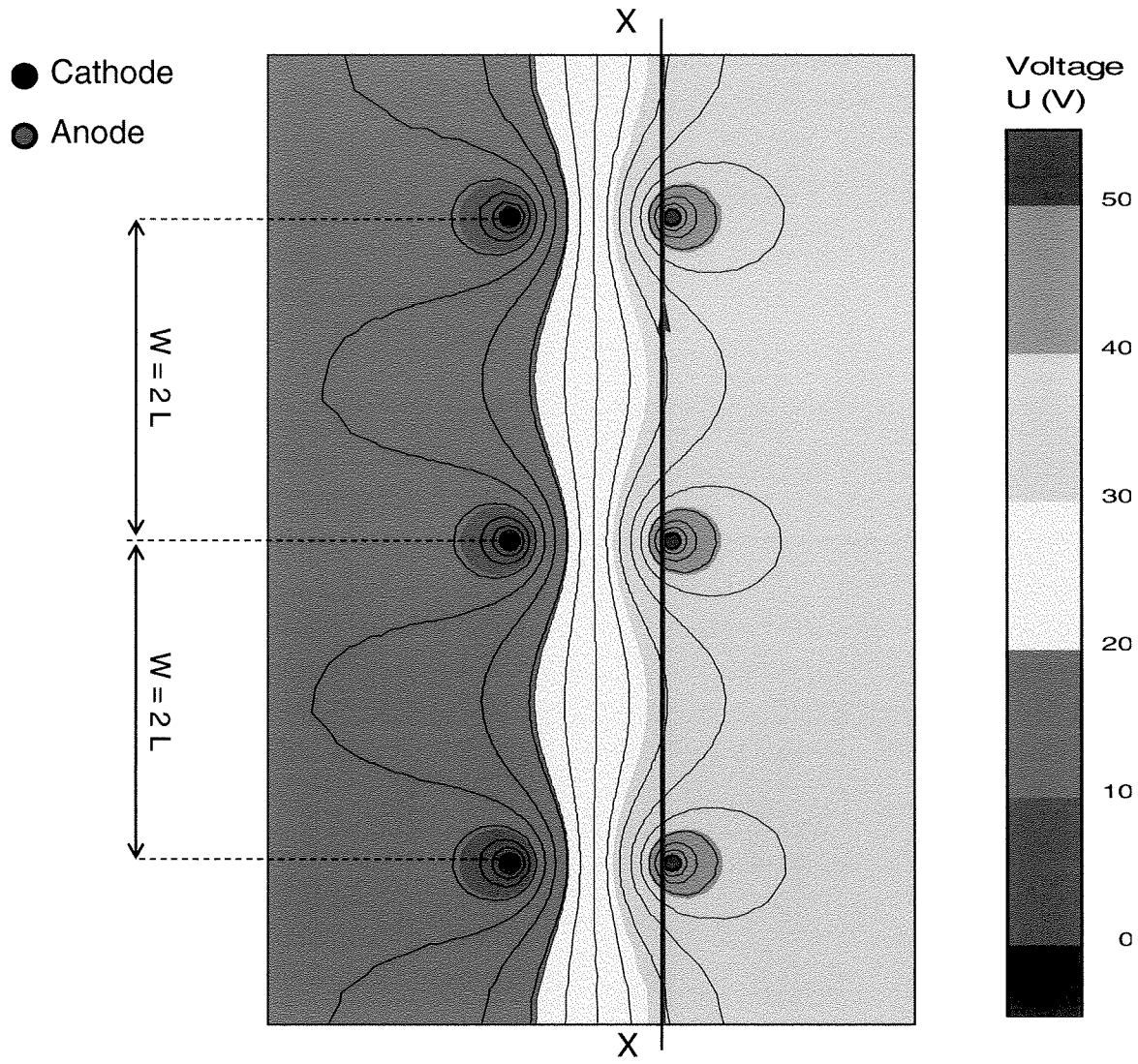

Figure 5.25.A Voltage distribution of the electrokinetic barrier with configuration of W = 2 L.

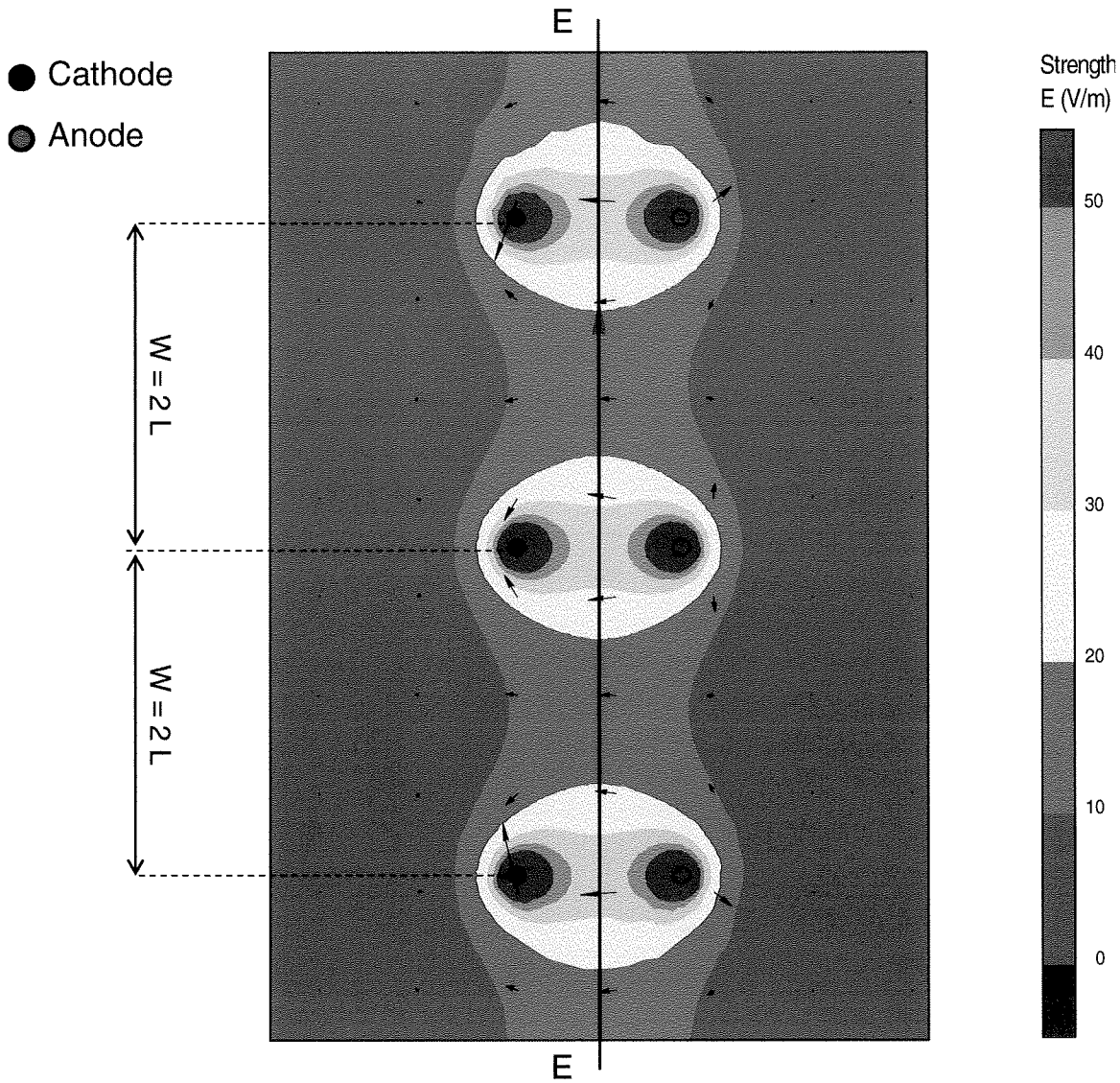

Figure 5.25.B Electric field intensity distribution of the electrokinetic barrier with configuration of W = 2 L.

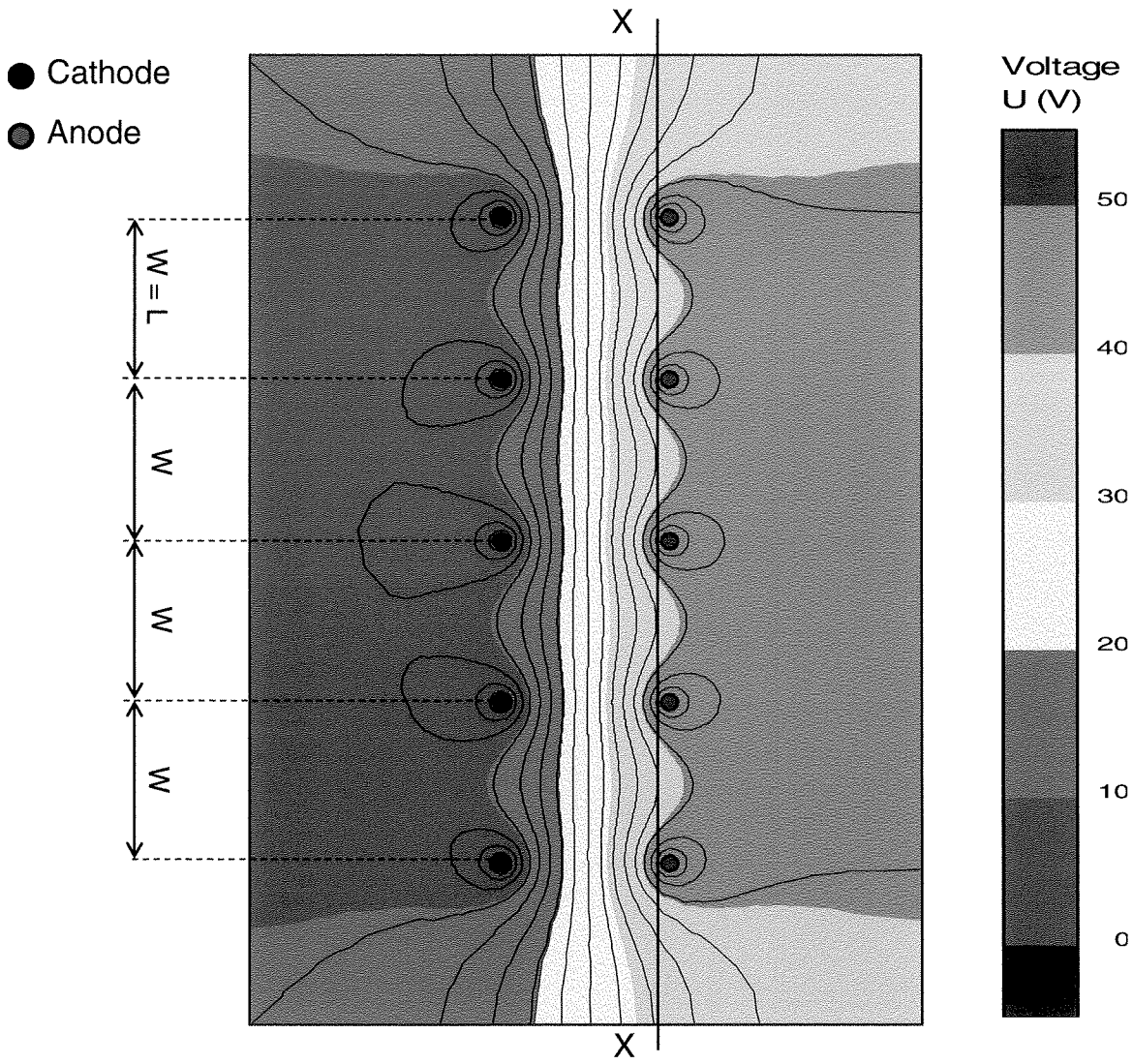

Figure 5.26.A Voltage distribution of the electrokinetic barrier with configuration of W = L.

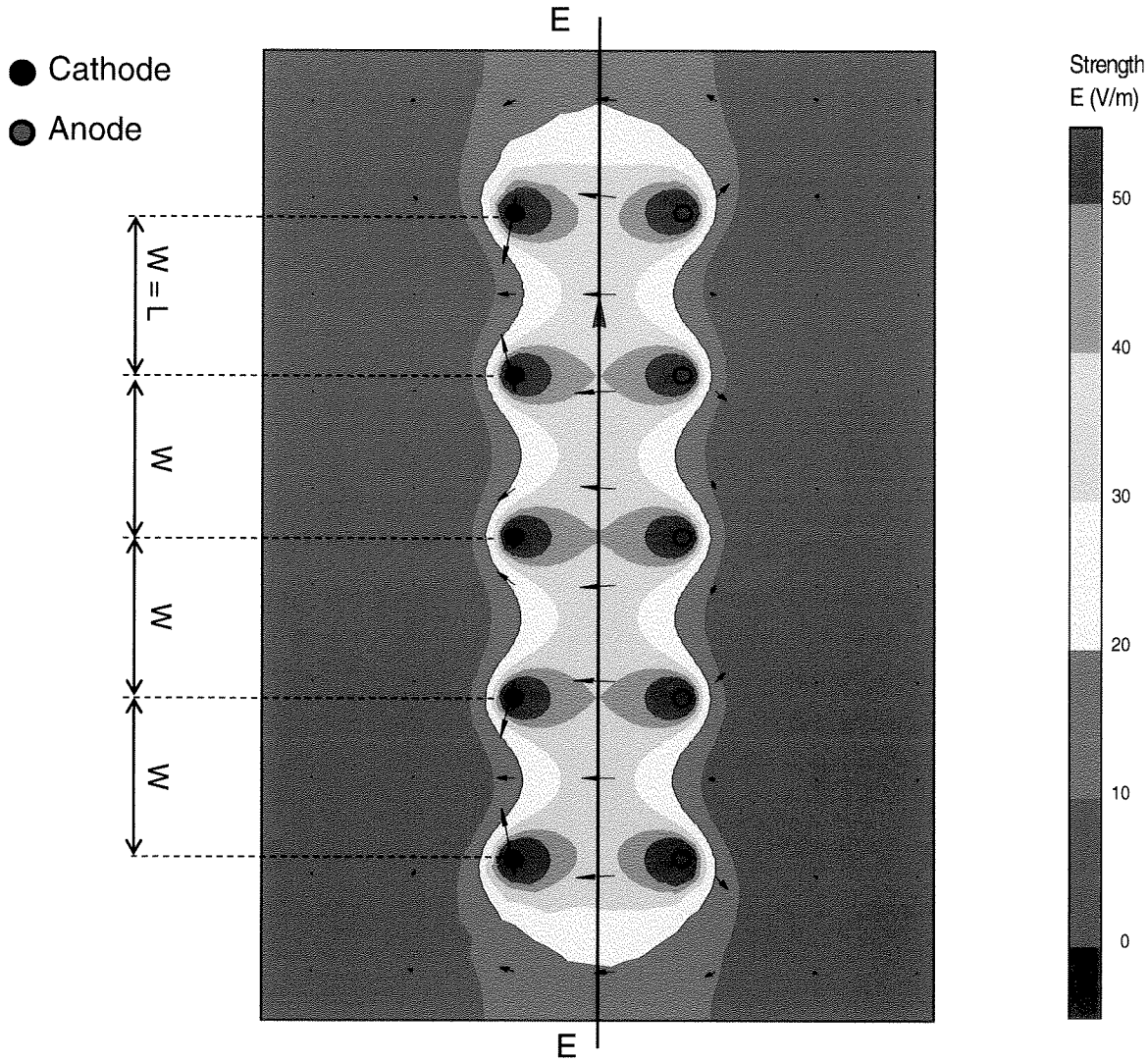

Figure 5.26.B Electric field intensity distribution of the electrokinetic barrier with configuration of W = L.

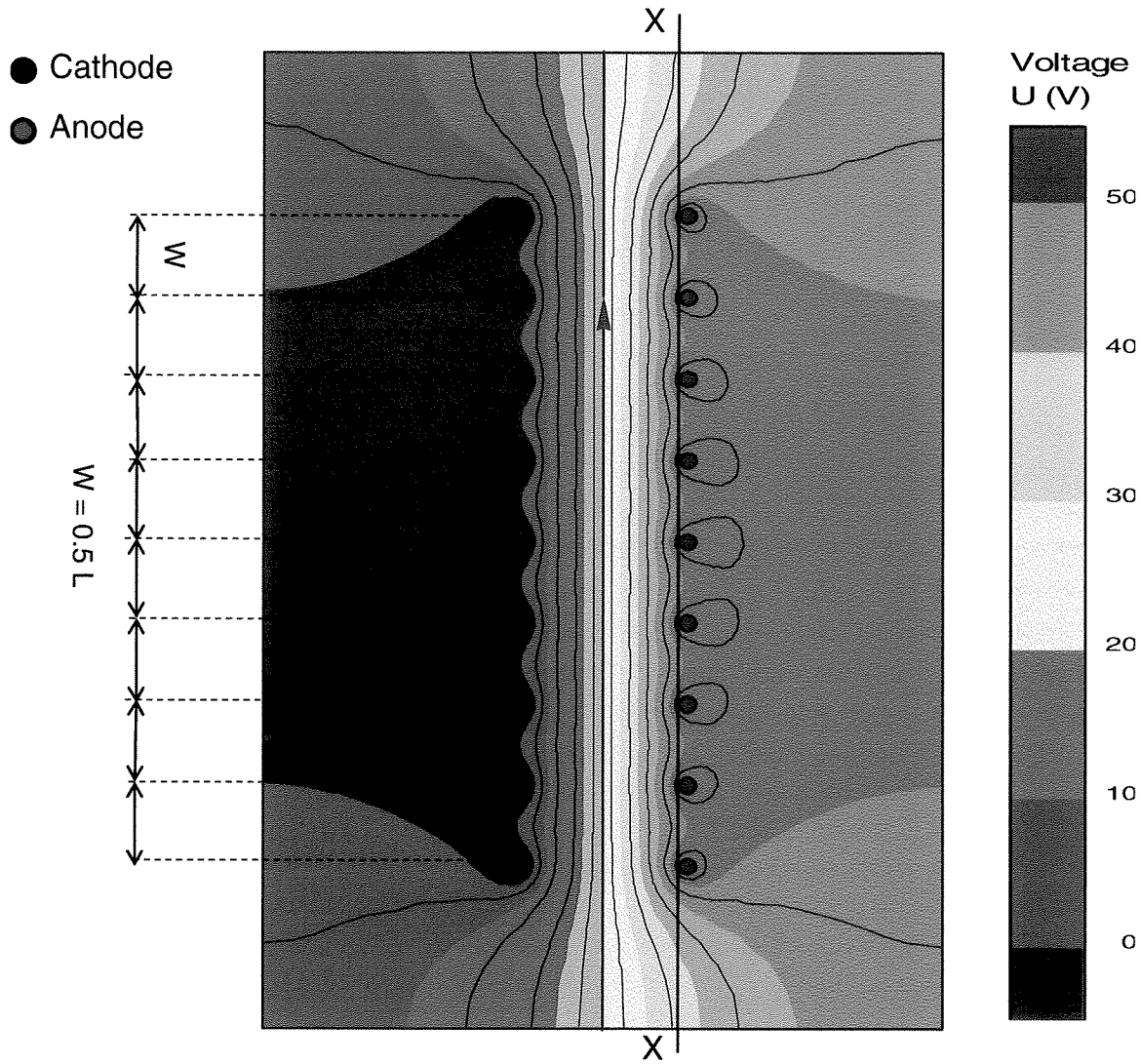

Figure 5.27.A Voltage distribution of the electrokinetic barrier with configuration of W = 0.5 L.

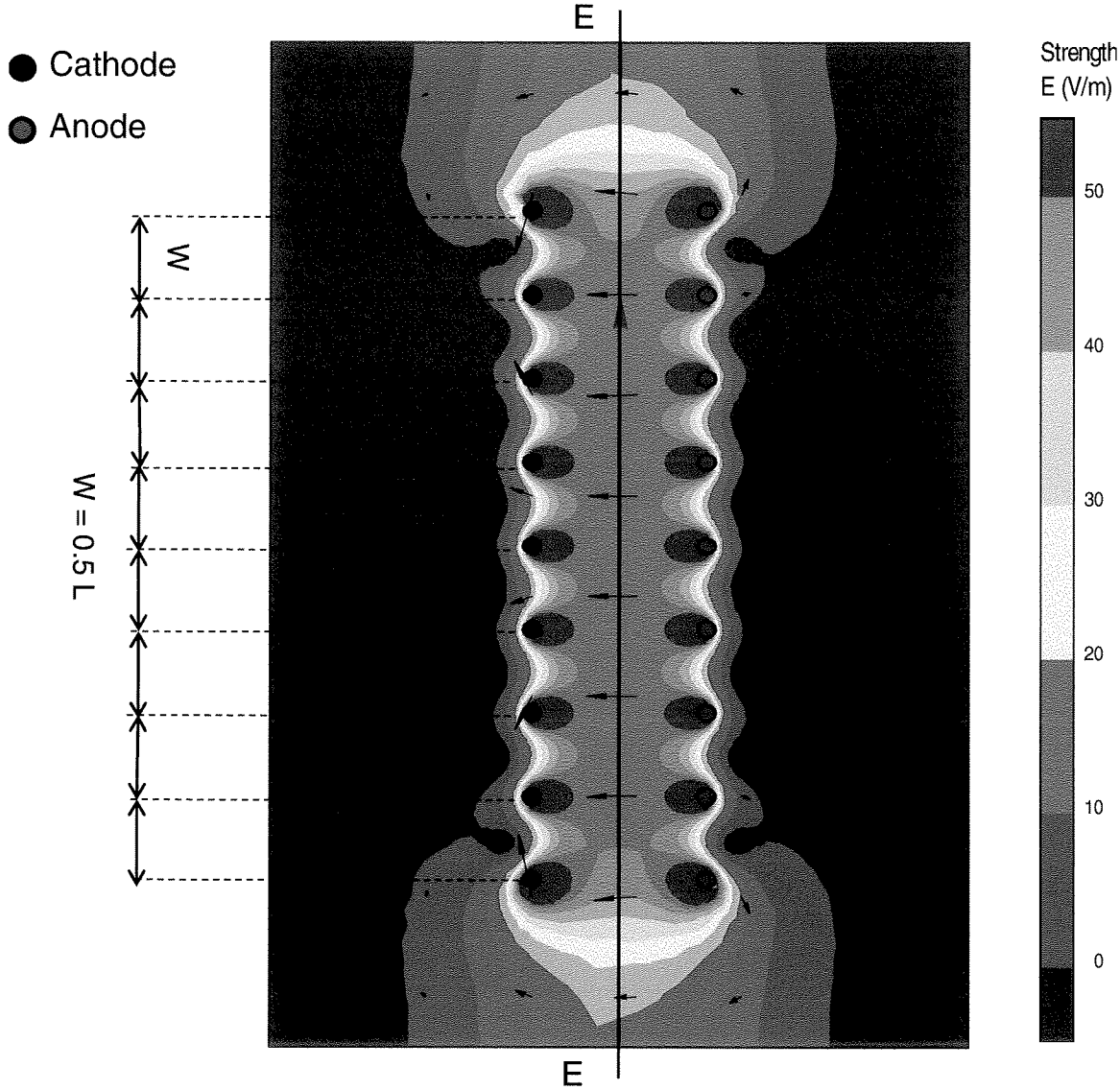

Figure 5.27.B Electric field intensity distribution of the electrokinetic barrier with configuration of W = 0.5 L.

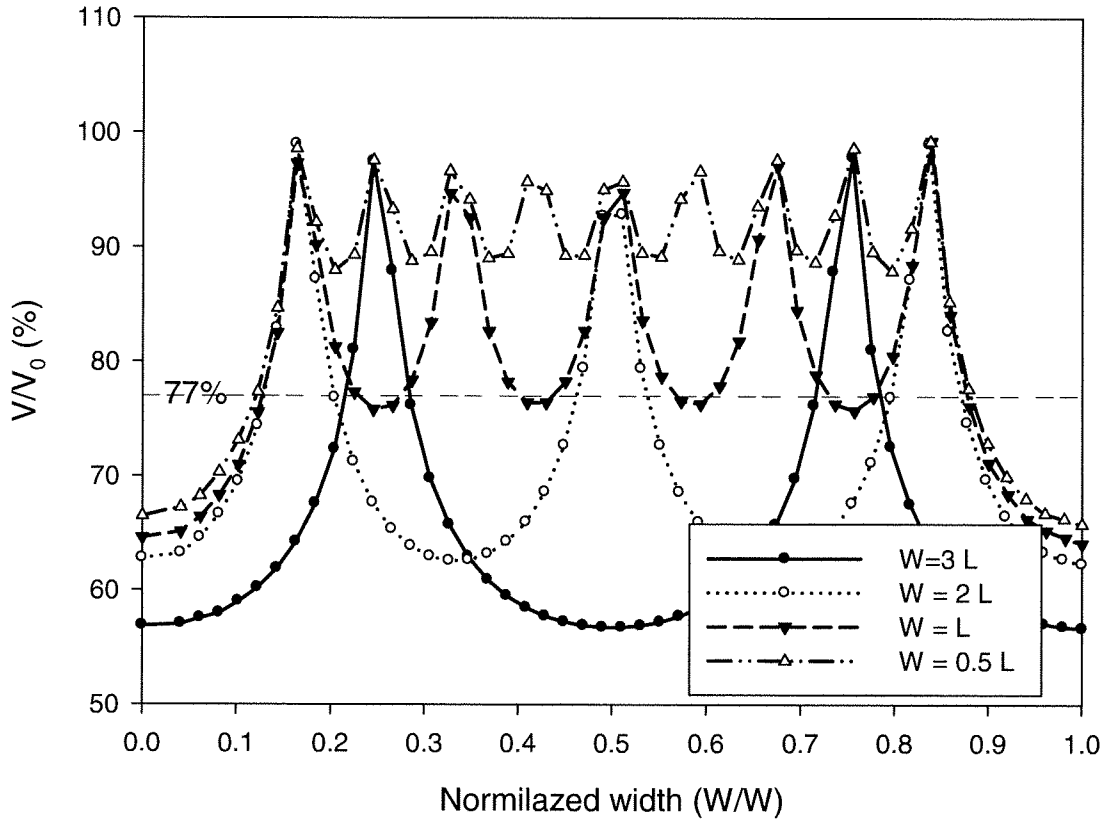

Figure 5.28.A Voltage distribution along cross section X-X of the electrokinetic barrier at the anode electrode for the suggested configurations.

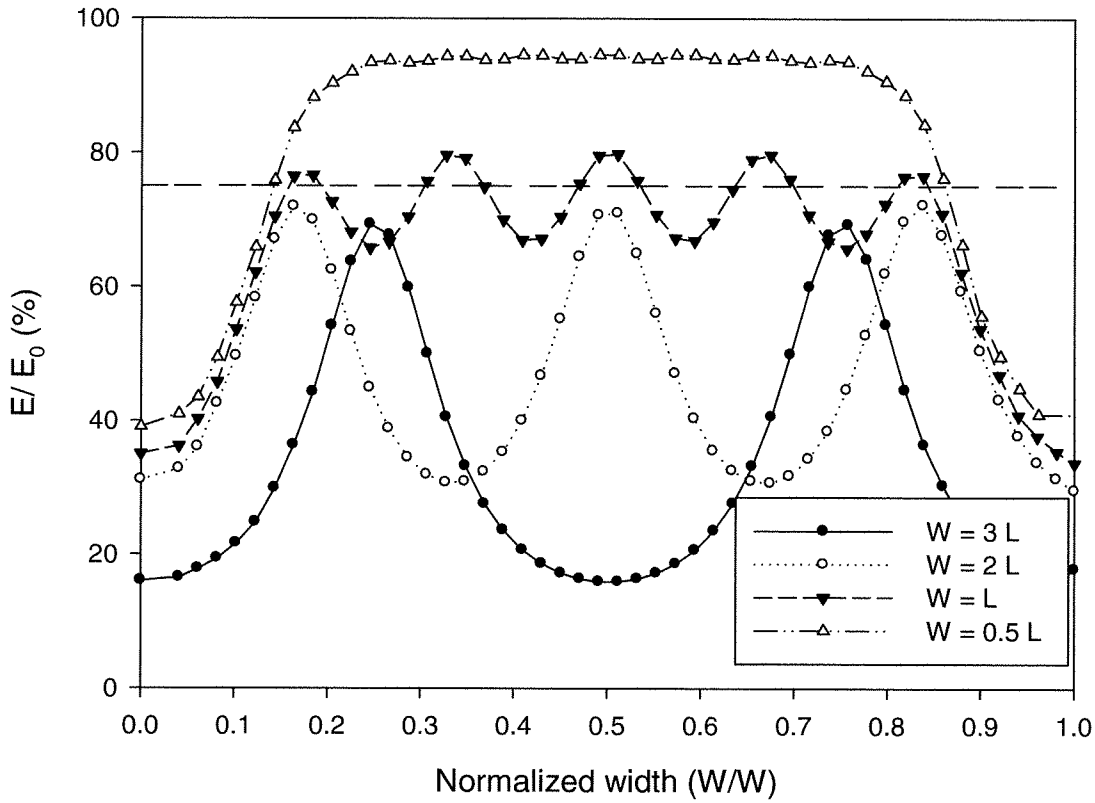

Figure 5.28.B Electric field intensity distribution of along cross section E-E at the centre of the electrokinetic barrier for the suggested configurations.

5.6 CONCLUSIONS

This study examined the effectiveness of integrated solar electrokinetic barrier. Total of 5 tests were conducted with one and two-dimensional electric filed configurations. A sand-clay mixture was tested with hydraulic flow with concentration of 1000 mg copper per liter of water. Control test was terminated after effluent collection of 2000 mL in 192 h. Accordingly, time comparative tests were carried out with electrokinetics. For the one-dimensional configuration, simulation of solar powered (12 h ON/ 12 h OFF) were used as potential source of energy. Another test with continuous application of the dc electric current was carried out for comparison. The effluent copper concentration, pH, soil residual copper concentration and current distribution were presented and discussed for each test. The continuous test completely prevents the transport of the copper compared to the control test. The one-dimensional solar-powered barrier significantly minimized the migration rate of the copper compared to the control test. Moreover, a high pH zone was created near the cathode that increased the soil adsorption capacity for the copper. Through simplified numerical analysis, electro-migration was found to be the dominant mechanism that countered the migration of the copper towards downstream. Similarly, tests with two-dimensional electrode configurations were performed. For the two-dimensional continuous-powered test, the electric field in 2-dimoinsonal configuration substantially minimized the copper migration where only 10% of the influent copper concentration had passed through the electrokinetic barrier. The use of solar power configuration also showed encouraging results. Although the effluent collected was around 75% of the control, the effluent

copper concentration was reduced to 19% of the influent copper concentration. Therefore, stand-alone solar system is a potential source of energy to prevent the migration of the contaminant. The two-dimensional electric field distribution of the electrokinetic cell plan was modeled. The minimum effective voltage near the anode along the width of the soil was found to be 77% of the maximum applied voltage. Optimization of the electrode configurations and appropriate spacing was discussed for proposed large-scale field. A software modeling of the voltage distribution was used to determine the applicable distance between the same-polarity electrodes. Configuration with spacing W= L was found to be in good agreement of the laboratory test values.

CHAPTER SIX

Results: Integrated solar Electrokinetic Remediation of copper contaminated slurries

6.1 INTRODUCTION

Electrokinetic remediation is recognized as a promising alternative to treat contaminated sediments (Yeung and Hsu, 2005). Electrokinetics requires only low-level direct current. Solar energy can be effectively used to provide electric current sufficient for electrokinetic applications. Yuan et al., (2009) showed that the cost of the electric power was reduced when solar cells was used to generate the power for an electrokinetic remediation study. In this research, solar energy was used to generate the electric field required to remediate artificially contaminated slurries. Tests were carried in one or two phases. Phase one was electrokinetic sedimentation of the slurry and phases two electrokinetic dewatering/decontamination. This chapter presents and discusses the results.

6.2 TEST PROCEDURE

Eight set of tests were carried out. Four sets were prepared with kaolinite clay (Plainsman clay) with solid concentration (mass of dry soil/ mass of water) of 10%, 15%, 20% and 25%. The other four sets were prepared with a mixture of 85% (by weight) kaolinite and 15% bentonite (kaolinite-bentonite mixture) with solid concentrations

similar to the previous set. The grain size distributions for both clayey soils are shown in Figures 3.1.A and 3.1.B. Several tests were conducted using the two types of slurries with one-dimensional (1-D) and two-dimensional (2-D) electric field configurations. The 1-D configuration tests consisted of two phases; electrokinetic sedimentation (phase 1) and electrokinetic dewatering/ decontamination of the settled clay (phase 2). Based on the results of the 1-D tests, only electrokinetic sedimentation was explored for the 2-D configuration. The procedure described in Section 4.3.3 was followed during the test.

6.3 RESULTS AND DISCUSSION

The following sections will present and discuss the results of the two phases of the test.

6.3.1 Phase 1: Electrokinetic Sedimentation

The electrokinetic sedimentation was assessed through the following procedure (Mohamedelhassan and Shang, 2001):

1. From the hydrometer test, the grain size distribution of the suspension was plotted (see Figure 3.1.A and 3.1.B).

2. The particle settling velocity induced by gravity, u_g, was determined for the various grain sizes in the suspension using Eq. [2.32].

3. Equation [2.33] was used to calculate the average particle settling velocity of the suspension by gravity $\overline{u_g}$. $\overline{u_g}$ was averaged for particles with d < 5 μm.

4. From Chapter Three, an average zeta potential, ζ, was selected and used to calculate the particle velocity induced by electrokinetics, u_{ek}. High pH zone was considered to dominate during the settlement process.

5. The average particle settling velocity due to gravity and electrokinetics $\overline{u}$ was calculated from Equation [2.35].

6. Equation [2.36] was used to determine the coefficient of free settling, β, in the gravitational and electrokinetic sedimentation processes. The free settling velocity of a dilute suspension, U_f, is measured by the drop of the mudline.

8. The coefficient of sedimentation was obtained from the experimental results of the gravitational, r_g, and the electrokinetic-enhanced, r, settling tests.

9. The change in the coefficient of sedimentation due to electrokinetics,Δr, was determined to evaluate the effects of electrokinetics.

6.3.1.1 Applied voltage and electric current

Figures 6.1 to 6.4 show the applied voltage and electric current during the sedimentation of the electrokinetic tests. As shown in the figures, the maximum applied voltage during the tests was 44 V reported during most of the day time and voltage of zero was observed during the night time. The electric current increased with the increase in the voltage and vice versa. As shown in Figures 6.1 to 6.4, in the electrokinetic sedimentation phase, the electric current increased with the solid concentration. This was due to the increase in electrical conductivity of the slurry. As the

solid concentration increased so were the copper concentration and subsequently the electrical conductivity. Generally, the electric current decreases with time during an electrokinetic test due to the decrease of electrical conductivity of the slurry (Chung et al., 2005). In the sedimentation phase, the current decreased towards the end of the test due to its relatively short duration.

As shown in Figure 6.1 and 6.2, higher electric current values were consistently reported in the kaolinite-bentonite tests. For example, at solid concentration of 25% the maximum current was 0.6 A compared to 0.27 A in the kaolinite test. The higher current was caused by the larger copper concentration in kaolinite-bentonite test 800 mg/kg compared to 400 mg/kg in the kaolinite test.

Figures 6.3 and 6.4 show the applied voltage and electric current during the sedimentation phase with two-dimensional configuration-A. The electric current reported during the test was lower than the current of the one-dimensional test. For example, at solid concentration of 25%, kaolinite-bentonite, for configuration-A, the maximum current was 0.3 A compared to 0.6 A in the test with one-dimensional configuration test.

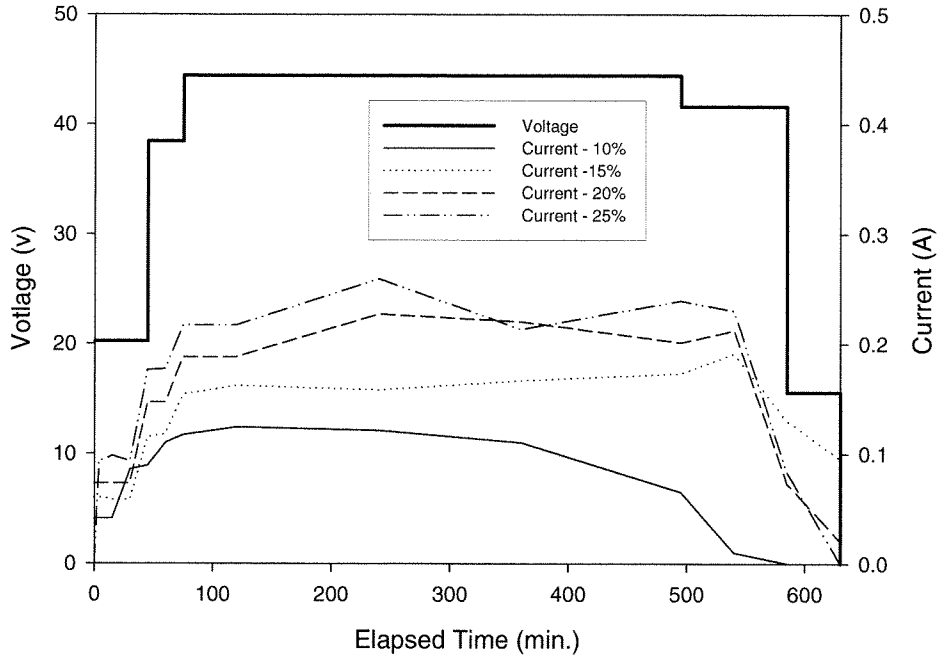

Figure 6.1 Applied voltage and electric current during the sedimentation phase with one-dimensional configuration (kaolinite).

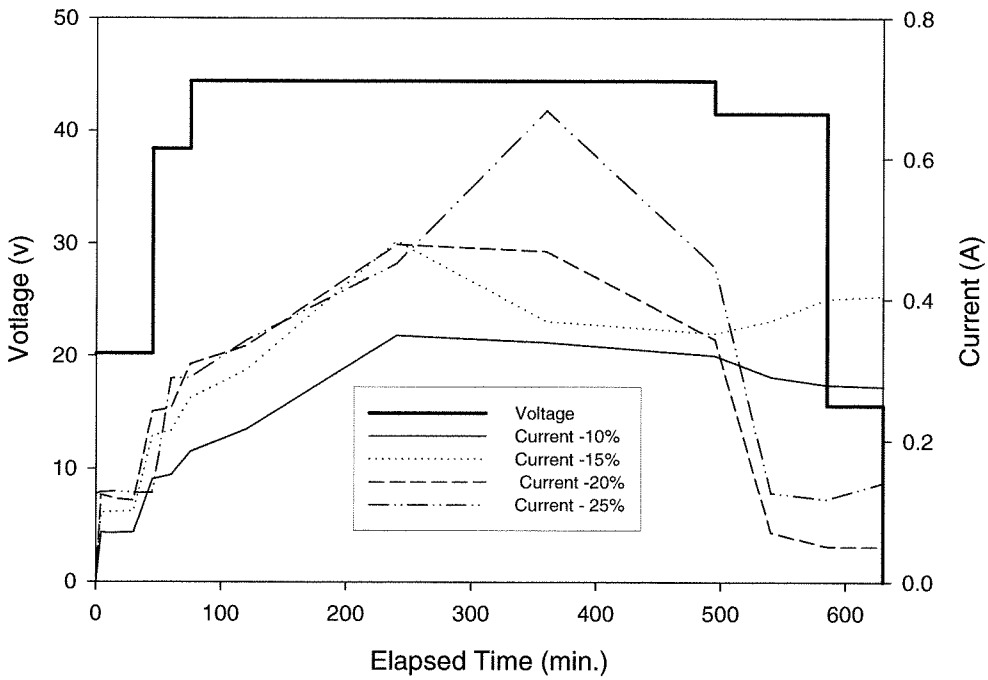

Figure 6.2 Applied voltage and electric current during the sedimentation phase with one-dimensional configuration (kaolinite-bentonite).

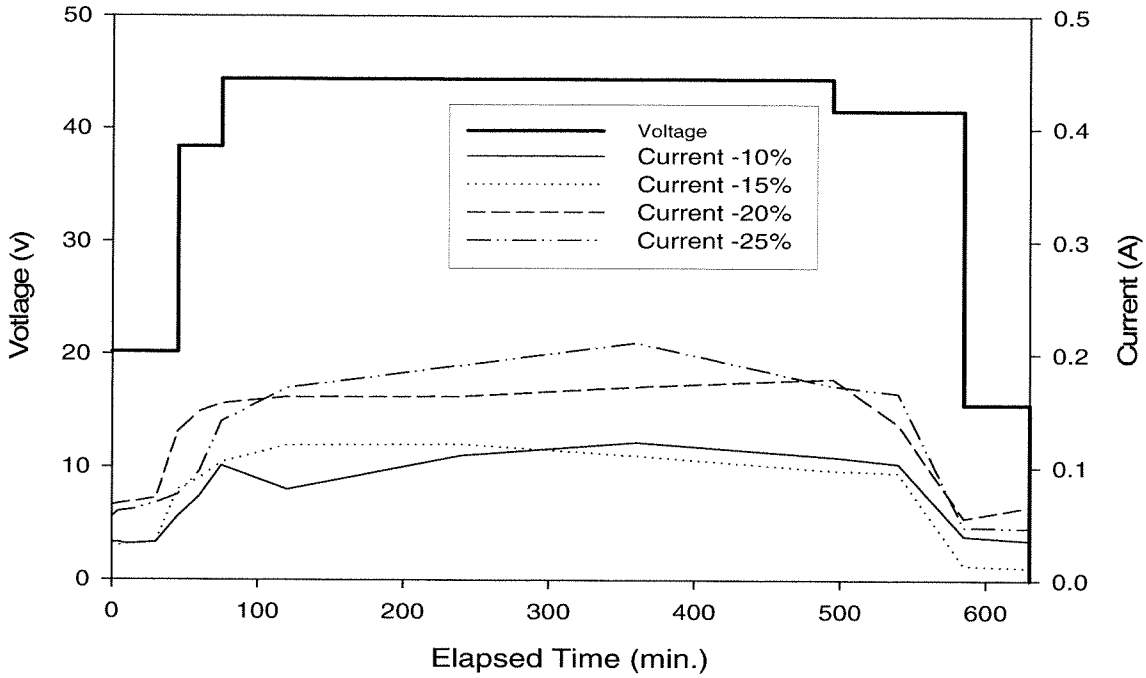

Figure 6.3 Applied voltage and electric current during the sedimentation phase with two-dimensional configuration, configuration-A (kaolinite).

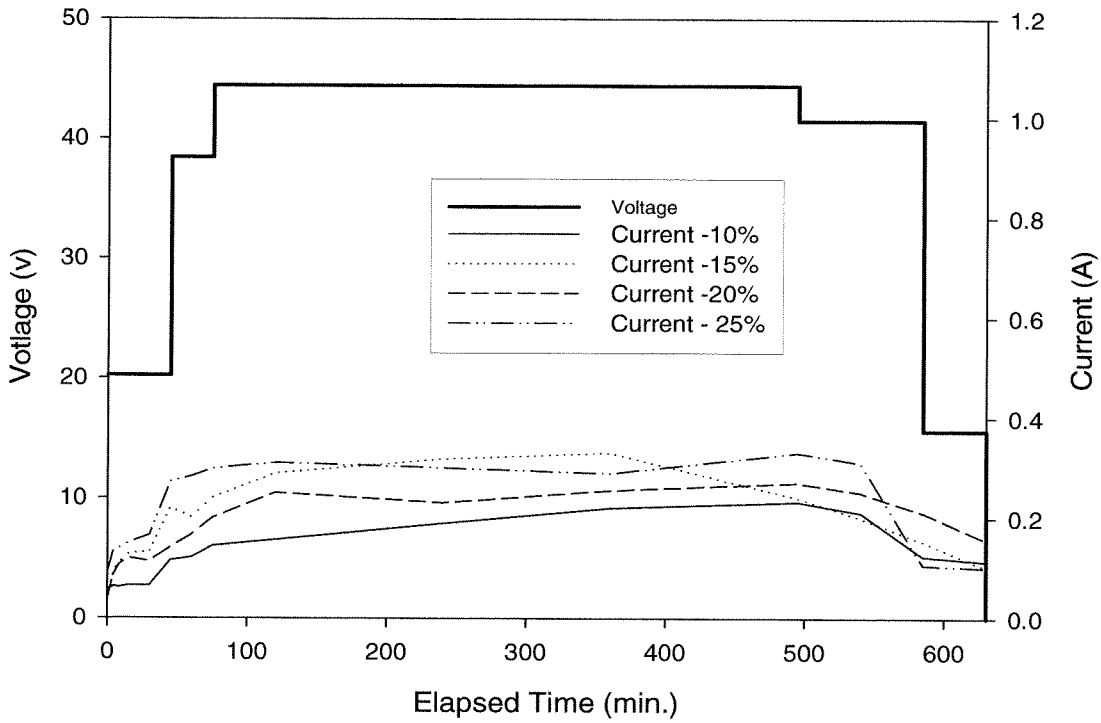

Figure 6.4 Applied voltage and electric current during the sedimentation phase with two-dimensional configuration, configuration-A (kaolinite-bentonite).

6.3.1.2 Particle settling velocity

Mohamedelhassan and Shang (2001) found that electrokinetics mainly accelerates the settling velocity of clay sized particles with grain size less than 5 μm. Figures 6.5 and 6.6 show three velocity zones, representing the gravitational particle settling velocity, u_g, the particle velocity induced by electrokinetics, u_{ek}, and the overall settling velocity, u, versus the grain size of the kaolinite and the kaolinite-bentonite. Electrophoretic velocity significantly increased the overall settling velocity for particles less than 5 μm, which is in good agreement with Mohamedelhassan and Shang (2001). An electric field intensity, E, of 160 V/m (the average of the voltage applied during the day time) was used to determine the electrophoretic velocity of the clay particles. Zeta potential of each clay type was obtained by the procedure described in Chapter Three. Figures 6.7 and 6.8 show the average gravitational settling velocity, $\overline{u_g}$, and the average settling velocity, $\bar{u}$, for kaolinite and kaolinite-bentonite slurries, respectively. At grain size < 5 μm, $\bar{u}$ for kaolinite was 0.035 cm/min while $\overline{u_g}$ was 0.028 cm/min as shown in Figure 5.7. Thus, electrokinetics increased the average velocity by 25%. For kaolinite-bentonite mixture, $\overline{u_g}$ was found to be 0.017 cm/min. The addition of the bentonite increased the fraction of particles sized less than 5 μm (see the grain size distribution curves in Figure 3.1.A and 3.1.B) and thereby deceased $\overline{u_g}$ as compared with kaolinite slurry. $\bar{u}$ was 0.023 cm/min which was 66% of $\bar{u}$ of the kaolinite slurry. This was expected since the bentonite increases the hydrostatic forces in the slurry which in turn keeps the sediments suspended. Nevertheless, the increase percentage of $\bar{u}$ at particles less than 5 μm was 35%, indicating the great effect of the electrophoresis velocity in the average

settling velocity of the kaolinite-bentonite mixture. The values of the average gravitational velocity and the overall velocity were used to evaluate the free and the hindered settling.

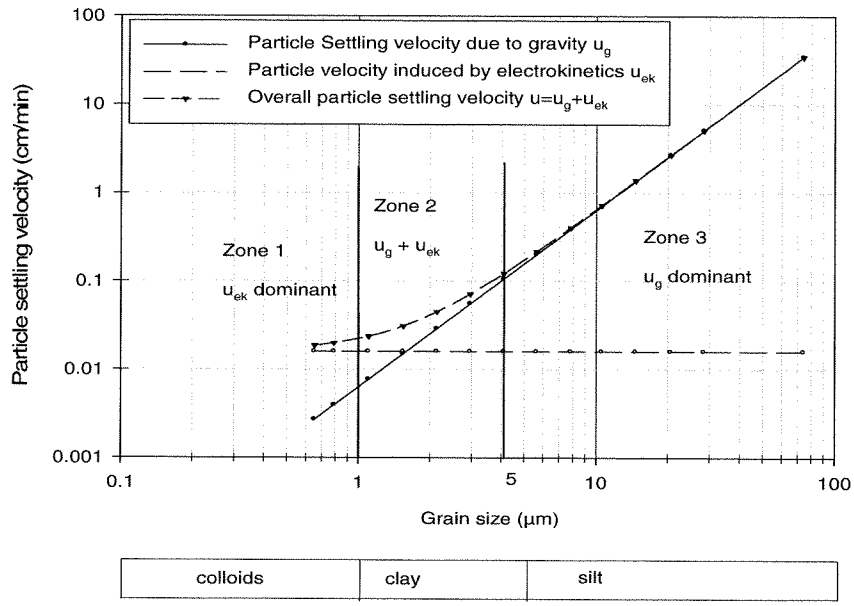

Figure 6.5 Particle settling velocity vs. grain size (kaolinite).

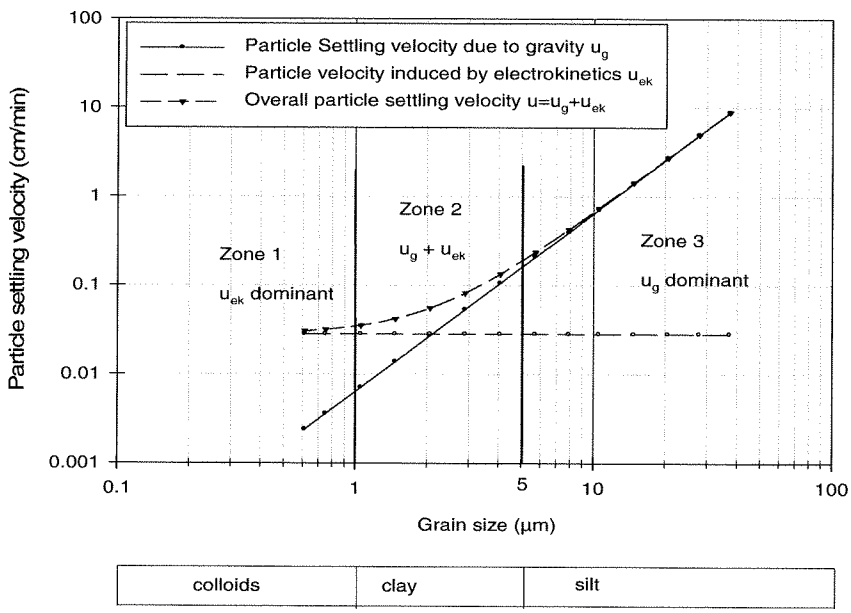

Figure 6.6 Particle settling velocity vs. grain size (kaolinite-bentonite).

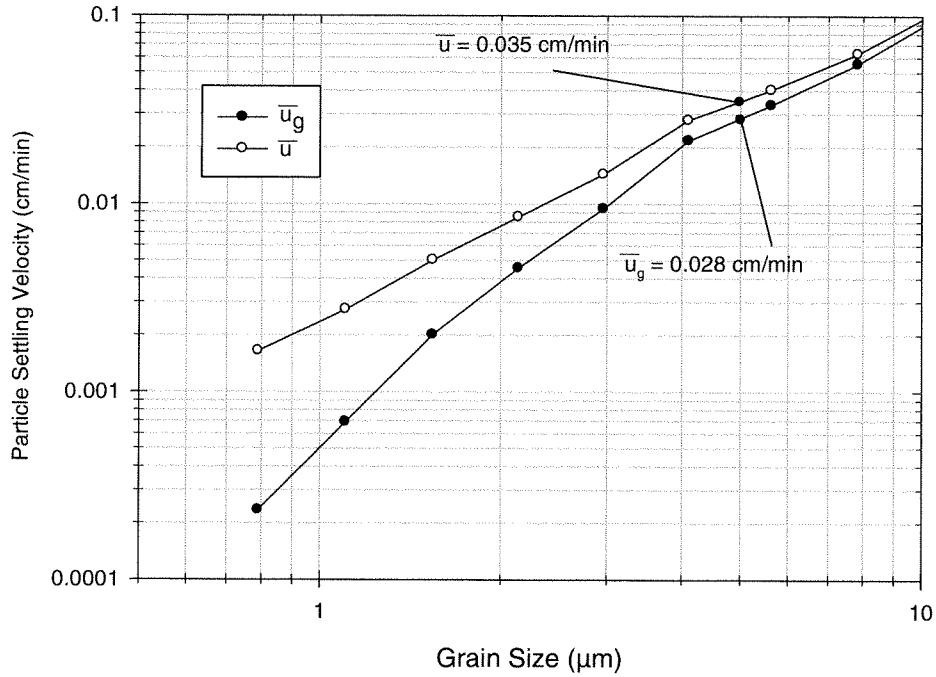

Figure 6.7 Average particle settling velocity vs. the maximum grain size (kaolinite).

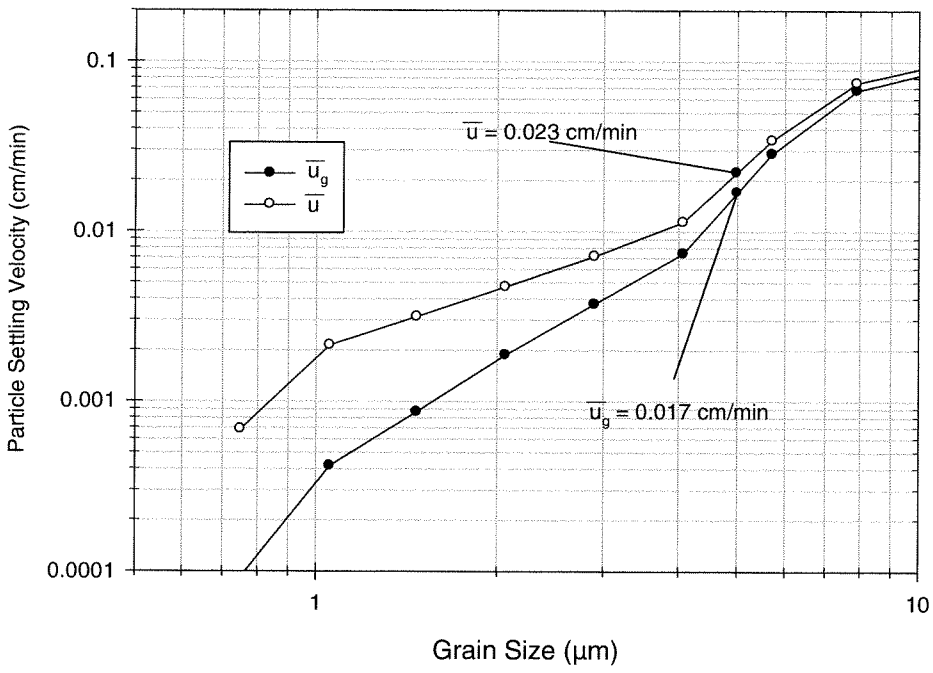

Figure 6.8 Average particle settling velocity vs. the maximum grain size (kaolinite-bentonite).

6.3.1.3 Free settling

The settlement characteristics of the slurries investigated in this study are shown in Figures 6.9 to 6.16. The drop of the mudline during the test which represents the free settling velocity, U_f, was recorded and plotted. As seen in the figures, in all the tests electrokinetics (with 1-D and 2-D configuration-A) accelerates the free settling as compared to the control test. However, the influence of electrokinetics was significant in the kaolinite-bentonite mixture tests.

The coefficient of free settling, β, was calculated using Eq. [2.36]. Tables 6.1 and 6.2 show summary of the sedimentation analysis of the kaolinite and the kaolinite-bentonite mixture slurries. The increases of $U_f$and β due to electrokinetics are included in the tables. Figures 6.17 and 6.18 show that trends of U_f for the electrokinetic and control tests were similar and U_f decreased with the increase of the solid concentration. Figures 6.19 and 6.20 show higher β values in the electrokinetic tests as compared with the control and β decreased with the increase in the solid concentration. As summarized in Tables 6.1 and 6.2, for slurries, the lowest percentage increase in β due to electrokinetics were reported in the tests with the lowest solid concentration (i.e. 10%) and the biggest percentage increase in the tests with solid contents of 20%. Shang and Mohamedelhassan (2001) also found the increase in β by electrokinetics is influenced by the solid concentration.

The increase in U_f and β due to electrokinetics were particularly remarkable in the kaolinite-bentonite slurries tests (see Table 6.2). For example, at a solid concentration

of 20%, the magnitudes of U_f and β in the electrokinetic test were 50 and 46 times those of the control test.

In general, the innovative two-dimensional electrodes configuration (configuration-A) demonstrated a higher U_f values compared with the one-dimensional configuration. For instant, at solid concentration of 10% (kaolinite-bentonite), Configuration-A increased β by 23% while the one-dimensional configuration increased β by only 5%. Similar trend was observed in most of the tests (see Tables 6.1 and 6.2).

Table 6.1 Summary of the free settling analysis of the kaolinite slurry

Initial Solid Concentration	Test	U_f (cm/min)	U_f Increase due to EK %	β	β Increase due to EK %
10%	C-10K	0.120	-	4.2	-
	EK-10K	0.150	20%	4.28	1.9%
	EKA -10K	0.178	42%	5.10	21%
15%	C-15K	0.070	-	2.50	-
	EK-15K	0.100	42 %	2.85	14%
	EKA-15K	0.113	61%	3.22	29%
20%	C-20K	0.045	-	1.60	-
	EK-20K	0.078	74%	2.22	39%
	EKA-20K	0.090	97%	2.57	60%
25%	C-25K	0.040	-	1.42	-
	EK-25K	0.055	37%	1.58	11%
	EKA-25K	0.059	47%	1.68	18%

Note:
C: Control test.

EK: Electrokinetic test with one-dimensional configuration.

EKA: Electrokinetic test with two-dimensional configuration (Configuration-A).

Table 6.2 Summary of the free settling analysis of the kaolinite-bentonite mixture slurry

Initial Solid Concentration	Test	U_f (cm/min)	U_f Increase due to EK %	β	β Increase due to EK %
10%	C-10B	0.120	-	7.06	-
	EK-10B	0.170	41%	7.39	5%
	EKA-10B	0.200	66%	8.69	23%
15%	C-15B	0.010	-	0.58	-
	EK-15B	0.051	410%	2.22	282%
	EKA-15B	0.077	670%	3.34	475%
20%	C-20B	0.00064	-	0.03	-
	EK-20B	0.032	4900%	1.39	4533%
	EKA-20B	0.031	4743%	1.34	4366%
25%	C-25B	0.00043	-	0.02	-
	EK-25B	0.015	3388%	0.65	3150%
	EKA-25B	0.019	4318%	0.83	4050%

Note:
C: Control test.

EK: Electrokinetic test with one-dimensional configuration.

EKA: Electrokinetic test with two-dimensional configuration (Configuration-A).

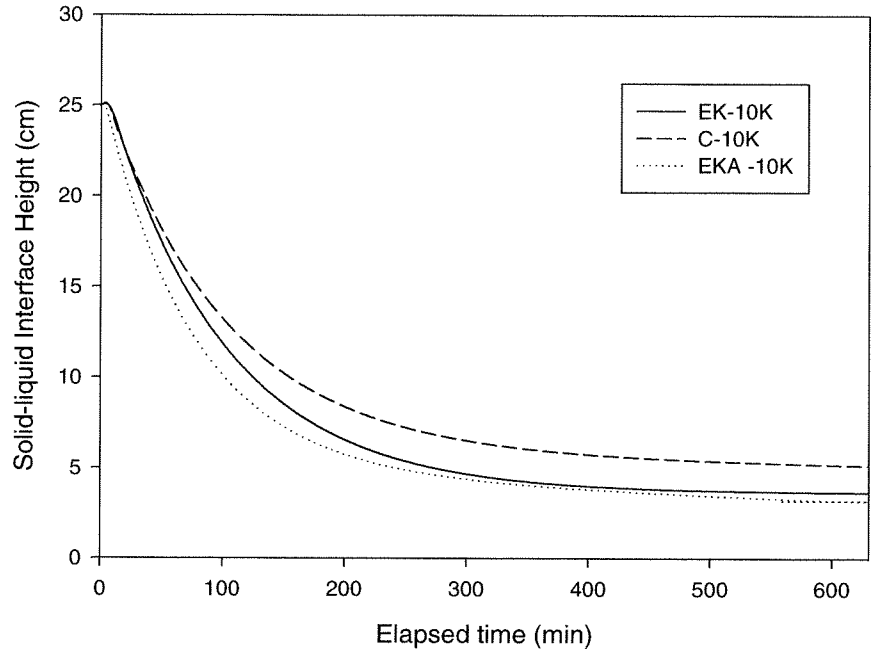

Figure 6.9 Solid-liquid interface (mudline) during tests with initial solid concentration of10% (kaolinite).

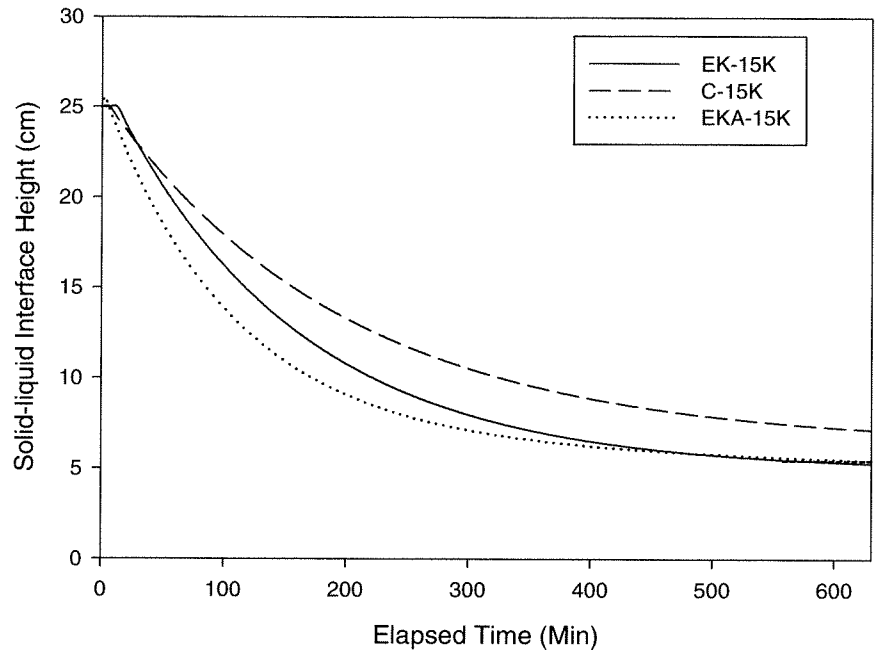

Figure 6.10 Solid-liquid interface (mudline) during tests with initial solid concentration of 15% (kaolinite).

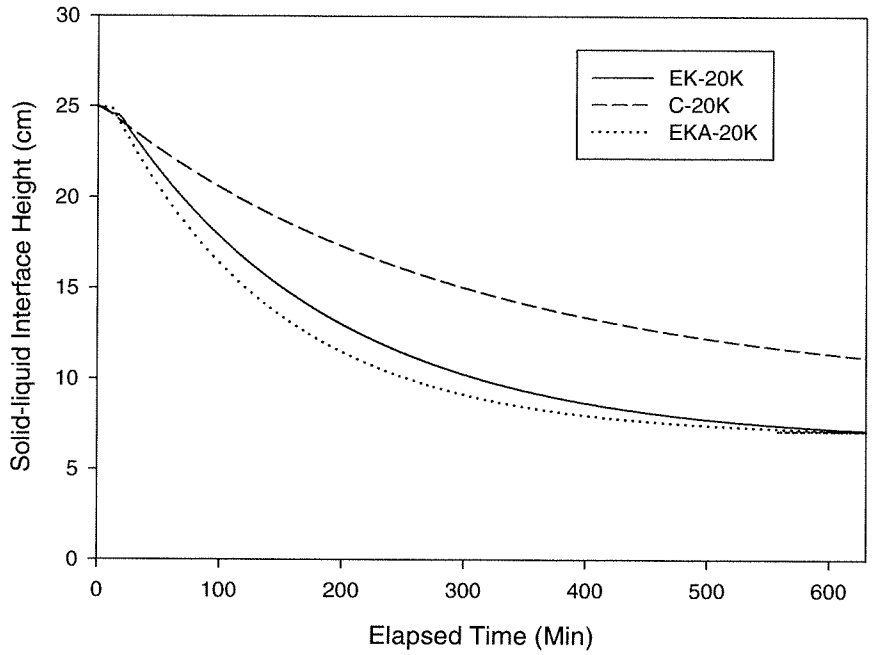

Figure 6.11 Solid-liquid interface (mudline) during tests with initial solid concentration of 20% (kaolinite).

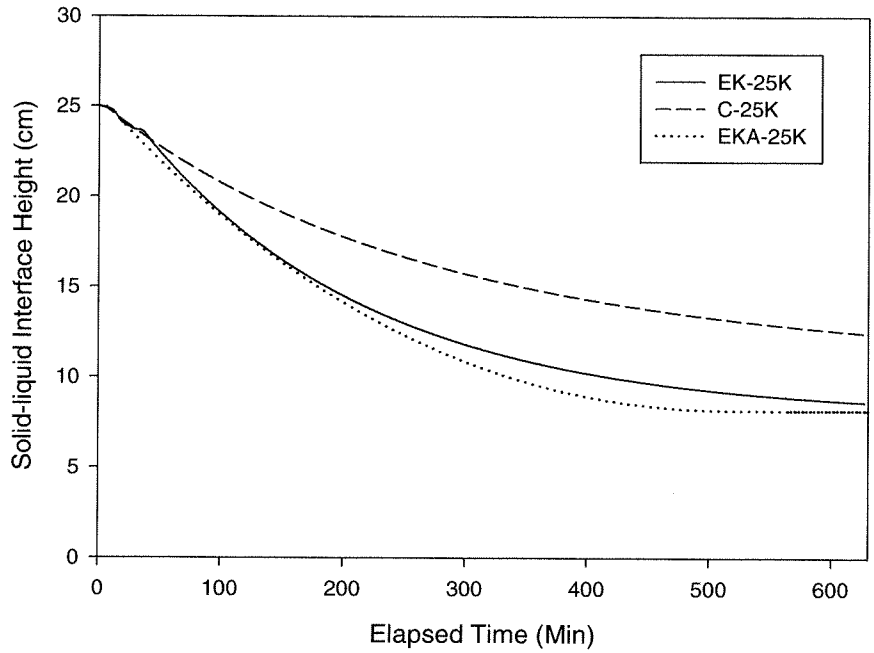

Figure 6.12 Solid-liquid interface (mudline) during tests with initial solid concentration of 25% (kaolinite).

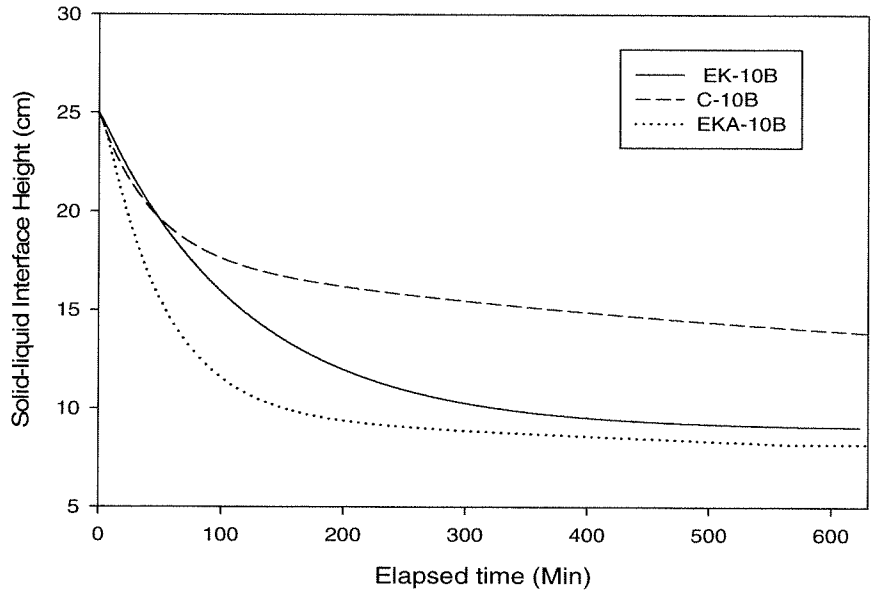

Figure 6.13 Solid-liquid interface (mudline) during tests with initial solid concentration of 10% (kaolinite-bentonite).

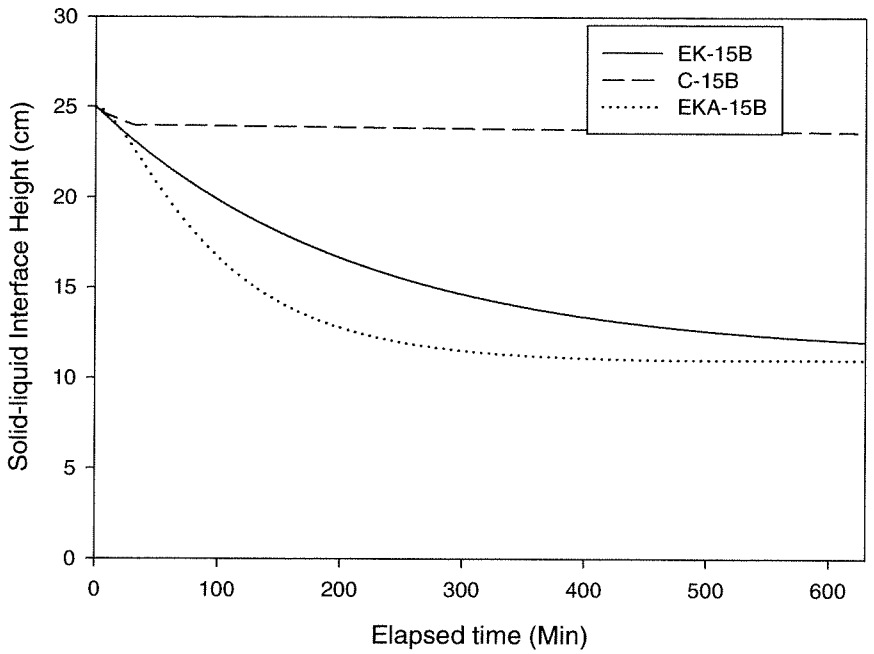

Figure 6.14 Solid-liquid interface (mudline) during tests with initial solid concentration of 15% (kaolinite-bentonite).

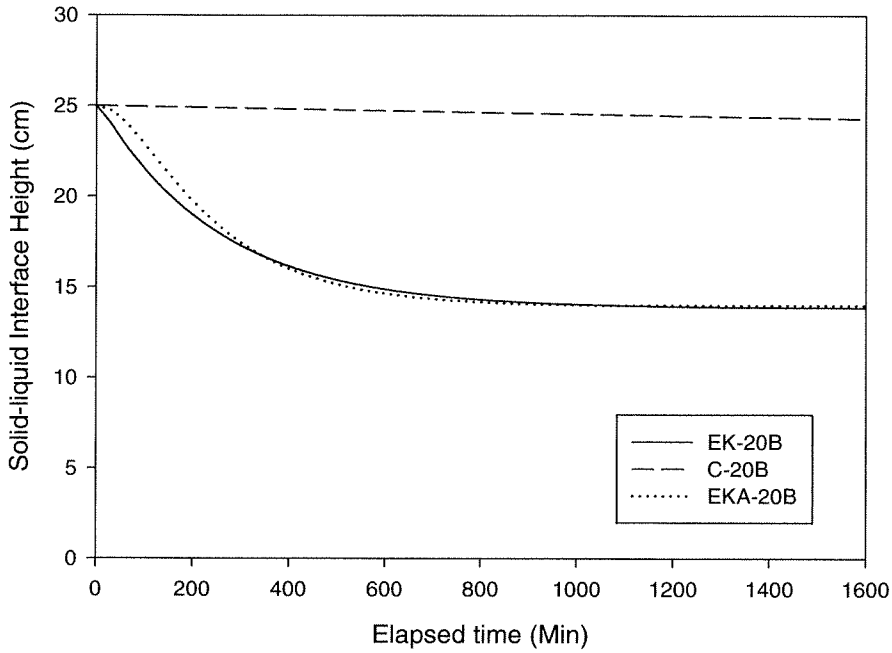

Figure 6.15 Solid-liquid interface (mudline) during tests with initial solid concentration of 20% (kaolinite-bentonite).

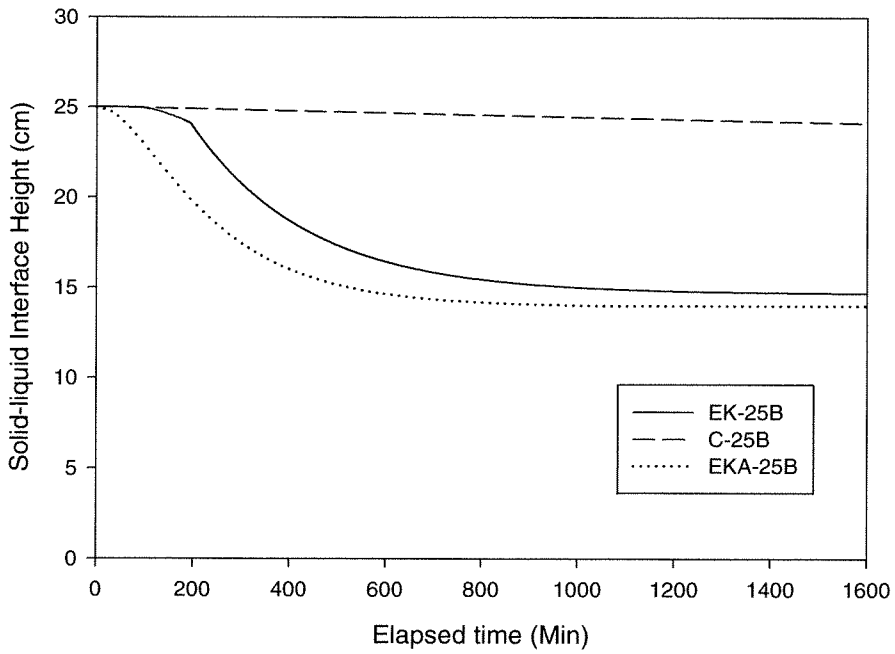

Figure 6.16 Solid-liquid interface (mudline) during the tests with initial solid concentration of 25% (kaolinite-bentonite).

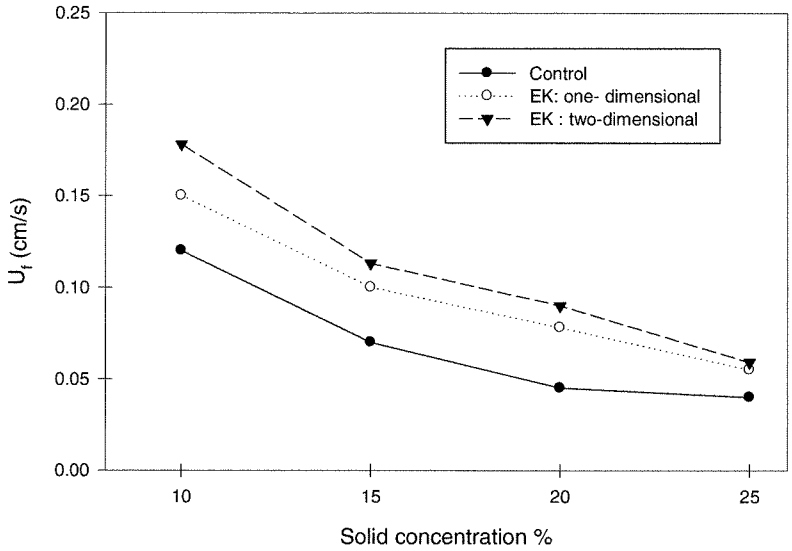

Figure 6.17 Free settling, U_f, vs. solid concentration (kaolinite).

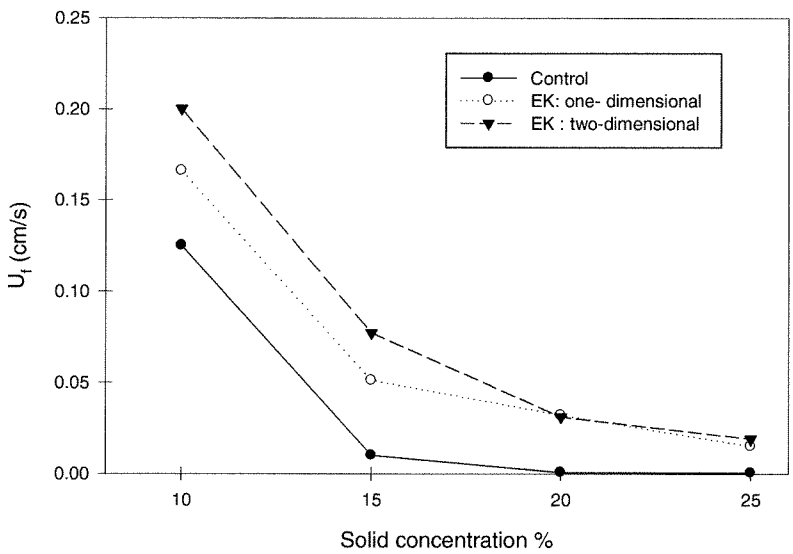

Figure 6.18 Free settling, U_f, vs. solid concentration (kaolinite-bentonite).

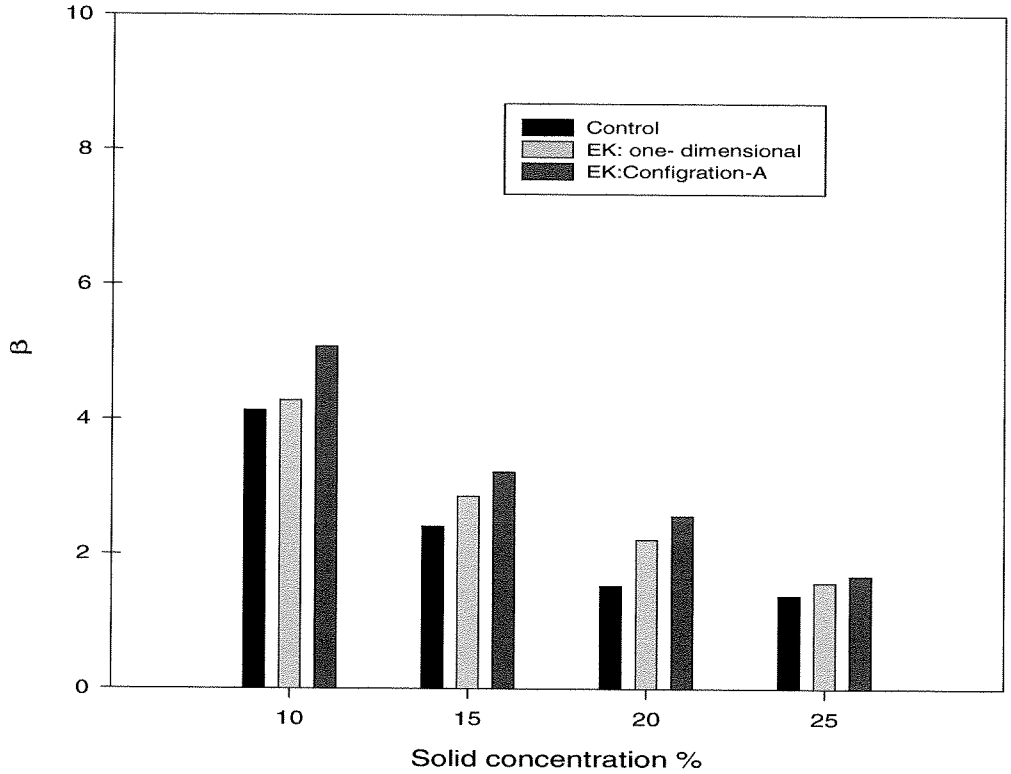

Figure 6.19 Coefficient of free settling, β, vs. solid concentration (kaolinite).

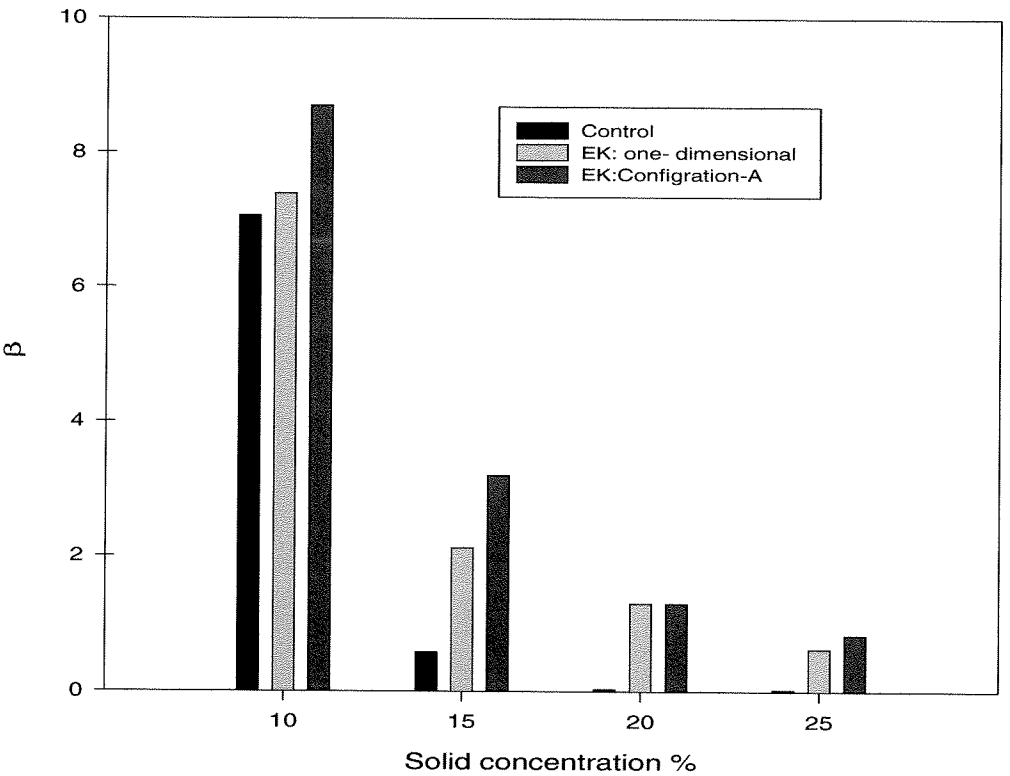

Figure 6.20 Coefficient of free settling, β, vs. solid concentration (kaolinite-bentonite).

6.2.1.4 Hindered settling

As the sedimentation process continues the solid concentration in the suspension increases while the porosity and settlement velocity decrease. This represents the hindered settling stage. The increase in the hindered settling velocity due to electrokinetics can be quantified by the decrease in the coefficient of sedimentation, r, as shown in Equation [2.39] (Mohamedelhassan and Shang, 2001). Accordingly, Δr was introduced and determined in order to evaluate the effect of electrokinetics on the higher solid concentrated slurry. Table 6.3 summarizes the values of r and Δr for the tests. As seen in the table, for kaolinite at the same initial concentration, r of electrokinetic test was consistently less than that of the gravitational test (control). The changes in the coefficient of sedimentation due to electrokinetics, Δr, were in ranged between 5.1 and 12.6, representing a decrease of 26.8 to 61.4%, as compared to the control. For kaolinite-bentonite tests, at solid concentration of 10%, Δr was 75.6% of r_g (the coefficient of sedimentation in the control test). At higher solid concentrations (15, 20 and 25%), r_g was very difficult to obtain as the gravitational hindered settlement was negligible and hence r_g was significantly high. Configuration-A tests had r values approximately similar to the one-dimensional tests. The values of r acquired from the electrokinetic tests put emphasis on the magnitude of the electrophoretic velocity, as it was the main mechanism that caused the increase in the hindered settlement. For kaolinite-bentonite slurries, r at solid concentration of 25% with the one-dimensional configuration was 12, compared to 37.2 and 41.4 for the 15% and 20% solid concentration, respectively. In fact, electrokinetics shows important influence on the

sedimentation of kaolinite-bentonite mixture compared to the control tests, particularly with the higher solids concentrations 20% and 25%.

Table 6.3 Coefficients of sedimentation, r_g, r and Δr evaluated from the tests

Initial Solids Concentration	Test	Kaolinite slurry		Kaolinite-bentonite slurry	
		r	Δr	r	Δr
10%	Control-(r_g)*	21.6	-	180.5	-
	EK	13.5	8.1	43.6	136.4
	EKA	13.6	8.0	44.8	136.2
15%	Control-(r_g)	19.6	-	-	-
	EK	11.9	7.8	37.2	-
	EKA	14.0	5.1	42.5	-
20%	Control-(r_g)	20.1	-	-	-
	EK	13.0	7.0	41.4	-
	EKA	14.3	5.8	50.0	-
25%	Control-(r_g)	20.5	-	-	-
	EK	10.5	10.0	12.0	-
	EKA	8.0	12.6	18.6	-

*(r_g): Gravitational settling coefficient

*EK: Electrokinetics.

6.3.2 Phase 2: Electrokinetic Dewatering and Decontamination

In this phase of the experiment, which started after the completion of sedimentation, the water above the mudline that remained from the sedimentation stage was removed. At this time, the solid concentration in the slurry was much higher than the initial concentration. The polarity of electrodes was reversed with the top electrode now serving as anode and the bottom electrode as cathode. The applying electric field on the slurry induced movement of water and copper from the slurry by electro-osmosis and electro-migration. The electric current, water removed, reduction in the volume of slurry, finial solid concentration, pH and copper concentration were presented and discussed in the following sections.

6.3.2.1 Applied voltage and electric current

Figures 6.21 to 6.22 show the variation of the applied voltage and electric current during the dewatering and decontamination phase of the electrokinetic tests. Maximum voltage of 44 V was applied during most of the day time and a zero voltage was observed during the night. As shown in Figures 6.21 and 6.22, the electric current decreased during the dewatering phase of the test. This was caused by the change of the electrical conductivity of soil resulted from the reduction of the water content of the soil. Compared to the sedimentation phase, higher electric current values were reported in tests during the dewatering phase. This was caused by the shorted distance between electrodes in such tests and subsequently higher electric field intensity and electric current.

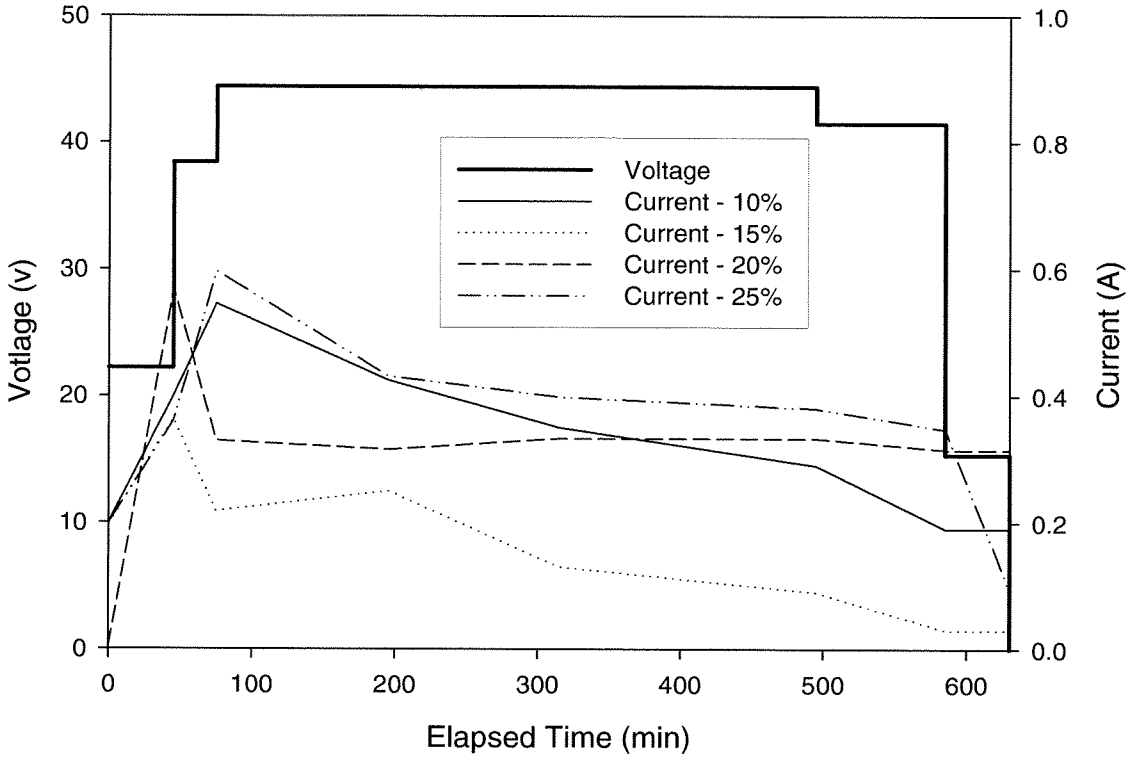

Figure 6.21 Applied voltage and electric current during the dewatering and decontamination phase with one-dimensional configuration (kaolinite).

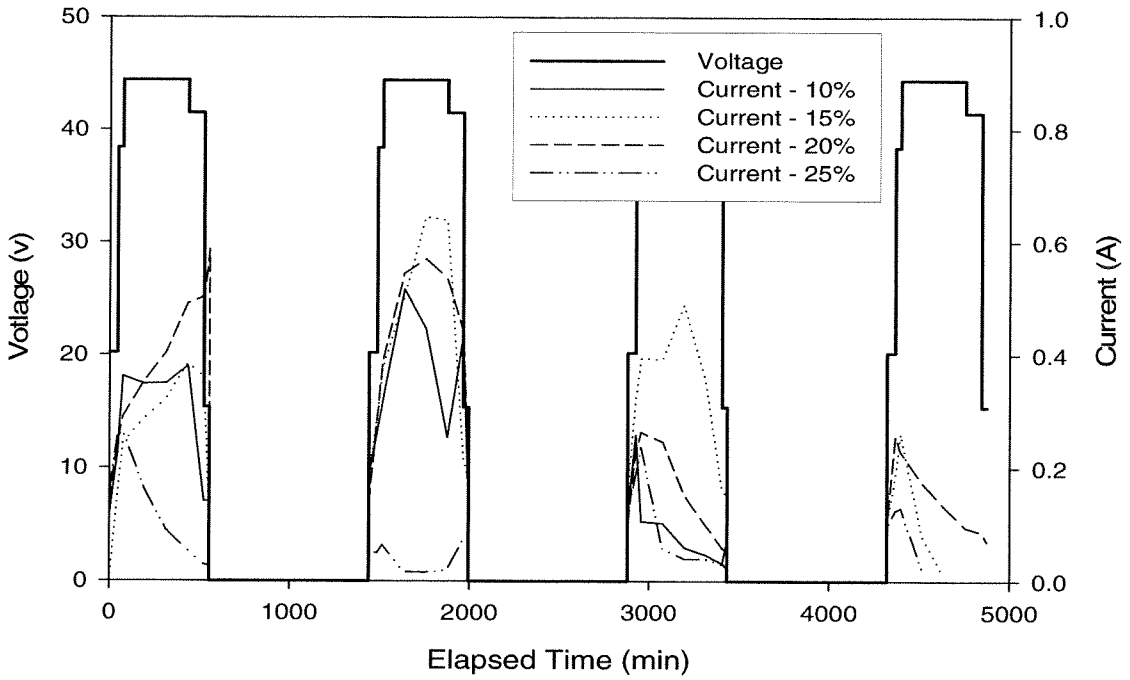

Figure 6.22 Applied voltage and electric current during the dewatering and decontamination phase with one-dimensional configuration (kaolinite-bentonite).

6.3.2.2 Electrokinetic dewatering

The accumulative volume of water collected during the dewatering phase for the kaolinite and kaolinite-bentonite mixture tests are shown in Figures 6.23 and 6.24. Table 6.4 summarizes the total volume of water removed during the dewatering phase along with the percentage increase in water removal due to electrokinetics. As seen in the table, electrokinetics was successful in removing more water from the slurry of both clay soils as compared with the control test. The removal of water was more significant from the tests with kaolinite-bentonite mixture. For example, in the test with 10% solid concentration, the percentage increase of water removal was 1880% in the kaolinite-bentonite mixture slurry compared to an increase of 126% in the kaolinite slurry. The extreme increase in water removal the kaolinite-bentonite mixture was due to the effectiveness of electro-osmosis in drainage water from soils with very small pore size such as bentonite.

The dewatering phase was considered complete when the drainage of water from the electrokinetic column had ceased and the current had dropped to a value less than 0.01 A. The time required to complete the dewatering for kaolinite was around 10 h compared to more than 80 h for kaolinite-bentonite. In view of that, the coefficient of electro-osmotic permeability, k_e, was calculated for the both slurries using Equation [2.8]. The average k_e was 9.6×10^{-6} m^2/s V for kaolinite and 8.5×10^{-6} m^2/s V for kaolinite-bentonite mixture.

Table 6.4 Volume of water removed during phase-2 (dewatering and decontamination)

Initial Solids Concentration	Test	Kaolinite	Kaolinite-bentonite
		Water Removed	Water Removed
10%	Control-	75 mL	25 mL
	EK	170 mL	495 mL
	% Increase due to EK	126%	1880%
15%	Control-	46 mL	30 mL
	EK	150 mL	254 mL
	% Increase due to EK	226%	746%
20%	Control-	110 mL	37 mL
	EK	215 mL	515 mL
	% Increase due to EK	95%	1292%
25%	Control	73 mL	47 mL
	EK	265 mL	412 mL
	% Increase due to EK	260%	777%

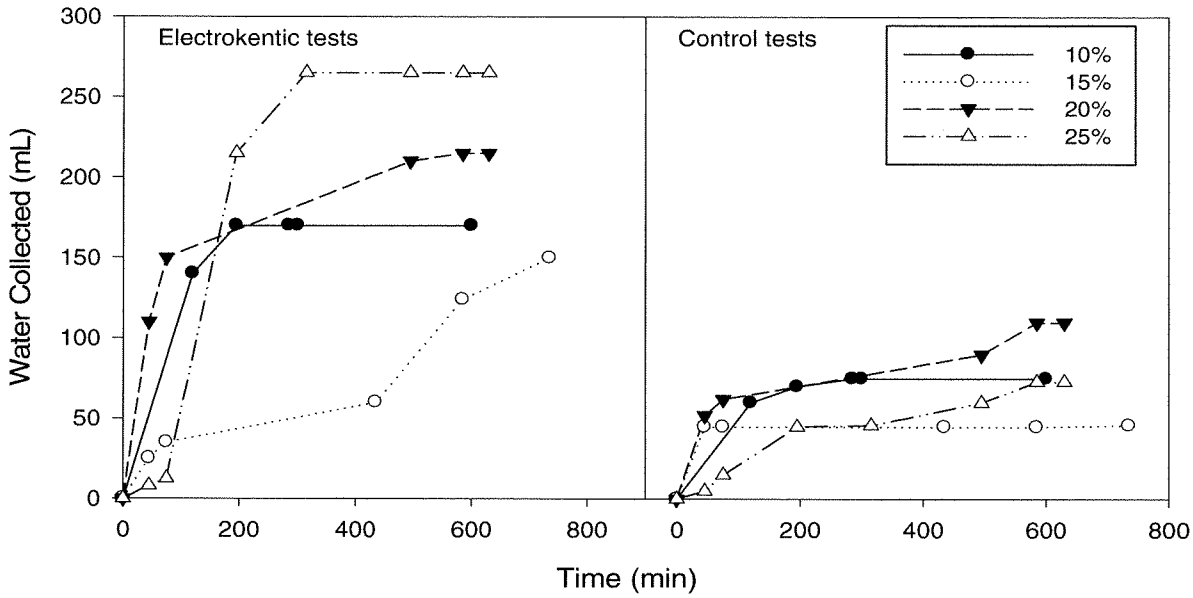

Figure 6.23 Volume of water collected from the kaolinite slurry during phase-2 (dewatering and decontamination).

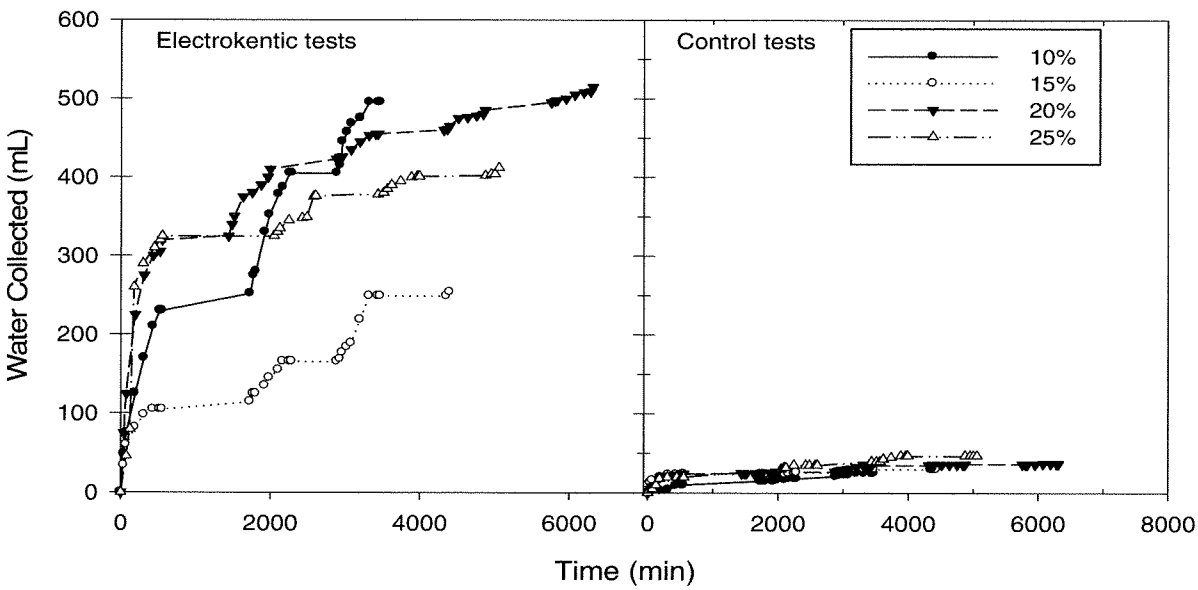

Figure 6.24 Volume of water collected from the kaolinite-bentonite slurry during phase-2 (dewatering and decontamination).

6.2.2.3 Total volume reduction

The need for reducing the volume of contaminated slurries is increasingly important in order to reduce the waste management costs and reuse the ponds basin (Shang, 1997). The total volume reduction of the slurries was calculated to emphasis the advantages of electrokinetic dewatering and consolidation. Table 6.5 shows the percentage of volume reduced in the sedimentation phase (phase 1) and the final volume reduction (phase-1 and 2). As seen the table, the final volume reduction in electrokinetics test was determinedly greater than the reduction by gravity alone (control test). As summarized in Table 6.5, the reduction in volume during electrokinetic sedimentation phase was dominant, yet the dewatering phase after the polarity reversal contributed significant reduction, particularly, in the kaolinite-bentonite slurry. The final volume reduction was significantly high in the kaolinite-bentonite mixture tests. For example, at the 25% solid concentration, 59% volume reduction was achieved by the electrokinetics comparing to 8% in the control test. The corresponding volume reduction in the kaolinite slurry test was 75% in the electrokinetic test and 62% in the control.

The final solid concentration for each test was determined and presented in Table 6.6. In comparison with the control, the combination of electrokinetic sedimentation and dewatering evidently increased the final solid concentration by the end of each test. The average final solid concentration for the kaolinite slurry with initial solid concentration of 20% was 65% in the electrokinetic test and 50% in the control, representing a 30% increase by electrokinetics. For the same initial solid concentration the final concentration in kaolinite-bentonite tests was 50% with electrokinetics and 27%

in the control. This represents an increase in solid concentration of 85% due to electrokinetic as compared with the control. Thus, electrokinetics was more effective on the kaolinite-bentonite mixture slurry, which is harder to dewater and consolidate by gravity alone.

Table 6.5 Volume reduction of the slurry during the sedimentation and dewatering processes.

Stage	Initial Solids Concentration	Test	Kaolinite	Kaolinite-bentonite
			Volume reduction	
Volume reduction in Sedimentation phase	10%	Control	83%	57%
		EK	85%	64%
	15%	Control	74%	12%
		EK	79%	56%
	20%	Control	65%	9%
		EK	72%	44%
	25%	Control	60%	6%
		EK	67%	45%
Final volume reduction	10%	Control	86%	58%
		EK	91%	81%
	15%	Control	76%	13%
		EK	84%	64%
	20%	Control	68%	10%
		EK	79%	60%
	25%	Control	62%	8%
		EK	75%	59%

Table 6.6 Final solid concentration after the end of the tests.

	Initial solid concentration	Kaolinite		Kaolinite-bentonite	
		Control	EK	Control	EK
Solid concentration sedimentation phase	10%	45%	49%	21%	25%
	15%	46%	53%	17%	30%
	20%	46%	54%	22%	32%
	25%	51%	57%	26%	40%
Polarity reversal					
Finial solid concentration	10%	51%	66%	22%	41%
	15%	48%	63%	17%	36%
	20%	50%	65%	22%	42%
	25%	53%	69%	27%	50%

6.3.2.4 Decontamination of copper

The magnitude of copper concentration was selected so the copper was mostly adsorbed by the soil. Accordingly, a concentration of 400 mg/kg of dry soil was used in the kaolinite slurry tests and a concentration of 800 mg/kg of dry soil in the kaolinite-bentonite slurry tests. After the completion of the sedimentation phase, the water on top of the settled slurry was collected and tested for pH and copper content. Table 6.7 presents the results. As seen the table, the amount of copper in the top water was found to be very small in the control and electrokinetic tests. The pH of the water varied between 10.5 and 11.8 in the electrokinetic test and 6.5 to 7.9 in the control tests. The low copper content in the electrokinetic tests may be due to the higher pH of the top

water caused by the hydroxide ions generated by electrolysis reaction at the cathode. Although electromigration transports cations (i.e. copper) towards the cathode (i.e. top water), the pH environment of the top water promotes copper precipitation (Evengelou, 1998). This may explain the lower copper content of the water in particular for the kaolinite-bentonite tests.

Table 6.7 Copper concentration and pH of the water above the mudline after the sedimentation phase.

Test		Copper Concentration mg/L		pH	
Slurry type	Initial solid concentration	Control	EK	Control	EK
Kaolinite	10%	0.01	0.13	6.5	10.7
	15%	0.21	0.05	6.6	11.0
	20%	0.01	0.05	6.1	11.1
	25%	0.17	0.29	6.6	11.2
Kaolinite-bentonite	10%	1.30	0.04	7.6	11.2
	15%	0.51	0.01	7.8	11.6
	20%	0.10	0.10	7.9	11.7
	25%	0.65	0.11	7.9	11.8

6.3.2.4 .1 Copper concentration and pH of Outflow water during the dewatering

Table 6.8 presents the copper concentration and pH of the water collected during the dewatering phase, where the bottom electrode served as cathode and the top as the anode. Under such configuration, the copper is removed by electro-osmosis, electro-migration and gravitational drainage in the electrokinetic test and by gravitational drainage alone in the control test. Accordingly, Table 6.8 shows the copper concentration of the water collected in the electrokinetic tests to be consistently higher

than in the water collected during the control tests. As shown in the table, the concentration of copper in the water collected from the kaolinite slurry was generally lower than that of the kaolinite-bentonite slurry. This may be due to initial amount of copper in the slurry which was 800 mg/kg in the kaolinite-bentonite and 400 mg/kg in the kaolinite. The amount of copper removed in electrokinetic tests increased in the kaolinite-bentonite slurries compared to the kaolinite. This further illustrates the effectiveness of electrokinetics in kaolinite-bentonite tests.

The pH values of the removed water were lower in the electrokinetic tests as compared with the control, with the lowest value reported in the kaolinite-bentonite tests. Low pH water contributes to dissolution of copper from the soil and subsequently more removal of copper from the soil which contributed to the higher copper removal in the kaolinite-bentonite tests.

Table 6.8 Copper concentration and pH of the water removed during the dewatering phase.

Test #		Copper Concentration mg/L		pH	
Slurry type	Initial solid concentration	Control	EK	Control	EK
Kaolinite	10%	0.13	0.17	8.1	7.4
	15%	0.23	0.41	8.1	7.6
	20%	0.06	0.22	8.1	7.9
	25%	0.03	0.67	7.8	6.6
Kaolinite/ bentonite	10%	0.44	4.53	7.0	2.6
	15%	0.20	17.5	7.6	2.9
	20%	0.39	24.6	7.7	3.0
	25%	0.54	32.9	7.7	3.9

6.3.2.4 .2 Copper concentration in pore fluid

After the completion of the test, soil pore fluid was recovered from the soil using the squeezer cell (described in Chapter Four) and tested for copper concentration. Two samples of pore fluid, one near the anode and one near the cathode, were recovered and tested for each test. Table 6.9 summarizes the results. The amount of copper in pore fluid was found to be higher in the electrokinetic tests as compared with the control. In the electrokinetic test, the copper in the section near the cathode was much higher than in the section near the anode. The decrease of pH near the anode by electrolysis reactions causes the dissolution and desorption of copper from the soil to the pore fluid. The released copper travels by electro-osmosis and electro-migration toward the cathode (Alshawabkeh and Acar, 1996). This may explain the higher copper concentration near the cathode. One representing sample was tested for the control test as the initial copper concentration. The residual water content after the test near the electrodes is presented in Table 6.9. The water content of the soil near the anode was consistently found to be lower than near the cathode. That resulted from electro-osmosis flow.

6.3.2.4 .3 Residual copper concentration in the dewatered slurry

Table 6.9 shows the total copper concentrations (mg/kg dry soil) after the dewatering of the test for the both slurry types. These concentrations have been obtained from the digestion test described in Chapter Four. The copper concentration near the anode and the cathode parts are presented as a percentage ratio of the initial concentration (c_o).

As seen in Table 6.9, electrokinetics had considerably minimized copper concentration near the anode. For example, at solid concentration of 10% (kaolinite-bentonite), the copper concentration near the anode was 31% of the initial concentration while the cathode part was 115%. The percent concentration clearly shows that electrokinetics pushed the contaminant towards the cathode through the combination of the electro-osmosis and electro-migration mechanisms. Further, the high pH near the cathode increased the adsorption of the copper by the soil solids.

Table 6.9 Copper concentration in pore fluid, total copper concentration and water content after the test (1- D configuration).

Clay type	Initial Solid Conc.	Sample #	Residual Water content %	Pore fluid Copper Conc. mg/L	Pore fluid Copper Conc. mg/kg	Total Copper Concentration mg/kg	C/C_0 %
Kaolinite	10%	Anode	37.6	1.87	0.70	164.39	41%
		Cathode	38.3	15.74	6.04	475.60	119%
		Control c_0	88.3	0.133	0.12	400	-
	15%	Anode	25.2	0.50	0.13	205.5	51%
		Cathode	27.5	67.30	18.51	555.5	139%
		Control c_0	70.3	0.23	0.16	400	-
	20%	Anode	23.4	0.38	0.09	344	86%
		Cathode	32.8	127.60	41.83	388.4	97%
		Control c_0	55.1	0.06	0.00	400	-
	25%	Anode	21.0	15.91	3.34	362	90%
		Cathode	27.0	191.80	51.79	489.25	122%
		Control c_0	47.9	0.031	0.02	400	-
Kaolinite - bentonite	10%	Anode	45.5	7.56	3.40	245	31%
		Cathode	57.5	39.67	22.81	925	115%
		Control c_0	78.3	0.44	0.35	800	-
	15%	Anode	51.3	2.03	1.04	619.5	77%
		Cathode	60.2	14.21	8.56	1174.2	143%
		Control c_0	82.0	0.442	0.36	800	-
	20%	Anode	41.0	8.23	3.38	648	81%
		Cathode	40.3	36.87	14.85	1731.5	216%
		Control c_0	41.3	0.399	0.17	800	-
	25%	Anode	48.4	10.36	5.01	777.5	97%
		Cathode	51.4	46.38	23.84	1893	236%
		Control c_0	72.1	0.546	0.39	800	-

6.3.3 Two-Dimensional Configuration-B

According to the previous results, electrokinetics significantly accelerated the sedimentation of the contaminated kaolinite-bentonite slurries. Innovative two-dimensional electrodes configuration, configuration-B, was introduced to simulate field conditions (see Figure 4.7). During this experiment, the voltage and current were monitored and reported along with the pH and the electrical conductivity. The change in the zeta potential during the test was determined and used to evaluate the sedimentation factors. The following sections discuss the analysis of the results.

6.3.3.1 Voltage and current distribution

Figure 6.25 shows the voltage and current distribution during the tests. At solids concentration of 10%, the maximum current was 3.5 A compared to 4.8 A at 25% solids concentrations. As discussed before, the current is function of the electrical conductivity of the soil (solids + water). The increase of the solids concentration leads to increase of the electrical conductivity and subsequently the electric current. Configuration-B had 4 electrodes covered 30% of the surface area of the slurry (cathodes) and only one electrode covers 9% of the bottom area. The following section discusses the electric field intensity.

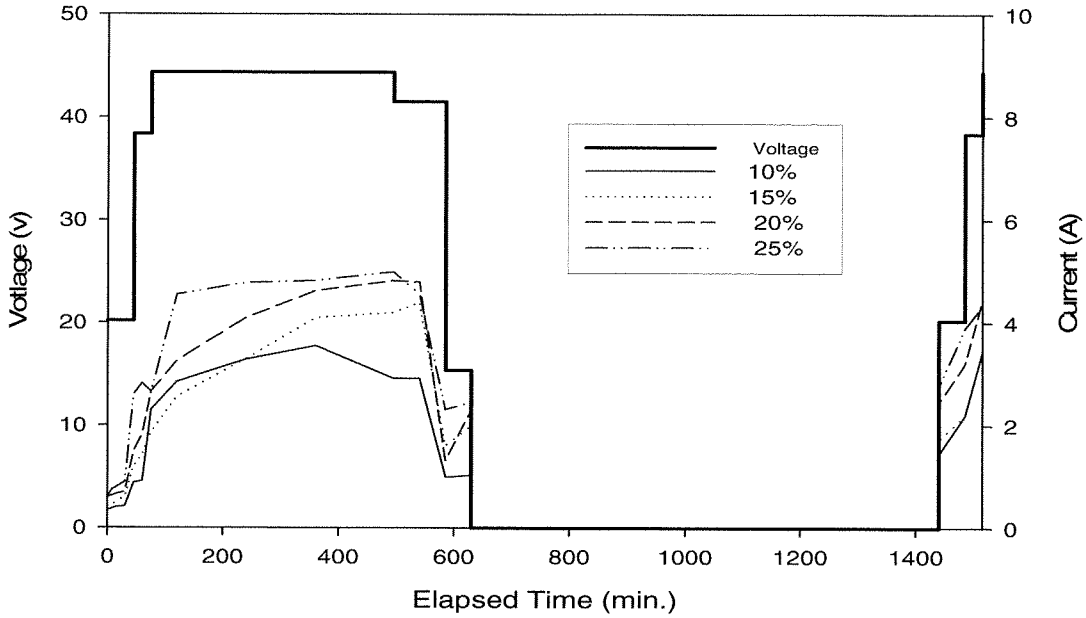

Figure 6.25 Applied voltage and electric current during the test (two-dimensional configuration-B).

6.3.3.1.1 Voltage distribution and electric field intensity of the 2-D configuration-B

The electrode configuration of the test (Configuration-B) was discussed in Chapter Four. For an average conductivity of 3 mS/cm and average applied voltage of 40 V, the distribution of the electric field in two-dimensional configuration was modelled using QuickFiled^{TM} (Tetra Analysis Ltd., 2011). Since configuration-B was a two dimensional configuration, 2 cross-sectional locations were chosen to represent the voltage and the electric field intensity distribution as shown in Figure 6.26. The voltage distribution across A-A and B-B are shown in Figures 6.27 and 6.28, respectively. Figures 6.27 and 6.28 show that values of the voltage varies from 40 V (maximum) near the anode to zero at the cathodes. Figure 2.29 illustrates the voltage across A-A and B-B at the

centre of the electrokinetic tank at the beginning of the test. As shown in the figure, a little steeper voltage gradient develops in A-A, while low gradient develops in B-B due to their electrode configuration.

For applied voltage of 40 V and distance between electrodes of 25 cm, the electric field intensity, E, for one-dimensional electric field is 160 V/cm. Figures 6.30 and 6.31 shows the electric field intensity across A-A and B-B, respectively. For the cross-section A-A, electric field of 140 to 160 V/m dominated the area between the electrodes as shown in figure 6.30. For B-B, the dominant E was in range of 100 to 120 V/m.

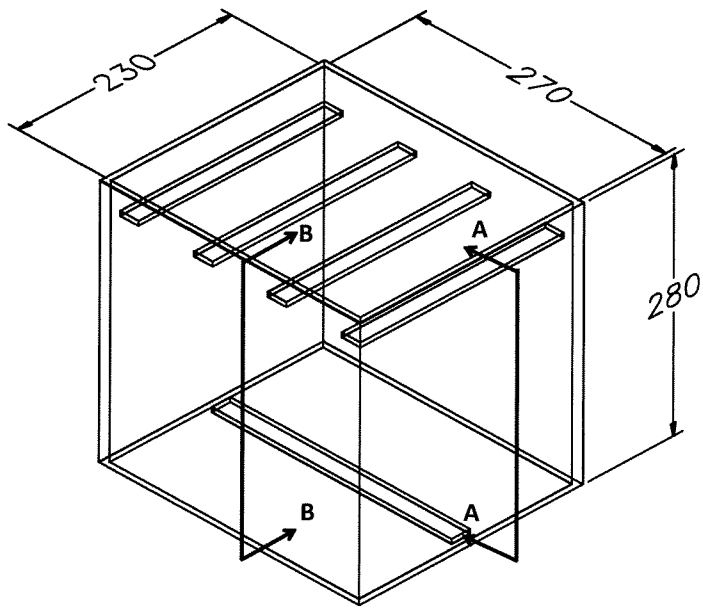

Figure 6.26 Schematic for the electrokinetic tank with the location of the cross-sections A-A and B-B.

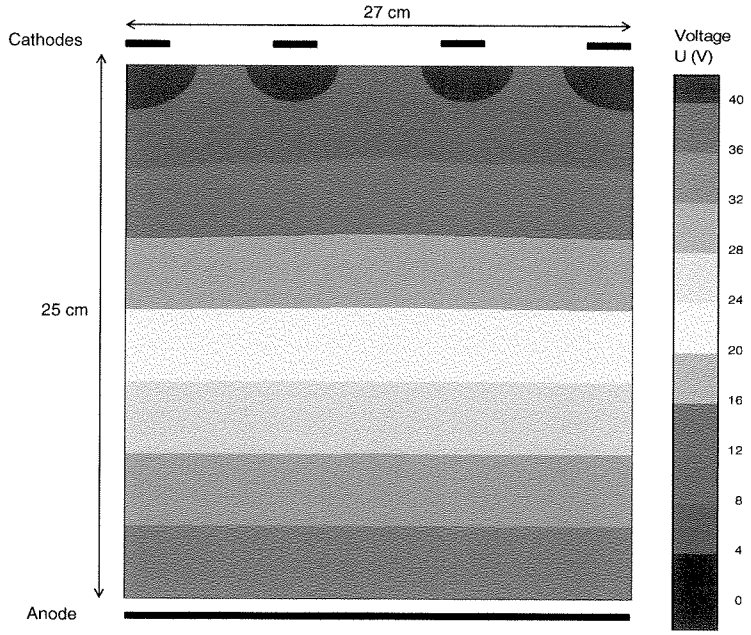

Figure 6.27 Voltage distribution for the cross-section A-A.

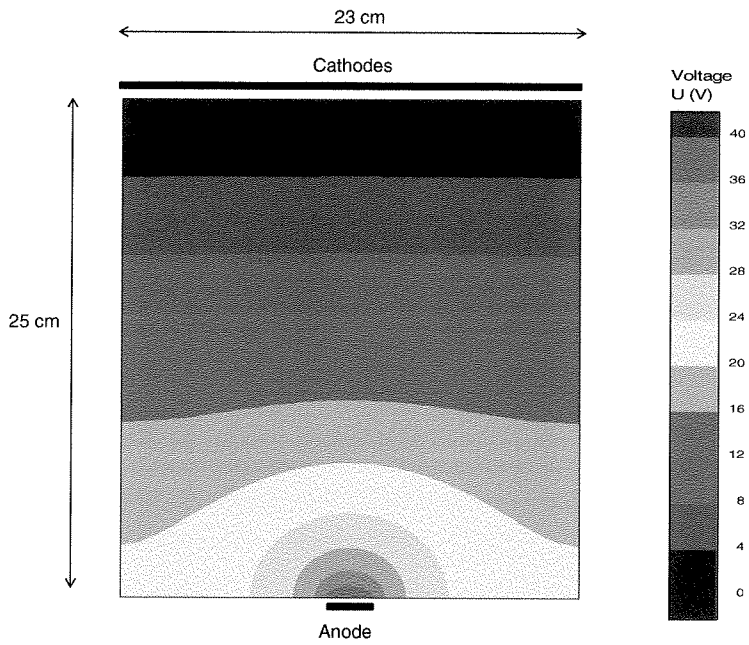

Figure 6.28 Voltage distribution for the cross-section B-B.

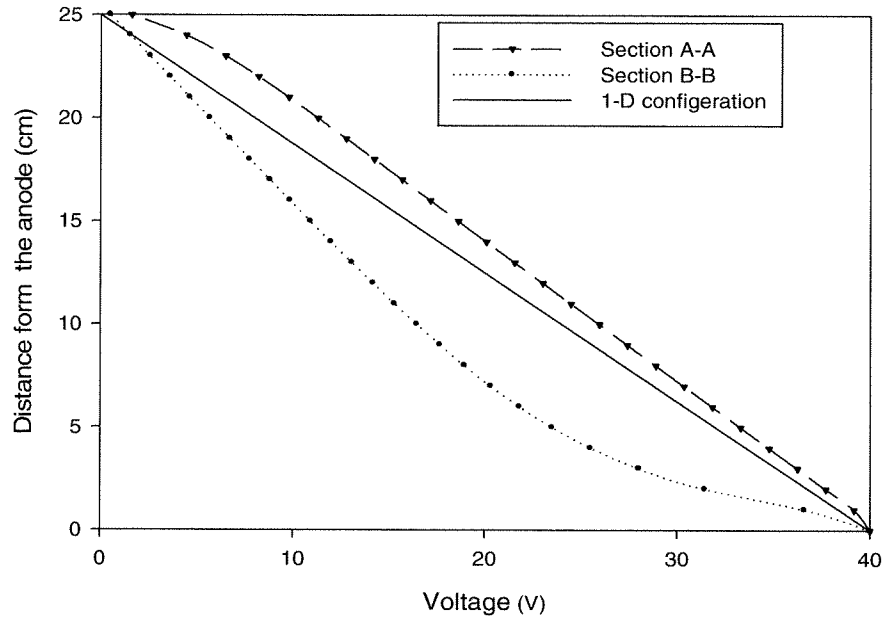

Figure 6.29 Voltage distribution at the centre of the cell for the cross-sections A-A and B-B.

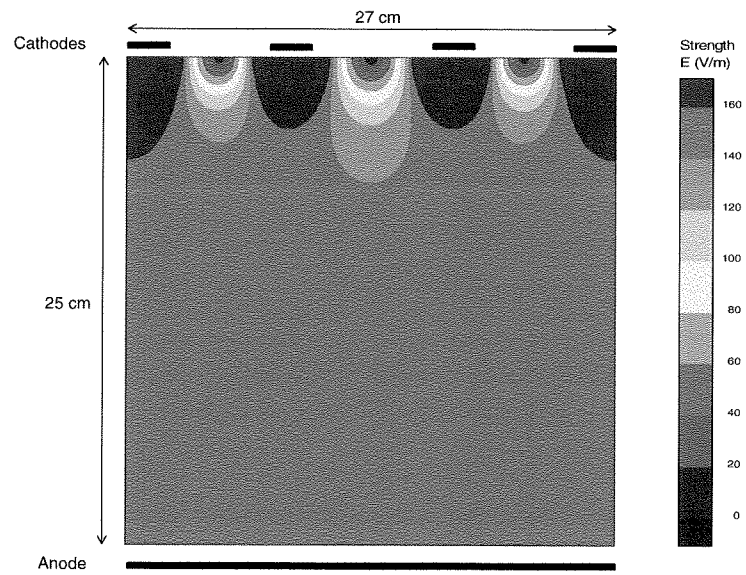

Figure 6.30 Electric field intensity for the cross-section A-A.

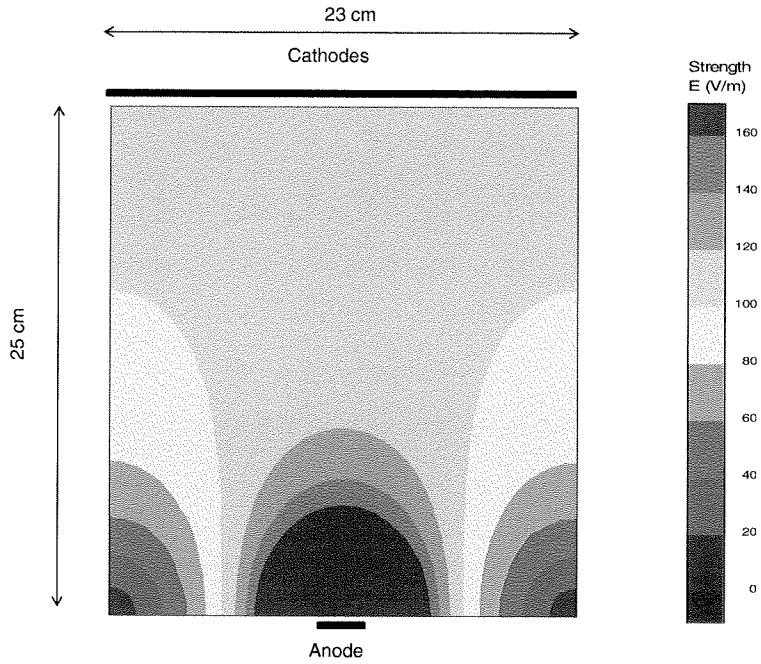

Figure 6.31 Electric field intensity for the cross-section B-B.

6.3.3.2 pH and electrical conductivity

Figures 6.31 to 6.34 show pH profiles for the tests with solid concentrations of 10, 15, 20 and 25%. The initial average pH of the slurries was about 7. Samples for pH and electrical conductivity readings were taken from three zones of mudline movement during the tests, Zone 1 mudline between 25-20 cm; Zone-2 mudline between 20-15 cm; Zone-3 mudline between 15-10 cm. As shown in Figures 6.32 - 6.34, the pH profiles were consistent with electrolysis reactions as high pH values were reported near the cathode and low values near the anode. From the figures, the pH values near the cathode increased during the test while the values near the anode had decreased. For example, the pH near the cathode was between 10 and 10.6 earlier during the test

(mudline in Zone-1) and between 11 and 11.8 by the end of the test (mudline in Zone-3).

Figure 6.35 shows the electrical conductivity along the electrokinetic tank during sedimentation phase. In general, the electrical conductivity increased with the increase in the solid concentration. Similar to the pH, the electrical conductivity near the cathode increased from 2.5 to 3.5 mS/cm at the beginning of the test to between 5.5 and 8.5 mS/cm at the end. Near the anode, the change in electrical conductivity was less significant. The bulk electrical conductivity of slurry is function of the conductivity of the soil solids and the pore fluid. Typically, the electrical conductivity of the pore fluid is much higher than the electrical conductivity of the solids. Thus, as the solids settle during the test, the pore fluid increases and subsequently the bulk conductivity increases. Also, the electrical conductivity of water increases during electrokinetics due to electrolysis reaction. This explains the increase of the bulk electrical conductivity near the cathode. Near the anode, the bulk electrical conductivity was decreased due the reduction of water content as the soil solids increases during the test. This may explain the little change seen on the conductivity near the anode.

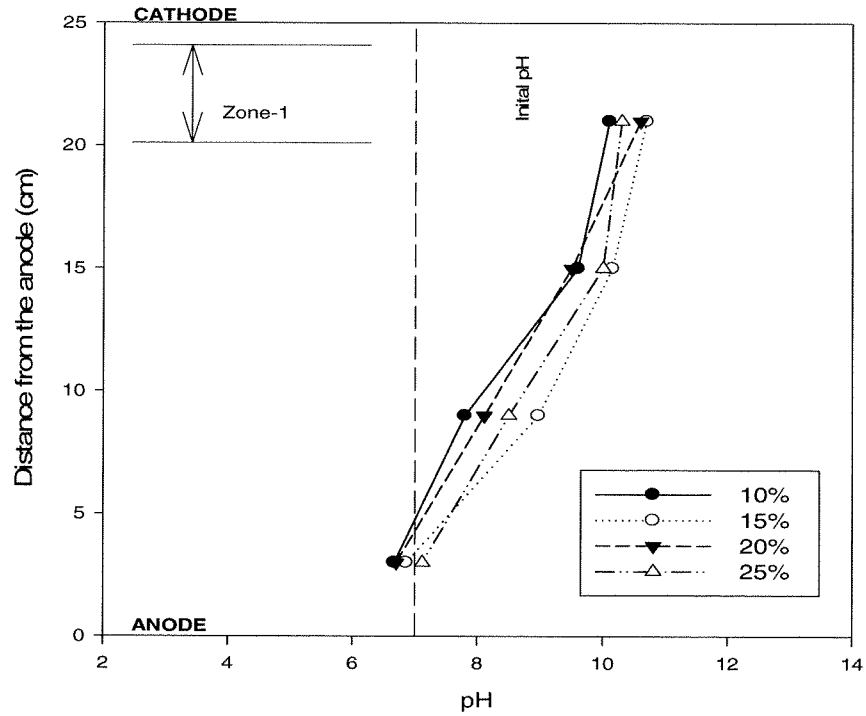

Figure 6.32 pH profile, mudline in Zone-1.

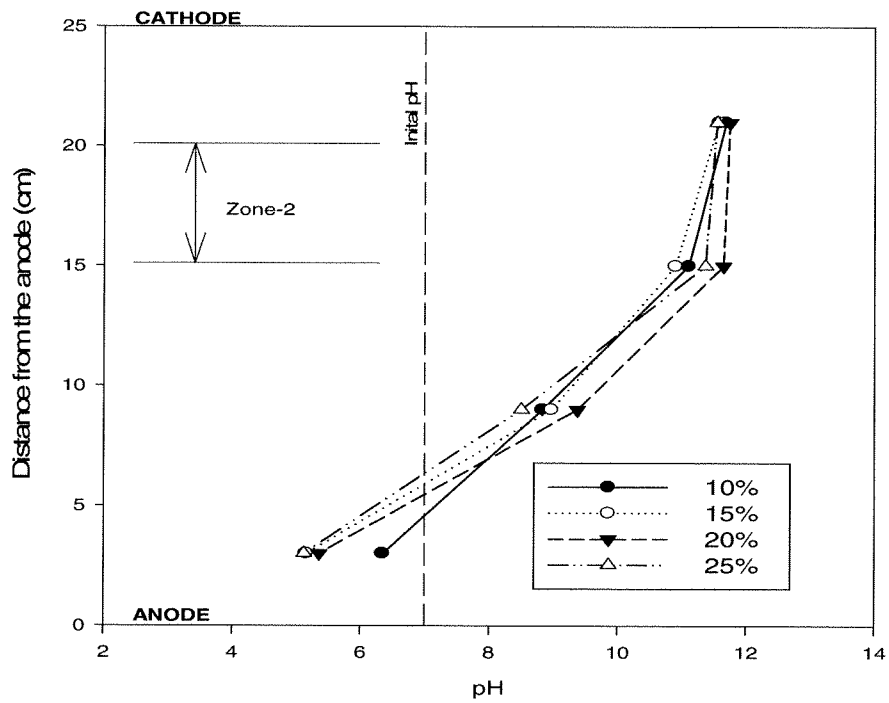

Figure 6.33 pH profile, mudline in Zone-2.

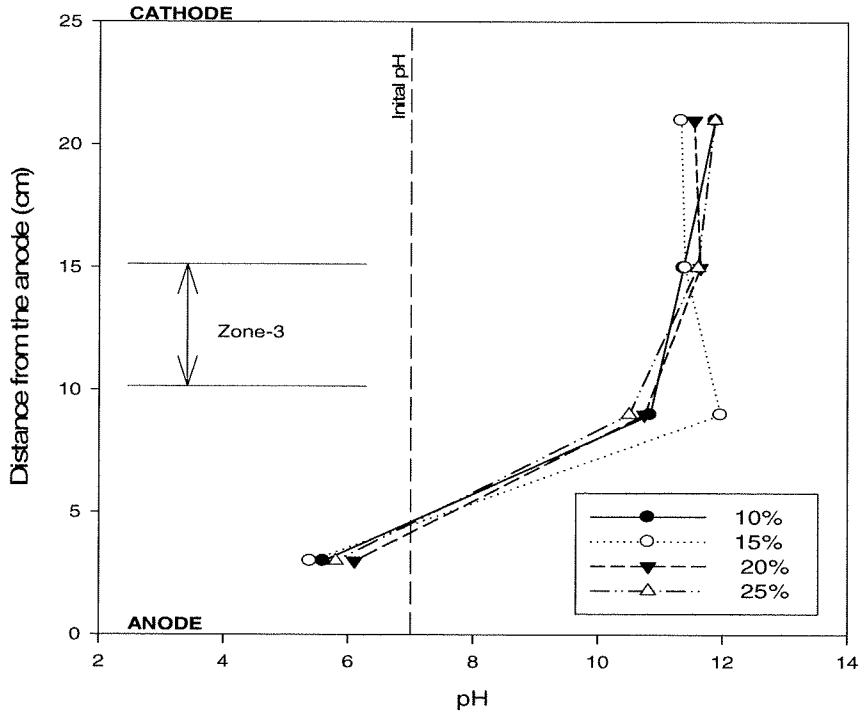

Figure 6.34 pH profile, mudline in Zone-3.

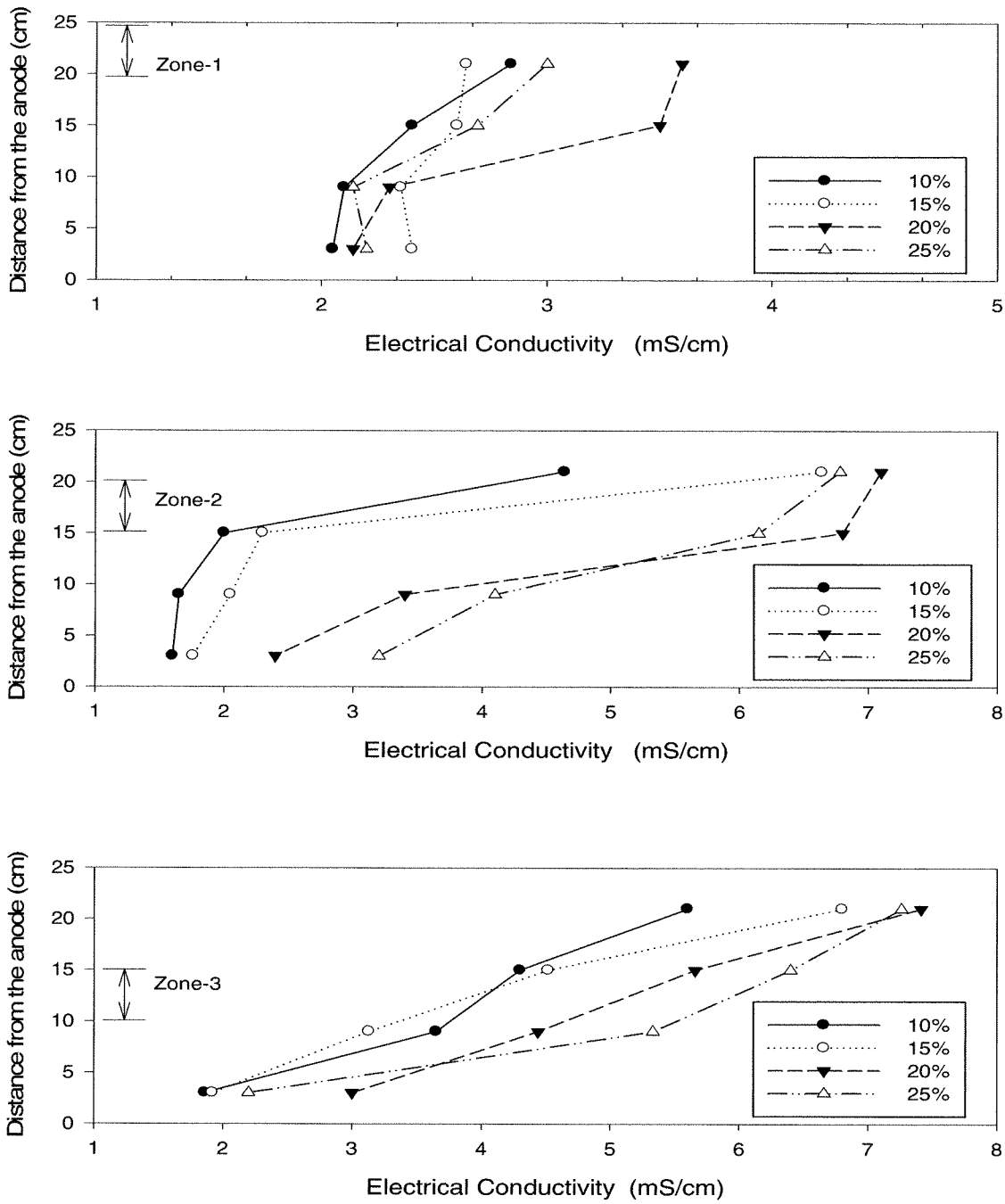

Figure 6.35 Electrical conductivity during the sedimentation phase.

6.3.3.3 Zeta Potential change

During the sedimentation, the pH and electrical conductivity changed with time along the electrokinetic tank as previously discussed. Consequently, the zeta potential,ζ, changed during the test. The mudline represents the free settling velocity which is function of the average settling velocity $\bar{u}$. Figure 6.36 shows the effect of ζ on $\bar{u}$ for kaolinite-bentonite slurry. In general, as ζ decreases (become more negative), $\bar{u}$ increases. According to Figure 6.36, the relationship between $\bar{u}$ (cm/min) and ζ (mV) is linear and is given by:

$$\bar{u} = -0.0001\,\zeta + 0.017 \qquad [6.1]$$

The term, 0.017, represents the average gravitational settling velocity $\overline{u_g}$ (cm/min).

ζ were obtained as an average value from Figure 3.9. The change of the electrical conductivity and pH during the three ranges was considered. Each solid concentration was treated individually and ζ was found to be between -20 and -30 mV. Accordingly, using Eq. [6.1], $\bar{u}$ varies between 0.019 and 0.020 cm/min (i.e. approximately the same). Therefore, an average ζ of -25 mV was used to determine the free settling velocity for the all solid concentrations.

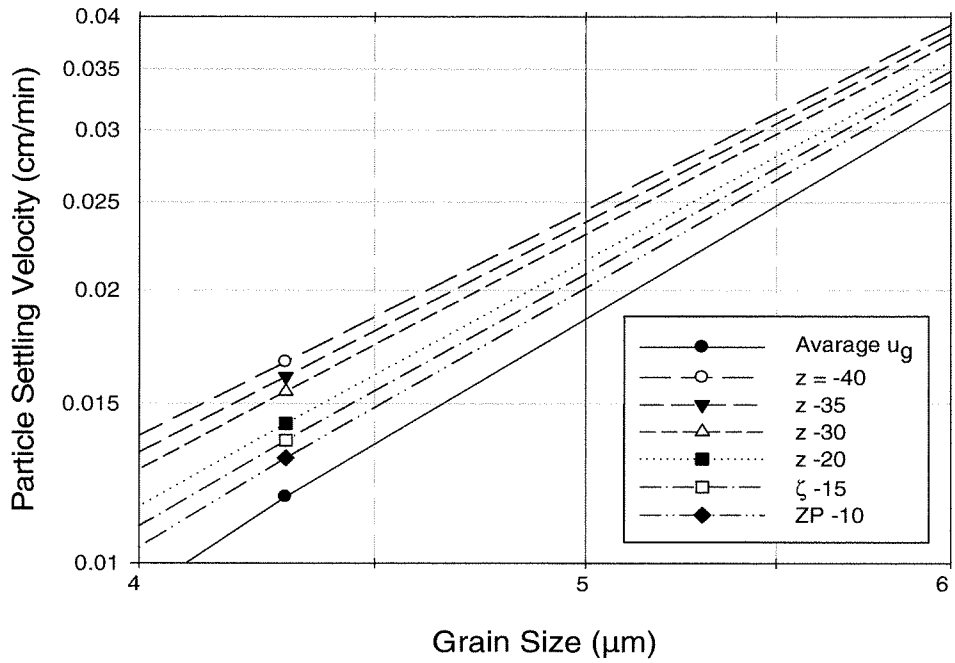

Figure 6.36 Average particle settling velocity vs. the maximum grain size for different zeta potential values.

6.3.4.3 Free settling and hindered settling

Figure 6.37 shows the mudline curves for electrokinetic tests with initial solid concentrations of 10, 15, 20 and 25%. As seen in the figure, the settling velocity decreased with the increase of the solid concentration. This was due to the increase of the surface forces with the solid concentration that hindered the settlement. The free settling velocity, U_f, the free settlement coefficients, β, and the coefficients of sedimentation, r, were determined for each solid concentration and summarized in Table 6.10. Figure 6.38 displays that both U_f and β decreased with the increasing of the initial solids concentration. Figure 6.39 shows r versus initial solid concentrations. Mohamedelhassan and Shang (2001) obtained similar curve and they suggested that

the lowest value of r in the curve coincides with the optimum initial solid concentration for electrokinetic sedimentation. Accordingly, for the kaolinite-bentonite slurry used in this study, 20% represents the optimum initial solid concentration.

Table 6.10 Settling velocities, U_f, the coefficient of the free settling, β, and the coefficient of the sedimentation, r, for 2-D configuration-B tests

Initial Solid Concentration (mass/mass)	U_f cm/min	β	r
10%	0.4	19.05	38.5
15%	0.20	9.67	37.2
20%	0.14	6.57	30.6
25%	0.1	4.72	35.4

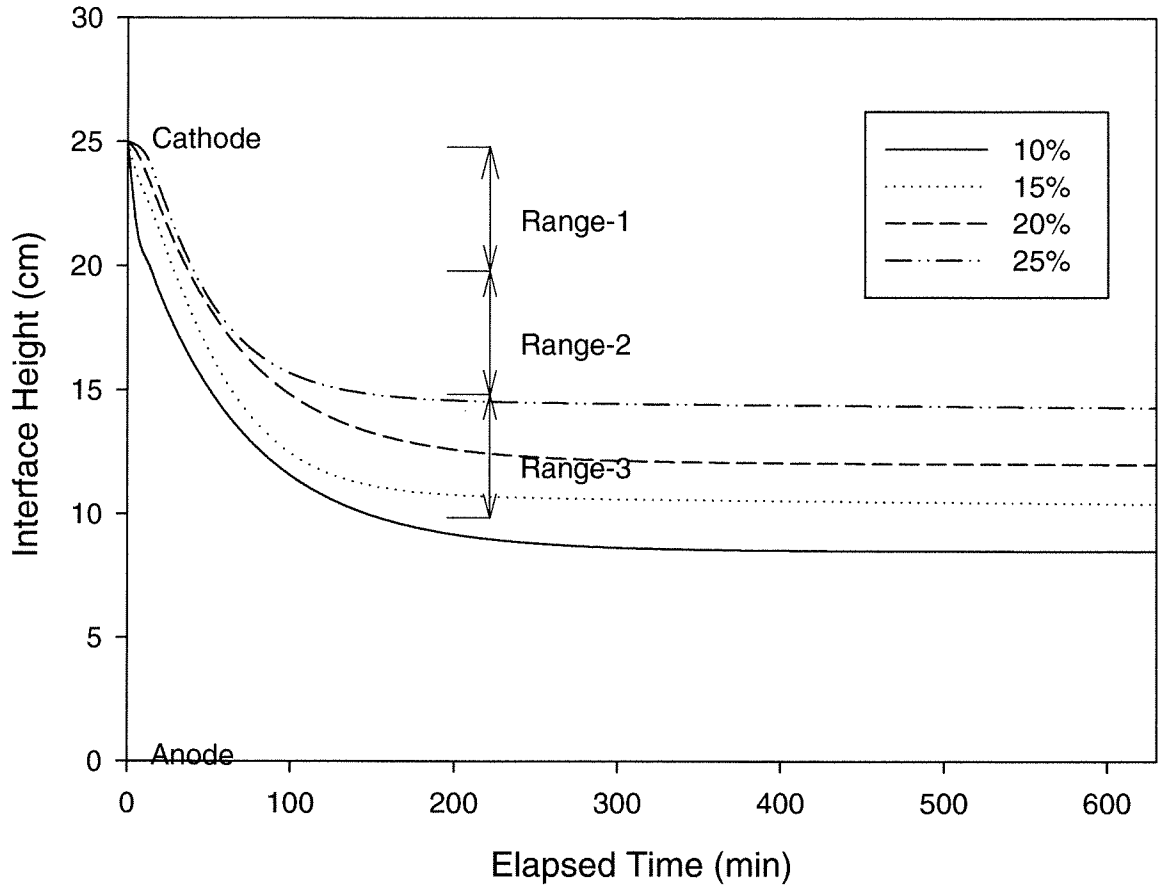

Figure 6.37 Solid-liquid interface (mudline) during the test (Configuration-B).

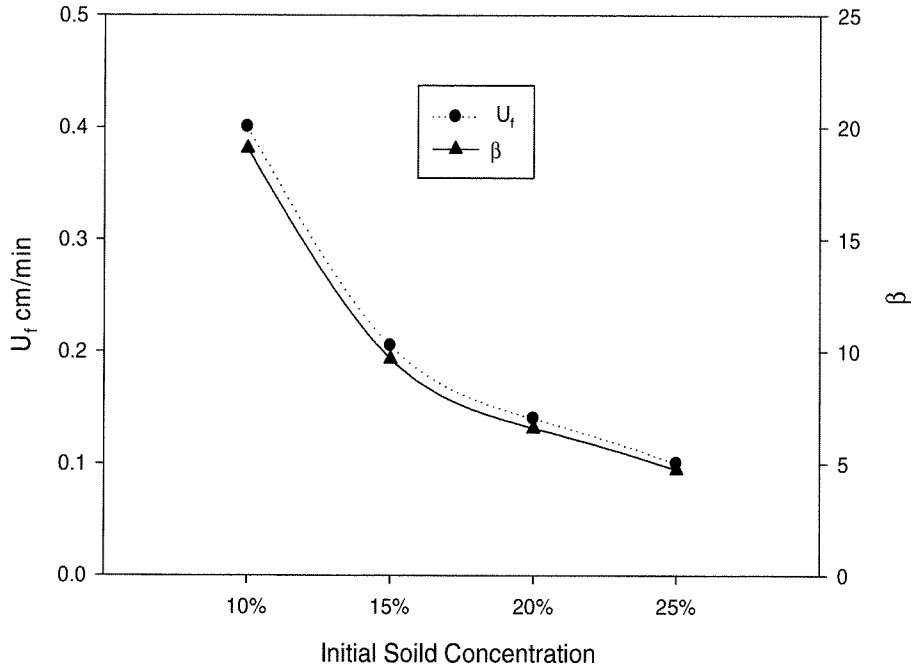

Figure 6.38 The free settling velocity, U_f, and coefficient of the free settling, β, vs. initial soil concentration

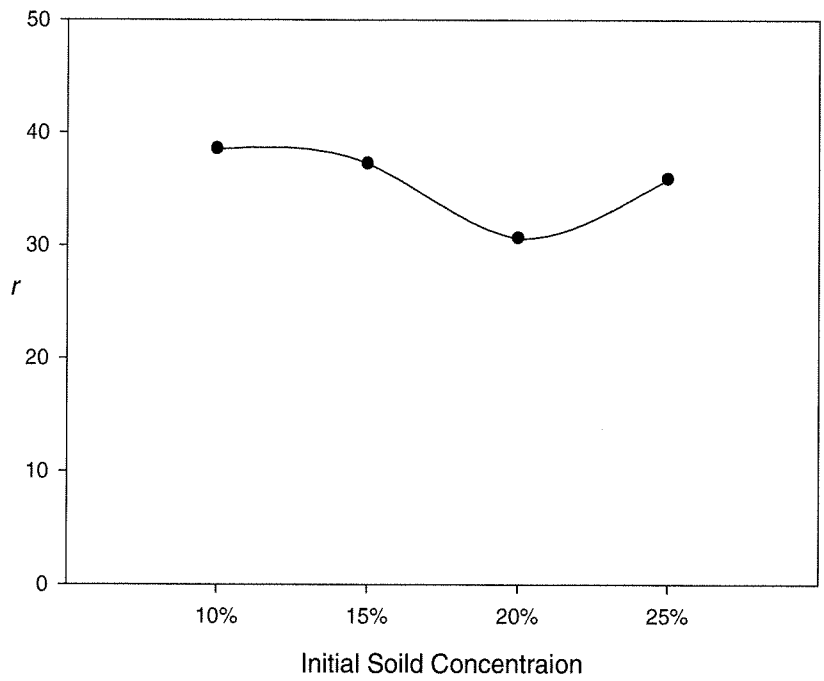

Figure 6.39 The coefficient of sedimentation, , vs. initial soil concentration

6.4 CONCLUSIONS

This study investigated electrokinetic remediation of contaminated slurry using solar cells as the source of power. The tests were conducted with one and two-dimensional electric field configurations. Two types of clay soils were tested; kaolinite and 85%koalinite-15%bentonite (by mass) mixture. The one-dimensional configuration tests consisted of two phases; electrokinetic sedimentation and dewatering/decontamination. According to the results of the dewatering phase in the one-dimensional tests, only electrokinetic sedimentation was explored for the two-dimensional configurations. An innovative two-dimensional configuration (configuration-A) was introduced. Configuration-A shows a considerable improvement on settling acceleration when compared with one- dimensional configuration tests (both tests conducted using the electrokinetic column). In the sedimentation phase, solar-powered electrokinetics successfully accelerated the sedimentation processes for the kaolinite and the kaolinite-bentonite slurries with a superior acceleration for the latter. The coefficients of the free settling, β, and the coefficients of the sedimentation, r, were determined and compared. The increase in settling velocity, U_f, and β due to electrokinetics were particularly remarkable in the kaolinite-bentonite slurries tests. The dewatering phase was used to remove water, the copper concentration and reduce the volume of the slurry. The results showed that solar-powered electrokinetics effectively removed significant amount of water from the settled clay compared to the gravitational dewatering. Besides electrokinetics mobilized copper towards the cathode, however, the removal of copper contamination in the effluent water was minor. The total volume reduction in the electrokinetic tests was noticeable compared to the controls, particularly for kaolinite-

bentonite slurries. An innovative two-dimensional configuration (configuration-B) was suggested as applicable field solution. The change in the pH profile and the electrical conductivity was considered in the analysis of the sedimentation coefficients. A finite element modelling software was executed to simulate the electric field in the two-dimensional configuration. According to the tests result, solar power can provide sufficient electric field for electrokinetics remediation of contaminated slurry.

CHAPTER SEVEN

Conclusions and Recommendations for future work

7.1 CONCLUSIONS

This research consisted of two parts. The first part investigated the efficiency of a stand-alone solar electrokinetic barrier to prevent/minimize heavy metal pollution. The second part studied solar-powered electrokinetic remediation of the contaminated slurries. In the first part, several laboratory tests were performed with one and two-dimensional electric field configurations. An electrokinetic cell, 285×125×250 mm (Length × Width × Height), was used for the tests. A sand-clay mixture was tested under hydraulic flow of water contain 1000 mg of copper per liter.

The results of the one-dimensional configuration showed that electrokinetics significantly prevented the migration of the copper contamination under continuous or periodic (solar power) application of the electric field. The effluent concentration, pH, residual copper concentration and current distribution were presented and discussed for each test. The soil adsorption capacity of the copper increased as result of the high pH zone created near the cathode in the electrokinetic tests. According to the results in the one-dimensional tests, electro-migration was found to be the dominant mechanism that opposing the migration of the copper towards the anode. Applying electric field through the two-dimensional configuration showed promising results in preventing the migration

of the copper. Electro-migration was the dominant mechanism that contributed in decrease the copper concentration in the effluent. Optimization of the electrode spacing was discussed and a software modeling of the voltage distribution was used to determine the appropriate distance between the same-polarity electrodes.

The second part of this research discussed electrokinetic remediation of the contaminated slurries using solar energy. Two types of clay soils were tested, kaolinite and mixture of 85% (by mass) koalinite-15%bentonite mixture. The experiments were carried out with one and two-dimensional configurations using an electrokinetic column with 300 mm in height and 125 mm in diameter. The one-dimensional configuration tests consisted of two phases; electrokinetic sedimentation and dewatering/decontamination. In the sedimentation phase, solar-powered electrokinetics effectively enhanced the sedimentation processes for the kaolinite and the kaolinite-bentonite slurries particularly in the latter. In the dewatering phase, solar-powered electrokinetics effectively removed significant amount of water from the settled clay compared to the gravitational dewatering. Electrokinetics mobilized copper towards the cathode, although the copper removal in the effluent water was minor. 2-D configuration-B also showed results almost similar to the 1-D configuration. An innovative two-dimensional configuration (configuration-B) was introduced as field application of the technology. The tests conducted in an electrokinetic tank, with dimensions 270 mm × 230 mm × 280 mm (Length × Width × Height). The results showed that configuration-B can be viable for electrokinetic remediation of slurry ponds.

7.2 RECOMMENDATIONS FOR FUTURE WORK

Part 1: Solar-powered electrokinetic barrier

- The clay was only 20% of the soil used in this study; further studies should investigate the use of solar power in homogenous clay.
- The tests were terminated at 1.14 pore volumes to reduce the time of the experiments due to the small hydraulic gradient applied to the soil specimen. Further investigation for larger pore volumes values should be considered to evaluate the effectiveness of the electrokinetic barrier with time.
- Pilot scale studies should be conducted to verify the effectiveness of electrokinetic barriers in preventing the migration of the contamination. The use of the software modeling of voltage distributions should be taken into account in designing the large scale studies.

Part 2: Electrokinetic remediation of copper contaminated slurries

- The copper was used to represent the contamination in the test conducted; further studies have to be to examine other organic/inorganic contaminants or mixture of the contaminants.
- Large scale study should be carried on using the two-dimensional configuration.

REFERENCES

Acar, Y.B. and Alshawabkeh, A.N. (1993). "Principles of Electrokinetic Remediation."- Environmental since and technology 27 (13): 2638-2647.

Acar, Y.B. and Alshawabkeh, A.N. (1996). "Electrokinetic Remediation I: Pilot-Scale Tests with Lead-Spiked Kaolinite." Journal of Geotechnical Engineering-ASCE 122 (3): 173-185.

Acar, Y.B., Li, H. and Gale, R.J. (1992). "Phenol Removal from Kaolinite by Electrokinetics." Journal of Geotechnical Engineering - ASCE, A118 (11): 1837-1852.

Acar, Y.B.; Gale, R.J., Putnam, G. and Hamed, J.T. (1989). "Electrochemical Processing of Soils: Its Potential Use in Environmental: Geotechnology and Significance of pH Gradients" 2nd International Symposium on Environmental Geotechnology, Shanghai, China, Envo Publishing: Bethlehem.

Alshawabkeh, A.N. and Acar, Y.B. (1996). "Electrokinetic Remediation. II: Theoretical Model." Journal of Geotechnical Engineering 122 (3): 186-196.

Alshawabkeh, A.N., Yeung, A.T. & Bricka, M.R. (1999). "Optimization of 2-D electrode configuration for electrokinetic extraction" Journal of Soil Contaminant (8): 617-635.

American Society for testing and Materials (ASTM) D422-63, 2007. Standard test Method for Particle size Analysis of soils. ASTM international, West Conshohocken. PA.

American Society for testing and Materials (ASTM) D4318-05, 2005. Standard test Method for Liquid Limit, Plastic Limit And Plasticity Index of Soils. ASTM international,

West Conshohocken. PA.

American Society for testing and Materials (ASTM) D854-06, 2006. Standard test Method for Specific Gravity of Soil by Pycnometer. ASTM international, West Conshohocken. PA.

American Water Works, A. (1990). Water quality and treatment: a handbook of community water supplies/ American Water Works Association.

Arias, M., Barral, M.T. and Mejuto, J.C., (2002). "Enhancement of copper and cadmium adsorption on kaolin by the presence of humic acids." Chemosphere (48): 1081–1088.

Buckland, D., Shang, J.Q. and Mohamedelhassan, E. (2000). "Electrokinetic enhanced sedimentation of contaminated Welland River sediment." Canadian Geotechnical Journal, (37): 735-747.

Atanssova, i. and Ozaki M (1997). "Adsorption-desorption charactristics of high level of copper in soil fraciond" Water Air And Soil Polution 98 (3-4):213-228

Casagrande, L. (1952). "Electroosmosis stabilization of soils." Journal of the Boston Society of Civil Eng. (39): 51-83

Chen, H.M., (1996). "Heavy Metal Pollution in Sol-Plant System." Science Press, Beijing.

Chung, H.I., Sills, G.C. and Kamon, M. (2005) "Electrokinetically Enhanced Settlement and Remediation of Contaminated Sediment." ASTM (3): 1546-962.

Eykholt, G.R. & Daniel, D.E. (1994). "Impact of System Chemistry on Electroosmosis in

Contaminated Soil." Journal of Geotechnical Engineering 120 (5): 797-815.

Evangelou V. P. (1998). "Environmental soil & water chemistry" John Wiley & Sons, Inc.. USA.

Gray, D. H., and Mitchell, J. K. (1967). "Fundamental aspects of electro-osmosis in soils." J. Soil Mech. Found. Div., Proc. ASCE (6): 209-236.

Hamed, J., Y.B. Acar and R.J. Gale. (1991). "Pb(II) Removal from Kaolinite by Electrokinetics." Journal of Geotechnical Engineering 117 (2): 24 1-271.

J. K. Mitchell and K. Soga (2005). "Fundamentals of Soil Behavior: 3rd edition" John Wiley and Sons, New York.

Kim SS, Kim JH, and Han SJ (2005)." Application of the electrokinetic-Fenton process for the remediation of kaolinite contaminated with phenanthrene." Journal of Hazard Material B118: 121-131

Koryta, J. (1982). " Ions, Electrodes, and Membranes", John Wiley and Sons, New York.

Ottosen, L.M., Kristensen, I.V., Pedersen, A.J., Hansen, H.K., Villumsen, A., and Ribeiro, A.B. (2003). "Electrodialytic removal of heavy metals from different solid waste products" Separation Science and Technology (38):1269 –1289.

Lageman, R., Pool, W. & Seffinga, G.A. (1989). "Electro-Reclamation: Theory and Practice." Chemistry & Industry (18): 585-590.

Lockhart N. C. (1983). "Electro-osmotic dewatering of clays. III. Influence of clay type,

exchangeable cations, and electrode materials." Colloid and Surfaces (6): 253-259.

Lockhart, N.C. (1986). "Electro-dewatering of fine suspensions. In Advances in solid–liquid separation." Edited by H.S. Muralidhara.Batelle Press: 241–274.

Lynch, R.J., A. Muntoni, R. Ruggeri and K.C. Winfield, (2007). "Preliminary tests of an electrokinetic barrier to prevent heavy metal pollution of soils" Electrochemical .Acta,(10): 3432-3440.

Mitchell, J.K. & Yeung, A.T. (1991). "Electrokinetic Flow Barriers in Compacted Clay." Transp. Res. Record, (1288): 1-9.

Mitchell, J.K., and Soga, K, (2005) "fundamental of soil behaviour" .3rd Edidtion, john & Sons, new tork

Mohamedelhassan, E. (2011). "Laboratory Study on Integrated Solar Electrokinetic Barrier for Preventing Cadmium Contamination." Research Journal of Environmental and Earth Sciences (5): 521-533.

Mohamedelhassan, E., and Shang, J. Q. (2001). "Analysis of electrokinetic sedimentation of dredged Welland River sediment." Journal of Hazardous Materials (85): 91-109.

Mohamedelhassan, E., and Shang, J. Q. (2001). "Effects of electrode materials and current Intermittence in electroosmosis." Ground Improvement (5): 3-11.

Mohamedelhassan, E., and Shang, J.Q. (2003). "Electrokinetics generated pore fluid and ionic transport in an offshore calcareous soil." Canadian Geotechnical Journal (40):

1185–1199.

Narasimhan, B. and Ranjan, R.S. (2000). "Electrokinetic barrier to prevent subsurface contaminant migration: theoretical model development and validation." Journal of Hazardous Materials, (2-3): 1583-1587.

Page, M.M. & Page, Ch.L. (2002). "Electroremediation of Contaminated Soils." Journal of environmental Engineering (3): 208-219.

Phillips, I.R., Lamb, D.T., Warker, D.W., and Burton, E.D. (2004). "Effect of pH and salinity on copper, lead, and zinc sorption rates in sediments from Moreton bay, Australia. Bull." Environmental Contamination and Toxicology (73): 1041–1048.

Probstein, R.F. and Hicks, R.E. (1993). "Removal of Contaminants from Soil by Electric Fields." Science(260): 498-503.

Reddy KR, Ala PR, Sharma S, and Kumar SN (2006). Enhanced electrokinetic remediation of lead contaminated soil. Science and Technology (85): 123-132

Reddy, K.R. and Cameselle, C. (2009): Electrochemical remediation technologies for polluted soils, sediments and groundwater. Edited by Krishna R. Reddy, Claudio Cameselle

Reddy, K.R., Parupudi, U.S., Devulapalli, S.N. and Xu, C.Y. (1997). "Effects of soil composition on the removal of chromium by electrokinetics." Journal of Hazard and Material (55): 135-158.

Ricart, M.T. (2001). "Removal of Multiple Metallic Species from Sludge by

Electromigration". Proceedings EREM 2001 3rd Symposium and Status Report on Electrokinetic Remediation. Published by AGK University of Karlsruhe. (9): 4-10.

Shang, J. Q., and Mohamedelhassan, E. (2001). "Electrokinetic Dewatering of Eneabba West Mine Tailings: An Experimental Study." ASCE Geotechnical Special Publication No. 112: Soft Ground Technology, ASCE Press, Reston,VA, : 346-357.

Shang, J.Q. (1997). "Electrokinetic dewatering of clay slurries as engineering soil covers." Canadian Geotechnical Journal (34): 78-86.

Shang, J.Q. (1997). "Zeta potential and electroosmotic permeability." Canadian Geotechnical Journal. (34): 627-631.

Shang, J.Q. and Lo, K.Y. (1997). "Electrokinetic dewatering of a phosphate clay." Journal of Hazardous Materials. Special Edition (55): 117-133.

Shang, J.Q., Lo, K.Y. and Huang. K.M. (1996). "On influencing factors in electro-osmotic consolidation." Geotechnical Engineering, Journal of Southeast Asian Geotechnical Society (27): 23-26.

Shang, J.Q., Lo, K.Y. and Quigley, R.M. (1994). "Quantitative determination of potential distribution in Stern-Gouy double layer model." Canadian Geotechnical Journal (31): 624-636.

Shapiro, A.P. & Probstein, R.F. (1993). "Removal of Contaminants from Saturated Clay by Electroosmosis." Environmental Science and Technology (2): 283-291.

Sposito, G (1984). "The surface chemistry of soils." Oxford University Press, Inc., New

York.

Sprute, R. H. and Kelsh D. J. (1976). "Dewatering and Densification of Coal Waste by Direct Current - Laboratory tests." US Department of the Interior United States Bureau of Mines Report of Investigations No. 8197.

U.S. Environmental Protection Agency, USEPA (1998). Sandia National Laboratories In Situ Electrokinetic extraction Technology-Innovative Technology Evaluation Report, National Risk Management Research Laboratory, Office of Research and Development.

Undabeytia, T., Nir, S., Tytwo, G., Serban, C., Morillo, E., and Maqueda, C. (2002). "Modeling adsorption–desorption processes of Cu on edge and planar sites of montmorillonite." Environmental Science and Technology (36): 2677–2683.

Virkutyte, J., Sillanpää, M., and Latostenmaa, P. (2002). "Electrokinetic soil remediation – critical overview." The Science of the total Environmental. (289): 97-121.

West, L.J., and Stewart, D.I., (1995). "Electrokinetic decontamination: the effect of zeta potential." Geoenvironment 2000. American Society of Civil Engineers Special Publication(46): 1535–1549.

Xu, Y.H., and Zhao, D.Y., (2005). "Removal of copper from contaminated soil by use of poly(amidoamine) dendrimers." Environmental Science and Technology (39): 2369-2375

Yeung, A.T. (1990). "Coupled flow equations for water, electricity and ionic contaminants through clayey soils under hydraulic, electrical and chemical gradients."

J. Non-Equil. Thermodyn (3): 285-299.

Yeung, A.T. (1994). "Electrokinetic flow processes in porous media and their applications: Advances in Porous Media" (2): 309–395.

Yeung AT, and Hsu C. (2005) "Electrokinetic remediation of cadmium-contaminated clay" Journal of Environmental Engineering ASCE 131(2): 298–304.

Yuan, S., Z. Zheng, J. Chen and X. Lu (2009). "Use of solar cell in electrokinetic remediation of cadmium contaminated soil." J. Hazard. Mater. 162(2-3):1583-1587.

Yuan, S. H., Xi, X. M., Jiang, Y., Wan, J. Z., Wu, C., .Zheng, Z. H. and Lu, X.H. (2007). "Desorption of copper and cadmium from soils enhanced by organic acids" Cemosphere 68(7):1289-1297